Investigating The Role Of Platelet Proteins In The Regulation Of Atherosclerosis In Coronary Artery Disease

Thesis submitted for the degree of
Doctor of Philosophy (Science)
In
Biophysics, Molecular Biology and Bioinformatics

by

Apabrita Ayan Das

Department of Biophysics, Molecular Biology and Bioinformatics
University of Calcutta
2020

"Science may set limits to knowledge, but should not set limits to imagination"

-Bertrand Russell

Dedicated to

My family…

For their support

Declaration

I hereby declare that this thesis is a presentation of my original research work. Wherever contribution of others involved have been made to indicate clearly, with due references of literature, and acknowledgement of collaborations. To the best of my knowledge, the use of self-published material in the thesis is in accordance with the copyright policies of the concerned journal(s). This thesis work was done under the guidance of Dr. Arun Bandyopadhyay, at CSIR- Indian Institute of Chemical Biology, Kolkata, India. I declare no conflicts of interest.

Apabrita Ayan Das
Kolkata, India

ACKNOWLEDGEMENTS

At this memorable moment of submitting my doctoral dissertation, I would like to consolidate my excitement about the incredible journey to the present stage of my carrier. I am grateful and I want to convey my sincere thanks to those people who helped me persistently.

First, I want to express sincere gratitude to my Ph.D. guide Dr. Arun Bandyopadhyay as he allowed me to pursue my research in his esteemed laboratory. His persistent belief on my capabilities and ideas helped me to increase my creativity. He has always given me liberty to think independently and design experiments according to my choice. Additionally, he streamlined my ideas and helped me to focus when I was diverging out in other minor scientific possibilities. At the same hand, he never stepped back to criticize my work from a scientific point of view which helped me to build my logical thinking. His guidance does not only encompass precious advice about my research work, but his friendly and jovial attitude helped me in my rough times. His encouragement helped me to overcome the frustrations of scientific research. Under his supervision, I developed methods for hypothesis testing, logical thinking which encouraged me to pursue a higher scientific career. He will always remain an inspiration for me.

I am deeply grateful to Dr. Jaya Bandyopadhyay for her immense support during the communication of my manuscripts. Her English skill has inspired me a lot to improve my thinking about the application of English literature in scientific writing.

My life at CSIR-Indian Institute of Chemical Biology would have been incomplete without my lab mates. I want to thank my seniors especially Tanima di, Somaditya da, Dipak da, Kamalika di and Vivek vaiya. They were very supportive and helped me when they could with problems regarding my research. I particularly want to thank Priyam for his constant support. I owe him a lot. Sayantan was always a good friend to me. I am gonna miss our leisure sessions discussing weird scientific things. Dibyanti, Devasmita, Aleepta, Ritu and Sumanta were always a great sport. I also want to thank Pratitusti, junior most member of our lab. It had been fun discussing science with her. Swapan da was of immense support in laboratory activities. I learned a lot of basic laboratory chemistry from him. I also want to thank Jishu da and Santu da with whom I had nice collaboration during my Isothermal Titration Calorimetry and Orbitrap experiments.

During my second year of Ph.D, I got chance to collaborate with some eminent researchers. I would like to name Dr. Surajit Biswas and Dr. Mahesh J. Kulakarni for their constant support in peptide chemistry and proteomics studies, respectively. Our long scientific discussions helped me to build my rational thinking. I would also like to thank Jagdeesha and Debmalya for their constant input in my proteomics and peptide chemistry research.

Over the years of my research, I have collaborated with many clinicians without whom my research would not have been possible. I would like to name Dr. Prakash C. Mandal, Dr. K.N. Siddiqui for their constant support and valuable advice regarding clinical analyses. I would also like to thank some eminent clinicians with whom I have worked with. I would like to name Christina Vassalle, Claudio Marabotti, Alberto Marabotti and Alessandro Pingitore among them.

I would like to thank the faculties of the Department of Zoology, Banaras Hindu University especially Dr. S.C. Lakhotia, Dr. R. Raman, Dr. J. K. Roy whose guidance led me take the interest in cell biology. I am also thankful to my Masters Dissertation mentor Garima di for her support during those rough days. I would also like to thank the faculties of Department of Zoology, Visva-Bharati especially Dr. Samir Bhattacharya and Dr. Shelley Bhattacharya. Their classes were invaluable for me to build the basics. I would also like to thank my classmates from BHU.

I am especially thankful to my friends Alokesh and Abhishek. Our nightlong discussions about science had deeply enriched me. Abhishek with his wise enthusiasm as well as Alokesh with his poetic clarity made those discussions. We could not fathom in those days how much we were learning from those friendly yet serious discussions. I also express my deepest gratitude to Dr. Debaki Ranjan Pramanik for his immense effort to build our basics.

This thesis work was entirely done in the Department of Cell Biology and Physiology, CSIR-IICB. I sincerely acknowledge the financial support provided by University Grant Commission (UGC) towards my fellowship. I would like to thank Department of Biophysics, Molecular Biology and Bioinformatics, University of Calcutta.

I would also like to mention specially my inanimate friends, my books and my flute for their unconditional friendship in the frustrating times.

Last but not the least; I want to thank my parents for their unconditional support and encouragement in all conditions. Their unconditional love always boosted my self-confidence. They have never forced me into any carrier. I feel lucky to have them as my parents. I also want to thank my sister for her support. I specifically want to mention my wife Aditi, for her continuous support. It was always inspiring discussing science with her. She had been a great companion for me. We discussed almost everything and had fun. I am grateful having her in my life. I am fortunate to have such a lovely family.

Apabrita Ayan Das

TABLE OF CONTENTS

ABBREVIATIONS

Abbreviations	Extended form
CAD	Coronary artery disease
sTLT1	Soluble TREM like transcript 1
TREML	Triggering receptor expressed on myeloid cells like protein
IgG	Immunoglobulin G
Fcɣ RI	Fcɣ Receptor I
SYK	Spleen tyrosine kinase
ECG	Electrocardiogram
HBTU	O-(Benzotriazol-1-yl)-N, N, N′, N′-tetramethyluroniumhexafluorophosphate
DMF	*N, N′*-dimethylformamide
DCM	Dichloromethane
DIEA	Diisopropylethylamine
EDT	Ethanedithiol
HADDOCK	High ambiguity driven protein-protein docking
AIR	Ambiguous interaction restraint
LDL	Low density lipoprotein
oxLDL	Oxidized low density lipoprotein
DPBS	Dulbecco's phosphate buffer saline
ApoE	Apolipoprotein E
HDL	High density lipoprotein
LVEF	Left ventricular ejection fraction
TIMI score	Thrombolytic index of myocardial infarction score
ROC curve	Receiver Operating Characteristics curve
AUC	Area under the curve
PPI score	Protein-protein interaction score
ITAM	Immunoreceptor tyrosine-based activation motif
MAPK	Mitogen activated protein kinase
MAPKK	Mitogen activated protein kinase kinase
HCD	High cholesterol diet
TNF-α	Tumor necrosis factor- alpha
BTK	Bruton's Tyrosine Kinase
SYK	Spleen Tyrosine Kinase
NFkB	Nuclear Factor kappa B

PPARγ	Peroxisome Proliferator-Activated Receptor γ
AZGP1	Zinc alpha 1 Acid Glycoprotein
ABCA5	ATP Binding Cassette A 5
HAVCR2	Hepatitis A Virus Cellular Receptor 2
PGLYRP2	N-acetylmuramoyl-L-alanine amidase
TIM-3	T cell immunoglobulin and mucin domain-containing protein 3
C17ORF57	C17 Open Reading Frame 57
SR-A	Scavenger Receptor-A
CD36	Cluster Differentiation 36

ABSTRACT

The role of inflammation in all stages of atherosclerotic process is well-known and soluble TREM like transcript 1 (sTLT1), a platelet protein, is reported to be linked to chronic inflammation. Yet, no information is available about the involvement of sTLT1 in atherosclerotic cardiovascular disease. Initially, our results indicated plasma level of sTLT1 was significantly (p<0.05) elevated in clinical (2342±184pg/ml) and subclinical cases (1773±118pg/ml) than healthy controls (461±57pg/ml). Additionally, statistical analyses indicated that sTLT1 was associated with Coronary Artery Disease (CAD). Ex vivo studies on macrophages indicated that sTLT1 binds to Fcγ RI to activate MAP kinase signalling cascade to activate NF-kB which promotes secretion of pro-inflammatory cytokine TNF-α from macrophage cells. Atherosclerotic apoE-/- mice also showed high levels of sTLT1 and TNF-α in virtually occluded aortic stage indicating the contribution of sTLT1 in inflammation. As, sTLT1 is a platelet secreted protein with a significant role in CAD, we explored the plasma secretome of Coronary Artery Disease subgroups (STEMI, NSTEMI, UA) which may identify new candidate proteins responsible for the development of CAD.

It resulted into the identification of several unique proteins in each subgroup. Employing a case-control design, more than 2500 annotated proteins were identified using Orbitrap mass spectrometer in both STEMI and healthy control subjects; whereas in NSTEMI and UA the numbers were a little less (>800). Quantitative proteomics study on STEMI patients revealed that 26 proteins were decreased and 38 proteins were increased significantly in STEMI compared to healthy control. AZGP1, ABCA5, Calicin, PGLYRP2, HAVCR2, C17ORF57 appeared to be relevant to STEMI whereas soluble Galectin-3 seemed relevant to NSTEMI after cross-validation in human samples. Mechanistic significance in foam cells indicated the imbalance of RCT through the interaction of AZGP1 with CD36. Additionally, in silico studies of soluble Galectin-3 with Dectin-1 showed the activation of Dectin-1 mediated signalling which led to the secretion of pro-inflammatory cytokines. In summary, this study revealed a unique relationship of some novel proteins apparently responsible for impaired RCT and chronic inflammation leading to atherothrombosis and myocardial infarction in CAD.

INTRODUCTION

REVIEW OF LITERATURE

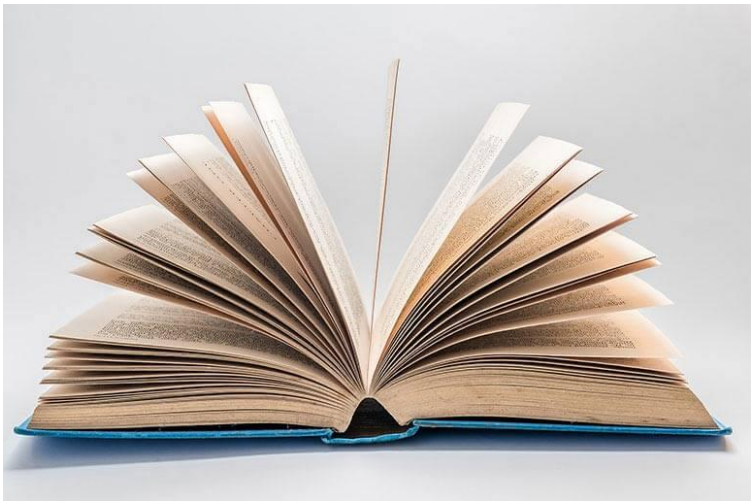

6.1.1. Human: anatomy and health issues

Human beings are a complex and unique trait which are difficult to explain because each of them is different. The keys to understanding a human being lie first in understanding our structure, then understanding our environment, and last in understanding our interactions with each other. To understand human beings, you must first understand the structure. This structure or the body functions as a machine, and the parts of the body are constructed to work together. The long mid part is called a torso which houses most of the major organs which provide the body with the things that the body needs to function. All these organs work to provide energy to the body, and one of the most important visceral organs is the heart. The heart is a pump that provides blood to the entire body with oxygen (the primary source of our internal energy). Human life and human health depends upon the availability of oxygen and perfect functioning of the vital organs. The human body is remarkably well designed as most of its organs have a great deal of extra capacity or reserve. Still, disease often affects anatomy, and changes in anatomy can cause disease. Because of the relationship between disease and anatomy, methods of exploring into the disease mechanism have become a mainstay in the diagnosis and treatment of disease. So, cardiovascular diseases are no exception to this trend.

6.1.2. Heart and the Cardiovascular System

The basic function of the heart is to act as a muscular pump propelling blood into and through vessels to and from all parts of the body. The arteries, which receive this blood at high pressure and velocity and carry it throughout the body, have thick walls that are composed of elastic fibrous tissue and muscle cells. The arterial tree, the complex branching system of arteries concludes in short, narrow, muscular vessels called arterioles, from which blood enters simple endothelial tubes (i.e. tubes formed of endothelial, or lining, cells) known as capillaries. These thin, microscopic capillaries are permeable to vital cellular nutrients and waste products that they receive and distribute. From the capillaries, the blood, now depleted of oxygen and burdened with waste products, moving more slowly and under low pressure, enters the venules that converge to form veins, ultimately guiding the blood on its way back to the heart. Because of the watertight lining of the heart (the endocardium) and the thickness of the myocardium, the heart cannot depend on the blood contained in its own chambers for oxygen and nourishment. It possesses a vascular system of its own, called

the coronary arterial system. In the most common distribution, this comprises two major coronary arteries, the right and the left; normally, the left coronary artery divides soon after its origin into two major branches, called the left anterior descending and the circumflex coronary arteries. The right, the left anterior descending, and the left circumflex coronary arteries have many branches and are of almost equal importance. Thus, there are commonly said to be three main functional coronary arteries rather than two. The right and left coronary arteries originate from the right and left aortic sinuses, which are bulges at the origin of the ascending aorta immediately beyond, or distal to, the aortic valve. The ostium or opening of the right coronary artery is in the right aortic sinus and that of the left coronary artery is in the left aortic sinus, just above the aortic valve ring. The left coronary arterial system is more important than the right because it supplies blood to the larger left ventricle, and the dimension of the left coronary ostium is larger than that of the right.

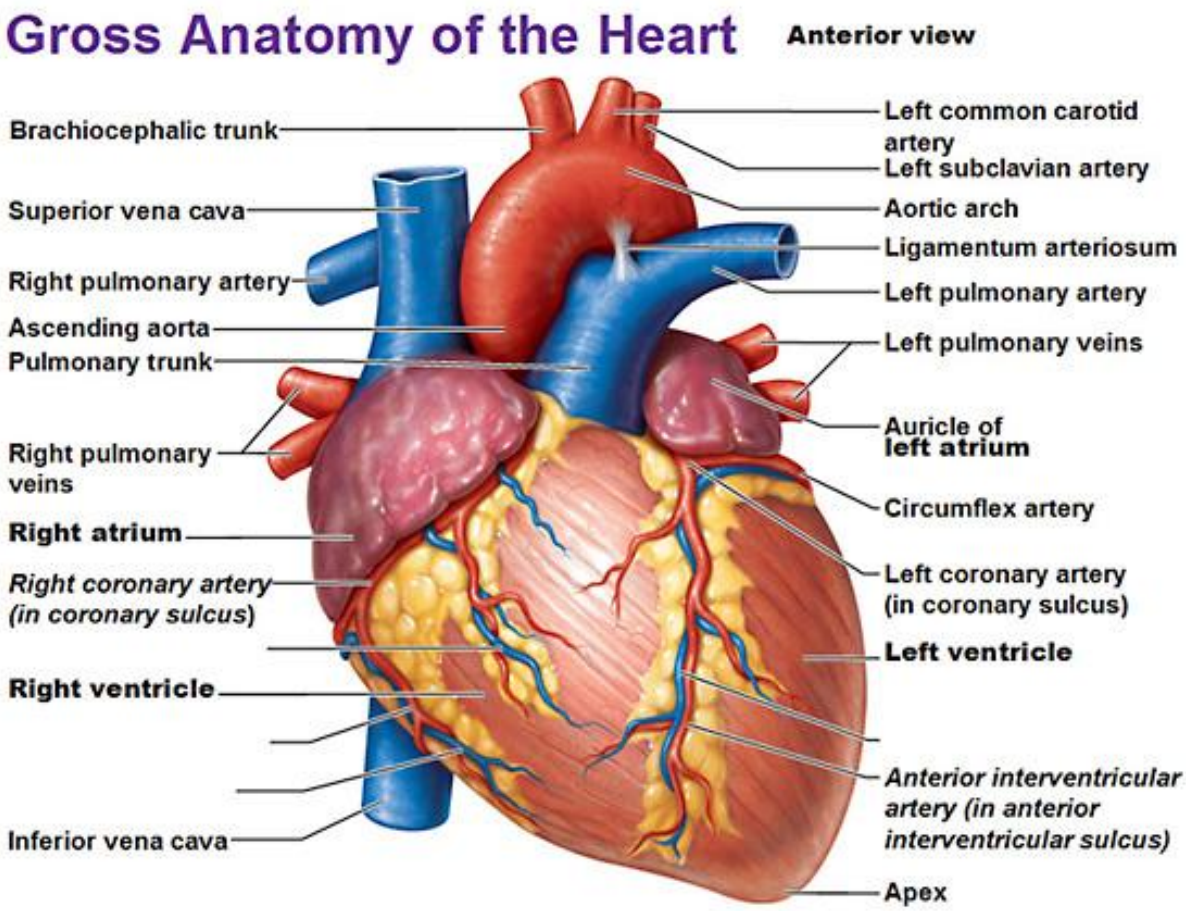

Figure 6.1.1. Anatomy of normal human heart [www.Britannica.com]

The right coronary artery has a lumen diameter of about 2.5 mm or more. It supplies the right ventricular outflow tract, the sino-atrial (SA) node, the atrio-ventricular (AV) node, and the bulk of the right ventricle, with branches extending into the inter-ventricular septum and joining with arteriolar branches from the left coronary artery more or less where the two ventricles join. The main stem of the left coronary artery has a luminal diameter often exceeding 4.5 mm. and is one of the shortest and most important vessels of the body. Usually, it is between 1 and 2 cm in length, but it may have a length of only 2 mm before dividing. Sometimes the main left coronary artery may actually be missing, with the left coronary ostium having two separate openings for the left anterior descending and the left circumflex arteries. The main left coronary artery divides into its two branches, the anterior descending and the circumflex, while still in the space between the aorta and pulmonary artery. The left anterior descending coronary artery usually begins as a continuation of the left main coronary artery, and its size, length, and distribution are key factors in the balance of the supply of blood to the left ventricle and the inter-ventricular septum. There are many branches of the left anterior descending artery; the first and usually the largest septal branch is important because of its prominent role in supplying blood to the septum.

The left circumflex artery leaves the left main coronary artery to run posteriorly along the atrio-ventricular groove. It divides soon after its origin into an atrial branch and an obtuse marginal branch. The former branch sometimes has a branch to the SA node (more usually supplied from the right coronary artery). The obtuse marginal vessel supplies the posterior left ventricular wall in the direction of the apex. These arteries are of utmost importance in progression and incidence of cardiovascular diseases as most of the blockage occurs in the cardiac arterial system. Anomalies in cardiovascular system, as stated above, can lead to cardiovascular disease.

6.1.3. Cardiovascular Disease: Classification

Cardiovascular disease occurs due to blockage of arteries with fatty deposits by a process known as atherosclerosis. There are broadly seven types of cardiovascular diseases e.g. Coronary Heart Disease; Peripheral Artery Disease; Rheumatic Heart Disease; Congenital Heart Disease; Stroke; Aortic Aneurysm; Deep Venous Thrombosis. Most of these cardiovascular diseases (CVD) lead to myocardial infarction or MI which results into heart failure (World Health Organization, 2018).

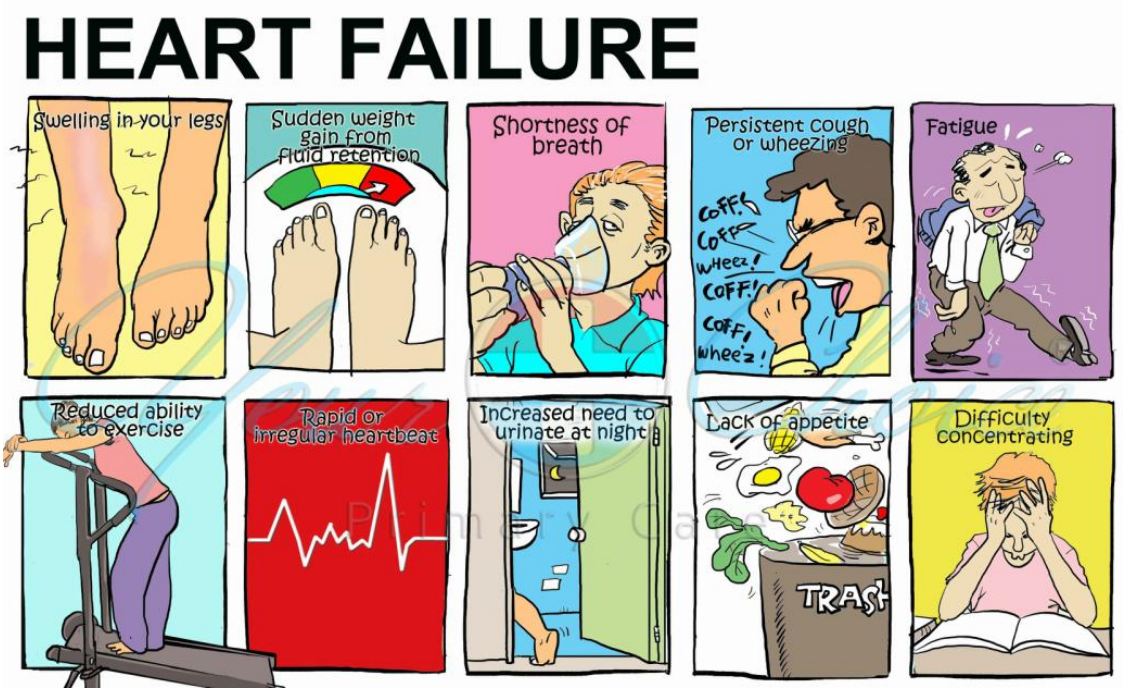

Figure 6.1.2. Cartoon showing signs of having a heart failure [www.wikihealth.com]

6.1.4. Global Burden of Cardiovascular Disease

According to the 2019 reports of American Heart Association (AHA), on the basis of NHANES 2013 to 2016 data, the prevalence of CVD in adults over 20 years of age is 48.0% overall (121.5 million in 2016) and it increases with advancing age in both the sexes. CVD prevalence excluding hypertension is 9.0% overall (24.3 million in 2016). In 2016, there were 2,744,248 registered resident deaths in the United States. 10 leading causes of CVD, accounted for 74.1% of all registered deaths. The 10 leading causes of death in 2016 were the same as in 2015; these include: 1) heart disease 2) cancer 3) unintentional injuries 4) chronic lower respiratory diseases 5) stroke 6) Alzheimer 7) DM 8) influenza and pneumonia 9) kidney disease and 10) suicide. In 2016, ≈17.6 million (95% CI, 17.3–18.1 million) deaths were attributed to CVD globally, which amounted to an increase of 14.5% (95% CI, 12.1%–17.1%) from 2006. The age-adjusted death rate per 100 000 population was 277.9 (95% CI, 272.1–284.6), which represents a decrease of 14.5% (95% CI, −16.2% to −12.5%) from 2006. An estimated 7.0 million Americans over 20 years of age have reported to have a stroke, and the overall stroke prevalence is an estimated 2.5%. Prevalence of current training in cardiopulmonary resuscitation was 18%, and prevalence of having cardiopulmonary resuscitation training at some point was 65% in a survey of 9022 people in the United States in 2015. The prevalence of cardiopulmonary resuscitation training was lower in Hispanic people, older people, and the lower-income group (Benjamin EJ et al, Circulation,2019).

Data from the BRFSS (Behavioral Risk Factor Surveillance System) 2016 survey indicated that 4.1% of respondents had been told that they had angina or CHD. From 2006 to 2016, the annual death rate because of CHD declined to 31.8%. CHD age-adjusted death rates per 100,000 were 132.3 for NH white males, 146.5 for NH black males, and 95.6 for Hispanic males; for NH white females, the rate was 67.9; for NH black females, it was 85.4; and for Hispanic females, it was 54.6 (unpublished National Heart, Lung, and Blood Institute tabulation). Compared to nonparticipants, participants in SNAP have twice the risk of CVD mortality, which reflects differences in socioeconomic, environmental, and behavioral sides. Similar trends follow for other CVDs too.

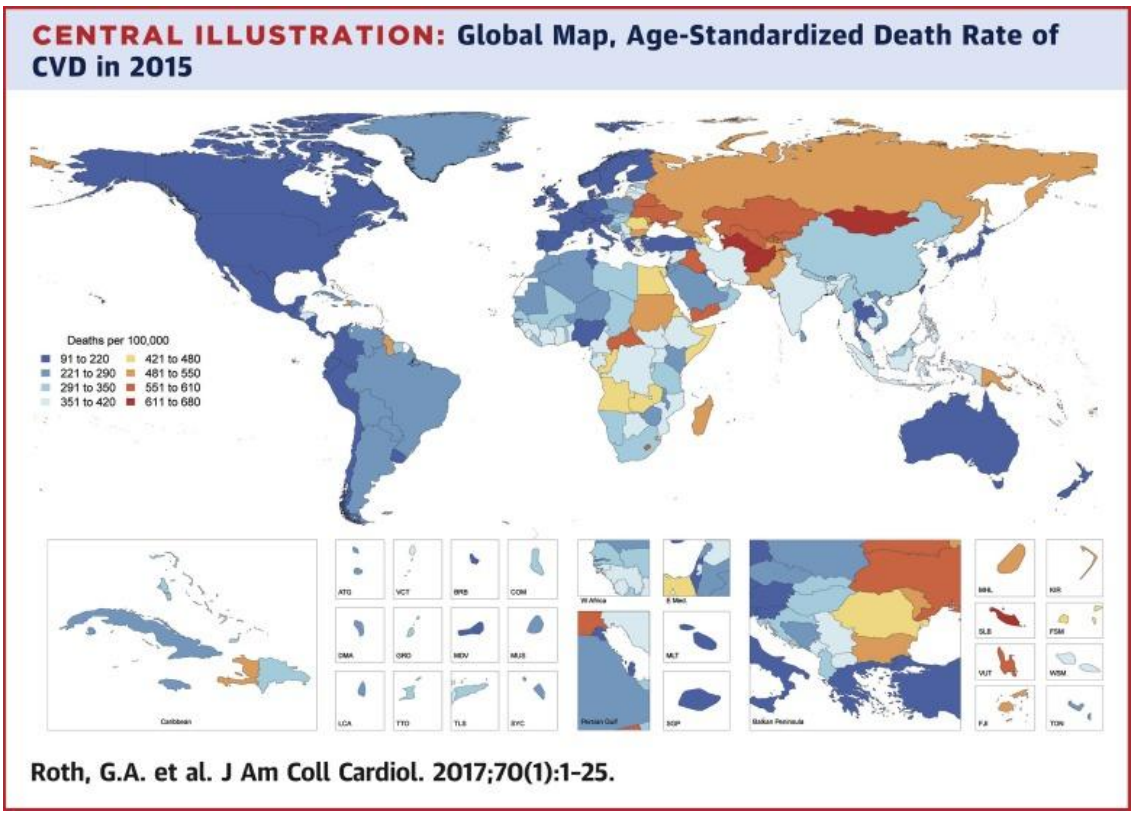

Figure 6.1.3. Global map of age standardized death rate of CVD in 2015 (Roth GA, Johnson C, JACC, 2017)

On the other hand, cardiovascular diseases are responsible for 28·1% (95% UI 26·5–29·1) of the total deaths and 14·1% (12·9–15·3) of the total disability-adjusted life-years in India, compared to 15·2% (13·7–16·2) and 6·9% (6·3–7·4), respectively, in 1990 (Roth GA et al, JACC,2017). In 2016, the difference was nine times between states in the DALY rate for ischemic heart disease, a 6 times difference for stroke, and a 4 times difference for rheumatic heart disease. An estimated, 23·8 million (95% UI 22·6–25·0) prevalent cases of ischemic heart disease were reported in India in 2016, and 6·5 million (6·3–6·8) prevalent cases of

stroke, a 2·3 times increase in both disorders from 1990. The age-normalized prevalence of both ischemic heart disease and stroke increased in all ETL state groups between the same years. Though, rheumatic heart disease is decreased between same time points; the increase for ischemic heart disease was highest in the low epidemiological transition level (ETL) state group. 53·4% (95% UI 52·6–54·6) of crude deaths were due to cardiovascular diseases in India in 2016 (Prabhakaran Dorairaj et al,The Lancet Global Health, 2018). "The leading risk factors in 2016 included dietary risks [56·4% (95% CI 48·5–63·9) of cardiovascular disease DALYs], high systolic blood pressure [54·6% (49·0–59·8)], air pollution [31·1% (29·0–33·4)], high total cholesterol [29·4% (24·3–34·8)], tobacco use [18·9% (16·6–21·3)], high fasting plasma glucose [16·7% (11·4–23·5)], and high body-mass index [14·7% (8·3–22·0)]" (Roth GA et al, JACC,2017).

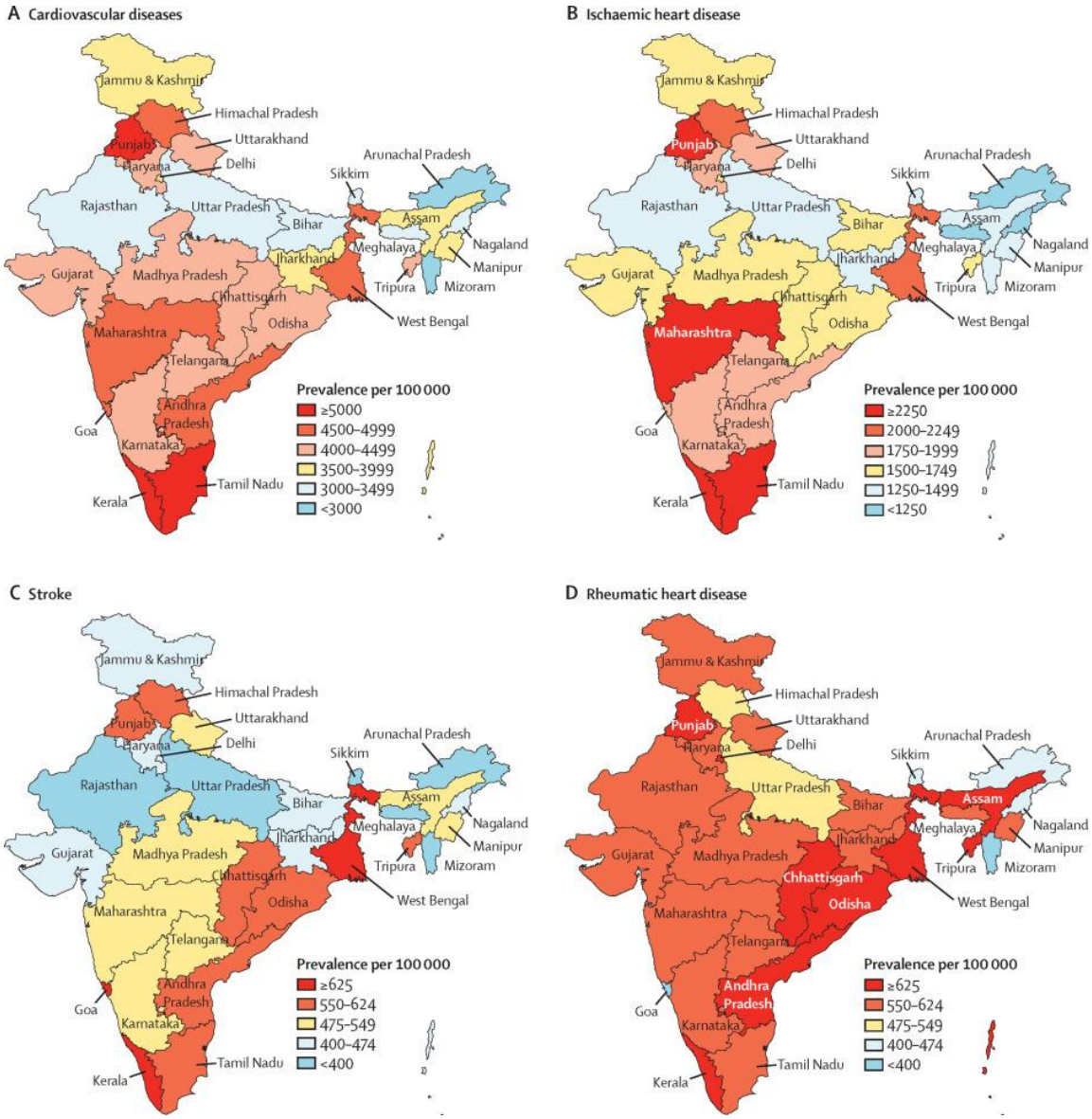

Figure 6.1.4. Prevalence of cardiovascular disease in India in 2017 (Prabhakaran Dorairaj et al,The Lancet Global Health, 2018)

6.1.5. Coronary Artery Disease: Types and clinical classification

Coronary artery disease (CAD) is the narrowing or total blockage of the coronary arteries, usually caused by atherosclerosis. Atherosclerosis is the accumulation of cholesterol and fatty substances (called plaques) on the inner side of the arteries. These plaques restrict blood flow to the heart muscle by clogging the artery. Without an adequate blood supply, the heart becomes hypoxic and it does not get the vital nutrients to work properly. This can cause chest pain or angina. If the blood circulation to a portion of the heart muscle is cut off entirely, or if the cardiac energy demands become much greater than its blood supply, a heart attack can occur.

Acute coronary syndrome (ACS) is a type of CAD also known as acute CAD. There are basically three types of acute CAD: a) ST-segment elevation myocardial infarction (STEMI) b) Non-ST- segment elevation myocardial infarction (NSTEMI) c) Unstable Angina (Thomas George, International Journal of Cardiology, 2003). Based on the severity of the symptoms of ACS as well as CAD, clinically MI can be grouped into four subcategories: a) Class I b) Class II c)Class III d)Class IV (El-Menyar Ayman et al, The American Journal of Emergency Medicine,2012).

- **Killip class I** includes individuals with no clinical signs of heart failure.
- **Killip class II** includes individuals with rales or crackles in the lungs, and elevated jugular venous pressure.
- **Killip class III** describes individuals with frank acute pulmonary edema.
- **Killip class IV** describes individuals in cardiogenic shock or hypotension (measured as systolic blood pressure lower than 90 mmHg), and evidence of peripheral vaso-constriction (Oliguria, cyanosis or sweating).

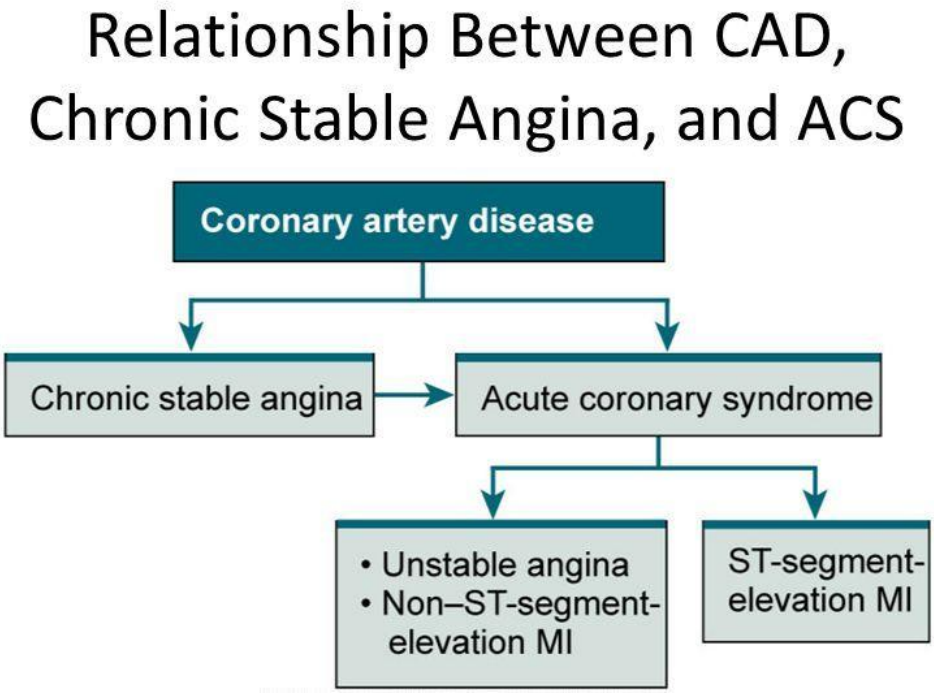

Fig.6.1.5. A. Types of Coronary Artery Disease

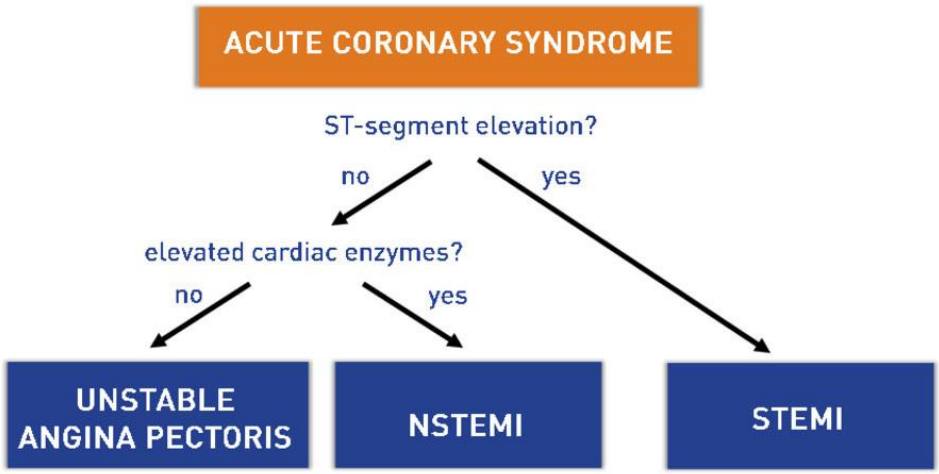

Figure 6.1.5. B. Basis of classification in acute coronary syndrome

6.1.6. Pathophysiology of Coronary Artery Disease

During the past ten years, our understanding of the pathophysiology of coronary artery disease (CAD) has evolved. As CAD patients generally present with either chronic or acute manifestations, the discussion will consider these two distinct modes in separate sections under this heading.

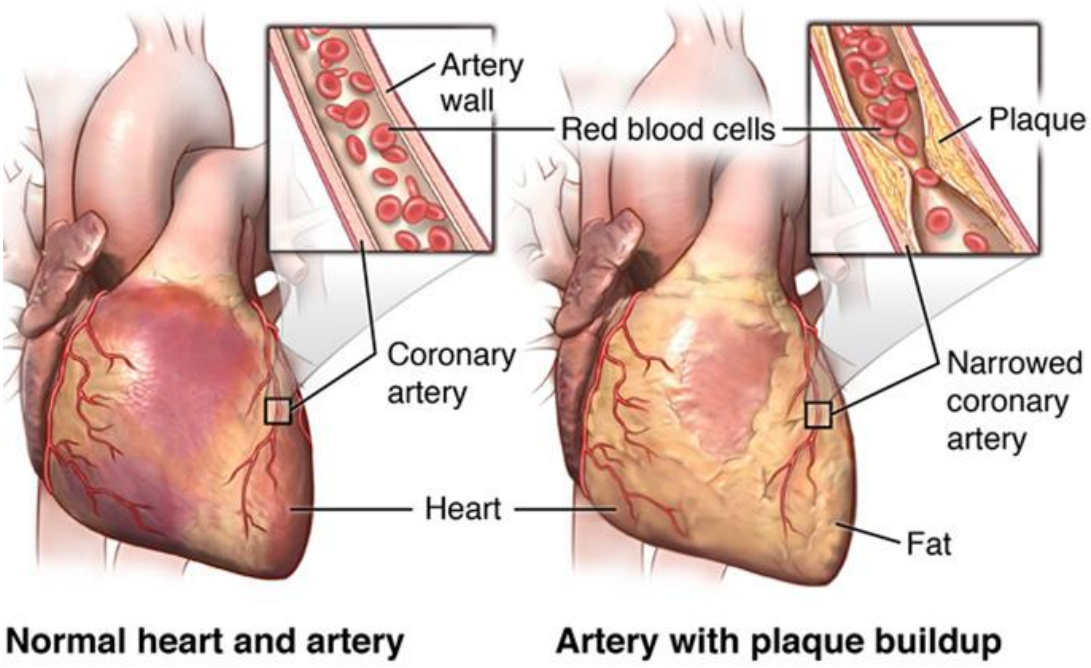

Figure 6.1.6. Differences between normal and diseased artery in human heart (Medicine Online, 2018)

6.1.6.1. Chronic CAD

6.1.6.1.1. Atherosclerotic Lesion Formation

It is currently well established that atherogenesis is a complex interaction of risk factors including cells of the artery wall and the blood and their molecular crosstalk. Inflammation as established plays a major role in all stages of atherosclerosis (Hansson GK et al, An. Rev. Path,2006). When the arterial endothelium encounters any of the risk factors e.g. dyslipidemia, vasoconstrictor hormones involved in hypertension, the products of glycoxidation associated with hyperglycemia, or pro-inflammatory cytokines derived from adipose tissue mass and inflammatory cells, augment the expression of cell adhesion molecules that promote the attachment of blood leukocytes to the inner surface of the arterial wall (Tousoulis D et al, Heart,2006). Transmigration of the adherent leukocytes depends on the expression of chemo-attractant cytokines regulated by signals associated with risk factors for atherosclerosis (Jones DP, Mediators Inflammation,2017). Once housed in the arterial intima, the leukocytes—mainly macrophages and T lymphocytes—communicate with endothelial and smooth muscle cells (SMCs). Major cross-talks exchanged among the cell types responsible for atherogenesis depend on mediators of inflammation such as prostanoids

and the leukotrienes (Riccioni G. et al, Curr. Drug Targets, 2010). As a result of the inflammatory condition undergoing in the early atheroma, SMCs migrate from the tunica media into the intima. These cells proliferate and help to make a rich and complex extracellular matrix. In harmony with endothelial cells and monocytes, they secrete matrix metalloproteinases (MMPs) in response to various oxidative, hemodynamic, inflammatory signals. MMPs, in equilibrium with their endogenous tissue inhibitors, modulate numerous functions of vascular cells, including activation, proliferation, migration, and cell death etc. Few constituents of the extracellular matrix (mainly proteoglycans) bind to lipoproteins, prolong their stay in the intima, and make them more vulnerable to oxidative modification and glycation (Vacek TP et al, Vascul. Health Risk. Manag. 2015). These products of lipoprotein modification, including oxidized phospholipids and advanced glycation end products, maintain and transmit the inflammatory response. As the lesion progresses, calcification may then occur through mechanisms similar to those in bone formation. In addition to proliferation, apoptosis commonly occurs in the atherosclerotic lesion. The death of lipid-laden macrophages can lead to extracellular deposition of tissue factor (Bourantas et al, BMJ Heart,2016). The extracellular lipid that builds up in the intima can join together and form the classic, lipid-rich "necrotic" core of the atherosclerotic plaque.

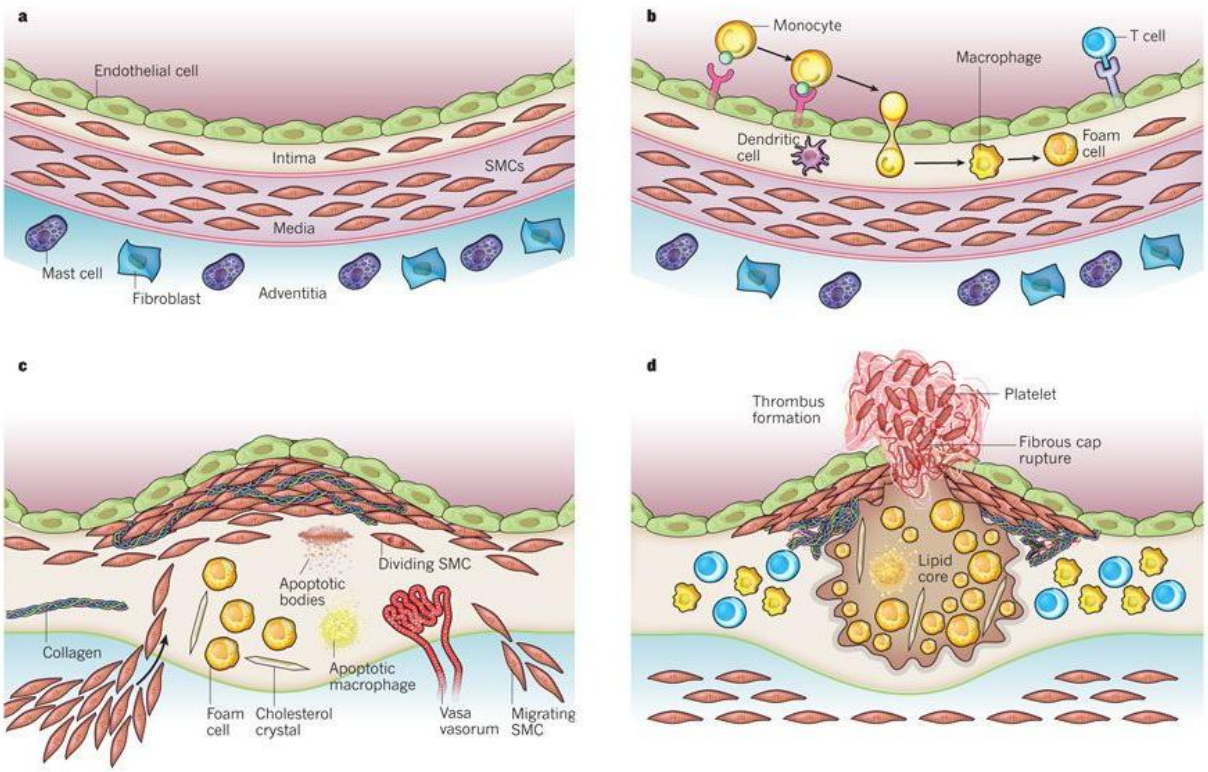

Figure 6.1.7. Overview of the process involving atherosclerotic lesion formation (Nature Medicine, 2011)

6.1.6.2. Acute CAD

In early 1980s, advanced imaging techniques and clinical examination as well as research on human atheromatous plaques led to the conclusion that physical disruption of the atherosclerotic plaque accounted for almost all acute coronary thromboses. Disrupted plaques aggravate thrombosis by several means (Insull Jr. Williams, The Am.J.Med., 2009). First, contact with collagen in the plaque's extracellular matrix can activate platelets. Second, TF produced by macrophages and SMCs activates the coagulation cascade. The disrupted plaque thus signifies a "solid-state" trigger to both thrombosis and coagulation; these pathways support each other, as thrombin generation amplifies the activation of platelets and other cells in the lesion. Conversion of fibrinogen to fibrin and release of von Willebrand factor (VWF) from activated platelets can offer the cross-linking molecular bridges between platelets that yield the dense, 3D network of platelets entrapped in fibrin of the "white" arterial thrombus (Sakakura K et al, Heart Lung Circ.2013).

These fluid-phase changes led to the idea of the "vulnerable patient," thus expanding our idea of the so-called "vulnerable plaque." In the context of acute CAD, the distal embolization of TF-rich debris discharging into the bloodstream from the core of the suddenly disrupted plaque may cause distal thrombosis in the microcirculation. Such distal embolization explains in part the "no-reflow" phenomenon that can complicate both natural and iatrogenic plaque disruption and prevent effective reperfusion of the distal microcirculation (Virmani Renu et al, ATVB,2005).

6.1.6.2.1. Pathophysiology of Vulnerable Plaque

Anatomicopathological studies recognized characteristics of the rupture-prone plaque, including a thin, fibrous cap and a large lipid core populated by numerous inflammatory cells and relatively lacking in SMCs. Recent results, however, point to the multiplicity of such "high-risk" plaques and the extensive nature of inflammation in patients prone to develop acute CAD. Both autopsy and intravascular ultrasound studies have highlighted the disperse nature of intimal disease in patients with acute CAD. Even sections of the coronary arterial tree that appear perfectly normal by angiographic criteria often have an extensive burden of atherosclerosis. In particular, plaques with extensive outward remodeling can have thin, fibrous caps and large lipid pools without invading on the lumen (Stefanadis C et al, JAHA,2017). Such "hidden" lesions not only avoid angiographic detection, but also do not

generate any symptoms until they set off thrombosis, as they do not produce ischemia. Moreover, the use of markers of inflammation such as myeloperoxidase points to a trans-myocardial step-up in levels of this inflammatory marker, even in the effluent of regions not perfused by the artery responsible. Thus, clinical presentations often involve focal lesions, arterial inflammation directing the underlying biology that influences to the local complications appears diffuse (Fuster Valentin,JACC,2015).

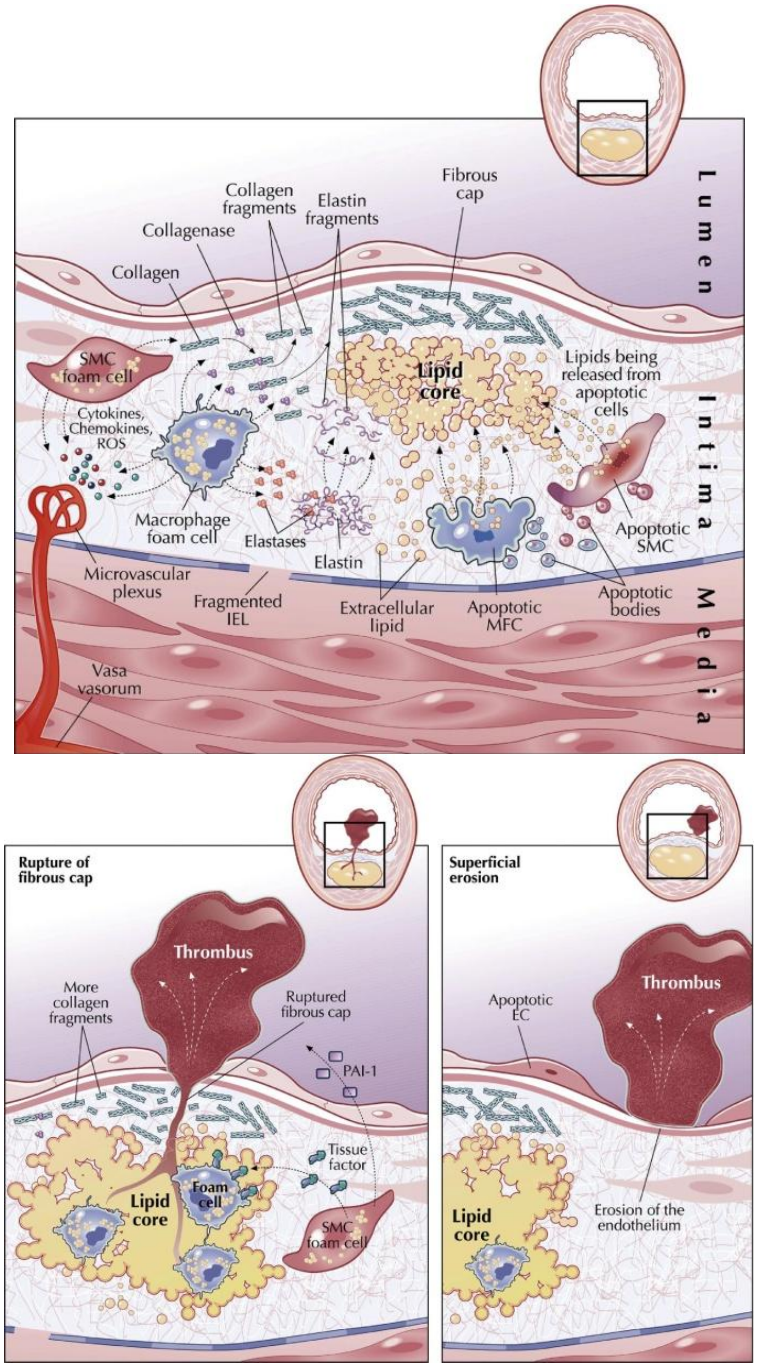

Figure 6.1.8. Mechanism of vulnerable plaque development and rupture (Peter Libby, AJC, 2006)

These recent findings defy our traditional view of coronary atherosclerosis as a localized disease simply corrected by bypass surgery or percutaneous revascularization. Newer imaging technologies such as optical coherence tomography (OCT), thermography, Raman/near-infrared spectroscopy, electron beam computed tomography (ECT), magnetic resonance imaging (MRI), and multislice spiral computed tomography should provide further information related to the risk of progression of cardiovascular events with regard to the atherosclerotic burden and its activity (Bourantas CV et al, BMJ Heart,2016). In this regard, it is noteworthy, that these techniques though thought powerful, can't predict the risk and chances of a possible acute cardiac event. Such novel imaging strategies will likely prove most useful but they are not cost effective. So, to identify higher-risk individuals among asymptomatic populations, we need new marker which can help in prognosis and diagnosis of an acute cardiovascular event. Not only that, we need to find new proteins which can indicate the event of plaque progression with a statistically successful rate.

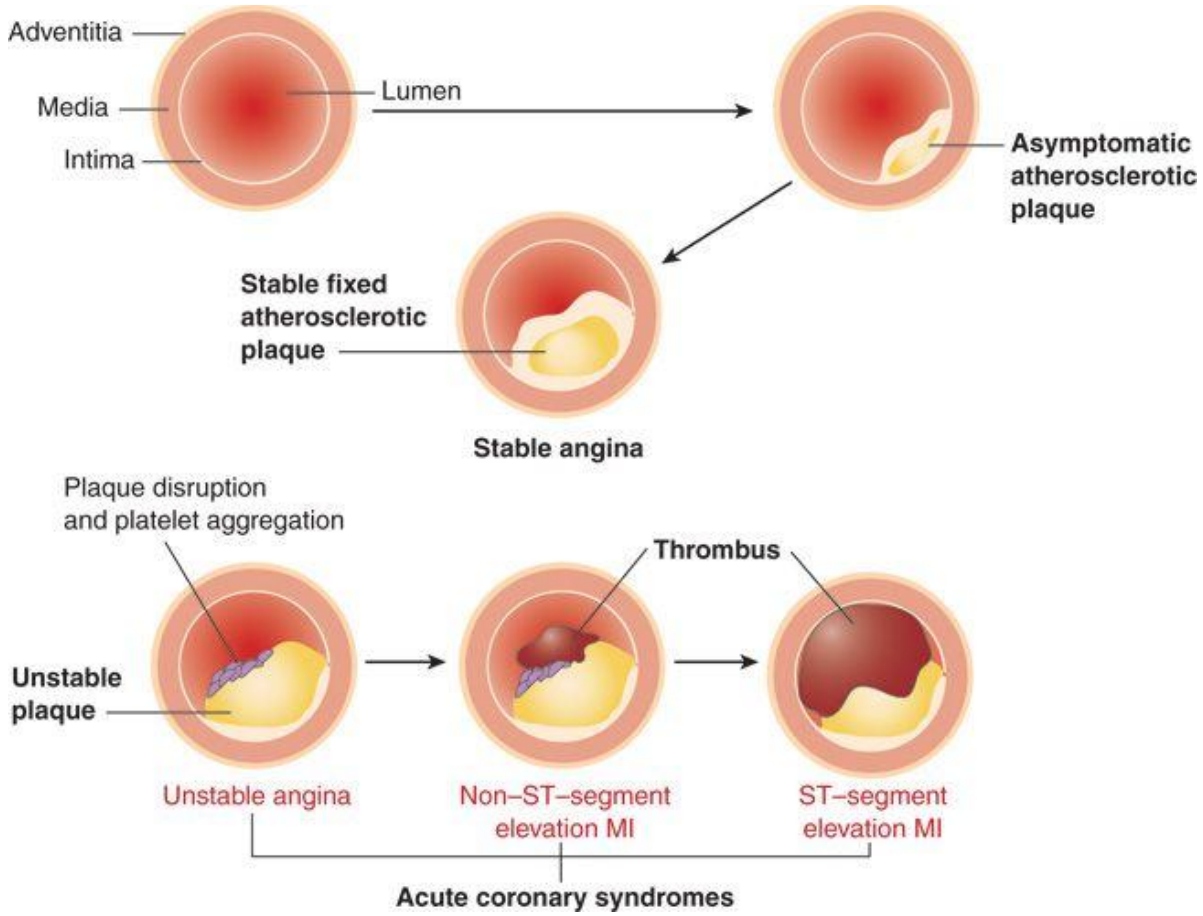

Figure 6.1.9. Physiology of plaques in different types of ACS and condition of vulnerable plaque (Circulation, 2011)

6.1.7. Blood and circulatory system

Technically, blood is a transport liquid pumped by the heart to all sections of the body, after which it is returned to the heart to repeat the process. Blood is a tissue as well as a fluid. It is a tissue because it is a collection of similar specialized cells that serve specific functions. These cells are suspended in plasma. Blood is comprised mainly of two types of cells; a) Erythrocytes or red blood cells (RBCs) b) Leucocytes or white blood cells (WBCs). Except these two types of cells, there is another special type of cells present in blood. These cells are smaller than RBCs and WBCs, known as platelets. Platelets play very important part in coagulation and thrombosis. A special type of cells among WBCs is monocytes. Monocytes differentiate into macrophage in response to different inflammatory stimuli. In the later sections, we will mainly discuss about these two cell types.

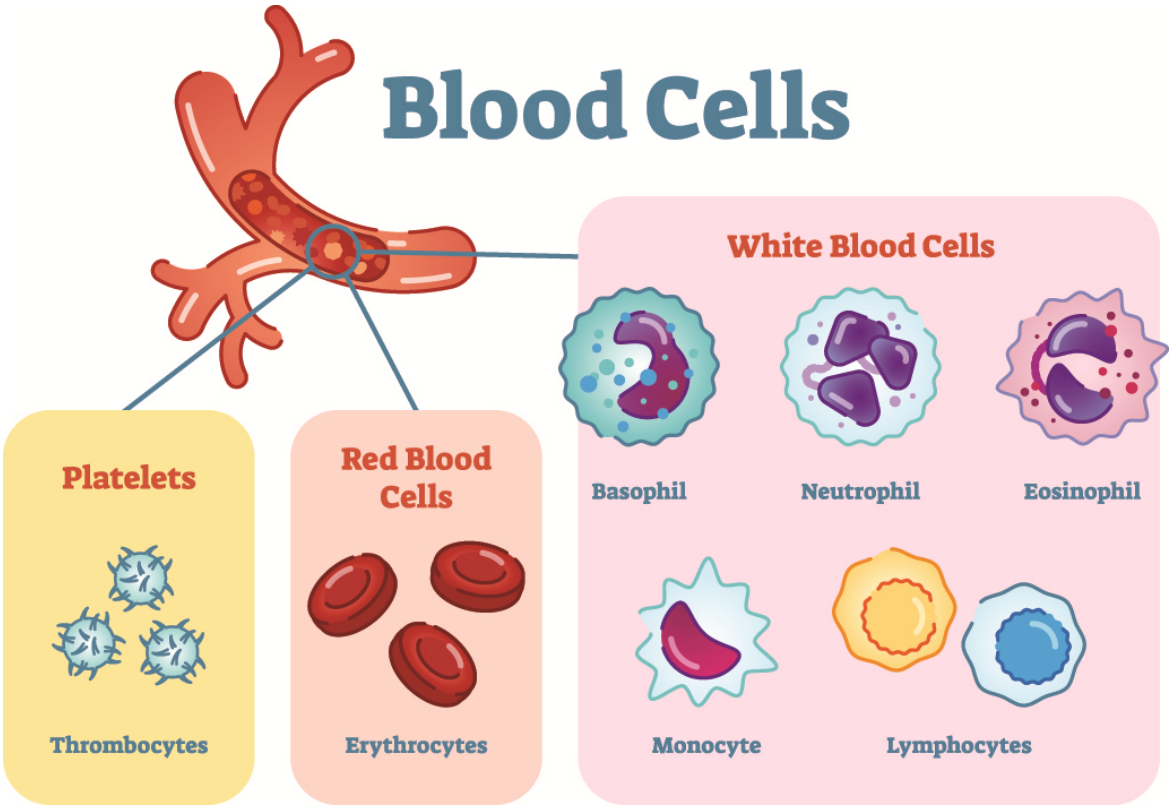

Figure 6.1.10. Diagrammatic representation showing different types of blood cells

6.1.8. Platelets and Atherosclerosis

Platelets are blood cells constantly produced from megakaryocytes in the bone marrow. These cells are involved not only in haemostasis and arterial thrombosis, but also in otherpatho-physiological processes. Signalling processes of platelet populations implicated in

thrombus formation is well understood. Genetic approaches have offered information on multiple genes associated with normal haemostasis, such as those encoding receptors and signalling or secretory proteins that decide platelet count and/or responsiveness. As highly responsive and secretory cells, platelets can modify the environment through the release of different growth factors, chemokines, coagulant factors, RNA species, and extracellular vesicles. On the other hand, platelets can also adapt to their environment (Patzelt J et al, Front. In Phys. 2015). In disease states, platelets can be primed to reach a pre-activated condition. At inflamed vessel wall, platelets interact with leukocytes, which is associated with thrombo-inflammation.

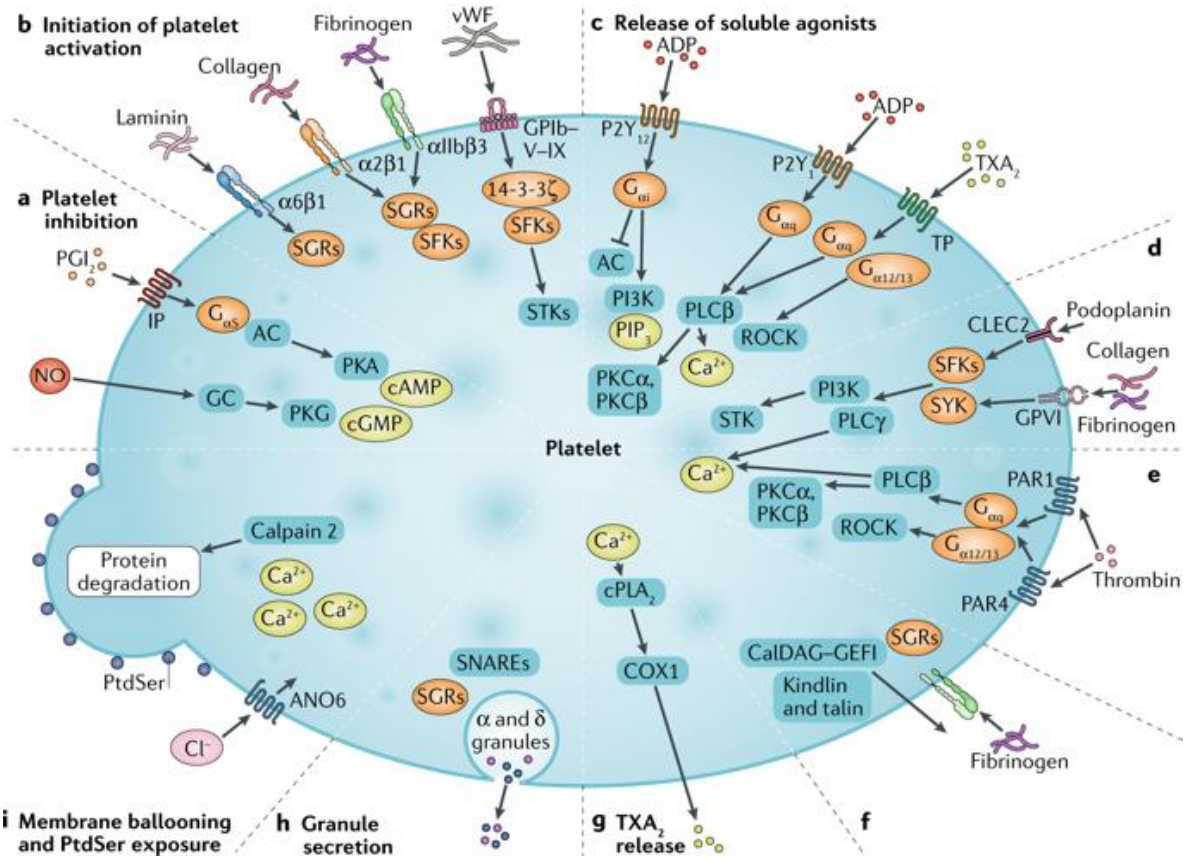

Figure 6.1.11. A cartoon of platelet showing all the functions with respect to specific stimuli (van der Meijden, Paola, Nat. Rev. Cardio. 2019)

Atherosclerosis is the principal reason for nearly all causes of coronary artery disease and peripheral arterial disease as well as many cases of stroke. Atherosclerosis is a systemic inflammatory process distinguished by the accumulation of lipids and macrophages within the intima of large arteries. The deposition of these materials and the successive thickening of the wall often considerably compromise the residual lumen leading to ischemic events distal to the arterial stenosis. However, these initial lesions may also advance into vulnerable

plaques prone to rupture or erosion. Plaque disruption begins both platelet adhesion and aggregation on the exposed vascular surface and the activation of the coagulation cascade leading to atherothrombosis. Yet, platelets have also been known to be transporters of regulatory molecules, to regulate the inflammatory response and mediate atherosclerosis progression (van der Meijden, Paola, Nat. Rev. Cardio. 2019).

Atherosclerotic lesions are the key event in the progression of atherosclerosis. It occurs as the consequence of a complex interplay between circulating factors and various cell types in the vessel wall, triggered by chronic exposure to several systemic stimuli. An elevated level of plasma lipids, particularly low-density lipoproteins (LDL), is a key reason of vascular damage. Apart from epidemiological confirmation for the pro-atherogenic role of lipoproteins, mechanistic studies propose that they play a role in related features for initiation and progression of lesions, such as endothelial dysfunction, intimal disorganization and thickening. In advanced atheromatous plaques, high extracellular and intracellular lipid deposits are associated with a high risk of vulnerability to rupture, causing thrombosis and its clinical problems (Yuqing Huo, Trends in cardio. Med.2004).

Platelets are very much involved in this atherosclerotic lesion formation. They do not adhere to the intact endothelium. However, inflammatory events in the early stages of the process lead to endothelial activation which, in turn, may provoke platelet attachment. Hence, endothelial disruption is not an absolute requirement to allow platelet activation and attachment to the arterial wall. Even though the mechanisms that lead to platelet–endothelial interaction remain to be fully illustrated, it has been hypothesized that platelet activation may be accredited to: (a) decrease in the mechanisms concerned with maintaining endothelial antithrombotic properties; (b) reactive oxygen species (ROS) produced by atherosclerotic risk factors; and (c) an enhancement in pro-thrombotic and pro-inflammatory mediators in the circulation. Activated endothelium lets platelets to roll on even under high shear rates. Platelet rolling, mainly mediated by P-selectin, is trailed by firm adhesion mediated by integrin binding. Therefore, platelet P-selectin, expressed due to activation, seems to be necessary to permit platelet–endothelium adhesion. Indeed, the absence of P-selectin has been proved to protect against the development of atherosclerotic lesions in both low density lipoprotein (LDL)-receptor and apoE-/- knock-out mice, particularly in the early stages of lesion development. Platelet attachment to intact but activated endothelium may also be started by interaction of GPIbα and αIIbβ3 (GPIIb/IIIa) with endothelial P-selectin and Von

Willebrand factor (VWF). Indeed, there is an augmented synthesis of VWF in atherogenesis, with practical consequences for platelet deposition on the vessel wall. Therefore, obstruction of platelet adhesion using either GPIbα or αIIbβ3 antagonists has been reported to decrease platelet adhesion, leukocyte recruitment and lesion size (Davi and Patrono, NEJM, 2007). Activated platelets, other than selectin and integrin expression, release several mediators stored within their granules that result in cell adhesion, survival and proliferation, coagulation and proteolysis, and synthesize chemokines and pro-inflammatory cytokines all of which speed up and enhance the inflammatory process promoting plaque development.

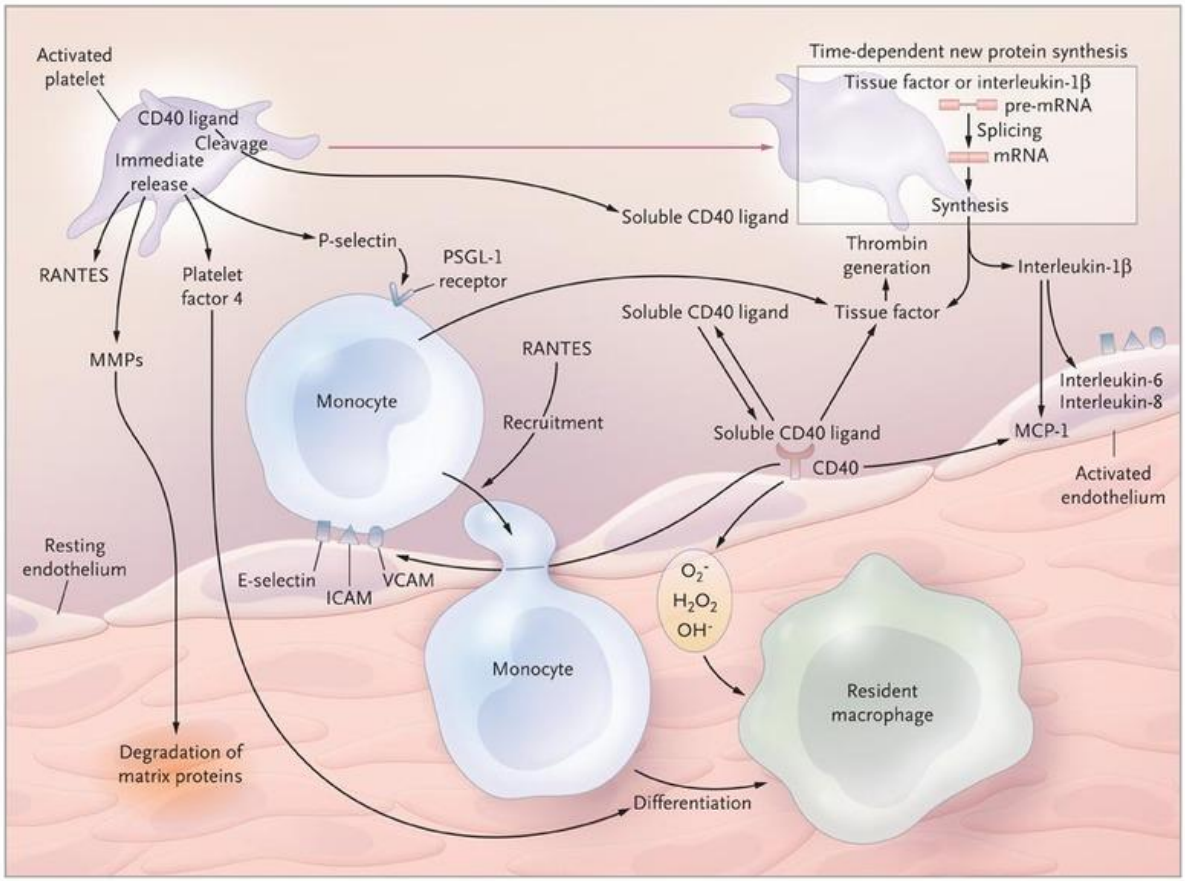

Figure 6.1.12. Platelet activation and initiation of atherosclerosis (Davi and Patrono, NEJM, 2007)

CD40 ligand secreted from platelets induces inflammatory responses in the endothelium. This ligand is a trimeric transmembrane protein in the tumor necrosis factor (TNF) family. CD40 ligand is stored in the cytoplasm of resting platelets and rapidly emerges on the surface after platelet activation. On the platelet membrane, it undergoes cleavage over to generate a functional soluble fragment. Platelet derived CD40 ligand can stimulate endothelial cells to produce reactive oxygen species (ROS), adhesion proteins, chemokines, and tissue factor, all

of which are parts of an inflammatory response. Blockade of the CD40–CD40 ligand signalling pathway strikingly inhibits the formation of atherosclerotic plaque and arterial lipid deposition in LDL-receptor $^{-/-}$ mice. Furthermore, several cardiovascular risk factors, including smoking and type 2 diabetes mellitus, are linked with platelet activation and increased release of the CD40 ligand. The amalgamation of hyperinsulinemia and hyperglycemia up-regulates the release of platelet CD40 ligand and monocyte-derived tissue factor. Contrary to the CD40 ligand, which is stored in the platelet cytoplasm, interleukin-1β is synthesized upon platelet activation. The amount of Interleukin-1β that activated platelets synthesize is enough to induce endothelial cells to express genes that mediate the adhesion of leukocytes. Interleukin-1β is an important factor for the platelet-induced activation of endothelial cells, causing them to the release of chemokines and up-regulate molecules that promote adhesion of neutrophils and monocytes to the endothelium. The stimulation of platelets by strong agonists can cause the shedding of small membrane vesicles from the platelet surface. The expression of P-selectin by activated endothelial cells or platelets can set off the recruitment of microparticles bearing the P-selectin glycoprotein ligand 1 (PSGL1) and tissue factor at sites of vascular injury. These microparticles have also been identified to be responsible for the upregulation of COX-2–dependent prostanoid formation in monocytes and endothelial cells, linking the transcellular metabolism of arachidonic acid. Activated platelets also release chemokines that can promote their differentiation into macrophages. Platelet factor 4 (PF4) is released upon platelet activation, induces the expression of E-selectin by endothelial cells. Activated platelets also release matrix metalloproteinases (MMPs) 2 and 9. Platelets have a rich supply of stimulators and inhibitors of angiogenesis and that’s why they play a central role in that process.

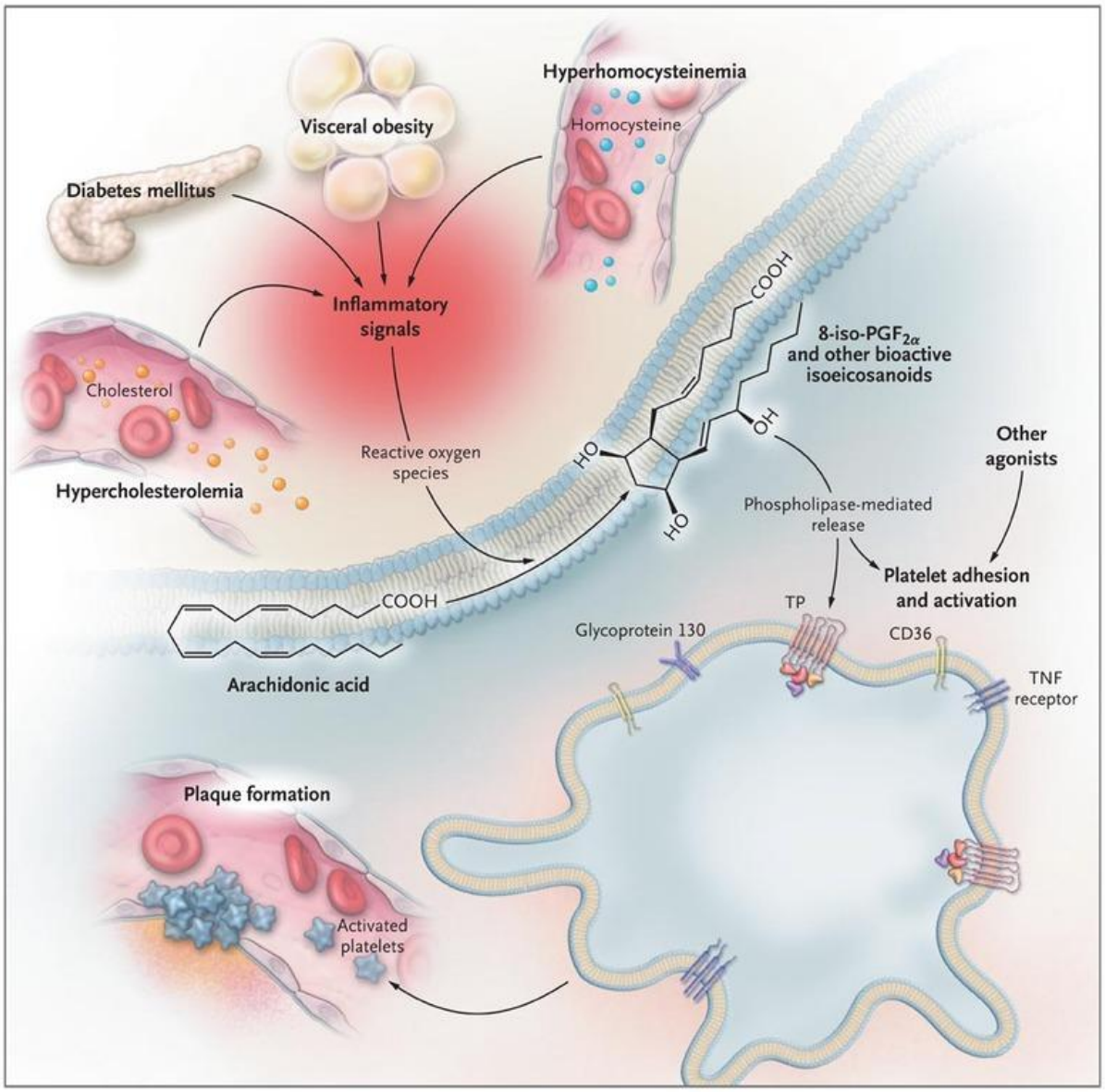

Figure 6.1.13. An overview of the relation between platelet activation and progression of atherosclerosis (Davi and Patrono, NEJM, 2007).

6.1.9. Inflammation in atherosclerosis: role of macrophages and foam cells

Atherosclerosis is the consequence of a maladaptive inflammatory response set in motion by the intramural retention of cholesterol-rich, apolipoprotein B-containing lipoproteins in vulnerable areas of the arterial vasculature. Lipoproteins sequestered in the arterial wall are prone to various modifications (such as oxidation, enzymatic and non-enzymatic cleavage and aggregation), which render these particles pro-inflammatory and activates the overlying endothelium. The resulting immune response is mediated by the recruitment of monocyte-derived cells into the subendothelial space, where they differentiate into mononuclear phagocytes that swallow the accumulated normal and modified lipoproteins, transforming

them into the cholesterol-laden "foam cells". Foam cells, typically classified as a type of macrophage, persist in plaques, inducing disease progression. While macrophage clearance of lipoproteins is likely to be helpful at the outset of this immune response, there is little negative feedback of uptake and thus these cells become grossly inflamed with lipids. The resultant dysregulation of lipid metabolism alters the macrophage phenotype and compromises critical immune functions. Notably, macrophages that accumulate in atherosclerotic plaques appear to have a diminished capacity to migrate, which contributes to failure to resolve inflammation and to progression of these lesions to more advanced, complex plaques in which other immune cell subsets and vascular smooth muscle cells participate in the inflammatory process (Nording HM, Front. Immuno.2015). In these advanced plaques, macrophages continue to be major contributors to the inflammatory response through their secretion of pro-inflammatory mediators (chemokines, cytokines and reactive oxygen and nitrogen species) and MMPs, through their eventual death by necrosis or apoptosis. Dying macrophages release their lipid contents and tissue factor, leading to the formation of a pro-thrombotic necrotic core, a key component of unstable plaques that causes their rupture and the ensuing intravascular blood clot that underlies myocardial infarction and stroke. Though many cell types contribute to the formation of atherosclerotic plaques, macrophages and foam cells play central role in the whole process.

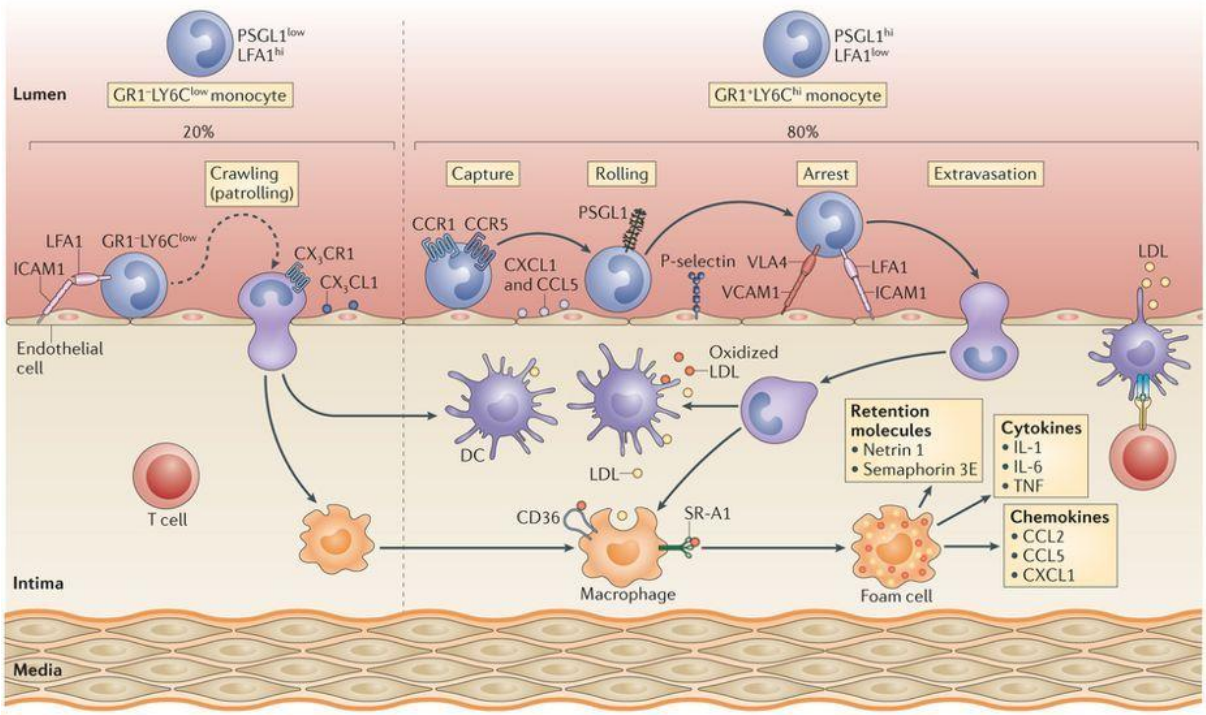

Figure 6.1.14. Mechanisms regulating monocyte recruitment and accumulation in plaque (Kathryn Moore et al, Nat. Rev. Imm., 2013)

The activation of the endothelium by platelets promotes the recruitment of circulating monocytes. These monocytes are mobilized to inflammatory sites like atherosclerotic plaques. Apparently, the steps regulating monocyte entry into the arterial intima are equivalent independent of the source of the cells and depend on the arrest of circulating monocytes by the leukocyte adhesion cascade. The capture and rolling phases of the monocytes depend on the immobilization of CCL5 and CXCL1 and on P-selectin. Vascular cell adhesion molecule 1 (VCAM1) and intercellular adhesion molecule 1 (ICAM1), which bind to the integrins VLA4 and lymphocyte function-associated antigen 1 (LFA1), respectively, are very important for the strong adhesion of monocytes to the luminal surface of the endothelium, with reasonably more LFA1 expressed by $LY6C^{low}$monocytes, which may trigger their greater tendency to adhere to, but not enter, the vasculature (Ramji DP et al, Cytokine Growth Factor Rev,2015).

Transmigration of monocytes across the endothelium is mediated by chemokines secreted by endothelial cells, intimal macrophages and smooth muscle cells. Although several chemokines have been implicated in atherosclerosis, the three major pairs involved in monocytes transmigration are CCR2–CCL2, CX3CR1–CX3CRL1 and CCR5-CCL510. It should also be noted that CCR2 and CX3CR1, over and above their effects on transmigration, have indirect roles in manipulating the number of monocytes that enter plaques. In particular CCR2 is also mandatory for the extravasation of $LY6C^{hi}$ cells from the bone marrow and CX3CR1 promotes their survival by inhibiting apoptosis. Overall, employment of circulating monocytes into plaques requires the integration of at least 3 discrete processes, their capture, rolling and transmigration, with each step synchronized with multiple, and sometimes overlapping, molecular factors (Hartmann P et al, Cell Mol Life Sci,2015).

On the other hand, scavenger receptors, which are a type of PRR expressed by macrophages, have an important role in atherosclerosis and were originally described by their skill to recognize and process modified LDL. Enumerable number of scavenger receptor family members including scavenger receptor A (SRA), MARCO, CD36, scavenger receptor class B member 1 (SRB1), lectin-type oxidized low-density lipoprotein receptor 1 (LOX1), scavenger receptor class E member 1 (SREC1) and scavenger receptor for phosphatidyl-serine and oxidized low-density lipoprotein (SRPSOX; also known as CXCL16) — can bind oxidized LDL and promote foam cell formation. These receptors internalize the lipoproteins, and transform them to free cholesterol and fatty acids. Free cholesterol in the endolysosomal compartment is then trafficked to the endoplasmic reticulum (ER), where it goes through re-

esterification by acyl-CoA: cholesterol ester transferase (ACAT) to cholesteryl fatty acid esters that provide the "foam" of foam cells. Along with this defective cholesterol esterification pathway can lead to defective cholesterol trafficking which may lead to atherosclerosis.

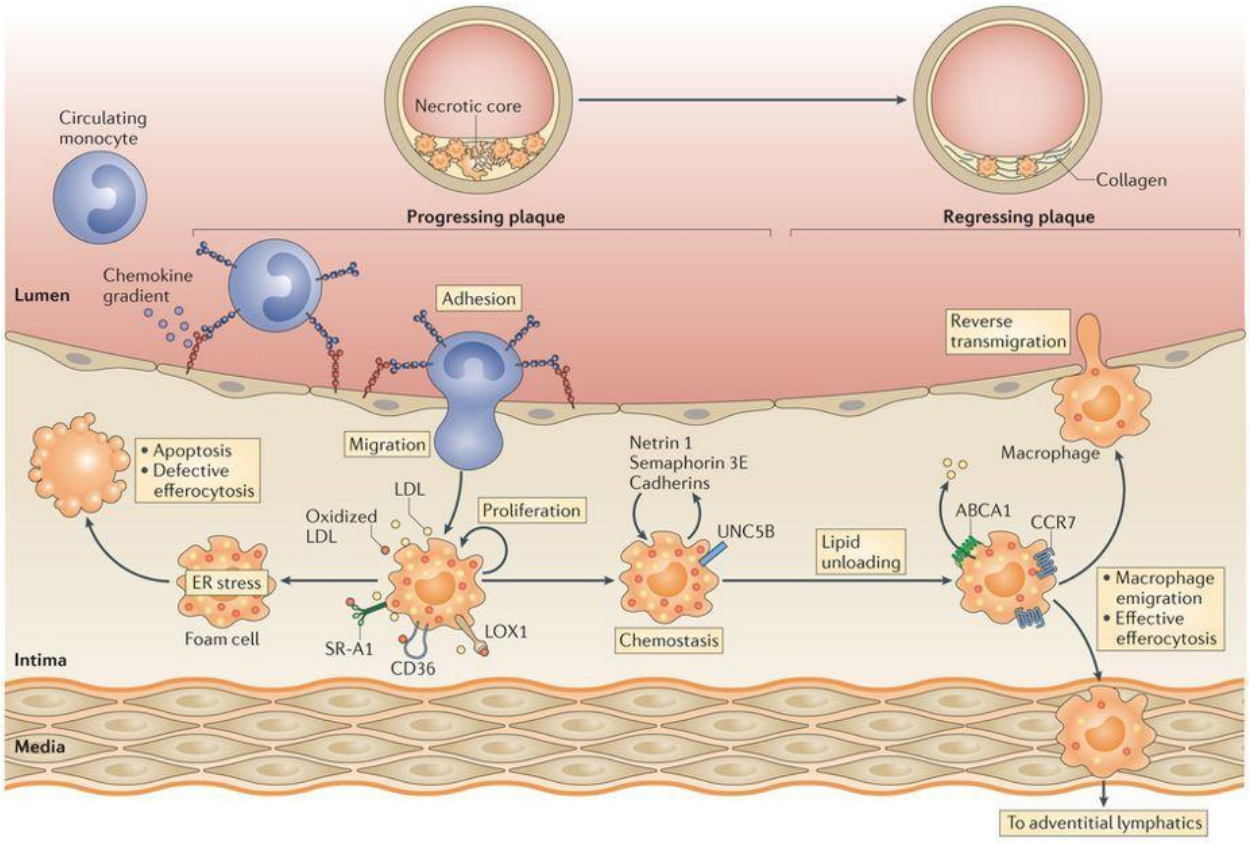

Figure 6.1.15. Pathways regulating macrophage retention, emigration and cholesterol efflux in plaques (Kathryn Moore et al, Nat. Rev. Imm., 2013)

Cells try to respond to excessive lipid accumulation by pathways that promote the removal of cholesterol and other lipids from them. In foam cells several macrophage transporters help this efflux of lipids — including ATP-binding cassette transporter A family member 1 (ABCA1), ABCG1 and SRB1— although passive diffusion from the plasma membrane also takes place. ABCA1 endorses cholesterol efflux to lipid-poor APOA1, which is the building block of HDL, whereas ABCG1 helps to efflux in mature HDL particles. The genes encoding ABCA1 and ABCG1 are transcriptionally upregulated in response to increased cellular cholesterol levels by liver X receptors (LXRs), which are ligand-activated nuclear receptors that act as sterol sensors. Autophagy also has a critical role in macrophage cholesterol efflux: lipid droplets in macrophages and other cell types are besieged to and hydrolyzed by the autophagy machinery in a process known as lipophagy. Fusion of the autophagosome with

the lysosome breaks cholesteryl esters and makes free and modified cholesterol accessible for efflux through an ABCA1-dependent pathway (Marchio P et al, Oxid Med Cell Long,2019). Furthermore, autophagy regulates innate and adaptive immune responses; including inflammasome activation, antigen presentation, and T cell activation. Thus, pathways that stimulate the efflux of cholesterol from the macrophage provide dual athero-protective functions by promoting lipid homeostasis and protecting from inflammation. Thus, macrophages and foam cells by their own inflammatory mechanisms affect the process of atherosclerosis well enough to claim their role as key players of the whole process. As most of the responsible proteins for atherosclerosis are secretory or soluble in nature, blood plasma is very important for prognosis of cardiovascular diseases.

6.1.10. Plasma: circulatory proteins and importance in prognosis of Coronary Artery Disease

Plasma is the liquid matrix of blood in which all the blood cells reside. Because of the presence of plasma blood appears as liquid. Plasma is colorless and it transports numerous acute phase secretory proteins which are important in pathophysiology of different diseases including coronary artery disease.

Acute-phase proteins (APPs) are a class of proteins whose plasma levels increase (positive acute phase proteins) or decrease (negative acute phase proteins) in response to inflammation. In response to injury, local inflammatory cells (neutrophils and macrophages) secrete numerous cytokines into the bloodstream, most important of which are the interleukins IL-1, IL-6 and IL-8, and TNF-α. The liver also produces a large number of APPs. APPs have a wide range of actions that augment host defense: they can directly counteract inflammatory agents, help to minimize the degree of local tissue damage, as well as contribute in tissue repair and regeneration. There is a huge increase in the plasma concentration of many complement cascade components, the activation of which results in the local buildup of neutrophils, macrophages and plasma proteins. These take part in the killing of infectious agents, the clearance of foreign and host cellular debris, and the repair of damaged tissue. Coagulation components, such as fibrinogen, play a necessary role in endorsing wound healing. The increased plasma concentration of some metal-binding proteins helps prevent iron loss during injury. The major APPs in mammals include serum amyloid A (Brown et al, Current Cardiology reports,2008) and C-reactive protein (CRP). During inflammation CRP levels can increase up to1000-fold from approximately 1 mg/L, depending on the disease and

its severity. CRP was originally named for its capability to bind the C-polysaccharide of Pneumococcus and has shown to have a number of calcium dependent binding specificities and biological activities associated with nonspecific host defense. Serum amyloid A is the collective name given to a family of polymorphic proteins transcribed by multiple genes in a number of mammalian species. Functionally, SAAs are small apolipoproteins that correlate quickly during the acute phase response with the third fraction of high-density lipoprotein (HDL3), on which they become the major apolipoproteins. SAA improves the binding of HDL3 to macrophages during inflammation, associated with a decrease in the binding capacity of HDL3 to hepatocytes. It proposes that SAA may remodel HDL3 and act as a signal to redirect it from hepatocytes to macrophages, which can then engulf cholesterol and lipid debris at sites of necrosis. Other supposed defensive roles for SAA are the inhibition of thrombin-induced platelet activation, as well as inhibition of the oxidative burst in neutrophils, which would help prevent oxidative tissue destruction. Other important APPs are H-FABP, Fibulin, NT-ProBNP, alpha-1-antitrypsin etc. As, APPs help in prognosis of cardiovascular diseases, recent researchers are still identifying new APPs by advanced techniques. The leading technique used to identify new candidate APPs is proteomics (Brown TM et al, Curr. Cardiol. Rep.2008).

6.1.11. Mass Spectrometry and Plasma Proteomics

Mass spectrometry is a valuable tool to measure the mass-to-charge ratio (*m/z*) of one or more molecules present in a sample. These measurements can often be used to calculate the accurate molecular weight of the sample components as well. Mainly, mass spectrometers are used to identify unknown compounds by molecular weight determination, to measure known compounds, and to establish structure and chemical properties of molecules.

Every mass spectrometer consists of at least these three main parts:

- Ionization Source
- Mass Analyzer
- Ion Detection System

6.1.11.1. The Ionization Source

Molecules are transformed to gas-phase ions so that they can be moved and manipulated by external electric and magnetic fields. The most commonly used technique is called

nanoelectrospray ionization. This method generates positively or negatively charged ions, based on the experimental requirements. Nanoelectrospray ionization is coupled to the outlet of a small-scale chromatography column directly to the inlet of a mass spectrometer. The flow from the column is passed from end to end through a needle that is 10-15 um at its tip.

6.1.11.2. The Mass Analyzer

After ionization, the ions are separated according to mass-to-charge (*m/z*) ratios. There are many mass analyzers currently on hand, each of which has swapped relating to speed of operation, resolution of separation, and other operational requirements. The mass analyzer often works in accordance with the ion detection system. Most commonly used mass analyzers are the Orbitrap and triple-quadrupole mass analyzers.

The Orbitrap is a high resolution mass analyzer with high mass accuracy (+/- 5 part-per-million m/z). In practice, the Orbitrap analyzer is the second generation of a hybrid mass spectrometer whose first generation is mostly a linear ion trap. Ions are injected into the Orbitrap tangentially and form oscillating rings around the central electrode, and get trapped in an electrostatic field. The frequency of axial oscillation can be linked by Fourier transform to the mass-to-charge ratio (m/z) of the ion. The Proteomics Platform exploits 5 Orbitrap mass spectrometers: three LTQ-Orbitraps, one LTQ-Orbitrap XL, and one LTQ-Orbitrap Velos.

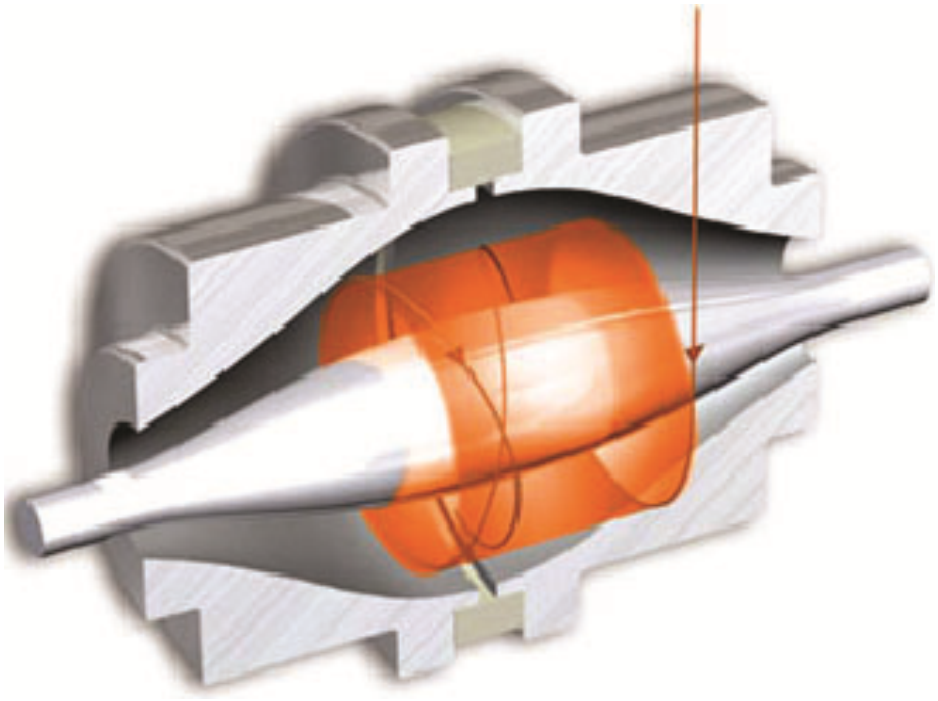

Figure 6.1.16. Diagram of orbitrap mass analyzer (after Broad Institute)

As in a linear ion trap, a triple quadrupole mass spectrometer exploits RF fields to manipulate ions. In this system, ions form a continuous beam rather than a trap. As the name entails, there are three quadrupoles. The first (Q1) and the third (Q3) quadrupoles are very much alike as they serve to recognize and sort out different masses while the second quadrupole (q) functions as a collision cell. In the collision cell the masses will undergo collision-induced dissociation (CID) which fragments the peptide into smaller ions. A triple quadrupole mass spectrometer lets the user to observe one or more "precursor" masses in Q1 as well as the fragment ions related to each precursor mass in Q3. The precursor mass is the mass of the peptide, typically in the +2 or +3 charge state, before it undergoes CID. By checking for both the precursor mass of a particular peptide and one or more fragment ions of the same peptide, it is possible to decide the presence of the peptide, even in a complex solution. The triple quadrupole is the type of instrument used for multiple-reaction monitoring (MRM) quantification assays.

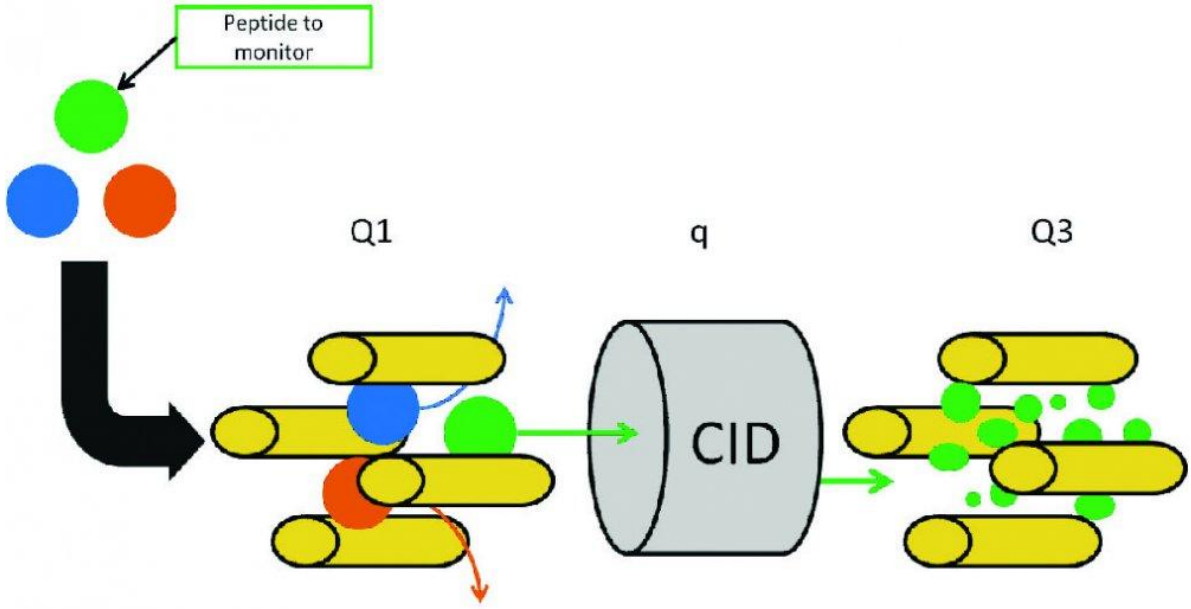

Figure 6.1.17. Diagram of triple quadrupole (after Broad Institute)

6.1.11.3. Ion Detection System

The separated ions are then quantitated and sent to a data system where the *m/z* ratios are stocked up together along with their relative abundance. A mass spectrum is simply the *m/z* ratios of the ions present in a sample plotted against their intensities. Each peak in a mass spectrum indicates a component of unique *m/z* in the sample, and heights of the peaks connote the relative abundance of the various components in the sample.

Plasma proteomics of cardiovascular disease has been developed and helped immensely in the identification of different APPs for better prognosis and diagnosis. In conjunction with the identification of probable prognostic proteins, plasma proteomics is a global approach to track down the signalling pathways and proteins involved in the pathophysiology of any disease through online pathway analyses. In cardiovascular diseases, especially in acute CAD, plasma proteomics has been used as a very powerful tool coupled with advanced nano-LCs and mass analyzer for sample fractionation and protein identification. This coupled approach led to the identification of many markers including Troponin-T,Troponin-C, NT-pro-BNP,CRP etc. But, in case of proteomics, minimizing false identification of proteins is very important. Though, mass analyzers and analyzing softwares do most of the minimizations, the importance of careful sample preparation during protein digestion can't be overlooked. So, it is important to discuss protein digestion in detail. Intact proteins have very complex, folded structures that make any kind of analysis by mass spectrometry very difficult. So, proteins and mixtures of proteins are typically unfolded and broken down into smaller, more convenient fragments before any analysis by mass spectrometry. Digestion protocols for proteins existing either in-solution or in-gel are very popular and consist of the following steps:

- Denaturation
- Reduction and Alkylation
- Digestion

Denaturation

It is the process of unfolding a protein from its intact to its single-stranded polypeptide form. The addition of a chaotropic agent, such as guanidine hydrochloride or urea, in combination with heat is the most common method. SDS-PAGE gels also inherently denature proteins, thus serving as a common and convenient step to both clean-up and denature proteins in one step. Rapigest (Waters Inc.) is also used as a chaotropic agent in most the cases.

Reduction and Alkylation

Even after being denatured, a protein may retain its structure due to disulfide bonds. The breaking of these covalent bonds requires a reduction step and the capping of the resulting free sulfur happens during an alkylation step. Alkylation is performed so that disulfide bonds

cannot reform, leaving the protein in a completely denatured state. Common reduction and alkylation agents include dithiothreitol (DTT) and iodoacetamide (IAA) respectively.

Digestion

The common process of digestion uses proteolytic enzymes that cleave peptide bonds at very specific amino acids along the polypeptide chain. This generates a series of smaller peptides that are now ready for analysis by mass spectrometry. Protein digestion preceding to mass spectrometry analysis is a very widespread proteomics tool and can be used for a variety of applications including sequence determination, post-translational modification analysis and biomarker discovery/verification.

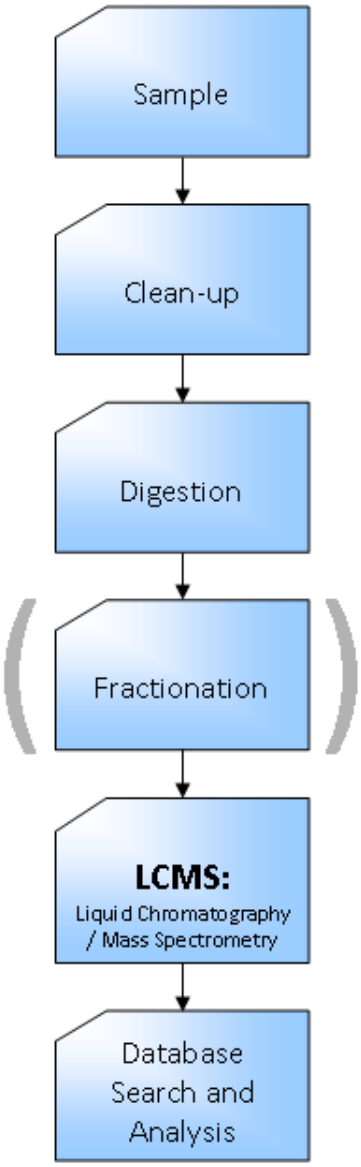

Figure 6.1.18. A simple workflow representing key steps of proteomic analyses (After Broad Institute)

6.1.12. Conclusion

Based on the above discussion, it became increasingly clear that cardiovascular disease as well acute CAD is caused mainly by atherosclerosis which occurs due to clogging of coronary arteries. Atherosclerosis is well connected to chronic inflammation which starts with the activation of platelets along with monocyte-macrophages. Though previous studies have pointed out the repertoire of proteins responsible for initiation and maintenance of inflammation, till date new information are accounted all the time. Still, the roles of the proteins involved in inflammation, reverse cholesterol transport as well as in pathophysiology of atherosclerosis remain baffling in acute CAD.

RATIONALE AND OBJECTIVES

6.2. Rationale

Previous studies on platelets and plasma secretome strongly established the role of these two components in Coronary Artery Disease. Although, the significance of most of the platelet as well as plasma proteins in CAD subtypes have not been reported. So, out work was focused on the role and association of a unique thrombin activated plasma protein sTLT1 with CAD as well as the identification and characterization of differentially expressed plasma proteins in different CAD subtypes.

Platelets are the smallest and specialized blood corpuscles that play vital roles in physiological processes including haemostasis, thrombosis, inflammation, wound healing, and host defense. In atherosclerosis, platelets augment the inflammatory milieu by the employment of inflammatory cells near the lesion sites and release of inflammatory mediators. The relationship between platelets, endothelial cells, circulating leukocytes and progenitor cells contributes to leukocyte activation, adhesion and transmigration. Once activated, the platelet released proteins set the course of next atherosclerotic events depending upon the very precise stimulus by which the platelets get activated. Thrombin, being a platelet agonist, acts as a pro-atherosclerotic mediator in cardiovascular diseases and remains constantly high in the plasma of coronary artery disease (CAD) patients. So, the proteins released from thrombin-activated platelets may have potential roles in the manifestation of atherosclerosis as well as CAD.

TREM like transcript 1(TLT1), which is identified to be expressed on the surface membrane of thrombin-activated platelets, is restricted to megakaryocytes as well as platelets in expression and is mostly considered to be associated with thrombus formation. The truncated part of TLT1 (17Kda), a part of the extracellular domain of the main protein, is released into the bloodstream as soluble TLT1 (sTLT1). It has already been established, this protein helps in platelet endothelial cell interaction, actin polymerization, platelet aggregation and leucocyte activation in microbial sepsis, but its function in CAD as well as atherosclerosis still need to be understood. In CAD, increased levels of thrombin not only activates platelets to mediate thrombosis but also gets involved in chronic inflammatory process along with atherosclerosis through the secretion of pro-inflammatory cytokines. However, sTLT1 is not yet reported to be connected to inflammation. Moreover, the blood thrombin levels in CAD patients and subclinical subjects with associated risk factors remain high, no information is available about the role of circulating sTLT1 in cardiovascular

pathology. It is reported that TREML group of proteins mostly bind with proteins possessing SYK domain in their intracellular part and induce inflammation. TLT1, being a member of TREML protein family, has a high likelihood of involvement in inflammation. But, the specific receptors involved and the intracellular effect of this protein upon receptor binding remain largely unknown.

Fc receptors are well conserved among species and play a critical role for maintaining cellular effector functions. Fcɣ RI, being a SYK domain associated protein, may have a claim as a receptor for sTLT1. It binds to IgG with high affinity and is expressed on monocytes, macrophages, dendritic cells, and neutrophils. Fascinatingly, the docking mode of this protein is constant for most of its ligands. Since, the binding affinity between Fcɣ RI and IgG is very high, the receptors get oversaturated with IgG even after extravasations of immune cells. But the exact role of this receptor in atherosclerosis remains elusive. The association of Fcɣ RI with cardiovascular disease was established by a study which showed Fcɣ RI deficiency conferred protection against atherosclerosis in apoE$^{-/-}$ mice. Studies reported that saturated Fcɣ RI binds to other ligands in an inflammatory atmosphere to form an immune complex but the mechanism of such interaction and the role of Fcɣ RI in intracellular signalling are still to be understood.

So, it is likely that sTLT1 functions via conserved Fcɣ receptors and thereby contributes to coronary artery disease. In this study, we prove a strong association between plasma levels of sTLT1 with severity and progression of coronary artery disease using healthy control, subclinical subjects and CAD subjects. We also show that sTLT1 binds to Fcɣ RI on macrophage surface initiating SYK mediated signalling which might initiate inflammation and atherosclerosis.

On the other hand, plasma proteomic profile of AMI subjects led to the identification of several biomarker candidates including fatty acid binding proteins, pigment epithelium derived factors and several others. Moreover, several reports described the functional implication of the altered proteins in cardiovascular diseases in general. Nevertheless, very few proteomics studies uncovered mechanistic paths of atherosclerosis in relation to inflammation and lipid balance in CVD subjects and most of them were conducted mainly on blood plasma of randomly designated CVD subjects. To avoid the lipid overload, created as a result of abnormal lipid concentration in plasma, the body activates a multi-step process known as the reverse cholesterol transport (RCT) for efficient efflux of excess cellular

cholesterol from peripheral tissue to liver, bile and finally to feces. Apolipoproteins play major roles towards RCT modulation. Hence, transgenic mice with disrupted ATP-binding cassette transporter 1 (ABCA1) and patients with ABCA1 gene mutations indicated impaired RCT and cholesterol efflux, and increased risk for atherosclerosis. ABC transporters are the most important factors in RCT. They mediate the efflux of HDL. The influx is mediated by SR-B1 receptors present in macrophages as well as in tissues. The balance between these two lipoproteins keeps up RCT.

Therefore, to understand the pathophysiological significances of the proteins related to RCT and dyslipidaemia in atherosclerosis and in turn to CAD, we performed plasma proteomics specifically of the subjects in CAD subgroups and normal healthy controls both by qualitative and quantitative approaches. Furthermore, we were able to ascertain the clinical significance of the altered proteins involving RCT, inflammatory signals, and development of CAD.

The present work aimed on the following objectives:

- To show an association of a platelet protein (soluble TLT1) with Coronary Artery Disease.
- Understanding the role of sTLT1 in the manifestation of atherosclerosis.
- To identify the differentially expressed proteins in ST-segment elevation Myocardial Infarction (STEMI), Non-STEMI (NSTEMI) and Unstable Angina (UA) with the help of quantitative and shotgun proteomics.
- Understanding interplay between obesity, chronic inflammation and reverse cholesterol transport from the perspective of dyslipidaemia in STEMI.

MATERIALS AND METHODS

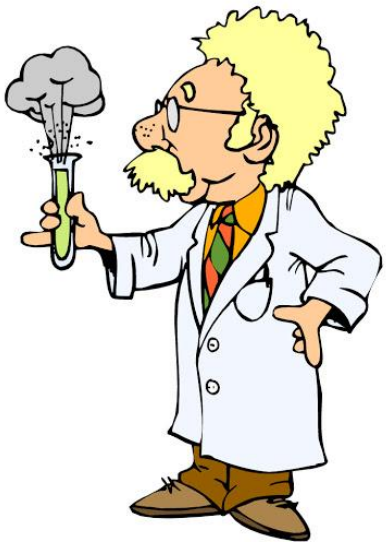

7.1. Materials

Reagents for mammalian cell culture, molecular biology, proteomics, as well as common laboratory chemicals were purchased from Merck (Germany), Calbiochem (Germany), Sigma-Aldrich (USA), Invitrogen (USA), Thermo-Scientific (USA) unless mentioned otherwise. Recombinant human proteins were purchased from MyBiosource (USA). Oxidized LDL was purchased from Alfa-Aesar (USA). All Fmoc protected amino acids and rink amide AM resin both were purchased from Novabiochem (Merck). *N, N′*-dimethylformamide (DMF), Dichloromethane (DCM), Trifluoroacetic acid (TFA), pipyridine, O-(Benzotriazol-1-yl)-N, N, N′, N′-tetramethyluroniumhexafluorophosphate (HBTU), Diisopropylethylamine (DIEA) and diethyl ether were purchased from Spectrochem (USA). Ethanedithiol (EDT) and phenol were bought from Merck (Germany). All the ELISA kits were purchased from Cloude-Clone corp. (USA) unless mentioned otherwise.

Phorbol Myristate Acetate (PMA) was procured from Sigma-Aldrich (USA). All the primary antibodies were purchased from Abcam (USA) or Santa-Cruz biotech (USA) or Cell Signalling technology (USA) unless mentioned otherwise. All the alkaline phosphatise conjugated secondary antibodies were purchased from Sigma-Aldrich (USA) and NBT-BCIP detection reagents were procured from Merck (Germany). Co-IP kits were purchased from Pierce Biotechnology (USA). SYK inhibitor R406 and BTK inhibitor Ibrutinib were purchased from Sigma-Aldrich (USA). Oil Red O staining kit for staining of foam cells were purchased from Biovision Inc. (USA).

Cell culture media, heat inactivated FBS were purchased from Gibco. Mass Spectrometry grade trypsin was purchased from Promega (USA). DTT, IAA was purchased from Bio-RAD (USA). MS grade ammonium bicarbonate was purchased from Merck (Germany). Nano-LC water and HPLC water were procured from Merck (Germany) and Spectrochem (India).

7.2. Ethics statement

The study on human subjects was approved by the ethics committees of CSIR-IICB and Apollo Gleneagles Hospital, Kolkata. Informed consents were obtained from each individual prior to blood collection. Samples were collected according to the Declaration of Helsinki (1975). Detailed information about each individual was collected in a proforma made according to the guidelines of Indian Council for Medical Research.

Wild type mice were obtained from CSIR-IICB animal house facility whereas ApoE$^{-/-}$ knockout mice was obtained from CSIR-Centre for Cellular and Molecular Biology, Hyderebad, India and maintained in the animal house of CSIR-IICB, Kolkata. The protocol was approved by the Institutional Ethics Committee (IICB/AEC-CERT/20115) and the animals were handled in accordance with the Committee for the Purpose of Control and Supervision of Experiments on Animals (CPCSEA), Ministry of Social Justice, and Government of India.

7.3. Study population and study design

Blood samples were collected from the subjects with ACS (*n*=60) on their arrival in Apollo Gleneagles hospital, Kolkata, India. Blood from healthy (*n* =16) as well as asymptomatic individuals (*n*=41) were collected from local population and during randomised routine check-up. For proteomics studies, 9 STEMI, NSTEMI as well as UA and 9 healthy subjects were selected by matching available information. Sample collection was done for the period of 5th October, 2013 to 5th October, 2016. Post-percuteneous intervention samples were taken from the same individuals who were considered as patients previously. Blood samples were centrifuged at 2500xg for 10 minutes to isolate plasma which then stored in -80°C freezer. The subjects with STEMI were chosen based on their electrocardiograph, M mode Doppler echocardiography and angiography reports. Healthy control subjects were age matched and not under any medication. They did not have any previous history of major illness. They have normal blood pressure, lipid profile, glucose, ECG and echocardiography. The levels of other blood parameters such as Na^+ -K^+, creatin, creatinin and bilirubin were in the normal range. Post PTCA samples were collected from the same subjects who were selected for STEMI. All samples were collected from the same institution, processed by the same individual and stored in similar condition for the same amount of time.

7.4. Inclusion and Exclusion Criteria

Subjects with CAD were enrolled for the study. Patients having diseases other than CAD like valvular heart disease, chronic coronary artery disease, diabetes, renal failure, hepatic failure, cancer, thyroid and other endocrinopathies, known genetic disorders, platelet related disorders, collagen related vascular disease, sepsis were excluded from the study. Healthy controls were chosen from normal population only if they don't have common risk factors and if their blood sugar, systolic/diastolic blood pressure, lipid profile, echocardiography and

electrocardiography, carotid intima-media thickness reports showed normal trend (<1mm) and the subjects with abnormal lipid profile and common risk factors, history of smoking or raw tobacco consumption, abnormal ECG and echocardiography reports, carotid intima-media thickness were >1mm were categorized as asymptomatic or subclinical subjects. We have selected the subjects with suspected disease and grouped them as subclinical or asymptomatic subjects. They are suspected to have the disease because they have the common risk factors for cardiovascular disease and they have carotid intima-media thickness >1 mm. Diabetic cardiomayopathy patients were also excluded from our study because of their medications, which might complicate the clinical association and further analysis.

For proteomics studies, age and sex matched individuals with ST-segment elevation in ECG having more than 70 percent blockage in major coronary arteries were selected as STEMI subjects whereas persons without any ST elevation were selected as NSTEMI. UA patients were categorized based on their Q wave inversion characteristics. The recruited healthy control subjects were also age and sex matched. Subjects with a previous history of diabetes, nicotine consumption/smoking, medication and major illness were excluded from the study. Subjects with chronic nephropathy and thyroid diseases were also excluded.

7.5. Plasma Isolation from isolated blood samples

Blood plasma was isolated after settling of collected blood samples at 4ºC followed by centrifugation at 1500g for 10 mins at 4°C. Isolated plasma was stored at -80ºC and freeze-thaw cycles, more than twice, were avoided.

7.6. Method of sample pooling

The mass spectrometry analysis by Orbitrap was performed in 3 independent sets (n_1,n_2,n_3) each of which contained pooled plasma of 3 different age and sex matched individuals. Thus data represent 9 plasma samples both in healthy control as well as STEMI.

SWATH- MS/MS was conducted in 6 independent sets (N_1,N_2,N_3,N_4,N_5,N_6) in which each set contained plasma samples pooled from 3 different individuals resulting into the inclusion of 18 individuals both in healthy controls and STEMI.

7.7. Echocardiography

Two-dimensional trans-thoracic echocardiography with targeted M-mode and Doppler were performed using commercially available systems by trained cardiologists. Echocardiography of CAD was confirmed to the recommendation of the 2012 World Heart Federation criteria. All measurements were made by blinded observers and mean of the three readings were recorded. Ejection fraction was calculated by Simpson's method. Carotid intima-media thickness was determined by trained physician using Duplex-Doppler vascular study.

7.8. Peptide synthesis

A scramble and active peptide (17 amino acids long) were synthesized. Sequences of the peptides were # **sequence 1: LQEEDAGEYGCMVDGAR (Active peptide) and # sequence 2: EDGQIYVPCLQYSLPQV (scramble).** The purity of the peptides was checked by both chromatogram and MALDI MS/MS (Figure 7.1). Synthesis was performed in the method described below. 300 mg of rink amide AM resin was placed in a peptide vessel and swelled overnight in DMF-DCM (1:1) solvent. Five equivalent of excess Fmoc protected amino acids (depending on sequence) were coupled successively followed by Fmoc deprotection using 20% piperidine solution in CEM microwave peptide synthesizer equipped with Liberty 1. Coupling and deprotection steps were maintained for eight and five minutes respectively. N, N′-diisopropylethylamine (DIEA) and HBTU were used as an activator base and activator respectively. DMF was used as solvent. After completion of the synthesis, the peptide attached resin was washed by DMF and DCM solvents. Peptides attached with resin were cleaved by standard resin cleavage cocktail solution containing 92.5% trifluoroacetic acid (TFA), 2.5% milli Q water, 2.5% EDT and 2.5% phenol. Resin attached peptide was kept for 3 h containing this peptide cleavage solution in a peptide vessel on shaker (Labnet international). After that, TFA was removed from the filtrate by nitrogen gas flow. The filtrate was added gradually to the cold diethyl ether solvent to ensure complete precipitation. The precipitation was separated by centrifugation. Finally, synthesized peptides were purified by using Shimadzu HPLC system equipped with C-18 reverse phase HPLC column and molecular weights were confirmed by MALDI-TOF mass spectrometry.Purity of these sequences were checked by HPLC and MALDI-MS/MS (Figure 7.1 A-D)

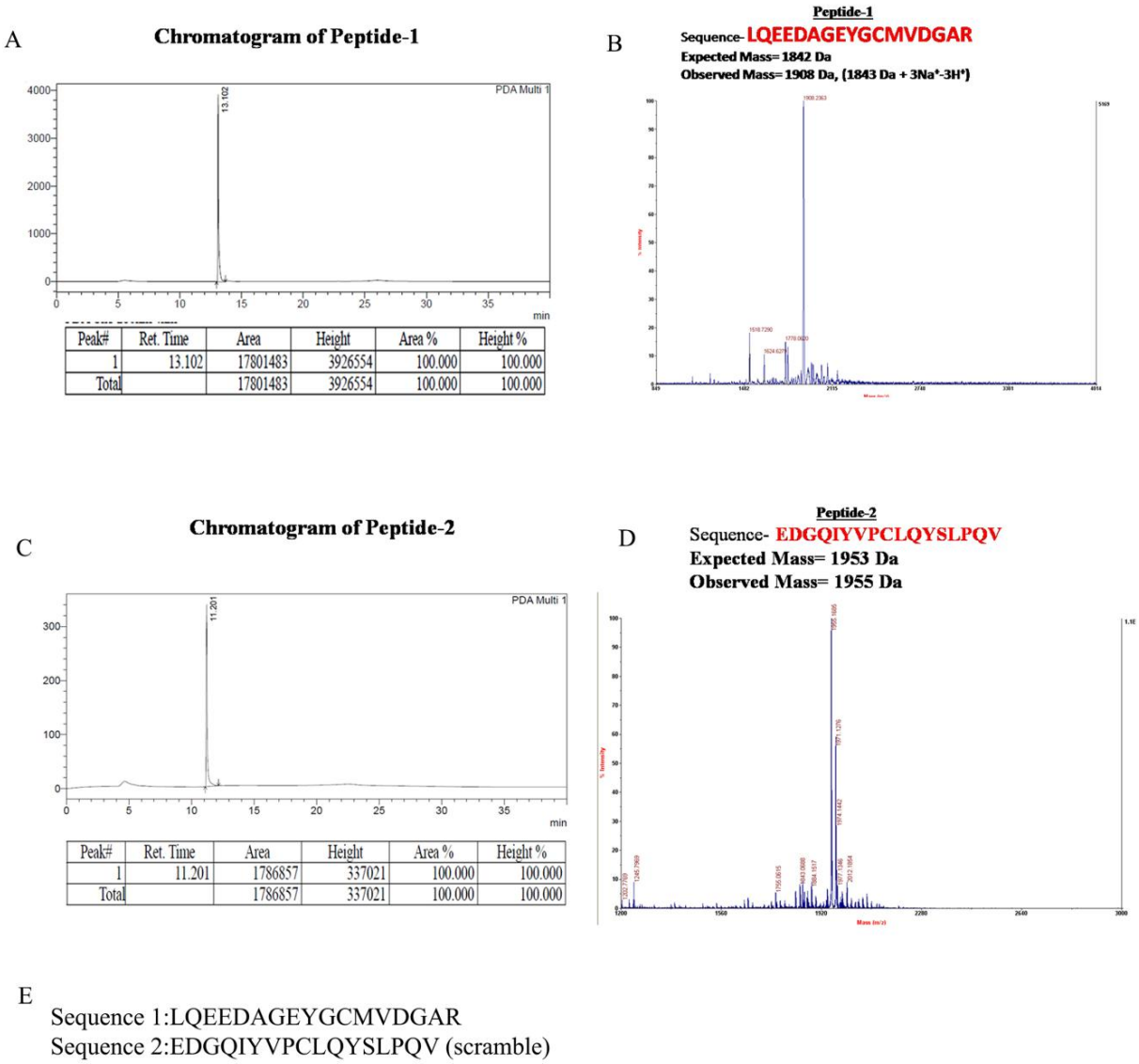

Peak#	Ret. Time	Area	Height	Area %	Height %
1	13.102	17801483	3926554	100.000	100.000
Total		17801483	3926554	100.000	100.000

Peak#	Ret. Time	Area	Height	Area %	Height %
1	11.201	1786857	337021	100.000	100.000
Total		1786857	337021	100.000	100.000

Figure 7.1. Chromatogram and mass spectra of peptide sequence 1 and sequence 2 (scramble)

HPLC chromatogram of peptide sequence 1 (A) and its corresponding MALDI-MS spectra (B) HPLC chromatogram of peptide sequence 2 (C) and its corresponding MALDI-MS spectra (D) Sequences of seq 1 (sTLT1 active peptide) and seq 2 (scramble) as synthesized chemically for treating monocyte derived macrophages (E).

7.9. ELISA

Cholesterol profiles of CAD subjects were determined by commercially available ELISA Kit using cholesterol probe (Sigma- Aldrich, USA). Cholesterol profile of healthy controls and asymptomatic individuals were obtained from the diagnostic centre where they were

recommended by cardiologists involved with this study (SK). Soluble TLT1 (R and D systems, USA), oxidized LDL (Uscn Life Sciences, USA) and N-terminus pro-BNP (Thermo-Scientific, USA) levels were measured by sandwich ELISA method as per the manufacturers' instructions. Detection limit of the kit was 10pg/ml. Intra assay CV was <10% and inter assay CV was <12% in all the ELISAs. The plasma level of HAVCR2 was measured by sandwich ELISA method (Cloud-Clone Corporation, USA). Briefly, plasma was diluted according to manufacturer's instruction. Samples (1:100) were incubated for 1hr inside the well. Then the wells were washed and detection reagent A was added. The wells were incubated for 1hr, and then washed again. Detection reagent B was added to incubate for 30 min at 37ºC. After the last wash, substrate solution was added in each well until the colour develops. Lastly, stop solution (1N H2SO4) was added and absorbance was taken at 450 nm.

7.10. Western Blotting

Plasma samples were diluted fifty times and resolved in 10% denaturing gel with prestained protein ladder (Fermentas#SM0671). Proteins were transferred to PVDF membrane with semi dry transfer apparatus (45 volts, 150 mA). The membranes were incubated with 5% non-fat milk solution, followed by incubation with primary antibodies (anti-TLT1, R&D systems, USA; anti-human alpha-transferrin, Sigma-Aldrich, USA) and secondary antibodies (anti-goat or anti-mouse AP conjugated) with alternating washing solution. Then, blots were incubated with NBT/BCIP solution until the bands were visible.Western blot analyses were performed using 10% SDS-PAGE.

Following antibodies were used for western blot analysis at the mentioned dilutions in 5% milk in TBST. Goat polyclonal anti-hZAG antibody (R&D Systems, USA) was used at a dilution of 1:300. Rabbit polyclonal anti-ABCA5 antibody (Abcam, USA) was used at a dilution of 1:1000. Rabbit polyclonal anti-C17ORF57 was used from Abcam, USA (1:1000). Rabbit polyclonal anti-PPARɣ (D69) (Cell-Signalling Technology, USA), was used at a dilution of 1:1000. Rabbit polyclonal anti-Calicin antibody was used in 1:1000 dilution (Novus biological, USA). Dilution used for Rabbit polyclonal anti-PGLYRP2/PGRP-L (Novus biological, USA) was 1:1000. Rabbit monoclonal anti-CD36 antibody was used at a dilution of 1:800 (Abcam, USA) with a loading control of alpha-tubulin (Santa-Cruz, USA). Mouse monoclonal anti-transferrin (E-8) (Santa-Cruz, USA) was used at a dilution of 1:6000. Following the primary antibody treatment, ALP-conjugated secondary antibodies were used

for western blots. Anti-Rabbit IgG-ALP (Sigma, USA) was used in a dilution of 1:6000. Anti-Mouse IgG-ALP was used at a dilution of 1:5000 (Sigma, USA) and for Anti-Goat IgG-ALP dilution used was 1:6000 (Sigma, USA).

7.11. Co-immunoprecipitation

Co-immunoprecipitation for CD36 and AZGP1 was performed by Pierce Classic Magnetic IP/Co-IP Kit (Cat no.88804) with the same antibody used for western blot (CD36,Abcam; AZGP1, R&D systems). Co-immunoprecipitation was performed in the following process. Cell culture media was carefully removed from the confluent culture. Cells were washed with cell culture grade PBS and lysed with ice cold co-IP lysis buffer with an incubation of 5 mins. After transferring the cells into microfuge tubes, cell lysate was centrifuged at 13000xg for 10 mins at 4ºC. The supernatant was transferred to a new tube and protein concentration was measured. Cell lysate was combined with 5 µg of antibody with a total protein amount of 400 µg. Then, the mixture was incubated overnight at 4ºC. 250 µg of magnetic beads were incubated and washed with IP lysis buffer twice. Then the beads were separated with the help of a magnetic stand and separated magnetic beads were mixed with sample-lysis buffer mixture. Beads were separated and unbound samples were collected for analysis. Then, the beads were again collected for wash. Samples bound to the beads were eluted with elution buffer and collected aliquots were run in 10% SDS-PAGE.Anti-GAPDH antibody was used as loading control (Cell signalling technology, USA, 1:800)

7.12. Cell culture and differentiation

Human THP1 monocytic cells (ATCC) were cultured in RPMI 1640 medium with 10% Foetal bovine serum in 5% CO_2 incubator at 37ºC. The cells ($2x10^6$) were seeded in fibronectin coated 6 well plates (Corning, Biocoat, Germany) in 1 ml of incomplete media and were differentiated using 100 nM PMA with appropriate controls for 24 h at 37ºC in 5% CO_2. Differentiated cells were attached to the bottom of the wells. Rest of the floating cells were washed by discarding remaining media and then each well was washed with cell culture grade DPBS (Gibco, USA). Differentiated THP1 cells were then treated with 10µg/ml oxidized LDL (low-TIBAR, Alpha-Aesar,USA) for 48 h to differentiate into foam cells. Synthetic sTLT1 treatment was performed in association with oxLDL for 24 h and oxLDL uptake was measured in presence of scramble and active sequence.

7.13. Cell staining

Cells were stained with Oil Red-O staining kit (BioVision, USA) to observe lipid particles in the cytoplasm with a counter-stain of Haematoxylin. Undifferentiated and differentiated THP1 cells were fixed with formalin and then incubated with isopropanol. Then, cells were stained with Oil Red-O for 10 min. The cells were then observed under microscope at 20x magnification in bright field.

7.14.Treatment of differentiated cells with chemically synthesized peptides (Sequence 1 or active sequence and scramble)

Differentiated macrophages were treated with Sequence 1 active peptide and scramble peptide (2ng/ml) for 6 h and protein was isolated after cell lysis with RIPA buffer for 30 min at 4° ºC at different time points for western blot. Protease inhibitor cocktail (Sigma-Aldrich, USA) and PhosStop (Roche) were used to prevent proteolysis and destabilization of phosphoproteins respectively. Cells were also treated with recombinant Gelctin-3 at physiological concentration.

7.15. Treatment of differentiated THP1 cells with chemically synthesized peptides (Sequence 1 or active sequence and scramble) along with SYK blocker (R406) and BTK blocker (Ibrutinib)

Differentiated THP1 cells were treated with SYK blocker R406 and BTK blocker Ibrutinib along with active sequence and scramble peptide (2ng/ml) for 6 h. R406 was added to the cell culture media in 0.5 µg and 4 µg concentrations whereas Ibrutinib was added in 1 µg and 2 µg concentrations. After treatment, cells were lysed with RIPA buffer for 30 min at 4ºC in addition with protease inhibitor cocktail (Sigma-Aldrich,USA) and PhosStop (Roche, Gremany) to prevent proteolysis and destabilization of phosphoproteins respectively.

7.16. Histopathological studies

ApoE$^{-/-}$ knockout mice was obtained from CSIR-Centre for Cellular and Molecular Biology, Hyderebad, India and maintained in the animal house of CSIR-India Institute of Chemical Biology, Kolkata. The protocol was approved by the Institutional Ethics Committee (IICB/AEC-CERT/20115) and the animals were handled in accordance with the Committee

for the Purpose of Control and Supervision of Experiments on Animals (CPCSEA), Ministry of Social Justice, and Government of India. ApoE$^{-/-}$ knockout mice were fed with normal chow diet (Kcal: Protein=25%; Carbohydrate=58%; Fat=17%) and high cholesterol diet (Research Diets Inc.; Open Source DIETS; Cat no. D12336; detailed composition has been attached in supplementary table 1) for 2 months. Then mice (n=10) were sacrificed after 45 days and 60 days to dissect out their aorta. 8 µm thick aortic sections were prepared from paraffin blocks by microtome. Sections were mounted on slides and observed under a microscope after haematoxylin-eosin staining.

7.17. Plasma isolation from wild type and ApoE-/- mice

ApoE-/- mice were fed with normal chow diet and high cholesterol diet for 45 days and 60 days. Afterwards, blood from these mice was collected by retro-orbital bleeding in EDTA coated vacutainer (BD, USA) for plasma collection. Isolated plasma was then kept at - 80ºC freezer for future experiments after aliquoting in a separate microfuge tube.

7.18. Methods for Mass spectrometry and proteomic studies

Plasma samples of subjects with STEMI, NSTEMI and UA as well as age and sex matched healthy individuals were pooled (n=3x3=9, please refer to statistical rationale section) separately for proteomic analysis. Initially, 900 µg proteins were pooled and major proteins (albumin, IgG) were depleted with the help of magnetic beads using Pure Proteome albumin/IgG depletion kit (Cat no. LSKMAGD12, Merck-Millipore, USA) and depleted plasma samples were collected separately. This method depletes about 70 percent of the plasma protein mass. Reproducibility of the samples was checked by running samples from different preparations and different fractions. About 100 µg protein was then used for in-solution tryptic digestion. Briefly, protein samples were treated with 100 mM DTT for 30 min at 60°C. Afterwards, it was cooled down to room temperature and treated with 200 mM iodoacetamide for 60 min. Then, samples were digested with 2 µl of porcine trypsin gold (Lysine, Arginine C-terminal, 1µg/µl, Promega) overnight in 37°C water bath. The processed plasma samples were lyophilized using Speed Vac (Savant, SC110). Lyophilized samples were again reconstituted in 50µl solution of 0.1% formic acid in water. Reconstituted samples then, proceeded for mass spectrometric analysis by Orbitrap mass spectrometer (LTQ-XL, Thermo-Fisher Scientific) after chromatographic separation and peptide fractionation through a C_{18} easy spray nano column (3µm, 100A) by nano LC (Easy-nLC1000). The injection

volume was 5µl for each sample. Total gradient was set for 185 min with a spray rate of 300 nl/min. The gradient was divided into 4 stages: 1) 0-5% for 5 min 2) 5% - 35% from 5 min to 155 min 3) 35% - 95% from 155 min to 172 min 4) 95% - 100% from 172 min to 185 min (Mobile phase A: 100% water with 0.1% (v/v) formic acid, mobile Phase B: 100% acetonitrile with 0.1% (v/v) formic acid). The acquisition was data dependent. Scan range for Orbitrap was from 350-2000 (m/z) with minimum 3 peaks and a resolution of 60000. Ionic fragmentation was done by collision induced dissociation (CID) method. Normalized collision energy for each run was 35. Detection and digitization of peaks were done by Fourier transformation and data acquisition was done in positive ion mode. Protein identification was performed by Thermo Proteome Discoverer version 1.4.0. MS/MS spectra were matched against both MASCOT and SEQUEST in assistance with fixed value PSM validator. Static modification was set for N-terminal acetylation and carbamido-methylation of Cysteine. Dynamic modification was set for Methionine (oxidation), Tyrosine (phosphorylation), Lysine (acetyl). Maximum missed cleavage number was two. Uniprot/Swissprot database (updated with Uniprot release 2015 and 46000 protein entries) was used as reference software for protein identification. Minimum number of peptides for assigning a protein was set two. Mass tolerance for precursor ion was set to 10 ppm. Raw spectra files were saved in Xcalibur raw format. Raw files can be accessed in Massive repository with the user ID: arun_123 and password: Orbitrap2018

7.19. SWATH-MS Analysis

For SWATH-MS, 9 plasma samples [control samples (3) were pooled and STEMI samples (3) were pooled for each biological replicate (N=3 for three biological replicates), (n=3xN=3x3=9, please refer to statistical rationale section)]; both the pooled samples were age and sex matched and these samples were the same samples which were used for orbitrap analyses. These Sample preparation and tryptic digestion were performed as described above. All the digested peptides were analysed on Triple- TOF 5600 (AB Sciex; Concord, Canada) mass spectrometer coupled with Micro-LC 200 (Eksigent; Dublin, CA) in high-sensitivity mode. To create the SWATH spectral library, 3µg of peptide from each sample was individually analyzed by information dependent acquisition (IDA). Accumulation time for MS was 0.25 ms and for MS/MS was 0.01 ms. Fragmentation was performed using rolling collision energy of 28kV.

For quantification, peptides were acquired by SWATH-MS mode (in technical triplicates) on Micro LC-Triple TOF 5600. Briefly, 1 µg of peptide was directly injected into Agilent C18-RP HPLC column (100×0.3mm, 3µm, 120 Å) and then separated using a 95-min gradient of 3% to 40% mobile phase (Mobile phase A: 100% water with 0.1% (v/v) formic acid, mobile Phase B: 100% acetonitrile with 0.1% (v/v) formic acid) at a flow rate of 8 µL/min. The quadrupole settings for the selection of precursor ion selection windows were 25 m/z wide. Using an isolation width of 26 m/z (containing 1 m/z for the window overlap), a set of 34 overlapping windows was constructed covering the precursor mass range of 400–1250 m/z. SWATH-MS/MS spectra were collected from 100 to 1999 m/z. The rolling collision energy was optimized for each window according to a charge 2+ ion centred upon the window with a spread of 15eV. Dwell time was used 70 ms for all fragment-ion scans in high-sensitivity mode, and for each SWATH-MS cycle acquired in high resolution mode for 100 ms resulting in a duty cycle of 3.4.

To get SWATH spectral library from IDA run, data were analyzed using Protein Pilot software using Uniprot reviewed human database (updated with Uniprot release 2015 and 46000 protein entries) with minimum 2 signature peptides assigned for each protein. Created spectral library (IDA runs) peptide tolerance were used with 20 ppm and for the quantification it was used (SWATH-MS acquisitions) with 50 ppm error at precursor level, 2 min retention time window and 99% confidence using Peakview software. Processed files were exported to Marker View software for the quantitative analysis of proteins, peptides and ions in different samples.

7.20. Pathway Enrichment Analysis

Pathway enrichment analyses for both Orbitrap and SWATH were performed mainly by Ingenuity Pathway Analysis (IPA) software (version 2.0, Qiagen, USA). Pathway enrichment was performed by core and expression analysis applications of IPA. Comparison of results between control and STEMI were also performed. The analyses were based upon IPA knowledge base and both direct and indirect relationships were taken into consideration. Confidence variable was set to consider both experimentally observed and highly predicted relationship tab. Prediction was based on probability values and Z scores. Species filter was set to human and statistical filter was set to stringent. Hierarchical clustering was performed with a p value threshold of 0.05. Colour intensity was assigned according to the amount of significance. Gene Codis 3 and PANTHER were used for further bioinformatic analysis.

7.21. *in-silico* analyses

PATCHDOCK, ClusPro V.2.0 and HADDOCK 2.2 (High Ambiguity Driven protein-protein Docking) servers were used to perform receptor-ligand docking. CD36, CD64 and Dectin-1 were defined as receptor and AZGP1, sTLT1 and sGalectin-3 were defined as the ligand in all the servers. Structure of ligands were uploaded in PATCHDOCK server (clustering RMSD was set to 2.0), which uses a fast Fourier transform (FFT) algorithm to search spatial degree of freedom between receptor and ligand. Moreover, this server reports each binding mode with an energy scoring function. The same pair was docked independently of PATCHDOCK with ClusPro V.2.0. It uses PIPER to find pair wise interaction potentials as well as rank on the basis of level of stability, semi-definite programming based underestimation (SDU) energy and cluster size. The cluster with the best statistics in both the cases was chosen for further studies by HADDOCK2.2. This server uses biophysical or biochemical interaction data such as chemical shift perturbation data from NMR to perform the docking analysis. The information about interacting residues was introduced as ambiguous interaction restraints (AIRs) to drive the docking. After calculation, the structures were docked according to their intermolecular energy that is the sum of electrostatic, Van-der-walls and AIR energy terms. So, lowest HADDOCK score represents the best possible interacting pair. Rigid body minimization, semi-rigid TAD-SA as well as final refinement in Cartesian space were also performed by HADDOCK2.2. To perform docking through HADDOCK, we specifically generated AIR restrained file for both the receptor and ligand as well as specified the probable interacting chains for both of them (as identified from other two servers) to get best cluster combination with minimum HADDOCK score. PYTHON algorithm was used to find out the common proteins among different orbitrap and SWATH runs.

7.22. Isothermal Titration Calorimetry

The purified human AZGP1 and CD36 (Gly30-Asn439) were procured from RayBiotech, USA in lyophilized form. For Isothermal Titration Calorimetry (ITC) lyophilized proteins were dissolved separately in 10 mM Tris-HCl (pH 8.0), 50 mM NaH_2PO_4, 0.3 mM NaCl solution and mixed in the sample cell.

Isothermal titration calorimetry was used to measure the enthalpy changes resulting from the titration of the ligand (2.5 µM in 1.8 ml buffer solution of AZGP1) into the buffer solution or

receptor (510.2 nM in 400 µl buffer solution of CD36) protein solution at 25ºC (VP-ITC, Microcal Inc., Northampton, MA, USA). Initially 10 µl of CD36 solution was injected in a 1.8 ml titration cell containing either buffer alone or AZGP1 solution. Each injection lasted for 20 seconds. The mixing of two solutions was conducted in 220 rpm and each set of mixing lasted for 180 seconds. Prior to data analysis, the measurements were corrected for the heat of dilution of buffer in the sample cell. The entropy change (ΔS) and the Gibbs free energy change (ΔG) of association were calculated using the following equation ΔGo = -RT InKa = ΔHo – TΔSo. Preliminary data analysis was conducted by Microcal LLC ITC. The thermodynamic parameters were determined by fitting the heat of the reaction data using Origin 7.0 software (Microcal Inc., Northampton, MA, USA).

7.23. Power calculation for the study population

We performed the power calculation by considering control to cases ratio 0.5. We used the following formula for calculating sample size for quantitative variables in case-control studies-

Sample size=$(r+1/r) \times \{SD^2(z_\beta+z_{\alpha/2})\}/d^2$

r= ratio of controls to cases

$z_{\beta=}$ standard normal variate for power(here for 80% its 0.84)

$z_{\alpha/2=}$ standard normal variate for level of significance (1.96 for p=0.05 i.e. 5% type I error)

SD=standard deviation

d= differences of mean between control and cases.

The power calculation between patient and subclinical group yielded sample size of 63 for patients and 32 for subclinical subjects whereas power calculation between subclinical and control group suggests a sample size of 24 for subclinical and 12 for control subjects. Hence, we included above mentioned number of subjects in each group. So, the number of subjects included in each group is statistically supported.

7.24. Experimental design and Statistical rationale

Data are expressed as mean ± SEM for continuous variables. Normal distributions for all continuous variables were tested using Kolmogorov-Smirnov test. One way analysis of

variance (ANOVA) was carried out to compare (1887) between three experimental groups. Otherwise non-parametric Kruskal-Wallis test was used. Differences among study groups were determined by Student's t test after testing their normality. Samples which were handled erroneously were considered as outliers. We also removed samples which were showing absurd values based on biological problems (chronic illness, ongoing medication, high number of platelets, diabetes etc.). These samples were categorized as biological outliers. Statistical outliers were detected by Z test and Grubb's test. The correlation between continuous variables was calculated using Pearson's Correlation Coefficient (r). The numbers of subjects taken into account in different correlation studies are different because of the exclusion of statistical and biological outliers from the data. Multiple logistic regression analysis was performed to determine the dependence and predictive value of sTLT1 on the established risk factors. ROC curve was plotted to assess the usefulness of changes in soluble TLT1 level in predicting the risk of having ACS and diagnosing the disease in patients. A probability value of $p \leq 0.05$ was considered as statistically significant. All these tests were performed by using GraphPad Prism 2.0 and MedCalc 6.2.0 software.

Three (N=3) age and sex matched samples were pooled to normalize inter-individual variability. Biological replicates (M=3) were run with three (M) different sets of pooled samples to normalize inter-sample variability. This resulted into the inclusion of 9 (n=NxM=3x3=9) different subjects in both STEMI and control subjects in both discovery and test set. Comparison between two continuous variables, parametric paired Student's t test was performed. Kolmogorov-Smirnov test was conducted to check normal distribution of the data. The significance among protein expression in western blotting and ELISA was performed also by Student's t test. Heat map was generated by IPA and ClustVis:BETA software and statistical relevance was calculated according to the Z score. Principal component analysis (PCA) was performed using ClustVis: BETA to normalize the inter-run variables in mass spectrometry. Ion intensities between Control and STEMI samples were compared by parametric student t test. Most of the analyses were done in Graph Pad Prism 6.0.

7.25. Monoclonal antibody production against sTLT1

Monoclonal antibody for sTLT1 was raised in mice and produced by the following protocol which involved immunization, fusion and clonal selection by Abclonex from KRIC.

RESULTS

CHAPTER 1

CLINICAL IMPLICATIONS OF sTLT1

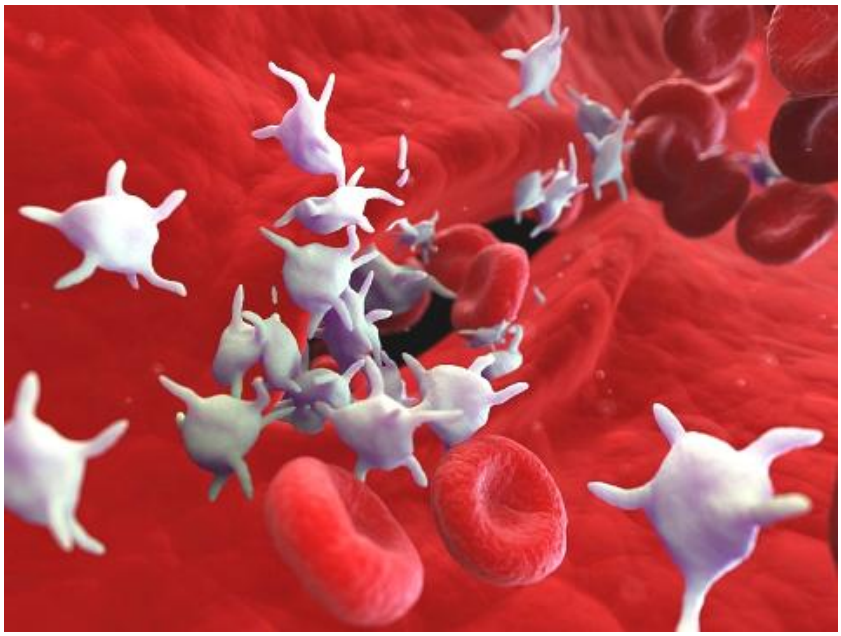

8.1.1. Introduction

As discussed earlier, platelets are the key cells to initiate the event of atherosclerosis as well as the process of plaque formation. Activation of platelets initiates major processes like monocytes activation and differentiation, endothelial cell activation, monocytes migration and secretion of pro atherosclerotic and pro-coagulant proteins which helps in the orchestration of the whole process of plaque formation as well as atherosclerosis (Reinger G ed et al, Platelets,2015). Platelets respond to different agonists in different ways. They secrete separate group of proteins in response to separate stimuli. So, there were several reports of platelet proteins being altered in the blood of coronary artery disease patients. But, most of them did not correlate in subclinical individuals and they had high false positives in clinical tests. So, for quite a few years, search of a platelet protein was very necessary which may indicate the prognostic condition of a CAD subject or a subclinical subject.

It has been reported that thrombin level increases in the blood plasma of CAD patients. But, blood thrombin level cannot act as good indicator for subclinical subjects as because in most of the subclinical subjects the plasma concentration does not differ significantly compared to normal healthy controls (Tosi F et al, Thromb Res,2017). On the other hand, thrombin being a potent platelet activator induces platelets to release several proteins in the blood plasma. Thrombin induction on platelets causes the release of a specific group of proteins which may have a high possibility of being related to atherosclerosis. So, we searched the literature to come across TREM like transcript 1 (Gattis JL et al, JBC,2006). It is a platelet membrane protein expressed in response to thrombin. Further studies, led us to identify that upon activation of platelets the extracellular domain of this protein is cleaved and released into the blood stream (Gattis JL et al, JBC,2006). So, we decided to check the clinical significance of this protein in CAD subjects as well as other groups.

8.1.2. Results

8.1.2.1. Baseline characteristics

The demographics and baseline of 117 individuals included in this study are shown in Table 8.1.1. About 13.7% individuals were control (n=16); 35% individuals were asymptomatic (n=41) and 51% subjects had CAD (n=60). In control group, about 75% were males and 25% were females; in asymptomatic,

78% were males and 22% were females; in CAD subjects 90% were males and 10% were females. 4 of the control subjects were smokers but still they were included because 3 of them started smoking recently (1 month) and one of them was an ex smoker (15 years ago and he smoked for 3 years only). All the patients in CAD had documented hypercholesterolemia, hypertension and abnormal ECG and echocardiography reports. Angiography was also performed to determine the extent and degree of the blockage which was helpful in determining the severity of the disease. The major clinical and demographic variables among three groups were determined through one way ANOVA analysis (Table 8.1.1). Patients mainly belonged to three Killip classes, a) Class I, 19 (31.67%); b) Class II, 31(51.67%); c) Class III, 10 (16.67%). No subjects belonging to Class IV were recorded. Majority of the CAD subjects were under anti-diuretic drugs (73.33%), and anti-platelet drugs (68.3%). Some patients (8.3%) were with anti-hypertensive drugs. However, sTLT1 level remained unaltered with the administration of drugs (anti-diuretics, p=0.927; anti-hypertensive, p= 0.467; anti-platelet, p=0.394) (Figure 8.1.2 C,D,E).

Table 8.1.1. Baseline Characteristics of Study populations

VARIABLES	GROUP 1 (n=16) Control	GROUP 2 (n=41) Asymptomatic	GROUP3 (n=60) CAD	P value
Age	39.6 ± 3.34	44 ±1.79	52 ±1.61	*0.04
M/F	12/4	32/9	50/10	0.1006
Total cholesterol (mg/dl)	159.4±7.64	174.4±5.72	217.5±9.44	***0.0001
HDL cholesterol (mg/dl)	45±3.15	41.6±1.35	36.8±1.5	0.07(ns)
LDL cholesterol (mg/dl)	95±6.32	107.78±5.02	120.4±8.20	**0.01
Triglyceride (mg/dl)	117.19±9.01	143.02±10.88	173.1±14.95	0.187(ns)
SBP(mm/Hg)	115±3	117±2	120±8	*0.02
DBP(mm/Hg)	75±2	77±2	80±2	0.096(ns)
Smoking status (current/ex)	3/1	12/9	19/2	0.2365

Data are expressed as mean ± SEM and compared by one-way ANOVA analysis.

8.1.2.2. Normalization of age and sex variables

No correlation with the age of each individual among the study groups was found (Figure 8.1.1A). To rule out the variability bias from platelet number, association of sTLT1 with platelet number was examined which revealed no significant correlation indicating that the variation of sTLT1 level was solely dependent upon the pathophysiology of the subjects (Figure 8.1.1B). Furthermore, multiple logistic regressions proved that age and sex were associated with disease risk but did not affect sTLT1 level in blood (Table 8.1.2).

Table 8.1.2. Results of multivariate logistic regression analysis

Logistic regression

Coefficients and Standard Errors

Variable	Coefficient	Std. Error	Wald	P
Age	0.079480	0.019585	16.4692	*<0.0001*
Smoking	1.49156	0.45949	10.5373	0.0012
Constant	-4.45074	0.99183	20.1369	*<0.0001*

Odds Ratios and 95% Confidence Intervals

Variable	Odds ratio	95% CI
Age	1.0827	1.0419 to 1.1251
Smoking	4.4440	1.8057 to 10.9372

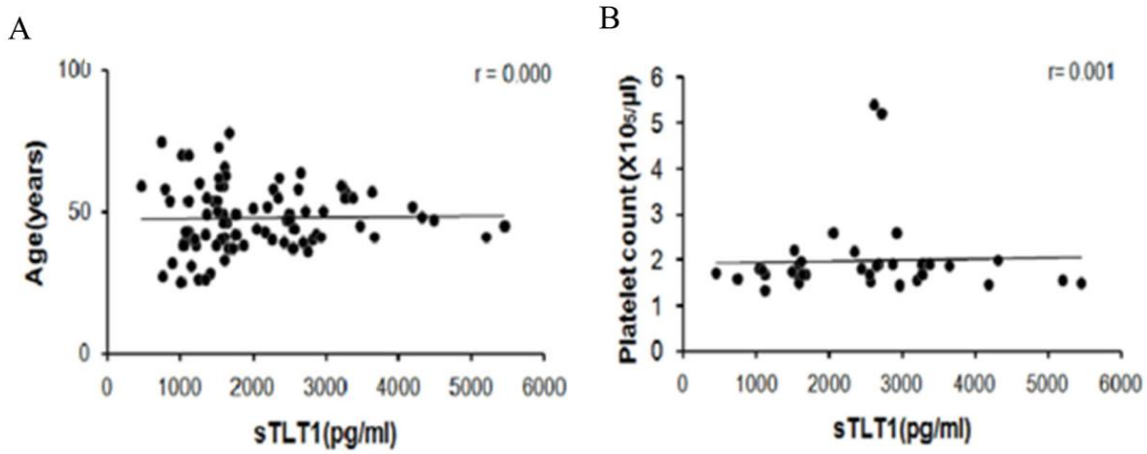

Figure 8.1.1. Correlation of sTLT1 level with age (A) and platelet number (B) indicating that it is independent of age bias as well as number of platelets ($r<0.4$ and $p>0.05$) (Das et al, Clin. Sc.2019)

8.1.2.3. Soluble TLT1 level increases in CAD patients and asymptomatic individuals

In CAD subjects (*n*=60), sTLT1 level (2342±184pg/ml) was significantly ($p<0.001$) increased compared to both asymptomatic (1773±118pg/ml) and control individuals (461±57pg/ml) (Figure 8.1.2A). There was a 4-fold increase in sTLT1 in asymptomatic compared to normal healthy controls ($P<0.001$). To validate these results, we performed western blotting with human plasma which displayed higher level of the protein in CAD patients (Figure 8.1.2 F). It was also observed that 48 h post pro-thoracic coronary angioplasty (PTCA) the protein level was (3055±246 to 1757±156) decreased significantly ($P<0.001$; Figure 8.1.2 B). Multiple logistic regression analysis also supports these findings as sTLT1 was associated with disease outcome ($p=0.045$, OR=1.02, 95%CI=1 to 1.04; Table 8.1.3).

Table 8.1.3. Results of multivariate logistic regression analysis for the disease risk prediction

Coefficients and Standard Errors

Variable	Coefficient	Std. Error	P
Hypertension	-0.243	2.346	0.917
sTLT1	*0.0199*	*0.001*	***0.045*
Constant	-15.93		

Odds Ratios and 95% Confidence Intervals

Variable	Odds ratio	95% CI
Hypertension	0.7844	0.0079 to 77.9517
sTLT1	*1.0201*	*1.0004 to 1.0402*

Significant values are highlighted in italics; sTLT1: soluble TREM like Transcript 1

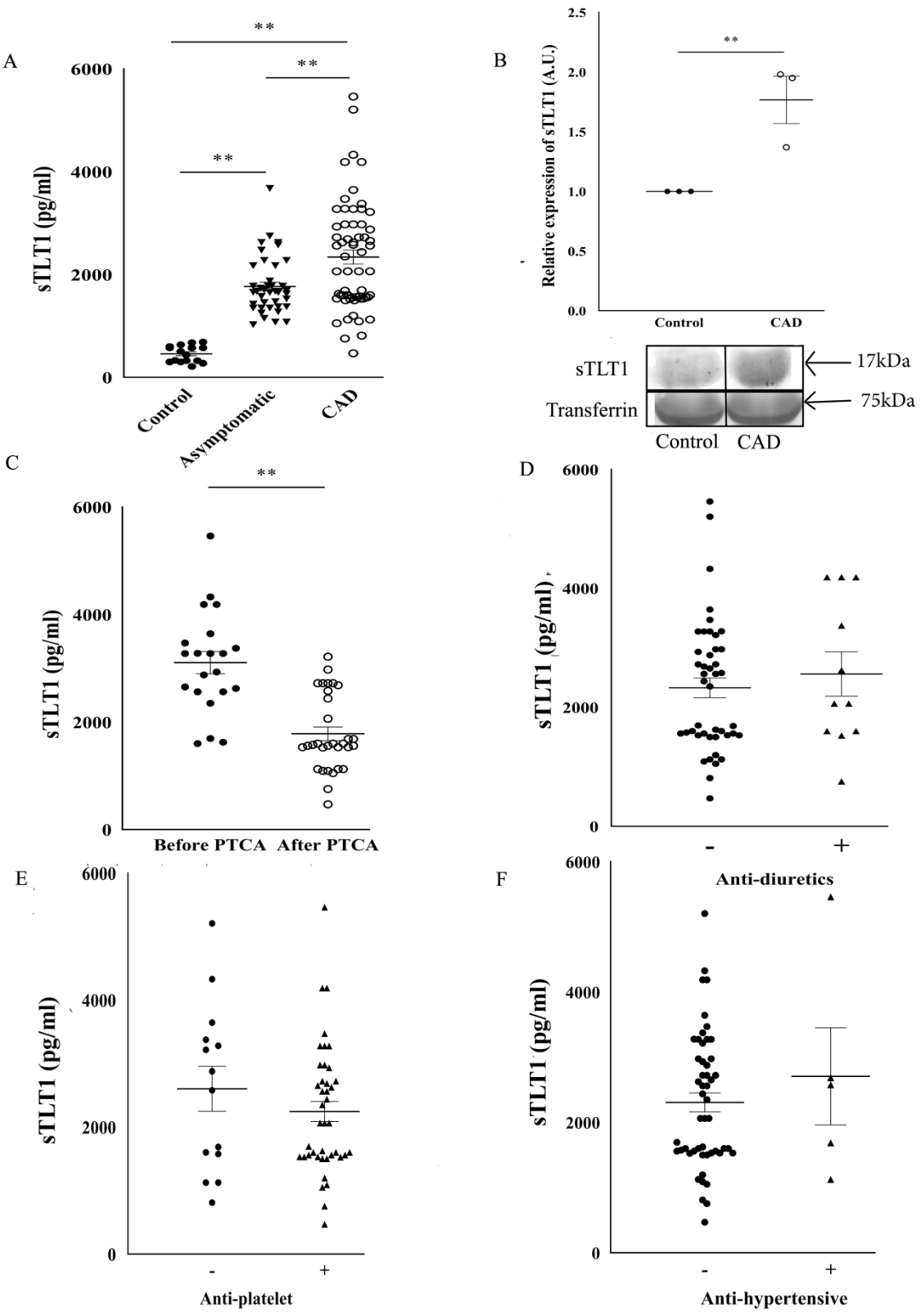

Figure 8.1.2. Estimation of soluble TLT1 in human plasma.

Scattered plots indicating plasma sTLT1 levels (mean ±SEM) in control (Black dots; n=16), subclinical (Inverted black triangle; n=41) and CAD (Black bordered white dots; n=60)

subjects as measured by ELISA (A). Representative western blot showing sTLT1 in CAD (Black bordered white dots) and healthy control (Black dots) in human plasma as well as its densitometric analyses by ImageJ software (B). The delineations in the representative blot image imply that they are cropped images from the same gel. The levels of sTLT1 are also shown in patients before (Black dots; n=21) and after PTCA (Black bordered white dots; n=31) (C); without (-) or with (+) anti-diuretics (D), anti-platelet (E) or antihypertensive (F) medicines. CAD subjects without medication (n = 44, 14, 51 representing anti-diuretics, anti-platelet and anti-hypertensive groups, respectively) are represented as black dots and CAD subjects with medications (n = 11, 41, 5 representing anti-diuretics, anti-platelet and anti-hypertensive groups, respectively) were symbolized as black triangles. Immunoblots shown were performed in triplicates. Double asterisk (**) indicates means are significantly different at $p<0.05$(Das et al, Clin. Sc.2019).

8.1.2.4. Correlation of sTLT1 level with LDL, LDL/HDL ratio and oxidized LDL

We examined the relationship of sTLT1 with the risk factors of atherosclerosis and severity of the disease, the correlation coefficient of soluble TLT1 with LDL level in asymptomatic individuals was calculated. Level of sTLT1 is positively correlated with LDL (r=0.401, p=0.03, n=35) and LDL/HDL ratio (r=0.435, p=0.016; n=30) in asymptomatic individuals (Figure 8.1.3A, B respectively). Similarly, sTLT1 level was also strongly and positively correlated with LDL concentration (r=0.6, $p<0.001$, n=35) and LDL/HDL ratio (r=0.59, p=0.02, n=14) in CAD subjects (Figure 8.1.3D, E respectively). It also positively correlated with oxidized LDL both in plasma of asymptomatic individuals (r=0.491, p=0.004, n=33) as well as CAD subjects (r=0.453, p=0.002, n=43). Interestingly, 81% CAD subjects (n=43) had high oxLDL level (n=35) despite of having normal LDL level (Figure 8.1.3 C, F respectively).

8.1.2.5. Association of sTLT1 with the severity of coronary artery disease

Correlation analyses with the left ventricular ejection fraction (LVEF) and GRACE score were performed to establish clinical significance with coronary artery disease. Figure 3G, showed sTLT1 level is inversely correlated with LVEF (r=-0.460, p=0.004, n=57). GRACE score was calculated for 6 months (predicts the risk of MI within 6 months) based on Killip

classification and it has strong positive correlation with sTLT1 level (r=0.508, p= 0.001, n=47) (Figure 8.1.3H). As low LVEF and higher GRACE score directly indicate disease severity; it is apparent that sTLT1 is mostly associated with severity of the disease and chances of acute coronary event when it crosses the threshold value. Furthermore, we calculated TIMI score for each patient and estimated the risk of individuals for the acute event within 14-30 days. The patients were categorized in two distinct groups according to their TIMI score. The subjects with TIMI score <5 was in lower risk of having another acute event whereas subjects with a TIMI score ranging from 5-8 are on the higher risk of having another event. Interestingly, low TIMI score group (n=17) corresponds to lower level sTLT1 (1621±174pg/ml) and high TIMI score group (n=38) corresponds to higher concentration of sTLT1 (2924±231pg/ml) with a very significant p value of <0.001 (Figure 8.1.3I). These results strongly support the hypothesis that the plasma level of sTLT1 can indicate the risk of acute coronary event also.

8.1.2.6. Receiver Operating Characteristics (ROC) Curve Analysis

To determine the specific cut off concentration and predictive performance of sTLT1, ROC curve analysis was performed. As shown in Figure 8.1.3J, the ROC curve analysis with asymptomatic and control subjects revealed a cut off value more than 875 pg/ml (p<0.001) with a sensitivity of 91.67% and specificity of 100% for association with CAD. The ROC curve analysis with sTLT1 concentration between asymptomatic and CAD subjects showed a cut off concentration of 2500 pg/ml with 65% sensitivity and 91% specificity (p<0.001) (Figure 8.1.3K). ROC curves do not determine disease survival and disease outcome but may predict performance level of sTLT1 as an associated protein. NT-pro-BNP levels were quantitated and compared with sTLT1 level in patients to compare its (sTLT1) sensitivity over NT-pro-BNP and was found to be performing better than NT-P-BNP (AUC= 89% for sTLT1 over 65% for NT-pro-BNP). Comparison of sensitivity of sTLT1 among asymptomatic or subclinical subjects was compared over oxLDL and sTLT1 was found to be performing better than oxLDL (AUC=100% for sTLT1 over 80% for oxLDL).

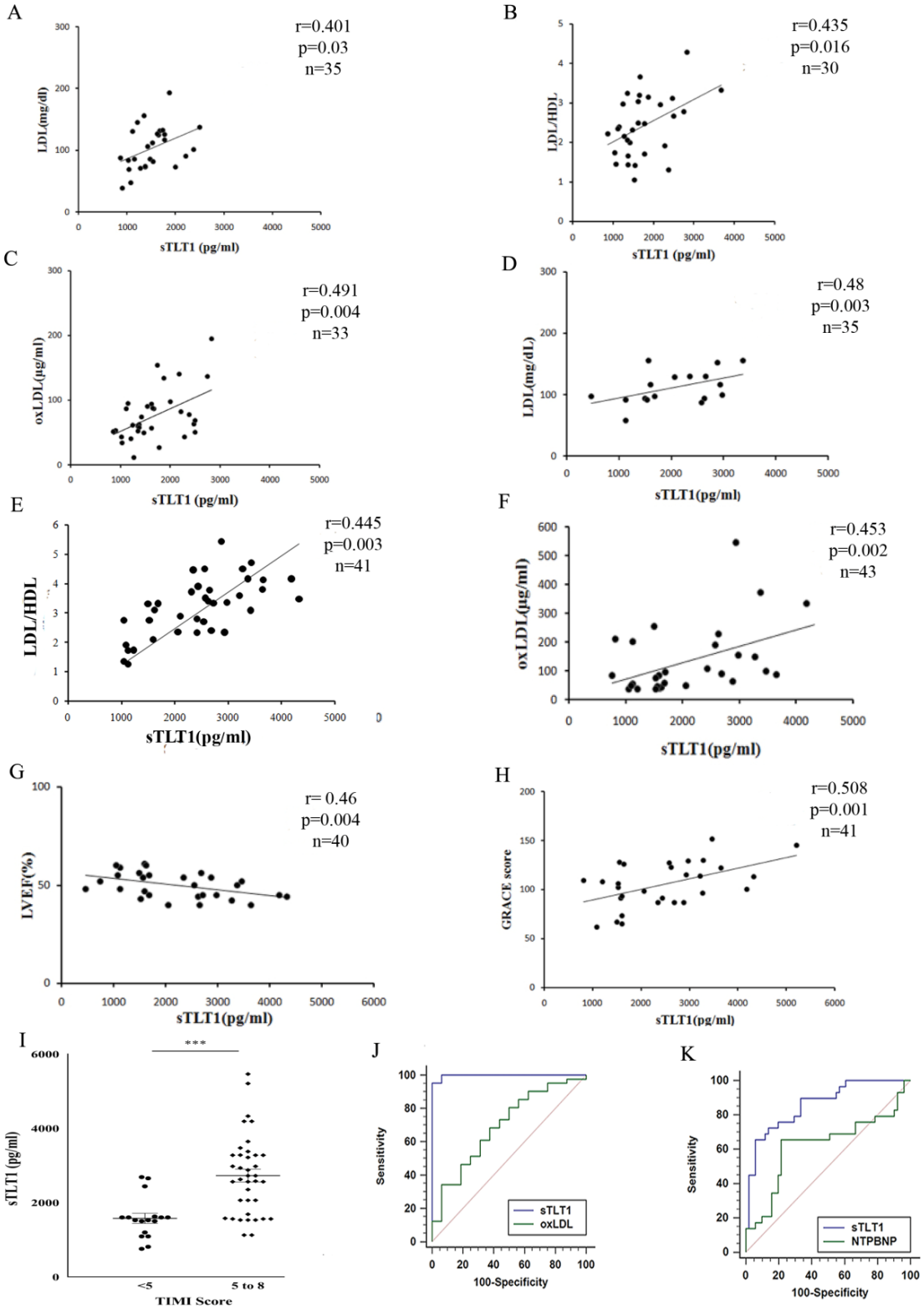

Figure 8.1.3. sTLT1 is linked to disease risk factors and it has a specific prognostic value for subclinical and clinical population.

Correlation of sTLT1 with LDL, ratio of LDL and HDL or oxLDL in subclinical individuals (A, B, C, respectively) and CAD subjects (D, E, F, respectively) (r>0.4 and p< 0.05).

Correlations of sTLT1 with LVEF (G) and GRACE score (H) are also shown to indicate association with disease severity. Scattered plot indicating association of sTLT1 with TIMI score (I) is also depicted to relate with disease risk (n=17 for the group with TIMI score <5 and n=38 for the group with TIMI score 5 to 8). Comparative ROC curve analyses of sTLT1 level with oxidized LDL in asymptomatic (J) and NT-proBNP in CAD subjects (K) reflecting its better performance for risk assessment. (Das et al, Clin. Sc.2019)

8.1.2.7. Correlation of sTLT1 with intima-media thickness

The carotid intima-media thickness of asymptomatic individuals was calculated based on Duplex Doppler study. The results showed that sTLT1 level (1338±375 pg/ml) was higher than the minimum threshold level in asymptomatic individuals who has intima-media thicknessmore than 1 mm. It clearly shows that sTLT1 can also be associated with total atherosclerotic burden of an individual and it is related to risk of coronary artery disease.

8.1.2.8. sTLT1 monoclonal development and testing

Two different immunogens from C terminal and N terminal was chosen to raise two monoclonal antibodies from two separate clones. Immunoblots with these two antibodies in subclinical and clinical plasma samples detected specific single bands against sTLT1 at a dilution of 1:500. On the other hand, ELISA with both these custom made antibodies detected significant colorimetric change which was measured and tallied against already established threshold values. The quantification for subclinical and clinical samples showed the concentration above the threshold value. So, we established an ELISA method to detect sTLT1 in plasma of suspected and diagnosed CAD subjects which may later help in the development of a kit.

8.1.3. Conclusion

The present work established that a platelet secreted protein induced by thrombin activation of platelets can act as a potential diagnostic candidate protein for clinical and subclinical CAD subjects. Through, biochemical and small population based statistical analyses on human plasma samples, we established the potential of this protein (sTLT1) as a probable risk predictor of the disease. To the best of our knowledge, this is the first report on characterization of a thrombin induced platelet protein as a possible candidate protein for disease risk prediction. Biochemical tests (sandwich ELISA and western blot) predicted that

sTLT1 is high in subclinical subjects and even higher in clinical subjects of CAD. Not only that, its level is increased with disease but its plasma concentration is significantly linked to most common cardiovascular risk factors like LDL level, HDL, oxidized LDL level in the plasma. Statistical analyses also showed that, other risk factors like hypertension, age and smoking are also related to the level of sTLT1 in CAD. We for the first time were able to determine specific cut-off values for sTLT1 in clinical and subclinical groups of CAD. Therefore, our results, all together present a platform for the identification of a new candidate protein (sTLT1) for disease risk prediction which has the ability to diagnose coronary artery disease in asymptomatic or subclinical population as well as clinical population.

CHAPTER 2

ROLE OF sTLT1 IN CORONARY ARTERY DISEASE AND ATHEROSCLEROSIS

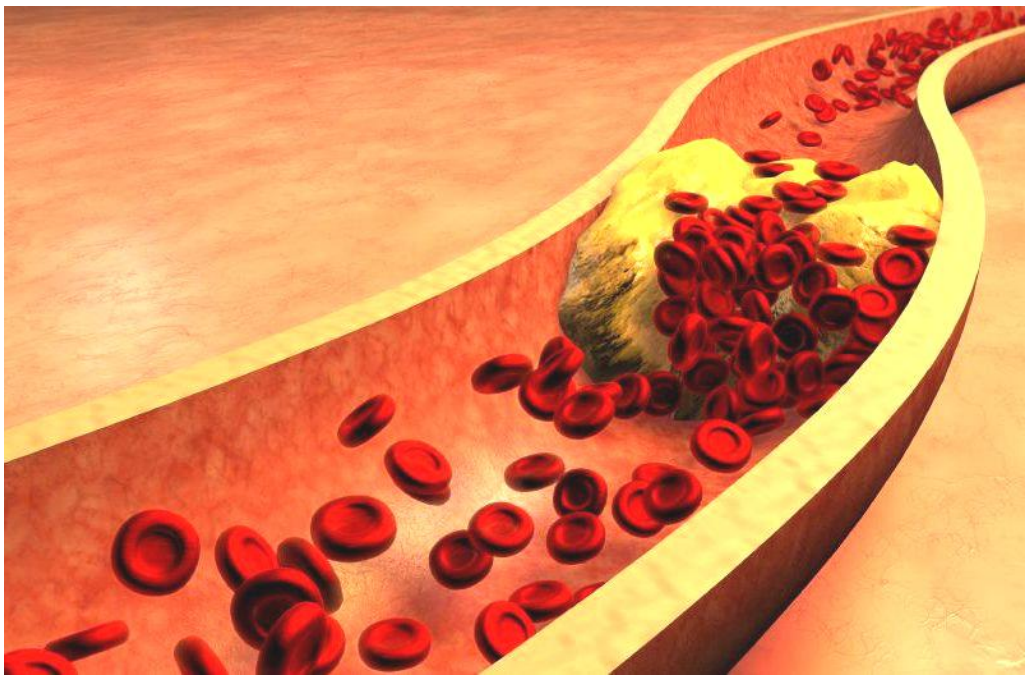

8.2.1. Introduction

Coronary artery disease is the most common cause of cardiovascular mortality in Indian subcontinent as well as all over the world. CAD occurs because of occlusion of coronary arteries by thrombus. Thrombus development is the result of plaque maturation and rupture for a long temporal scale. Though, plaque development goes on for a long time inside the body, without the presence of any agonistic factors, it is impossible for plaques to rupture. Build up and rupture of a plaque is mostly dependent upon two major cell types: the macrophages and the platelets. Platelets are involved for coagulation and recruitment of different cell types whereas the macrophages mainly deal with inflammation and cholesterol transport.

Platelets are the key cells in atherosclerosis. They, depending on their activators, release different repertoire of proteins. These proteins are mostly responsible for the progress and development of atherosclerosis. sTLT1 is a platelet protein released when activated by thrombin. Its role has been reported in maintaining chronic inflammation (Derive M et al, JI, 2012) and monocytes recruitment but there are no reports available regarding its contribution in atherosclerosis (Washington AV et al, JCI,2009). Based on the fact that plasma thrombin level remains high in CAD subjects, we established that sTLT1 level remain significantly high in CAD subjects in the previous chapter. But, the mode of action and the route downstream is still need to be elucidated.

Fc receptors are mostly conserved among species and play a vital role to maintain cellular effector functions. Fcɣ RI, a SYK domain associated protein, likely has its own claim as a receptor for sTLT1, as sTLT1 belongs to the TREM group of proteins and these proteins tend to bind receptors with SYK domain. Fcɣ RI binds to IgG with high affinity and is constitutively expressed on monocytes, macrophages, dendritic cells, and neutrophils. Interestingly, the docking mode of this protein is largely constant for most of its ligands. Since, the binding affinity between Fcɣ RI and IgG is very high, the receptors always remain oversaturated with IgG even after entry of immune cells (Mancardi DA et al,Blood,2013). But the precise role of this receptor protein in atherosclerosis remains unclear. The association of Fcɣ RI with cardiovascular disease was established by a study which indicated Fcɣ RI deficiency conferred protection against atherosclerosis in apoE$^{-/-}$ mice. Studies reported that saturated Fcɣ RI binds to other ligands in an inflammatory environment to form

an immune complex but the mechanism of such interaction and the role of Fcγ RI in intracellular signalling are still to be understood.

So, it is likely that sTLT1 functions via conserved Fcγ receptors and thereby contributes to coronary artery disease. In this chapter, we show that interaction of sTLT1 to Fcγ RI on macrophage surface initiates SYK mediated signalling which might contribute to inflammation and atherosclerosis.

8.2.2. Results

8.2.2.1. sTLT1 binds with the SH2 domain of SYK

Increased plasma level of sTLT1 led us to confirm the cause-effect relationship of this protein with the disease. Based on in-silico studies we predicted that sTLT1, being a secreted plasma protein, may interact with macrophage membrane proteins. Protein structure of sTLT1 indicated it has a IgV like domain. Based on literature mining in Uniprot, we predicted that "IgV like domain" family proteins may bind to SYK group of proteins. So, to identify potential interactors of sTLT1, we performed STRING interaction analysis. It identified 10 probable interacting proteins with significantly high PPI score ($p<0.05$) (Figure 8.2.1A). Among these, FCER1G (Fcγ RI) not only has a SYK domain but also had a high node to node PPI score of 0.6. Furthermore, Fcγ RI is plentiful on macrophage cell surface and involved in adaptive immune regulation. Based on these initial data, we inspected docking of Fcγ RI on sTLT1.

The aim was to discover the specific portion of the proteins (Fcγ RI and sTLT1) which frequently interacts with its partners. Searches in PDB and Uniprot led us to identify SH2 domain (9-262 amino acids) of Fcγ RI and IgV like domain of sTLT1 (amino acids: 20-125) as the most frequent interacting chains. So, to find out the best possible conformation, we docked IgV like domain of sTLT1 (amino acids: 20-125) (PDB ID: 2FRG) (Figure 8.2.1B:b,c,d Red portion showing the interacting surface) with SH2 domain (part of ITAM domain) of SYK in FCER1G (amino acids: 9-262) (PDB ID: 1A81) (Figure 8.2.1B:a Red portion showing the surface of interaction) with the assistance of PatchDock and ClusPro 2.0. Primarily, .gz files of both the domains were uploaded in PatchDock web server. The results presented 10 binding conformations with minimum free energy, minimum entropy and the maximum number of weak bodings. Further for cross-validation, we repeated the docking experiments using ClusPro 2.0 and one of the predicted interaction complex was found to be

common in both of the web servers. Further analysis was performed on the common cluster of interacting pairs. In figure 8.2.1C (a,b), a simple ribbon model of the common pair has been shown (IgV domain in red) from two different angles. We also determined the surface cleft of the interaction through initial docking [Figure 8.2.1D (zoomed in) and 8.2.1F (zoomed out)]. Figure 8.2.1E shows likely amino acids implicated in interaction in Ig V like domain in loop ribbon model. Then, we docked the proteins using HADDOCK to find out the possible angle of interaction and specific chains involved in interaction. HADDOCK results primarily indicated 8 different cluster combinations of interaction for the chosen pair. Clusters were numbered from 1 to 8 according to their HADDOCK score in increasing order. Scatter plots against HADDOCK score (Y axes) and other determining variables (X axes) for all the clusters are presented in figure 8.2.2 (A-G). These scatter plots point out cluster 1 (marked as red triangle in the plots) as the most suitable cluster of interaction since it earned minimum HADDOCK score and minimum inter-Root Mean Square Distance (i-RMSD) among the interacting chains (Table 8.2.1). Based on in-silico analysis, we performed co-immunoprecipitation of sTLT1 (chemically synthesized) and Fcɣ RI from cellular extracts of differentiated macrophages to find out the same conclusion (Figure 8.2.2H).

Table 8.2.1. Values of HADDOCK analysis for cluster 1

Variables	Values
HADDOCK score	-109.0 +/- 4.7
Cluster size	103
RMSD from the overall lowest-energy structure	1.4 +/- 0.8
Van der Waals energy	-33.4 +/- 4.4
Electrostatic energy	-396.4 +/- 88.1
Desolvation energy	1.1 +/- 10.5
Restraints violation energy	25.2 +/- 14.58
Buried Surface Area	1645.0 +/- 70.0
Z-Score	-2.2

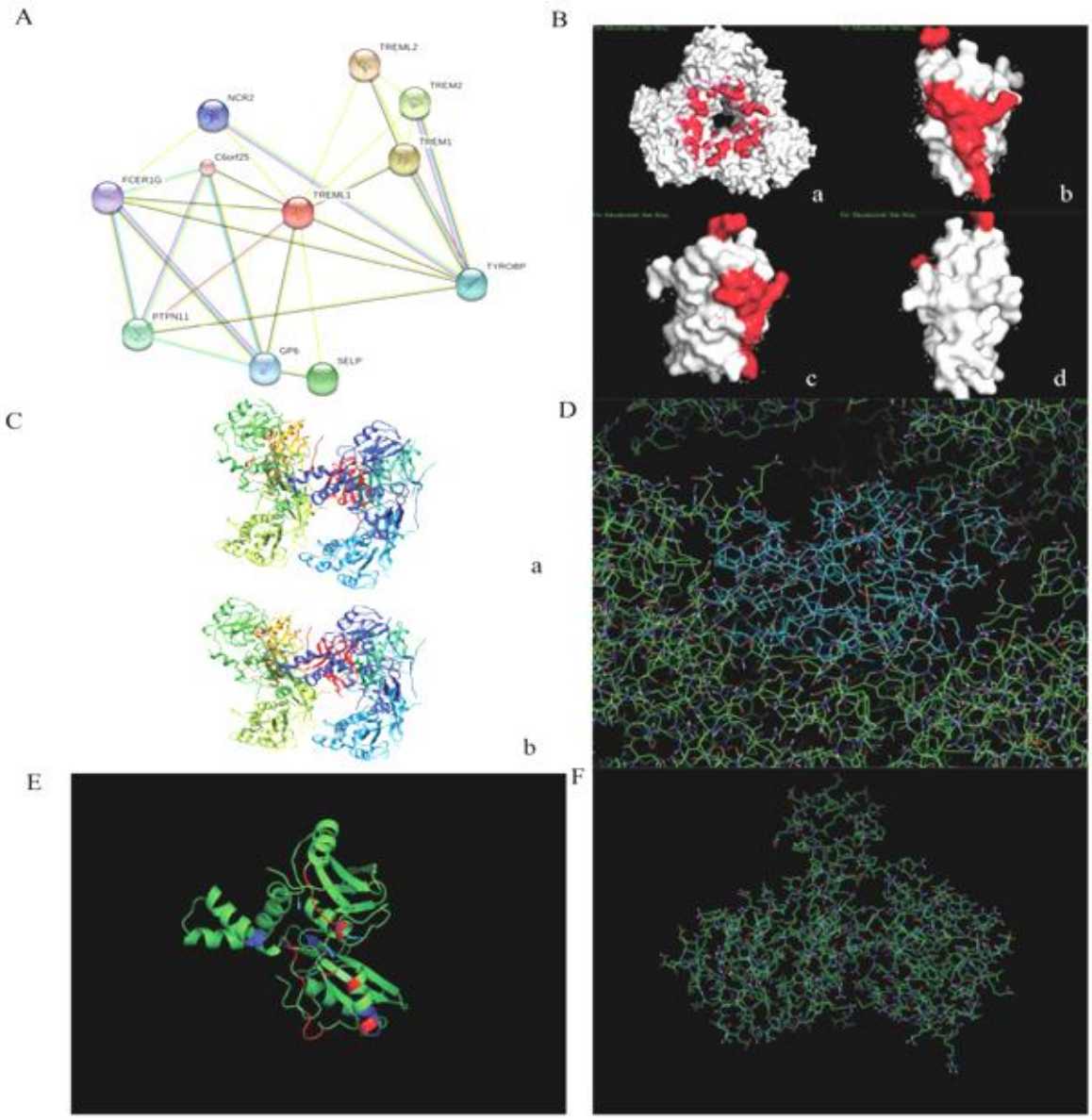

Figure 8.2.1. Molecular docking showing Fcɣ RI interaction with sTLT1.

Possible interactors for sTLT1 (TREML1) were determined by STRING analysis which indicated Fcɣ RI (FCER1G) as a possible receptor with fairly high PPI score ($p<0.05$) (A). 3D model of interacting protein domains and their surface of interaction (in red) of SH2 domain (a) and IgV like domain (b,c,d) were shown in PyMOL view(B). Common interacting complex from PatchDock and ClusPro is shown in Ribbon model (sTLT1 in red and SH2 domain of Fcɣ RI in multicolor) from two different angles (a,b) which was used for HADDOCK2.2 analysis (C). Ball and stick model of the zoomed in (D) and zoomed out (F) view of sTLT1 (sky blue) - Fcɣ RI (green) attachment cleft in HADDOCK cluster were shown as PyMOL view. Position of interacting amino acids of sTLT1 specifically highlighted in red and blue was represented as ribbon model (E). (Das et al, Clin. Sc.2019)

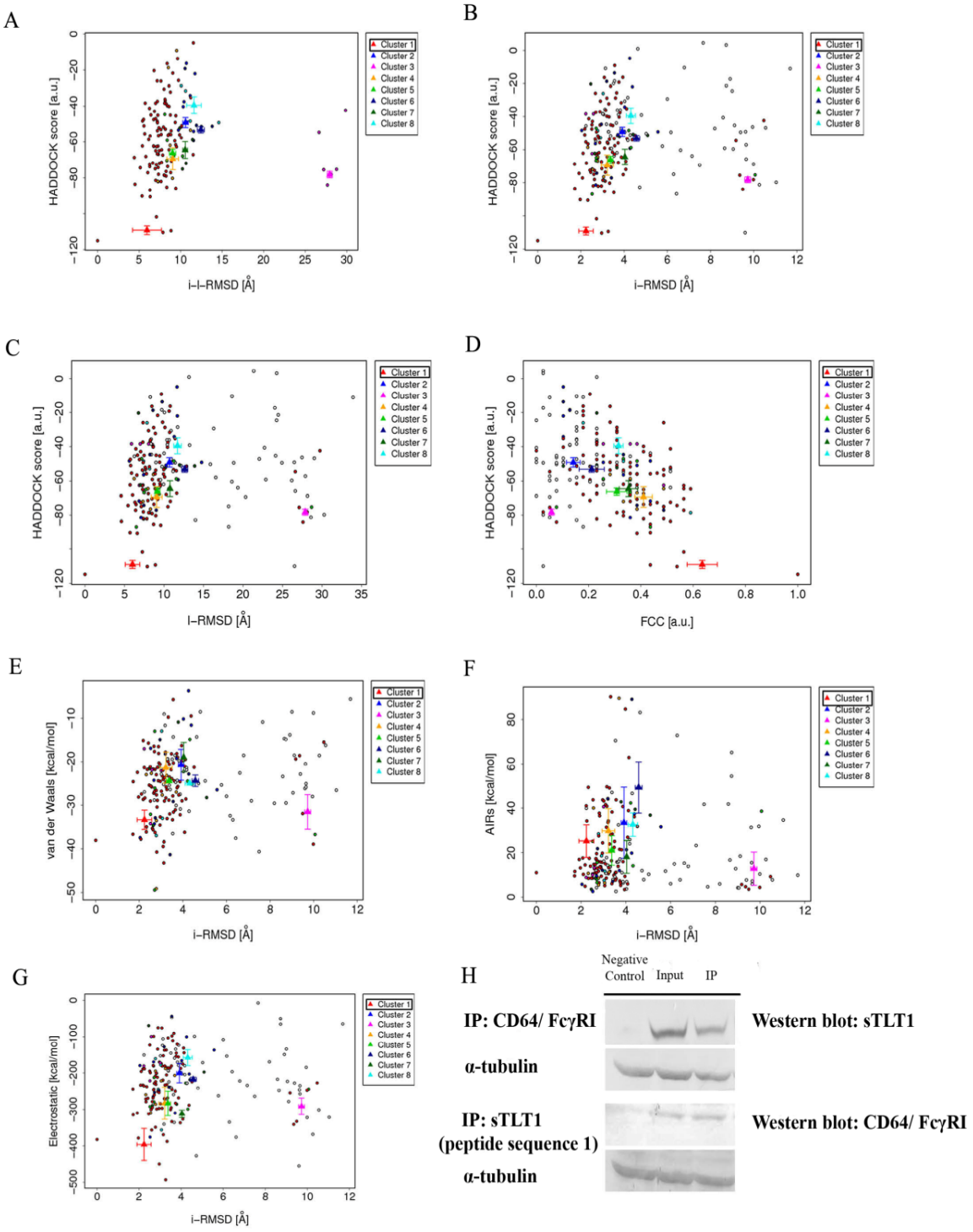

Figure 8.2.2. HADDOCK analysis and Co-IP confirms sTLT1-Fcɣ RI interaction.

The results and pictorials presented in Fig.8.2.2 (A to G) are based on water refined models generated by HADDOCK. The clusters (indicated in color in the graphs) are calculated based on the interface- ligand RMSDs calculated by HADDOCK, with the interface defined based upon all observed contacts. The various structural analyses (FCC, i-RMSD and l-RMSD) are made with respect to the best HADDOCK cluster (the one marked as red triangle) with the

lowest score. H. Co-immunoprecipitation (Co-IP) experiments in macrophage cells shows Fcɣ RI when immunoprecipitated with anti-sTLT1 antibody and vice versa; points towards the interaction of Fcɣ RI with sTLT1. Synthetic sTLT1 protein was used as input in Co-IP of sTLT1 and cell lysate was used as input in Fcɣ RI. α-tubulin was used in both the cases as loading control. IgG was considered as negative control for the whole experiment. (Das et al, Clin. Sc.2019)

8.2.2.2. sTLT1 activates SYK mediated MAPK pathway

Differentiated THP1 monocyte-macrophages were treated with sTLT1 active peptide (sequence 1) and scramble (sequence 2) to observe the effect of sTLT1- Fcɣ RI interaction. Sequence 1 treated cells showed a time-dependent phosphorylation pattern of SYK when compared to total SYK while scramble treated cells did not show any specific phosphorylation pattern. The level of activated SYK is 1.4 times higher at 15 min (Figure 8.2.3, panel A, $p<0.05$). Time-dependent study of activated BTK showed 2.9 fold increase against total BTK level at 10 min (Figure 5.3, panel A, $p<0.05$). But, scramble treatment did not show phospho-BTK indicating no activation. Downstream analyses of BTK pathway led us to track further into the phosphokinetics of this signalling cascade. MEK, next predominant member of this cascade, showed 4 fold initial increase at 15 min to 5 fold increase at 30 min compared to original levels (Figure 8.2.3, panel B, $p<0.05$) after active peptide treatment but not in scramble treatment. Activated ERK showed a significant (3 fold) increase at 15 min (Figure 8.2.3, panel B, $p<0.05$) only in cells treated with active sequence.

8.2.2.3. Activation of ERK-mediated MAPK pathway induces NF-kB canonical pathway

Increased level of phosphorylated MEK (MAPK) and ERK (MAPKK) led us to investigate further downstream in sTLT1 induced intracellular pathway. Our data indicated that phosphorylated IKKβ was 2 fold higher and the level of phosphorylated NF-kB-p65 was 1.5fold higher after 15 min of treatment with sTLT1 active sequence compared to the scramble peptide (Figure 8.2.3, panel C, $p<0.05$). These results may point to the fact that activation of IKKβ is directed to the phosphorylation of IkB and its gradual degradation through ubiquitination. On the other hand, this degradation of IkB results into the release of

NF-kB-p65 from the inactive complex of p65-p35 that makes nuclear translocation of the molecule possible. This correlates with the increased level of NF-kB-p65 in the cell lysate.

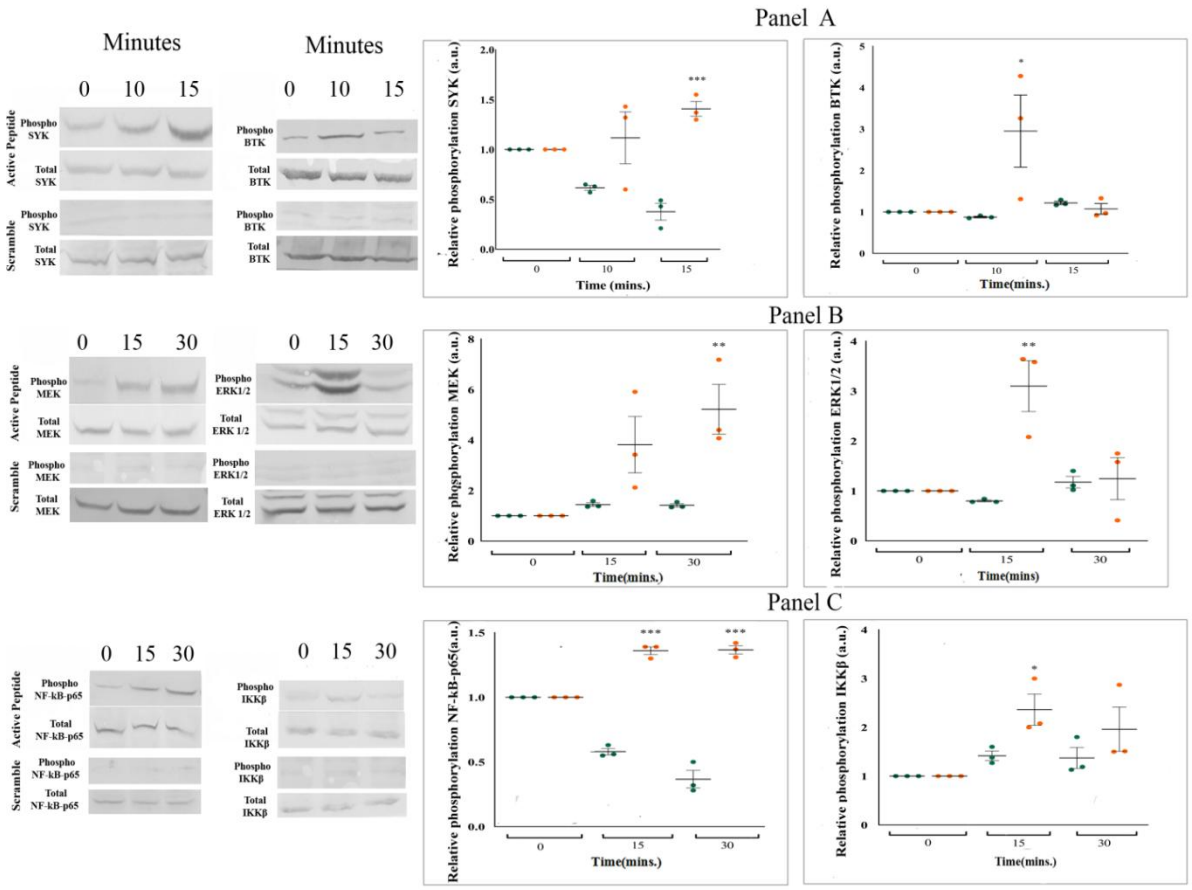

Figure 8.2.3. Induction of sTLT1 activates SYK mediated signalling to secrete TNF-α in vivo.

Immunoblots showing phosphorylation (activation) status of SYK, BTK, MEK, ERK1/2, NF-kB-p65 and IKK-β in macrophage upon treatment with active peptide of sTLT1 and its scramble for indicated times. Densitometric analyses of the immunoblots by ImageJ software are shown in the corresponding adjoining panels (A, B, C) to indicate the level of phosphorylation. All the blots shown are performed in triplicates. Green dots and yellow dots represent data for scramble and active peptide treatment at different time points, respectively. (Das et al, Clin. Sc.2019)

8.2.2.4. SYK antagonist R406 inhibits downstream signalling to decrease the secretion of TNF-α from THP1 derived macrophages

Differentiated macrophages were treated with SYK specific inhibitor, R406 in two different concentrations (0.5 µg and 2 µg) along with active peptides. Immunoblots indicated that SYK was inhibited by R406 (Figure 8.2.4A). Interestingly, BTK activation was also inhibited in response to R406 compared to active peptide alone (Figure 8.2.4A). This shows that BTK activation happens directly following SYK activation in response to active sTLT1 peptide. Moreover, ERK interestingly showed the same trend as of BTK and SYK (Figure 8.2.4A). To examine the functional significance of SYK inhibition, the level of secreted TNF-α in differentiation media was estimated in the presence or absence of SYK antagonist. TNF-α level reduced in a dose dependent manner ($p<0.001$) with SYK antagonist in active peptide treated group while it remains unaltered in response to scramble peptide (Figure 8.2.4B). These observations indicate that sTLT1 active peptide initiates a SYK-BTK-MEK-ERK axis to promote inflammation through TNF-α secretion.

8.2.2.5. Secretion of TNF-α is derceased by BTK antagonist

To confirm further the involvement of BTK-MEK-ERK axis, cells were treated in the absence or presence of BTK inhibitor, Ibrutinib, along with active peptide or scramble. Immunoblot demonstrated reduction of BTK activation by Ibrutinib. The normal pattern of activation even in the presence of BTK inhibitor in the cell culture indicates that SYK remains upstream to this axis. Ibrutinib treated cells did not show any activation of ERK suggesting that ERK remains downstream to SYK, BTK and MEK (Figure 8.2.4C). Furthermore, to check the downstream influence of this inhibition we measured secreted TNF-α from cells treated with active peptide and scramble along with BTK antagonist. TNF-α secretion decreased in a dose dependent manner ($p<0.001$) with Ibrutinib (Figure 8.2.4D). This data indicated the involvement of NF-kB-p65 and IKK-β in the signalling since the same cascade activates TNF-α secretion from macrophages. Thus the above observations suggested that sTLT1 acts through the major signalling axis consisting of SYK-BTK-MEK-ERK.

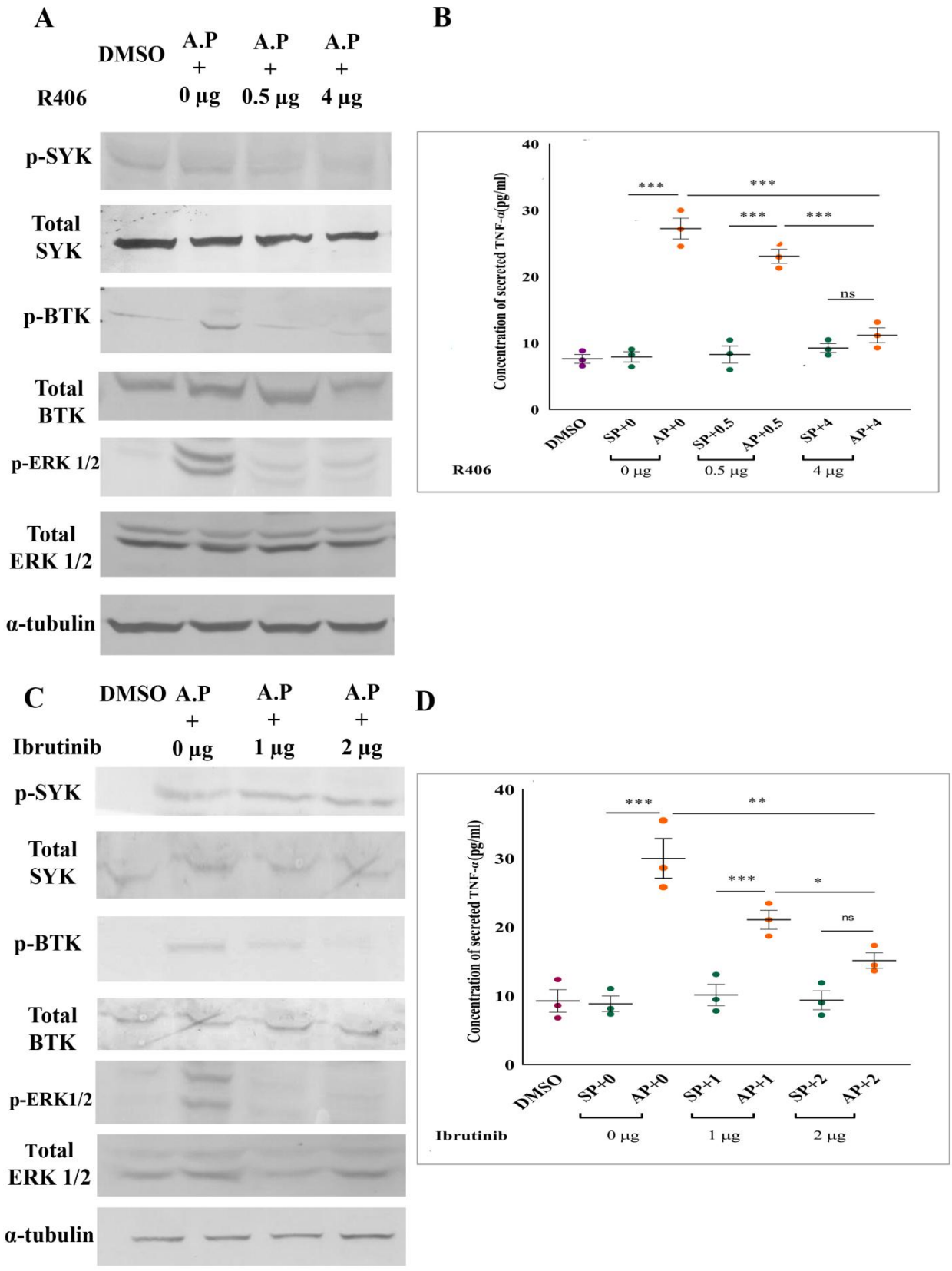

Supplementary figure 4

Figure 8.2.4. Decreased TNF-α secretion by SYK antagonist, R406 and BTK antagonist, Ibrutinib from differentiated macrophages.

Representative immuoblots with phosphorylated SYK, BTK and ERK antibodies from the whole cell lysates of the macrophage treated either with R406 (A) or Ibrutnib (C). Levels of secreted TNF-α (pg/ml) in the media are also calculated upon stimulation of the cells either with scramble (green dots) or active peptide (yellow dots) in absence of presence of the inhibitors (B, D). Levels of TNF-α after DMSO treatment are represented as violet dots in both the scattered plots. Asterisk (*) denotes significant difference at $p<0.05$ (Das et al, Cli. Sc. 2019).

8.2.2.6. sTLT1 stimulates secretion of TNF-α in THP1 derived macrophages as well as in apoE$^{-/-}$ mice

Differentiated macrophages from THP1 monocytes treated with synthetic peptides (sequence 1 and sequence 2) showed thrice the level of secreted TNF-α in seq1 (active peptide) treated group compared to scramble treated group. Release of TNF-α from differentiated macrophages was induced by sTLT1 active peptide compared to that of scramble one. To connect this finding with atherosclerosis *in vivo*, plasma levels of sTLT1 and TNF-α were measured in apoE$^{-/-}$ mice fed with HCD and compared to those of chow fed wild type mice of the same strain for 45 and 60 days. Histopathological analysis (Haematoxylin-Eocene staining) of the cross-section of the aorta shows plaque development after 45 days, which progressed to advanced level of occlusion after 60 days in HCD fed mice (Figure 8.2.5, Panel D). As mentioned earlier, induction of sTLT1 active peptide significantly increase TNF-α secretion in macrophage cells (Figure 8.2.5E, $p=0.0001$). So, to correlate further sTLT1 and TNF-α was measured in mice plasma. Plasma levels of sTLT1 increased significantly (amount ≈ 3500pg/ml, $p<0.05$) in HCD fed apoE$^{-/-}$ mice after 45 days (AEHCD45) and also increased further after 60 days (≈ 6000 pg/ml, $p<0.001$; AEHCD60) compared to chow fed mice (Figure 8.2.5F). Interestingly, sTLT1 level in chow fed apoE$^{-/-}$ mice (AEC60) was less ($p<0.001$) compared to that of HCD fed apoE$^{-/-}$ after 60 days (AEHCD60). Alternatively, the level of sTLT1 was similar in wild type mice either fed with chow (WTC60) or HCD after 60 days (WTHCD60). However, sTLT1 level differs significantly ($p<0.001$) between HCD fed wild type (WBHCD60) and apoE$^{-/-}$ mice after 60 days (AEHCD60).

For further understanding plasma TNF-α level was also measured in wild type and apoE-/- mice either fed with chow or HCD after 45 and 60 days. Interestingly, HCD fed atherosclerotic mice with distinct plaques had the highest level of TNF-α at day 60 ($p<0.05$; AEHCD60) compared to that of chow fed wild type mice (WTC60) or HCD fed wild type

mice (WTHCD60) or chow fed apoE-/- mice (AEC60, Figure 8.2.5G). As HCD fed apoE$^{-/-}$ mice showed an increased expression of both sTLT1 and TNF-α, it is obvious that sTLT1 induction in apoE$^{-/-}$ mice correlated with high TNF-α level and thereby indicates the maintenance of inflammation in mice as well as sTLT1 induced macrophages.

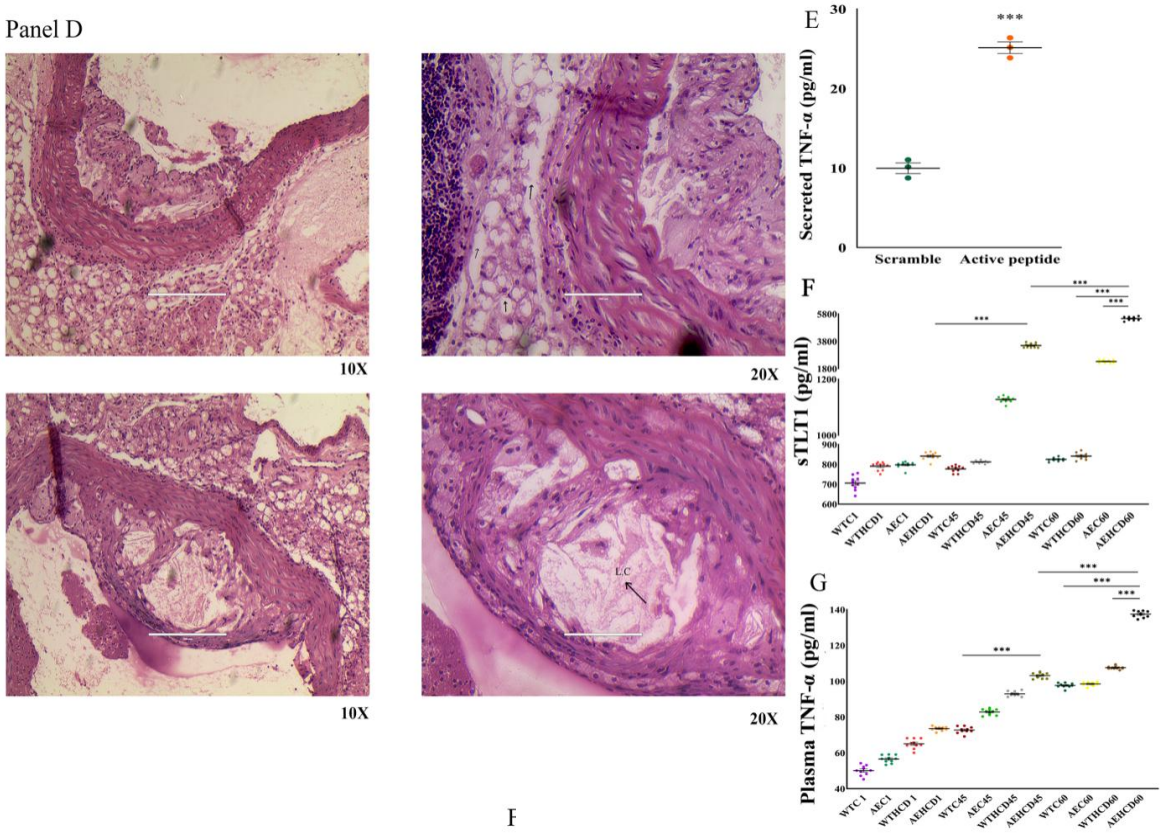

Figure8.2.5. Histopathology and biochemical studies indicate sTLT1 is connected to advancement of plaques through inflammation.

Histopathological images of aortic arches (cross sections) in apoE$^{-/-}$ mice (n=10) fed with HCD for 45 days (upper panel) and 60 days (lower panel) in 10X and 20X magnifications. Arrows indicate the lipid laden cells and L.C. designates necrotic lipid core (Panel D).

Scattered plots showing the concentration of secreted TNF-α (pg/ml) from macrophages treated with sTLT1 active peptide (yellow dots) and its scramble sequence (green dots) (E). Plasma concentration of sTLT1 (F) or TNF-α (G) in mice fed with chow or HCD after 45 days and 60 days indicating the inflammatory state of the mice in plaque forming stages. Asterisk (*) denotes significant difference at $p<0.05$. Abbreviations. WTC1, WTC45, WTC60: wild type mice fed with chow for 1 day, 45 days and 60 days respectively; WTHCD1, WTHCD45, WTHCD60: wild type mice fed with high cholesterol diet for 1 day,

45 days and 60 days respectively; AEC1, AEC45,AEC60: apoE$^{-/-}$ mice fed with chow for 1 day, 45 days and 60 days respectively; AEHCD1, AEHCD45, AEHCD60: apoE$^{-/-}$ mice fed with high cholesterol diet for 1 day, 45 days and 60 days respectively (Das et al, Cli. Sc. 2019).

8.2.3. Conclusion

Our study established that sTLT1, a platelet secreted protein binds directly to the SYK domain of FcγRI and initiates a mitogen activated protein kinase (MAPK) based signalling. Binding of sTLT1 with FcγRI activates SYK which itself is a tyrosine kinase. This activation is mediated by the intracellular ITAM motif of FcγRI. SYK activation via tyrosine phosphorylation causes the activation of BTK. BTK activation initiates further downstream cascades including MEK/ERK/NF-kB signalling. Nuclear NF-kB activation is the key event in this whole pathway. This activation leads to the increased expression and secretion of a major pro-inflammatory cytokine TNF-α in blood. Increased secretion of TNF-α in response to increased plasma sTLT1 proves direct cause-effect relation between these two proteins relating sTLT1 with the maintenance of inflammation as well as atherosclerosis.

CHAPTER 3

IDENTIFICATION OF PLASMA PROTEINS IN CORONARY ARTERY DISEASE AND THEIR ROLE IN ATHEROSCLEROSIS

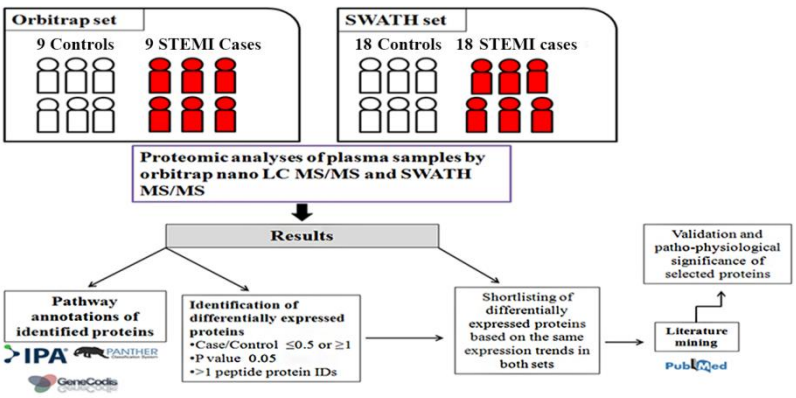

8.3.1. Introduction

Plasma is the liquid matrix in which different components of blood float. It mainly consists of blood cells which secrete several proteins in response to different stimuli. As a result, plasma carries several proteins which play definite roles to maintain the normal physiological environment in our body. As plasma consists of proteins important in every physiological function, it has always been a rich source to identify proteins responsible for any pathophysiological condition or disease. But, to identify the huge number of proteins or peptides present in plasma one needs a global and robust approach. Since, the beginning of this decade, clinical and translational research started to use proteomics as a tool for identifying novel and unidentified disease specific proteins in a global approach.

Proteomics is a tool to identify a large number of proteins in a specific sample and at a specific time point. It uses advanced mass spectrometers and chromatographic technique to yield a large number of proteins from a minimum amount of sample. Plasma, as it contains huge number of proteins, yields very convincing results through proteomic techniques. Plasma proteomics is a very common approach now for clinical biomarker studies as well as cellular studies to narrow down the pathways involved in the examined sample. Previous studies on cardiovascular disease identified several proteins important for atherosclerosis like FABP; several complement factors, numerous immunological proteins through advanced proteomic approach (Lygirou V et al,J.Trans.Med,2018)). But, there were very few studies on plasma proteomic changes in STEMI, NSTEMI and UA patients compared to healthy control subjects separately. In addition to this, little was known about the uniqueness of atherosclerotic mechanism in ST segment elevation myocardial infarction (STEMI), NSTEMI as well as UA compared to normal ACS or CAD patients.

So, here in this chapter we demonstrate plasma proteome changes in STEMI (part I), NSTEMI and UA (part II) subjects through proteomics approach respectively. Furthermore, we validated in larger sample size and and established the role of some of the proteins in atherosclerosis, STEMI as well as CAD.

8.3.2. Results

Total proteins identified from the STEMI, NSTEMI, UA and control samples were enlisted. Common proteins were identified manually between the experimental groups. The following

diagram summarizes the number of unique proteins identified in each groups and common proteins among them.

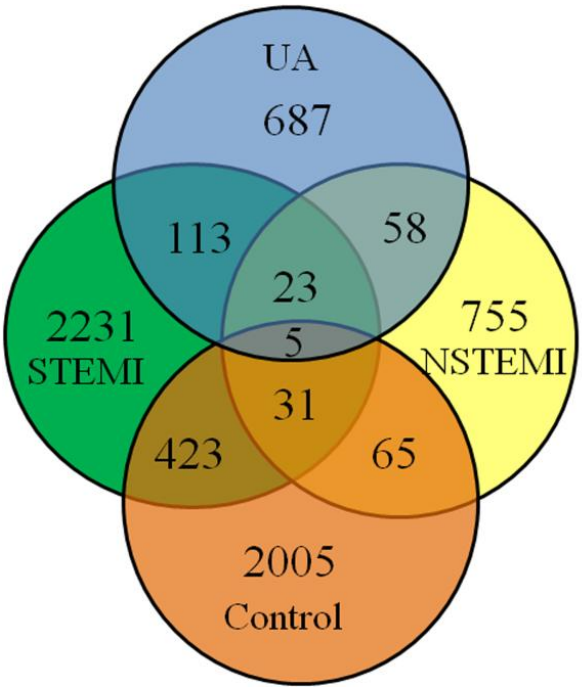

Figure 8.3. Venn diagram showing number of unique proteins identified in each group and the common proteins among them

PART I (STEMI)

8.3.2.1. Protein identification using Orbitrap mass spectrometer

By means of Orbitrap MS analysis of plasma samples collected from healthy control subjects and STEMI patients (demographic information are given in Table 8.3.1), we identified 2654 (blue circle) and 2428 (red circle) proteins, respectively, as shown in Figure 8.3.5A. Out of these 423 proteins (intersection in the Venn diagram) were common between the two groups (Figure 8.3.5A). Using technical triplicates of pooled samples for mass analysis (n=9 in each set; online file S2); quantification of these identified proteins was performed using Sieve v2.2 software which indicated differential expression of only 13 proteins ($p<0.05$). The proteins increased or decreased in the plasma include Cytoplasmic Actin 2, PGLYRP2 (up), ABCA5 (up), AZGP1 (down), Anti-thrombin 3, Complement C8-β chain, Calicin (down), Transthyretin, MyosinVII, Complement C1q subunit A, Complement C9, Complement C4A and C17 Open Reading Frame 57 (C17ORF57) (down). Probability values (Y axis) and logarithmic fold change (X axis) for proteins identified with Orbitrap were calculated using

Sieve v2.2 software (Thermo-scientific) which indicated a normalized distribution in a volcano plot (Figure 8.3.5B). Red dots in the plot indicate all the identified proteins with excellent scores (above threshold value) whereas black dots correspond to the proteins with low scores (below threshold value). Principal component analysis indicated that inter-run variability was minimum (Figure 8.3.5C). All the proteins identified by Orbitrap and its replication study are shown in online table file S2and online table file S3 respectively. Identified proteins in STEMI and healthy control were analyzed by Cytoscape to point out several inter-connections relevant to RCT (Figure 8.3.1 and Figure 8.3.2).

Table 8.3.1. Demographic parameters of subjects recruited for Orbitrap experiments

Variables	Control subjects (n=9)	STEMI subjects (n=9)	P value
Age	47.22±1.39	47.22±1.39	1 (ns)
Sex(M/F)	M	M	NA
Total cholesterol (mg/dl)	157.56±8.47	220.67±6.66	<0.0001 (s)
HDL cholesterol (mg/dl)	47.4±1.8	27.89±8.84	<0.0001 (s)
LDL cholesterol (mg/dl)	95.11±6.85	136±8.84	0.0021 (s)
Triglyceride (mg/dl)	130.78±10.49	191±4.87	<0.0001 (s)
SBP (mm/Hg)	120±1.67	138.44±7.89	0.04(s)
DBP (mm/Hg)	81.11±2.61	81.77±2.44	0.8558 (ns)
Smoking status	none	none	NA

a. Values are expressed as mean±SEM and comparison of groups was done by unpaired t test. $p<0.05$ was considered as significant

b. NA= Not applicable

c. ns= not significant

d. s= significant

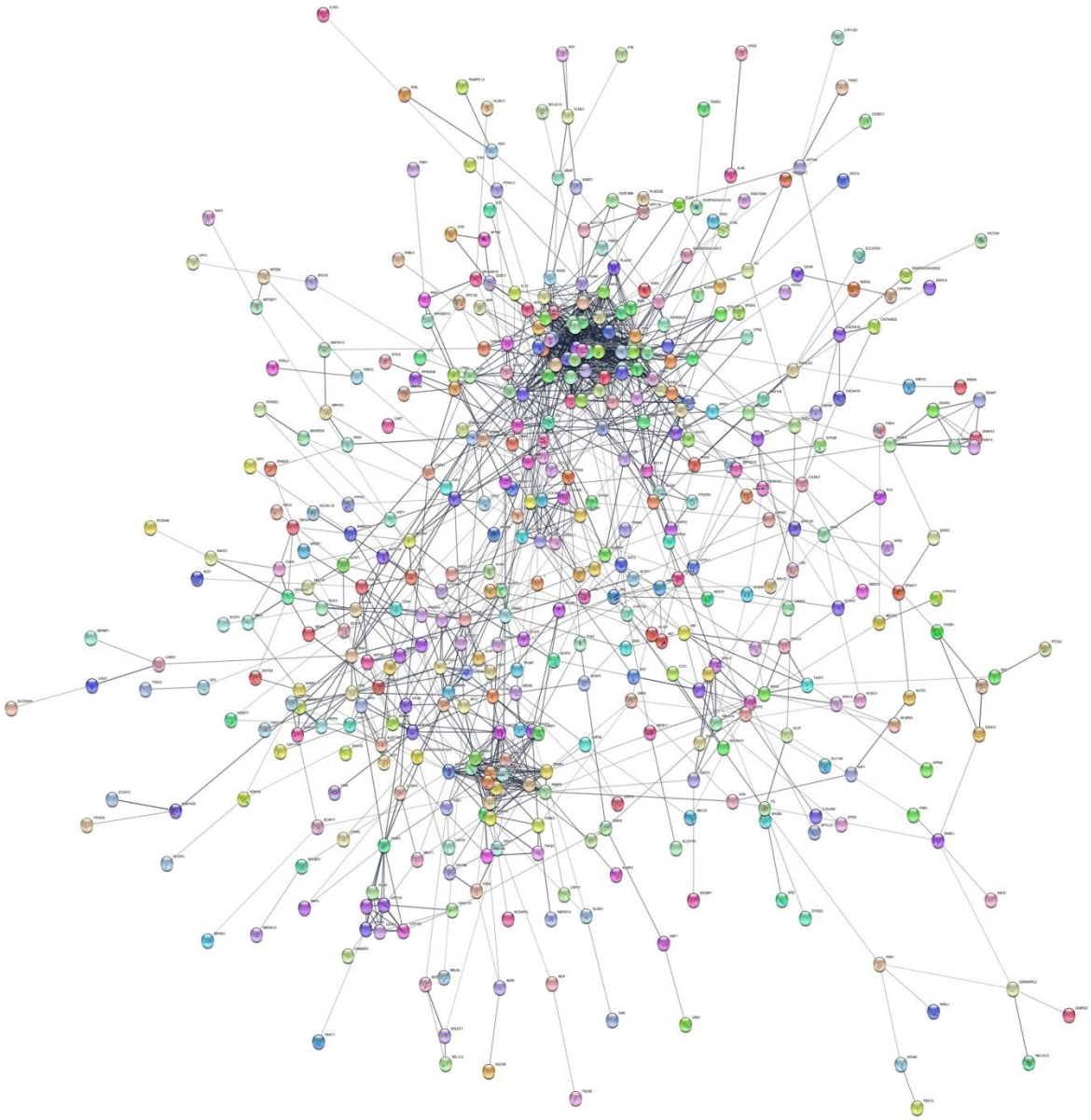

Figure 8.3.1. Network map of proteins identified in STEMI subjects

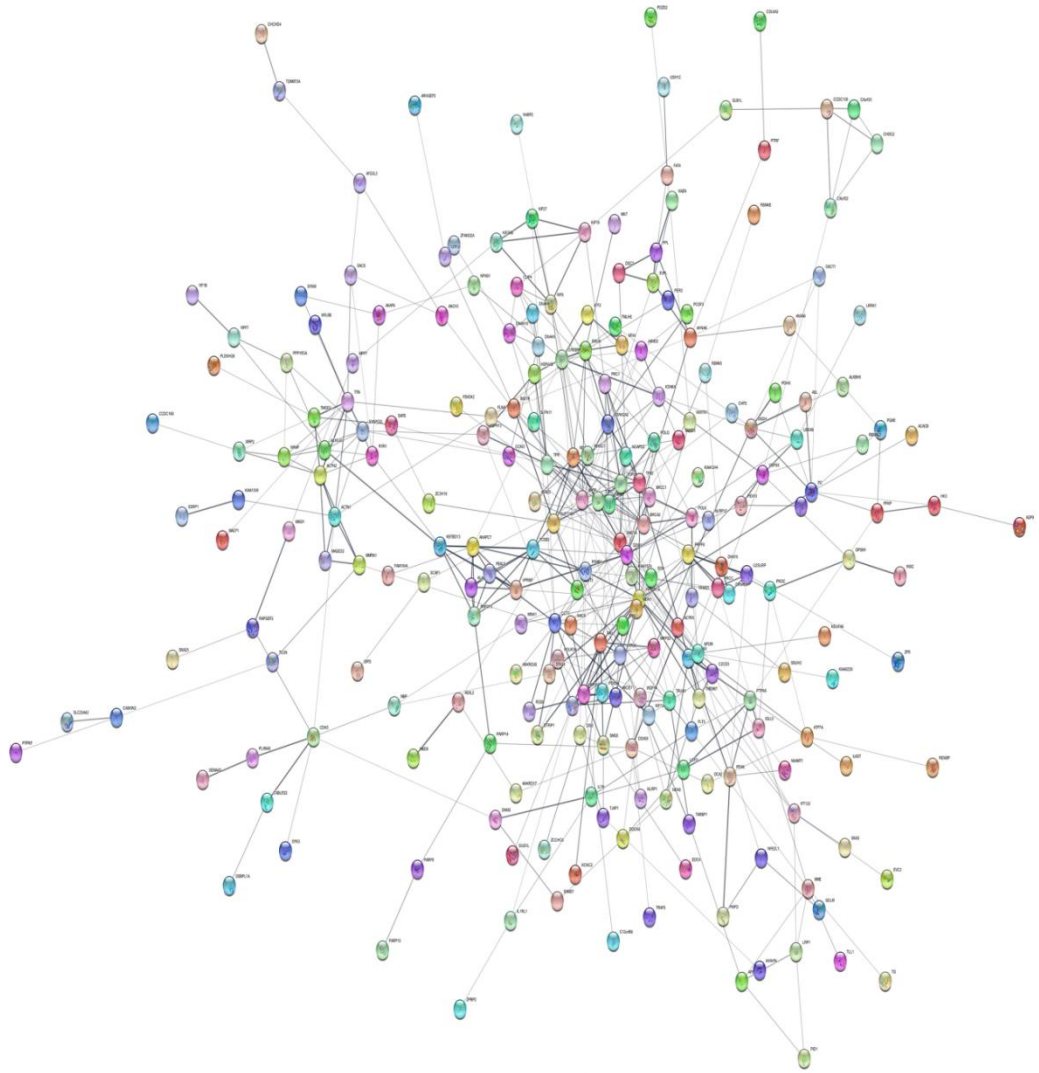

Figure 8.3.2. Network map of proteins identified in control subjects

8.3.2.2. Quantitative proteomics by SWATH-MS

Quantitative proteomics by SWATH-MS/MS was performed to narrow down the number of proteins based on their probability value (<0.05) to help with subsequent validation. Initial quantitative proteomics study gave evidence of the alteration of 64 proteins. Among the altered proteins, 26 proteins were decreased and 38 were increased (p value <0.05, $t \leq \pm 6$) (online table S1). The fold change, logarithmic fold change and probability value were plotted in a heat map in an increasing order indicated by color green to red. The Euclidean distance was plotted along the vertical axis to show the degree of neighbourhood among the identified proteins (Figure 8.3.5D). Some of the significantly decreased plasma proteins were relevant to atherosclerosis. They are Lipopolysaccharide-binding protein (FC=0.265,p=4.95E-06), alpha-1-acid glycoprotein-1(FC=0.434, p=0.0002), Galectin-3

binding protein (FC=0.417, p=0.0007), Zinc alpha-2-glycoprotein (ZAG/AZGP1) (FC=0.575, p=0.005), Calicin (FC=0.495, p=0.02), Hepatitis A Virus cellular receptor protein 2 (FC=0.319, p=0.05) etc. On the other hand, some of the proteins increased in the plasma were also relevant to RCT and inflammation. They were ApolipoproteinB-100 (FC=1.94,p=3.68E-05), Repetin (FC=2.08, p=0.002), Apolipoprotein-A-IV (FC=1.87, p=0.002) and N-acetylmuramoyl-L-alanine amidase (PGLYRP2) (FC=1.74, p=0.005). Data distribution is shown in a Volcano plot to clarify that logarithmic fold change of proteins are in normal distribution (Figure 8.3.5E). Altered proteins in SWATH were again analysed by Cytoscape to yield inter-connecting network maps which indicated the relation of these proteins with RCT (Figure 8.3.3). Demographic information of recruited individuals is provided in Table 8.3.2.

Table 8.3.2. Demographic parameters of subjects recruited for IDA and SWATH experiments

Variables	Control subjects (n=18)	STEMI subjects (n=18)	P value
Age	46±0.89	46±0.89	1 (ns)
Sex(M/F)	9/9	9/9	NA
Total cholesterol (mg/dl)	146.22±5.37	221.06±4.54	<0.0001 (s)
HDL cholesterol (mg/dl)	49±1.204	28.95±0.92	<0.0001 (s)
LDL cholesterol (mg/dl)	92.94±4.51	138.72±6.2	<0.0001 (s)
Triglyceride (mg/dl)	126.5±6.01	191.53±3.18	<0.0001 (s)
SBP (mm/Hg)	118.33±1.46	133.94±4.67	0.0031(s)
DBP (mm/Hg)	79.17±1.63	82.28±1.44	0.1619 (ns)
Smoking status	none	none	NA

a. Values are expressed as mean±SEM and comparison of groups was done by unpaired t test. $p<0.05$ was considered as significant
b. NA= Not applicable
c. ns= not significant
d. s= significant

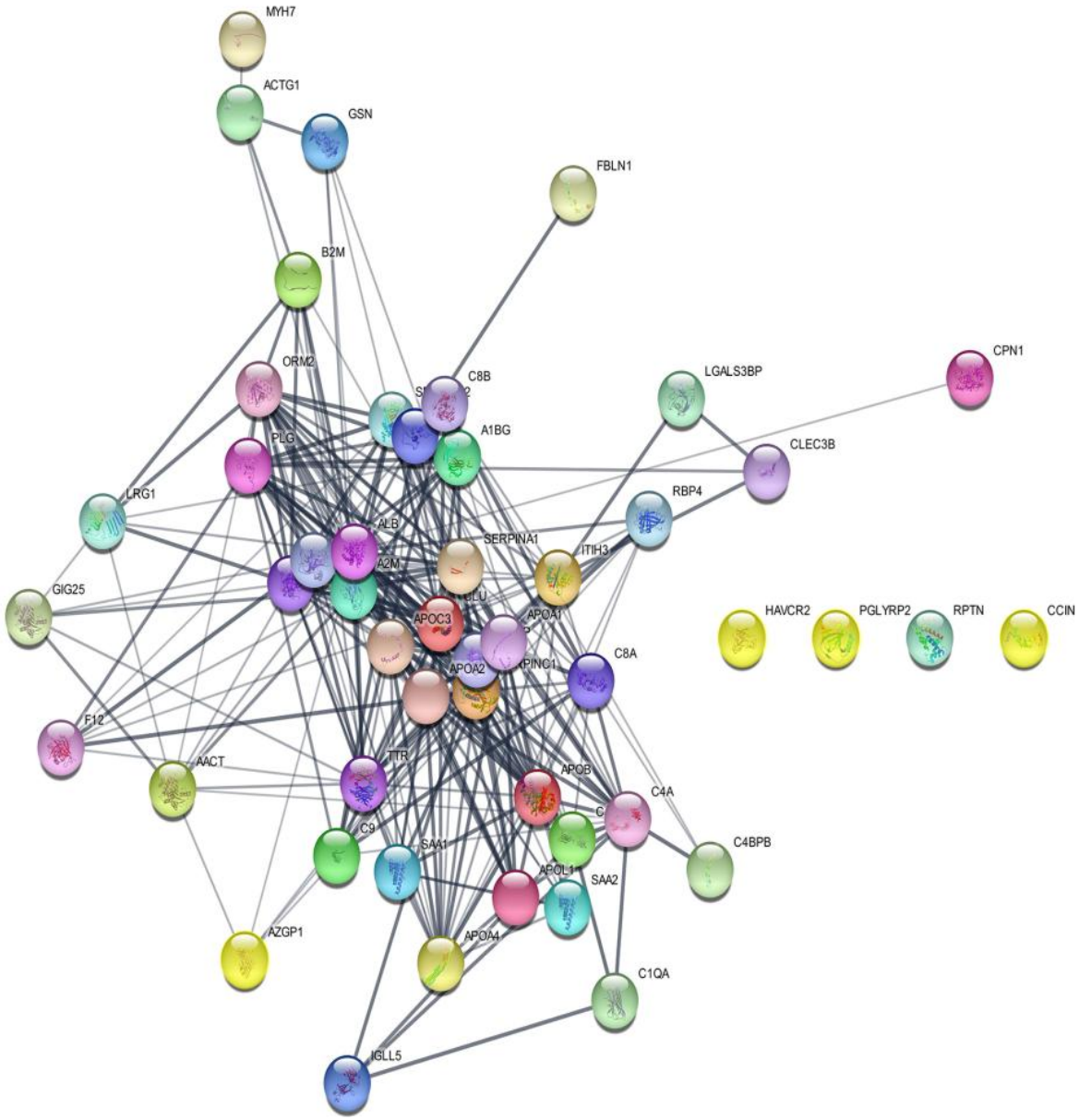

Figure 8.3.3. Network map of proteins identified by SWATH MS/MS

8.3.2.3. Enrichment of Biological Processes (BP) and KEGG pathways using Gene Ontology/ GeneCodis and Panther

As, Cytoscape analyses of both Orbitrap and SWATH identified proteins led to the identification of pathways related to RCT and inflammation; we analysed the protein lists more extensively by GeneCodis and PANTHER (http://geneontology.org/page/go-enrichment-analysis) with reference to total human proteome (Uniprot Homo sapiens 06.06.2012 release). The results indicated significant enrichment of 112 biological processes (BP) and 13 reactome pathways for proteins decreased in plasma of STEMI subjects ($p<0.05$)

in SWATH-MS. Similarly, 250 BP and 19 reactome pathways were observed to be significantly enriched ($p<0.05$) with proteins increased in SWATH-MS run. All results shown with and False Discovery Rate <0.05 (Fisher's Exact with FDR multiple test correction). Enrichment analysis for the differentially expressed proteins obtained in SWATH-MS using PANTHER v13.1 (http://pantherdb.org/geneListAnalysis.do) pointed out significant enrichment of 13 KEGG pathways and 9 biological processes (BP) for proteins increased in SWATH. Similarly, 6 KEGG pathways and 10 BP were enriched significantly with proteins decreased in SWATH run (Figure 8.3.4, see online submission).

Interestingly, GeneCodis (http://genecodis.cnb.csic.es/) analysis of proteins not common between healthy individuals and STEMI subjects revealed a significant enrichment of 6 and 9 functional protein groups, respectively, including ABC transporter family. The unique ABC family proteins for STEMI subjects were ABCA6, ABCA10, ABCA12, ABCA5, ABCB11, ABCB9, ABCC1, ABCC12, ABCC7, ABCC8, ABCD1, and ABCG8.

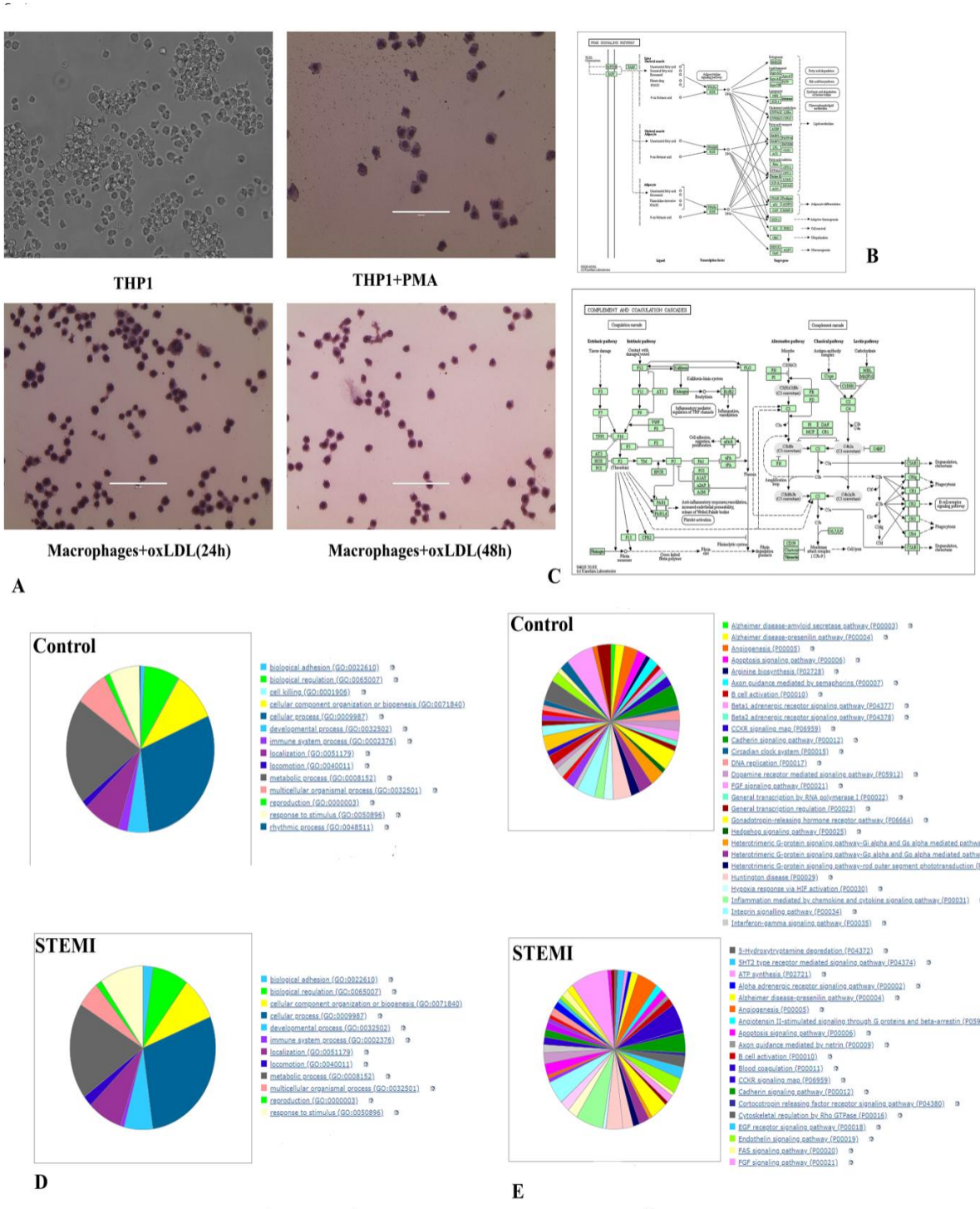

Figure 8.3.4 A. Microscopic images of THP1 cells before and after differentiation into foam cells. B and C. PPAR signalling pathway and complement and coagulation signalling pathway as obtained from pathway enrichment analysis. D. Pie chart showing biological pathways enriched in control and STEMI samples by orbitrap. E. Pie chart showing signalling pathways enriched in control and STEMI samples by orbitrap.

8.3.2.4. Pathway enrichment analysis by IPA

Ingenuity Pathway Analysis (IPA) was conducted with data obtained by SWATH-MS with reference to the set of regulated proteins to detect enrichment of the biological pathways, downstream signalling molecules as well as enrichment of related diseases with the proteins increased and decreased in STEMI plasma. Downregulated proteins revealed significant enrichment of 25 pathways including coagulation activation pathways, acute phase response, intrinsic and extrinsic prothrombin signalling, clathrin mediated endocytosis and interleukin pathways etc. ($p<0.05$) (Figure 8.3.5F). 38 proteins which were increased in the plasma indicated significant enrichment of 22 KEGG pathways. All the enriched pathways were plotted based on their z score to indicate their degree of significance and were found to be matching with previously stated probability calculation (Figure 8.3.5G). Interestingly, the relevant pathways identified in the study involved the fat digestion and absorption, PPAR signalling pathway, IL-12 induction and production cascade in macrophages, complement activation, activation of scavenger receptors, acute phase response signalling, intrinsic and extrinsic pro-thrombin signalling, activation of IL-10 and other cytokine secretion from related immune cells, activation of coagulation pathway, LXR/RXR and atherosclerosis signalling pathway ($p<0.05$, Figure 8.3.5H). These enrichments were further validated through z score statistics. All the canonical pathways found in the up SWATH and the down SWATH were compared using the IPA and plotted in a heat map according to their score and negative logarithmic p values. Interestingly, most of the highest scoring canonical pathways like LXR/RXR pathway, coagulation system, interleukin pathways, and inhibition of matrix metalloproteinases were associated with cardiovascular diseases and atherosclerosis (Figure 8.3.5I).

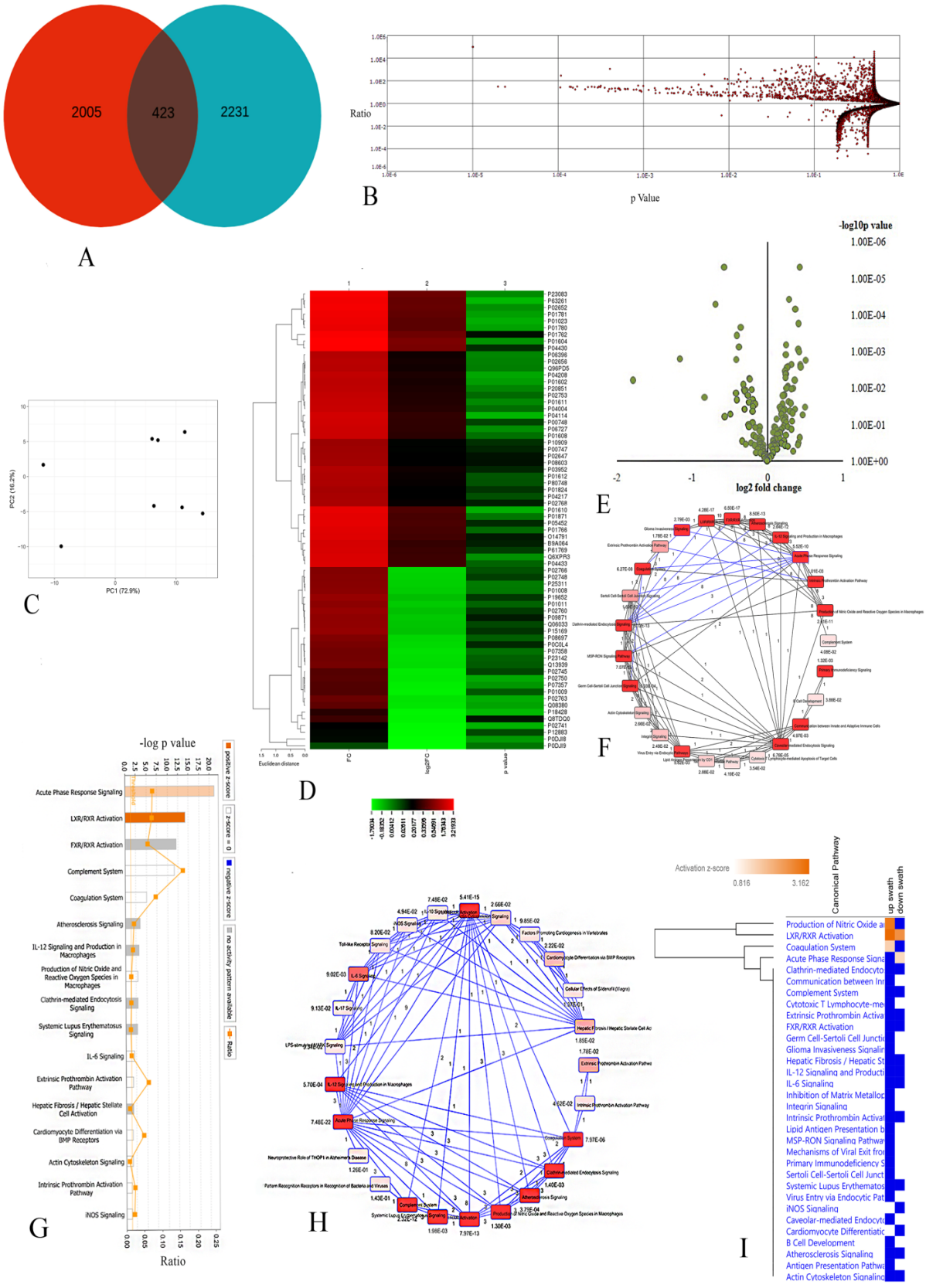

Figure 8.3.5. Identification and quantification by mass spectrometry analysis

A) Venn diagram shows the total number of proteins identified by orbitrap mass spectrometry in healthy controls (blue shade) and subjects with STEMI (red shade). The intersection denotes the number of common proteins between these two groups. B) Volcano plot indicates the axial distribution of identified proteins from orbitrap runs. Red dots represent proteins above the appointed threshold value as well as low FDR and black dots represent the proteins with high FDR. C) Principal component analysis of orbitrap runs was performed to show the inter run variability. D) Fold change (red=up and green=down), logarithmic fold change and p values (green indicates $p < 0.05$) of altered proteins were plotted in a heat map to show the clustering of differentially expressed proteins in SWATH through Euclidean distance. Clustering was done on fold change and indicated along the left vertical axis of the heat map whereas the right vertical axis shows the UniProt accession numbers of proteins included in the analysis. E) Volcano plot of SWATH identified proteins indicates the axial distribution of significant proteins (green dots) above a threshold p value. Higher the dot in the Y axis ($-\log_{10}p$) the more significant is the protein. F) Enrichment map of statistically significant pathways of downregulated proteins identified by SWATH $^{+}$. G) Statistically enriched pathways from the list of differentially expressed proteins in SWATH MS were plotted according to their z score (Yellow bars = high positive Z score). H) Enrichment map of statistically significant pathways of upregulated proteins identified by SWATH $^{+}$. I) Heat map shows comparative pathway mapping according to their score and p value. Pathways were clustered according to Euclidian distance.

$^{+}$The edges are represented by the number of common genes among the nodes and deeper shade represents higher significance in both the maps (F,H). Threshold p value is <0.05.

Analysis of the profiles obtained by orbitrap mass spectrometer revealed significant enrichment for 26 and 25 KEGG pathways with proteins annotated from control and STEMI samples, respectively. Figure 8.3.6A represents a heat map plotted according to the enrichment score of biological functions including atherosclerosis, cardiovascular disease, organ injury, metabolic diseases etc. in control samples (the deeper shade indicating a higher enrichment score). Figure 8.3.6B demonstrates a pathway enriched in cardiovascular disease from the aforementioned module of IPA analysis which includes Calicin and PGLYRP2; thus, providing further logic to validate these proteins through biochemical methods. Figure 8.3.6C shows significantly enriched pathways plotted according to their z score signifying

their relevance to the indicated signalling systems. Heat map constructed on z-scores of the biological functions in STEMI exhibits that the most significant biological functions were related to atherosclerosis (Figure 6.6D). Bar diagram plotted according to the z score of the enriched pathways of STEMI samples again indicated association with atherosclerosis (Figure 8.3.6E). Figure 8.3.6F showed the pathways identified in STEMI as nodes through IPA analyses indicating the enrichment of several important signalling pathways in atherosclerosis; the edges represent the common genes between the connecting nodes with indicated p values and deeper shade indicates higher statistical significance of the node. Interestingly, mass spectrometric analyses both by Orbitrap and SWATH identified some common pathways including IL-12 signalling, atherosclerosis signalling, coagulation system activation, thrombin activation pathways, and pathways related to chronic inflammation in plasma of healthy control and STEMI subjects.

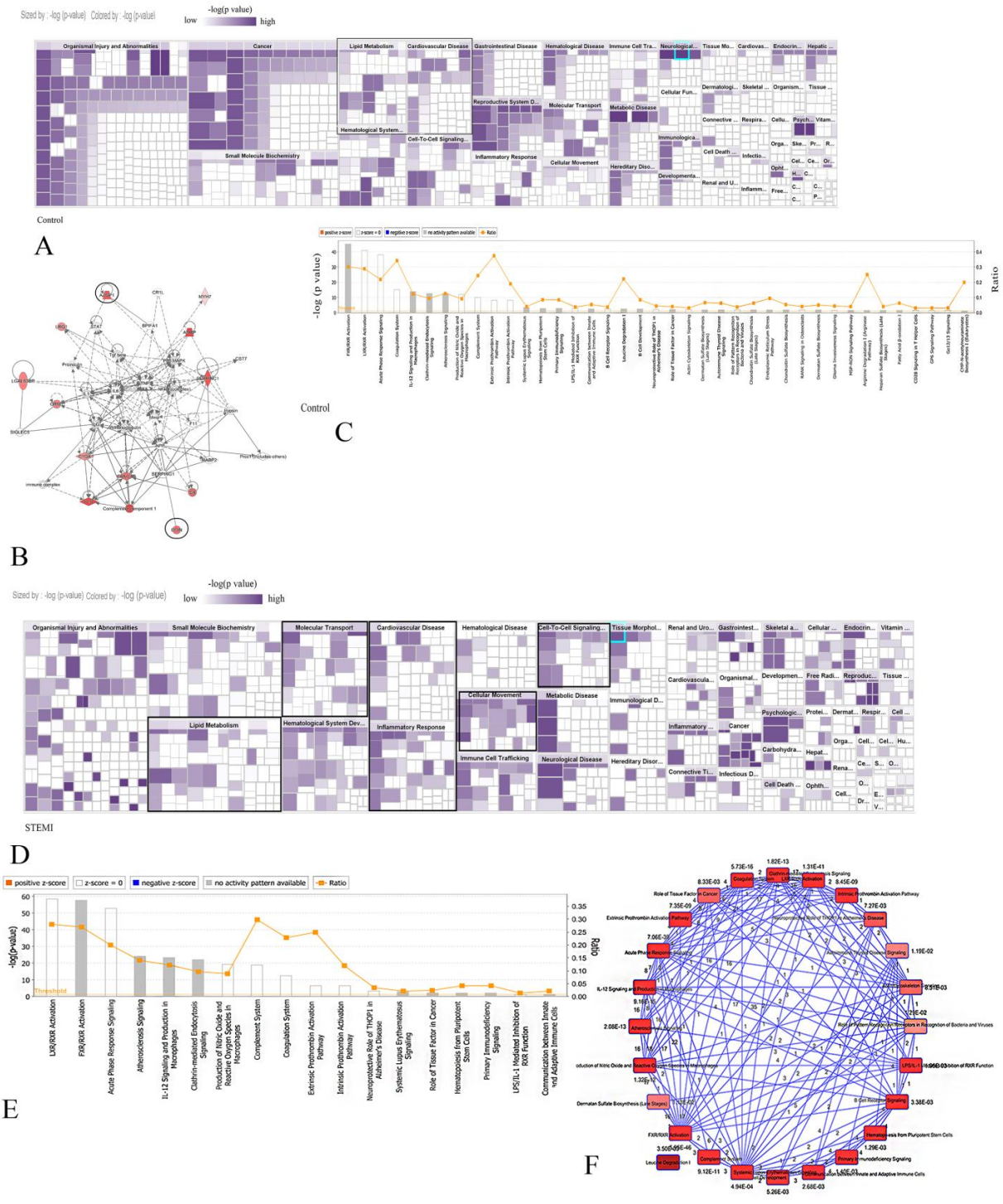

Figure 8.3.6. Pathway enrichment of proteins identified by orbitrap mass spectrometry of healthy control and STEMI subjects.

A) Heat map (plotted according to the z score) of proteins identified in control samples showing the pathways related to diseases. Deeper shade indicates more significant pathways ($p<0.05$). B) Pathway map related to cardiovascular diseases as found in (A). Proteins encircled (Calicin and AZGP1) are also validated by Western blot (Figure 8.3.7). C)

Statistically enriched pathways were plotted according to their z score and negative logarithmic p value using proteins identified in healthy control. D) Heat map of proteins identified in STEMI samples. E) Statistically enriched pathways plotted according to their negative logarithmic p value and z score ($p<0.05$) using the proteins identified in STEMI samples. F) Interaction of all the pathways involving proteins identified in STEMI samples (p values and number of common proteins among pathways were indicated; $p<0.05$).

8.3.2.5. Proteins altered in STEMI are related to reverse cholesterol transport

Some of the relevant proteins identified by Orbitrap mass analysis were chosen on their involvement of atherosclerotic pathways and validated by immunoblotting which indicated significant decrease of C17ORF57 (0.57-fold, $p<0.05$, n=6) and increase of ABCA5 (0.54-fold, p=0.003, n=9) in STEMI subjects in comparison to healthy controls (Figure 8.3.7, panel A). Interestingly the level of ABCA5 was only restored in post PTCA and it was found to be comparable to healthy control (0.59-old, p=0.003, n=9) after angioplasty. From our SWATH analyses, three differentially expressed candidate proteins, viz. AZGP1, PGLYRP2, and Calicin (Figure 8.3.7, panel B), were selected for further study. Immunoblotting of plasma samples showed about 0.59-fold (p=0.003, n=9) decrease in Calicin level in STEMI patients compared to control subjects. However, the levels of Calicin increased significantly (p=0.004) 48h post PTCA compared to STEMI subjects. On the contrary, PGLYRP2 increased by 1.73-fold in STEMI in comparison to healthy controls (p=0.002, n=9). The levels of zinc-α2 glycoprotein, a novel adipokine (AZGP1) decreased significantly (0.617-fold, $p<0.0001$, n=9) in STEMI subjects compared to healthy controls. Interestingly, PPARɣ was also found to be decreased by 0.59-fold (p=0.037, n=6) in STEMI patients when compared to healthy control indicating a shift of balance towards the disease through induction of inflammation and misbalance of RCT (Figure 8.3.7, panel B). All these validated proteins were directly or indirectly connected to RCT. It was interesting to note that plasma level of HAVCR2 decreased ($p<0.05$, n=3) in STEMI compared to control subjects as also observed in SWATH analysis. However, the levels of HAVCR2 in plasma measured by ELISA were not restored in subjects 48h post-PTCA (Figure 8.3.7C). A list of validated proteins and the corresponding fold changes are depicted in Table 8.3.3.

Table 8.3.3. Fold change of validated proteins by western blot at a glance

Protein	**Fold change(p value≤0.05)**
Orbitrap	
C17ORF57	0.57(down)
ABCA5	0.54(up)
SWATH MS/MS	
Calicin	0.59(down)
PGLYRP2	1.73(up)
AZGP1	0.617(down)

a. Fold change of validated proteins in STEMI subjects compared to control subjects obtained as in immunoblot analyses.

8.3.2.6. AZGP1 binds to the foam cell surface through CD36

Based on text mining and pathway interaction analysis related to cardiovascular diseases (Figure 8.3.7D) it appeared that AZGP1 may interact with CD36 based on the common interacting domains shared in their structure. In-silico interaction analyses through PatchDock and ClusPro between AZGP1 and CD36 ensured an energy favourable state of the docking. However, the most energy favourable structure was chosen from the previous docking experiment, and the interacting chains were determined by HADDOCK 2.2 (Figure 8.3.7E). Highest negative free energy interacting model predicted that AZGP1 and CD36 may possibly interact through predominant weak interactions in between the ligand and the receptor. In order to confirm our observation, we performed a co-immunoprecipitation experiment using cell lysates of macrophage and foam cell and our results indeed showed that CD36 binds with AZGP1 (Figure 8.3.7F).

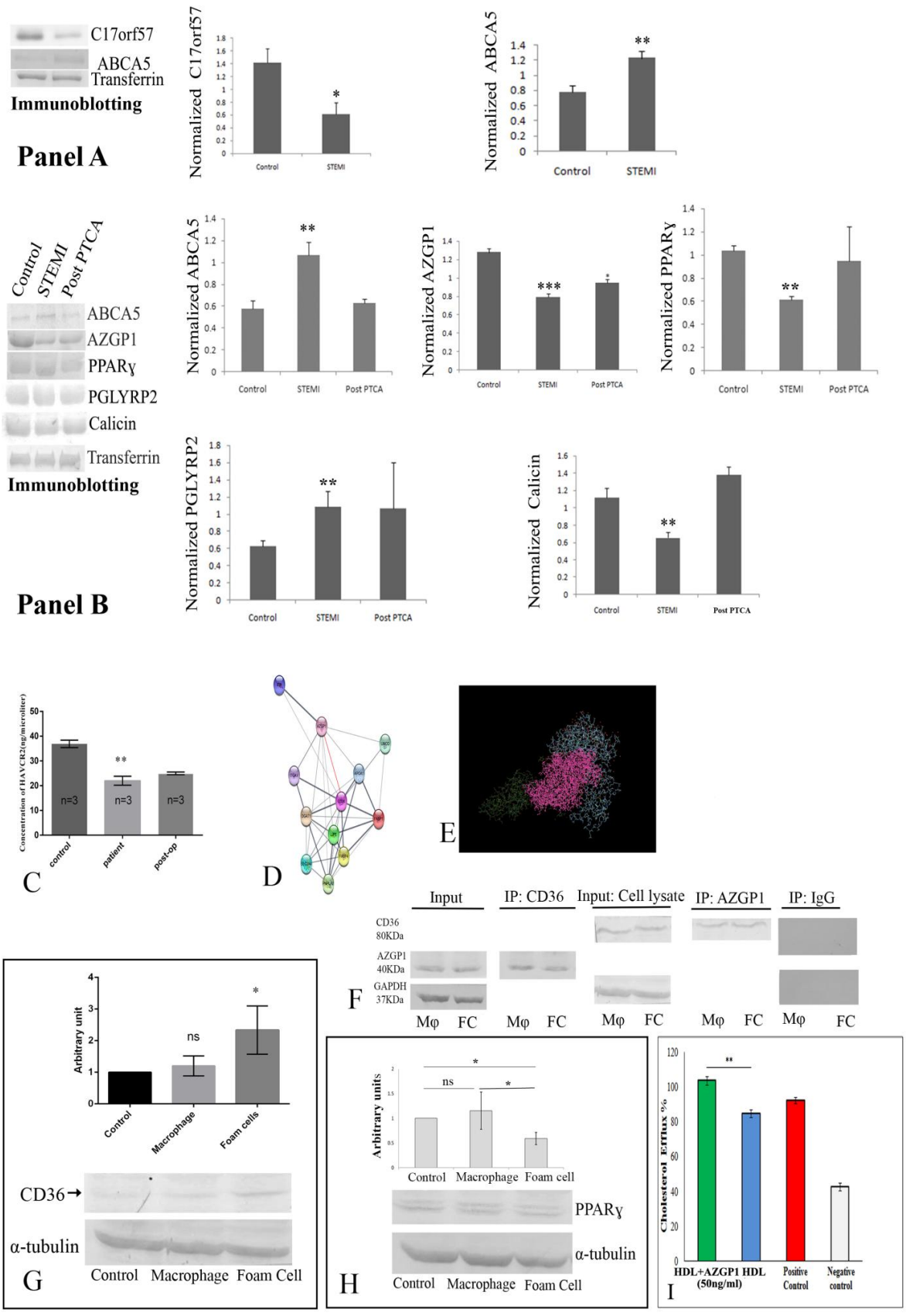

Figure 8.3.7. Validation, quantification and in-silico analysis of proteins

Panel A represents western blots showing the reduction of C17ORF57 and increase of ABCA5 in plasma of STEMI subjects. Panel B showing altered level of ABCA5, AZGP1, PPARγ, PGLYRP2 and Calicin in control, STEMI and post-PTCA subjects by western blot of the plasma samples. C) Plasma levels of HAVCR2 in control, STEMI and post PTCA subjects show a gradual decrease in ELISA. D) Cytoscape network analysis shows the proteins chosen for docking experiments and the red line indicates the proposed interaction of CD36-AZGP1. E) PyMol view of the most energetically favourable model of interacting AZGP1 and CD36 showing interacting surface (pink) and chains. F) Co-immunoprecipitation of CD36 with AZGP1 in macrophage and foam cells indicating the interaction between these two proteins (Mφ= Macrophage, FC= Foam cells). G) Western blot showing increase in cellular CD36 in foam cells ($p<0.05$). H) Expression of PPARɣ in monocytic and macrophage cells.

To characterize the complex formed by CD36 and AZGP1 in physiological pH and physiological solution, we measured thermodynamic parameters of interaction between CD36 and AZGP1 by ITC. Primarily, decrease in enthalpy change (Kcal/mole) was observed when compared to each injection of buffer pointing out the binding between injectant (CD36) and AZGP1 in the reference cell was endothermic (Figure 8.3.8 A, B). Moreover, the dissociation was indicated by the plot's shift towards an exothermic reaction after the saturation point also supports the above observation (Figure 8.3.8C).

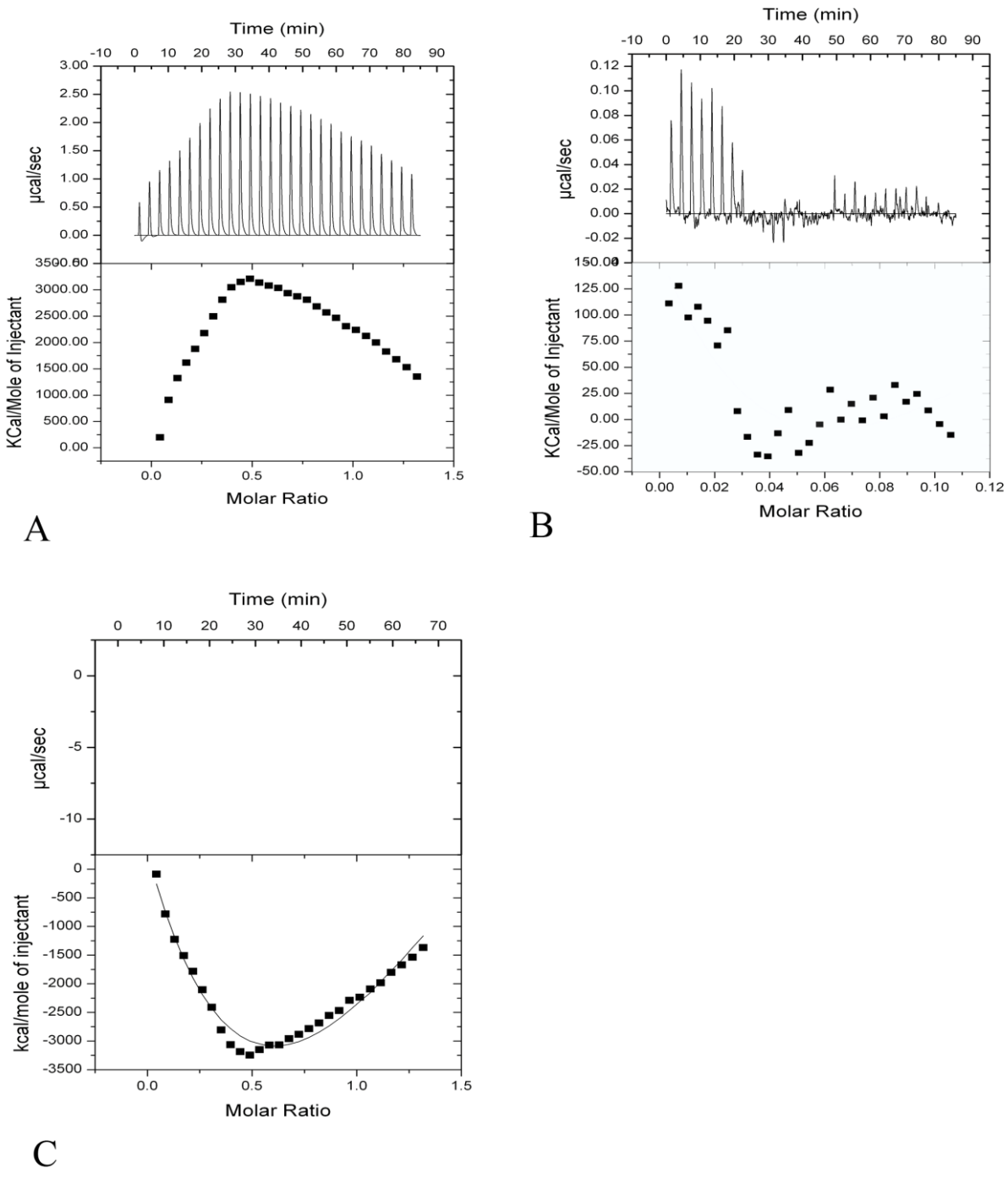

Figure 8.3.8. Determination of thermodynamic parameters of interaction between CD36 and AZGP1 by ITC.

A. Illustration of heat compensation in the sample cell containing dilution buffer.B. Plots of heat compensation (µcal/sec) and enthalpy change (Kcal/mole) as a function of time and molar ratio (CD36:AZGP1). C. Plot of enthalpy change as a function of molar ratio after buffer subtraction between CD36 and AZGP1.

After applying the non-linear curve fitting for all the data points obtained from ITC, we found a "3 attachment sites" curve as the best fit. This provided us the thermodynamic parameters of interaction for 3 possible attachment sites in CD36 (Table 8.3.4). Gibbs free energy (*Δ*G) calculation showed that first and third attachment sites had negative free energy leading to spontaneous reactions for the complex formation between both the proteins. On the other hand, the second attachment site had zero free energy indicating the binding at this site would not possibly be a spontaneous one. Moreover, positive enthalpy and entropy values for these two sites (1^{st} and 3^{rd}) indicated that probably the complex formation at these sites would be hydrophobic in nature. Estimation of error in enthalpy for the above sites helps us in proposing the preferred site of interaction between these two proteins. Table 8.3.4 demonstrates that the error rate in enthalpy (*Δ*H) estimation is higher for the first site (1.189E3 ± 6.93E3 Kcal/mole) than the third site (9.647E4 ± 5.6E5 Kcal/mole) which indicated that the third site as the most likely attachment site for CD36-AZGP1 complex.

Table 8.3.4. Thermodynamic parameters of CD36 and AZGP1 association at 25° C

Binding sites	Equilibrium constant (K) $Mole^{-1}$	Gibbs Free Energy (*Δ*G) Kcal/mole	Enthalpy (*Δ*H) Kcal/mole	Entropy (*Δ*S) Kcal/mole/K
First	2.78E4 ± 1.9E5	-6	1.189E3 ± 6.93E3	4.01
Second	2.93E5 ± 2.0E6	0	-1.193E4 ± 1.21E5	-64.5
Third	3.16E5 ± 1.7E6	-130	9.647E4 ± 5.60E5	324

a. Gibbs free energy were calculated by taking midpoint value of *Δ*H in each case

8.3.2.7. Ex-vivo studies as well as altered expressions of CD36, PPARγ indicate induction of RCT through AZGP1

We analyzed ex vivo the amount of secreted labelled cholesterol in the culture media. After 24 h of incubation, cholesterol secretion increased significantly from differentiated macrophage cells, among which rh-AZGP1 with HDL treated cholesterol-loaded macrophage cells showed highest secreted cholesterol concentrations in the culture media compared to

macrophages with HDL only treatment. This was also reflected in the cholesterol efflux percentage in the exact same manner supporting our observation in the media (Figure 8.3.7I). No significant difference between cells incubated either with HDL or positive control was observed in efflux percentage. Therefore, we next studied the key players of regulation of RCT ex vivo to see the effect of AZGP1 in the process. Interestingly, PPARɣ was found to be decreased ($p=0.037$, $n=6$) (Figure 6.7, Panel B) in the plasma of STEMI subjects indicating its possible link with CD36 and AZGP1 regulated downstream signalling.

Western blot analysis showed that CD36 was upregulated in macrophage derived foam cells compared to monocytes ($p=0.048$) but not in rh-AZGP1 treated macrophage group (Figure 8.3.7G). The protein expression of PPARγ was also found to be decreased ($p\leq0.05$) in foam cells when compared to control THP1 monocytes as well as rh-AZGP1 treated macrophages (Figure 8.3.7H). Decrease of PPARγ in foam cells along with unaltered expression of CD36 in macrophages indicates an imbalance of RCT in macrophages and foam cells. In addition, an increase of cholesterol efflux by AZGP1 in macrophages suggests its clear involvement in RCT.

8.3.3. Conclusion

Proteomic identification and validation of altered level of circulating proteins reveal the role of these proteins to understand the pathophysiology of coronary artery disease. We report, among the significantly altered proteins, AZGP1, a novel adipokine which might be responsible for decreased level of PPARɣ . This lowering of PPARɣ may primarily promote imbalance in RCT in conjunction with the increased level of ABCA5 in plasma. The data also supports chronic inflammation by macrophage showing an increased level of PGLYRP2. Additionally, decreased levels of HAVCR2 and C17ORF57 promote foam cell differentiation. So, cumulative effect of these altered proteins all together equivalently maintains chronic inflammation and deregulation of RCT which indeed play a significant role in atherosclerosis.

Part II (NSTEMI and UA)

8.4.1. Results

8.4.1.1. Identification and annotation of plasma proteins through Orbitrap from NSTEMI and UA patients

Plasma proteins of NSTEMI patients were digested in solution and run through nano LC for initial separation. These separated fractions were injected into Orbitrap mass analyzer to identify proteins through proteome discoverer version 4.0. We identified >800 proteins in NSTEMI and UA. Most of them related to complement activation, chronic inflammation and reverse cholesterol transport. Some of the important proteins identified through Orbitrap in NSTEMI and UA are listed in table 8.4.1. Some of the notable proteins include dectin-1, complement factor 1b, complement 3b, FABP1 etc.

8.4.1.2. Enrichment analyses by IPA identify pathways involved in acute phase response and chronic inflammation

Ingenuity pathway analyses of plasma proteome identified in UA and NSTEMI patients identifies several which are involved in acute phase response signalling and maintenance of chronic inflammation. IPA analysis revealed enrichment of FXR/RXR signalling and LXR/RXR signalling which is vital for maintenance of reverse cholesterol transport and chronic inflammation as well as secretion of chronic inflammatory cytokines like TNF-α, IL-1β etc. Moreover, this analysis indicated the enrichment of coagulation system activation, complement system activation, atherosclerosis signalling, ROS (Reactive Oxygen Species) production in macrophages etc. which are directly connected to plaque development, progression, stability and dissociation (Figure 8.4.1 and 8.4.2). Significantly enriched biological functions above the threshold probability value includes inflammatory response, hematological disease, cardiovascular disease, immune cell trafficking, cell mediated immune response and free radical scavenging. All of which are key processes in the development of atherosclerosis (Figure 8.4.3).

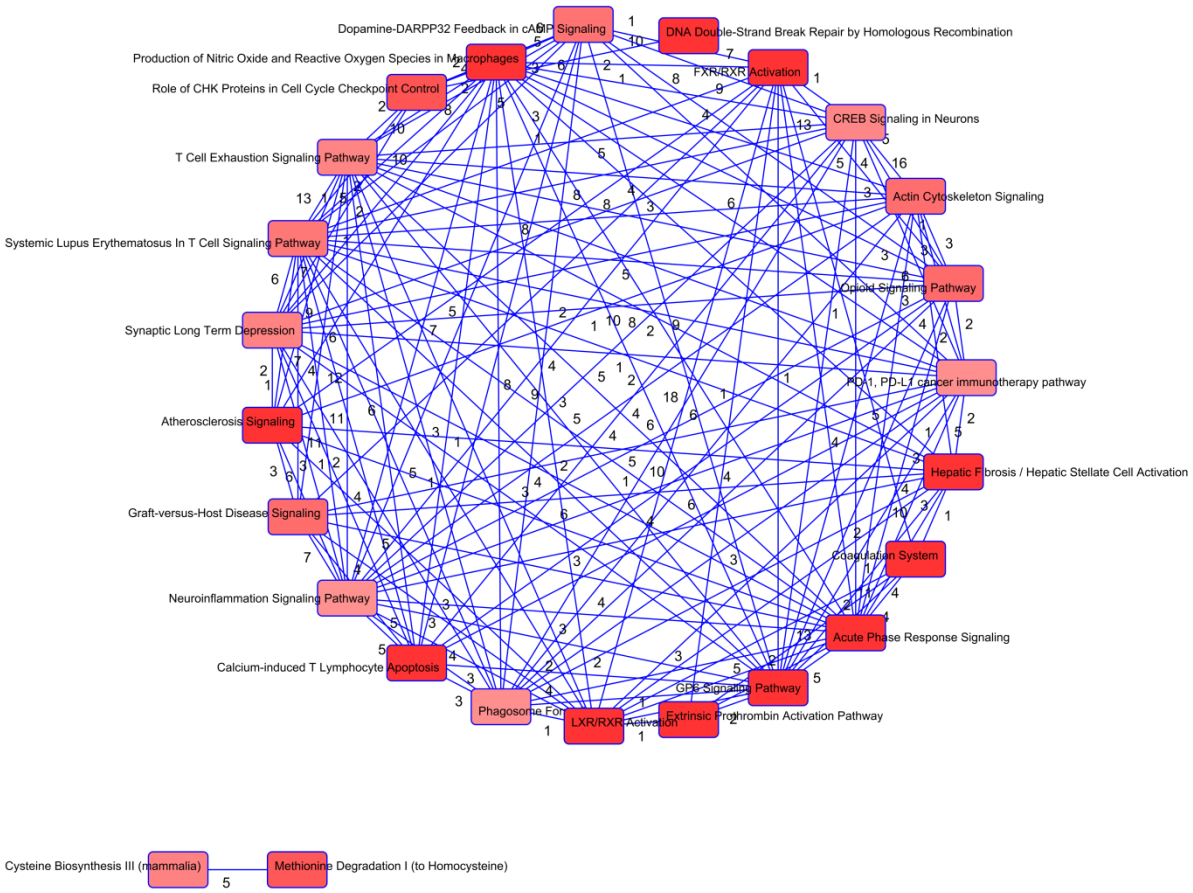

Figure 8.4.1. Circular representation of statistically enriched ($p<0.05$) pathways acquired after analyzing the plasma proteome of NSTEMI samples. Deeper shade indicates more significant pathways. Nodes are connected by blue edges. The numbers beside the edges represent number of common genes shared between the two connected nodes.

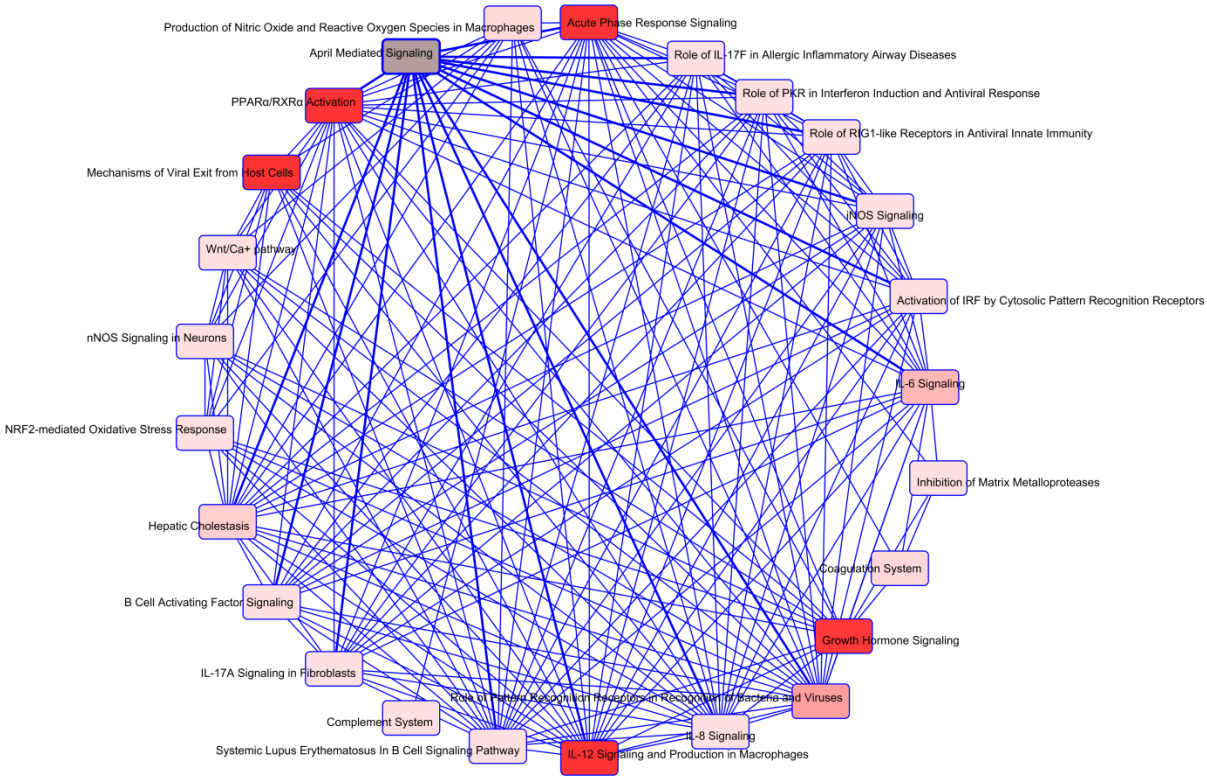

Figure 8.4.2. Circular representation of statistically enriched ($p<0.05$) pathways acquired after analyzing the plasma proteome of UA samples. Deeper shade indicates more significant pathways. Nodes are connected by blue edges. The numbers beside the edges represent number of common genes shared between the two connected nodes.

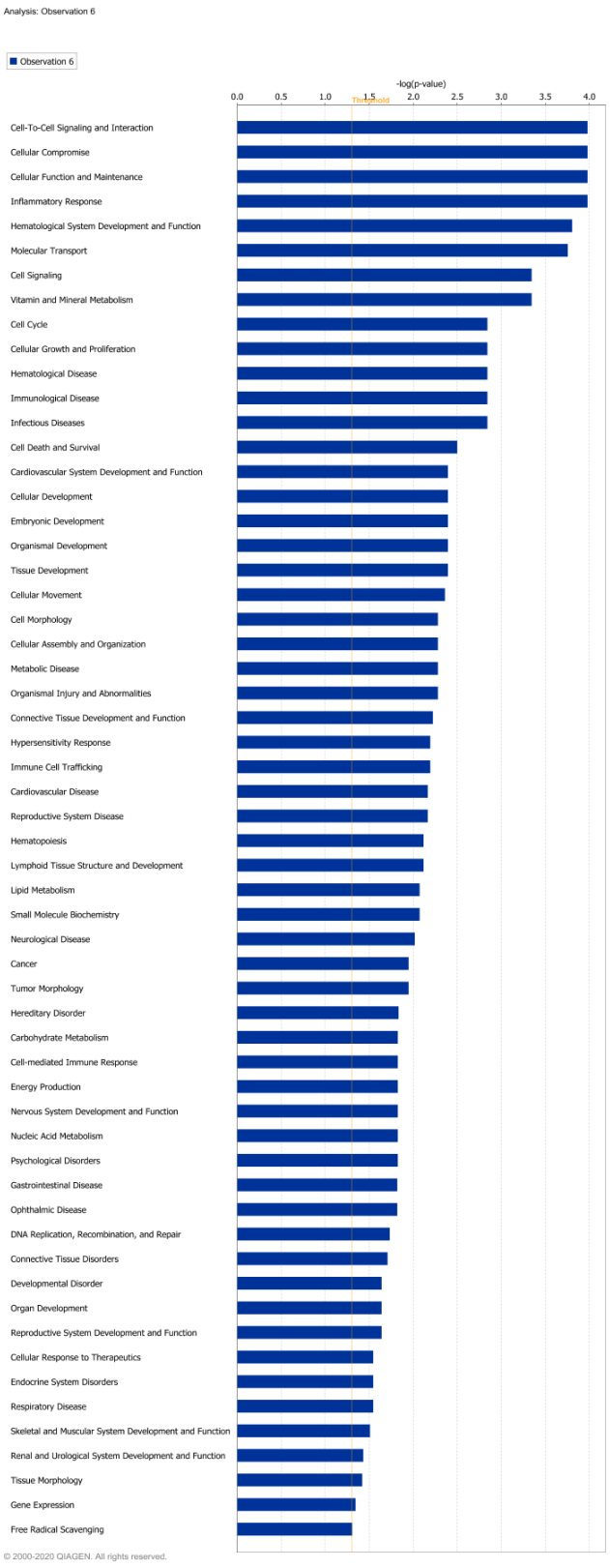

Figure 8.4.3. Significant cellular functions enriched after the analysis of plasma proteome of NSTEMI samples through Orbitrap were plotted in a bar graph according to their negative log (p) value (X axis) to indicate the relevance of NSTEMI proteome in the development of the disease. The yellow line indicates the threshold above which all functions were considered significant.

8.4.1.3. Disease enrichment analyses of NSTEMI and UA samples indicate biasness towards atherosclerotic and cardiovascular diseases

IPA core analyses of plasma proteome of NSTEMI and UA samples indicated that most of the proteins identified in the mass spectra of NSTEMI or UA plasma are responsible for causing cardiovascular disease. A heat map analyses of NSTEMI samples showed that most of the proteins identified are involved in the cellular functions like monocytes activation, monocytes movement, immune cell trafficking, chronic inflammatory response, endothelial cell development as well as activation and so on. On the other hand, heat map analyses of unstable angina (UA) samples indicate the involvement of most of the proteins in cellular processes like hematological system development, organismal injury, cell movement, immune cell trafficking etc. Heat map analyses, core analyses as well as expression analyses of both NSTEMI and UA samples direct the enrichment towards the role of atherosclerosis in vascular and cardiovascular diseases (Figure 8.4.4 and 8.4.5).

Figure 8.4.4. Heat map constructed by the core analyses of UA plasma proteome through IPA. Deeper shades (violet) indicate lower p value or more significance whereas sizes of the box indicate the number of proteins involved in that physiological function.

Figure 8.4.5. Heat map constructed by the core analyses of NSTEMI plasma proteome through IPA. Deeper shades (violet) indicate lower p value or more significance whereas sizes of the box indicate the number of proteins involved in that physiological function.

8.4.1.4. Pathway enrichment analyses using GeneCodis and Panther indicate cellular and biological functions involving coronary artery disease

The plasma proteome of NSTEMI when analyzed by Panther database the relevance of the identified proteins became prominent. 71 percent of the proteins were incorporated in the enriched pathways which include blood coagulation pathway, CCKR signalling, cytoskeletal protein mediated cell movement, FGF signalling, Rho-GTPase signalling etc (Fig.8.4.6). All these pathways are directly connected to plaque development in atherosclerosis indicating the fact that in the plaques of NSTEMI the active signalling pathways are different from that of STEMI plaques. Additionally, biological and molecular function enrichment led us to identify functions closely related to thrombus formation like cell adhesion, cell proliferation, immune system activation etc (Fig. 8.4.7 and 8.4.8). Additionally, GeneCodis analyses of the same proteome led to the significant enrichment of most of the pathways similar to the Panther analyses.

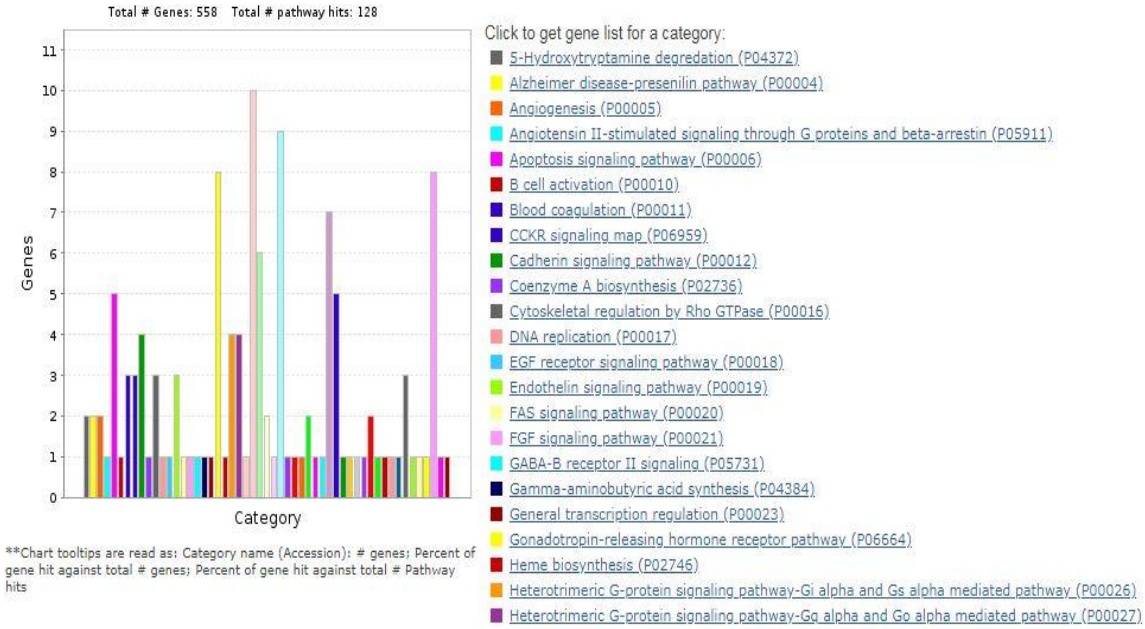

Figure 8.4.6. Bar chart showing enriched pathways in different color codes. List of the color codes are given at the right side of the graph.

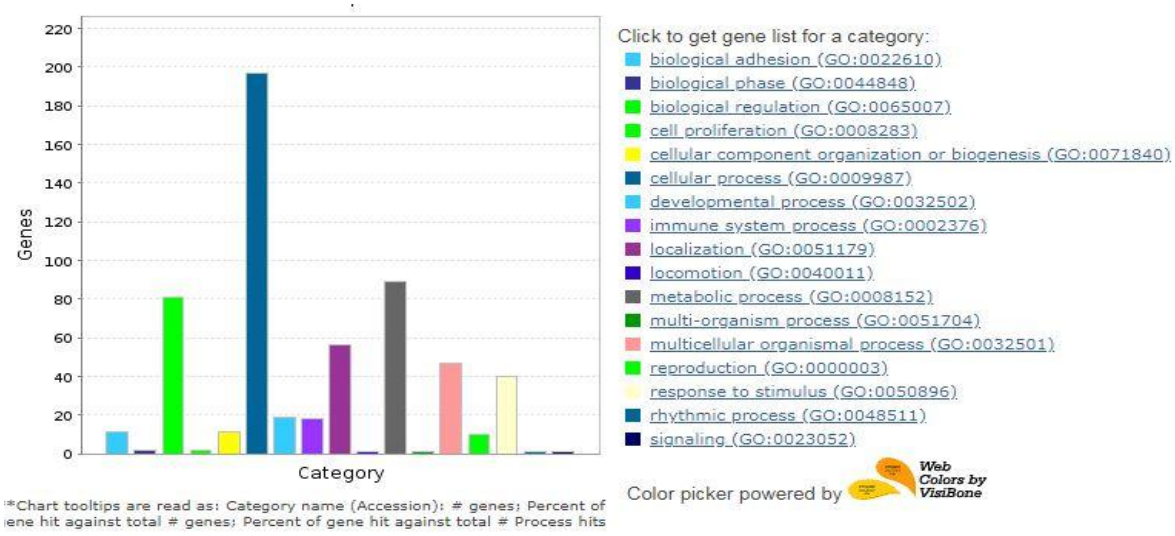

Figure 8.4.7. Bar chart showing enriched biological functions in different color codes. List of the color codes are given at the right side of the graph.

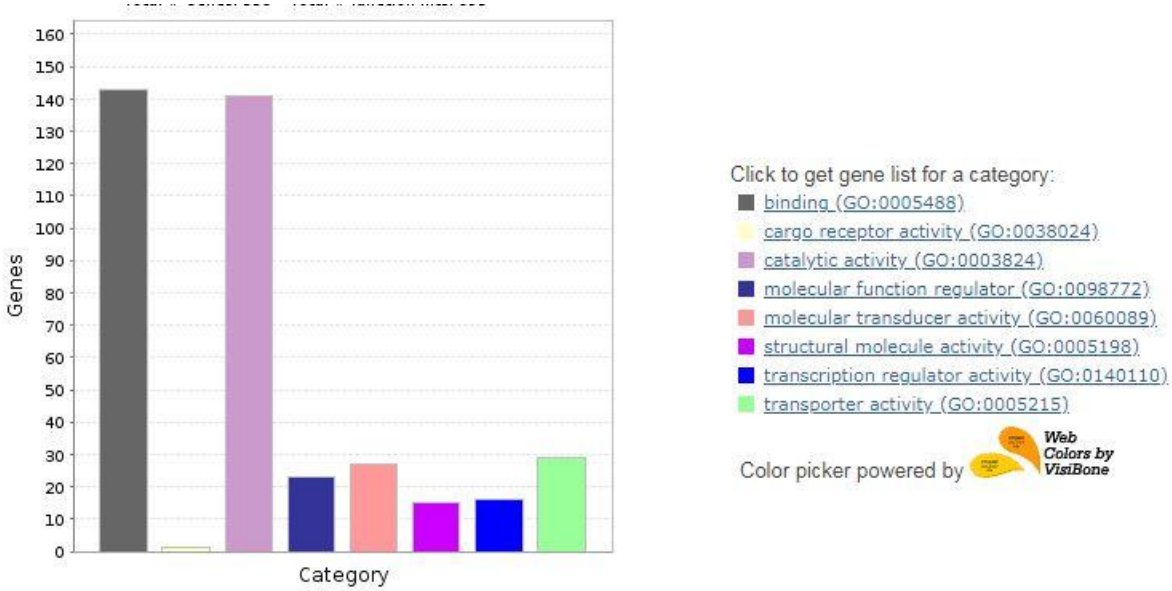

Figure 8.4.8. Bar chart showing enriched molecular functions in different color codes. List of the color codes are given at the right side of the graph.

Enriched pathways are shown in fig. 8.4.9, 8.4.10 and 8.4.11.

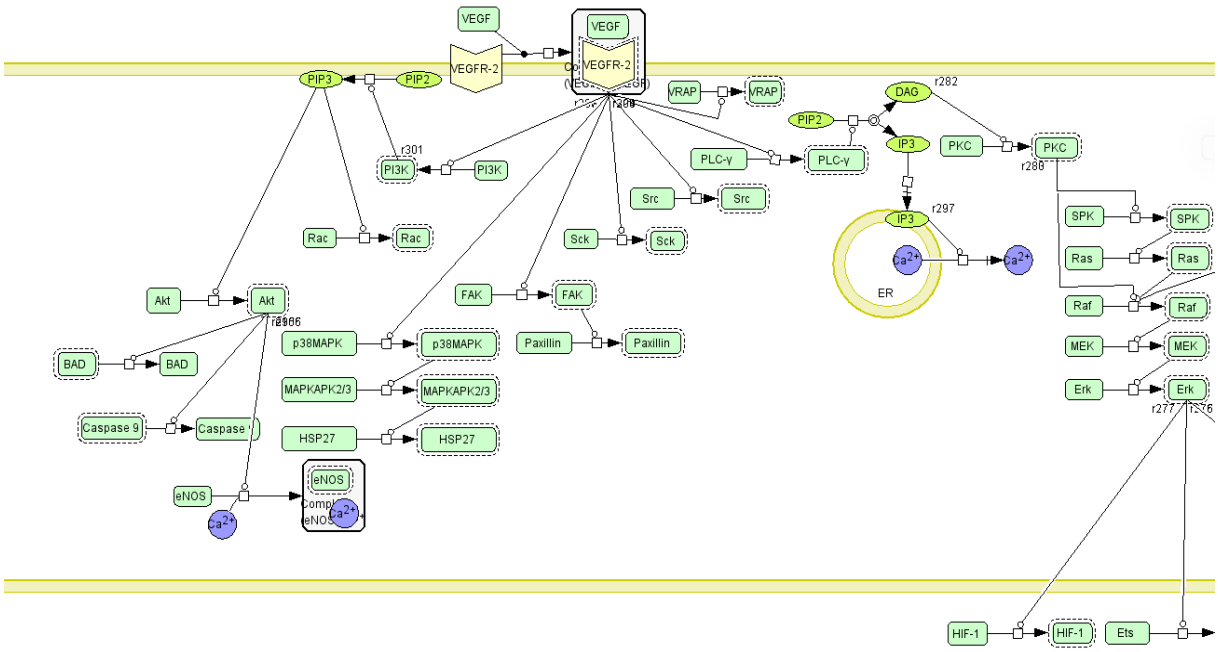

Figure 8.4.9. A part of angiogenesis pathway enriched in the plasma proteome of NSTEMI samples showing angiogenesis signalling by VEGF. Proteins shaded in green were identified in the Orbitrap analysis of NSTEMI samples.

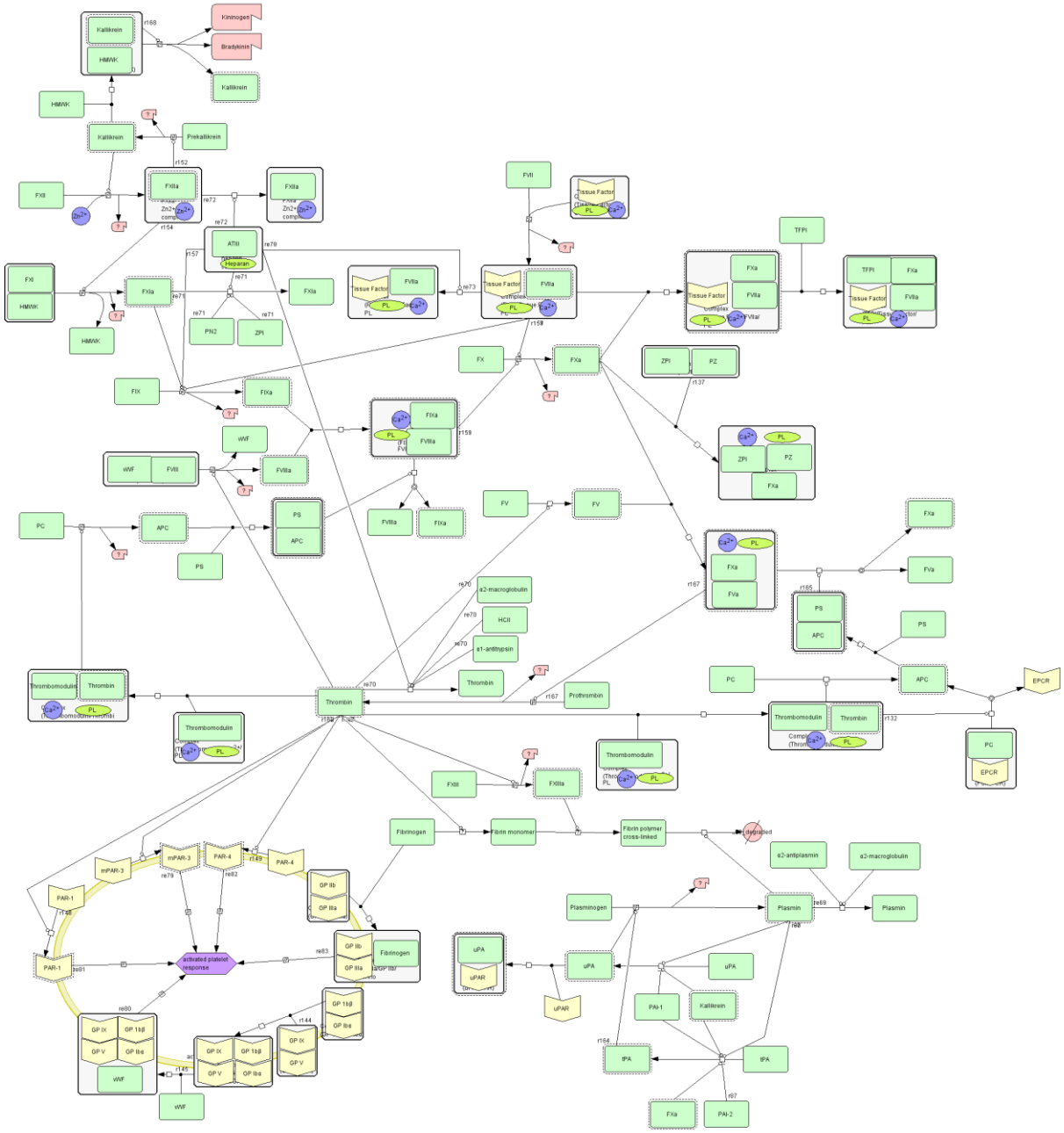

Figure 8.4.10. DAVID illustration of blood coagulation pathway enriched in the plasma proteome analyses of NSTEMI samples. Proteins shaded in green were identified in the Orbitrap analysis.

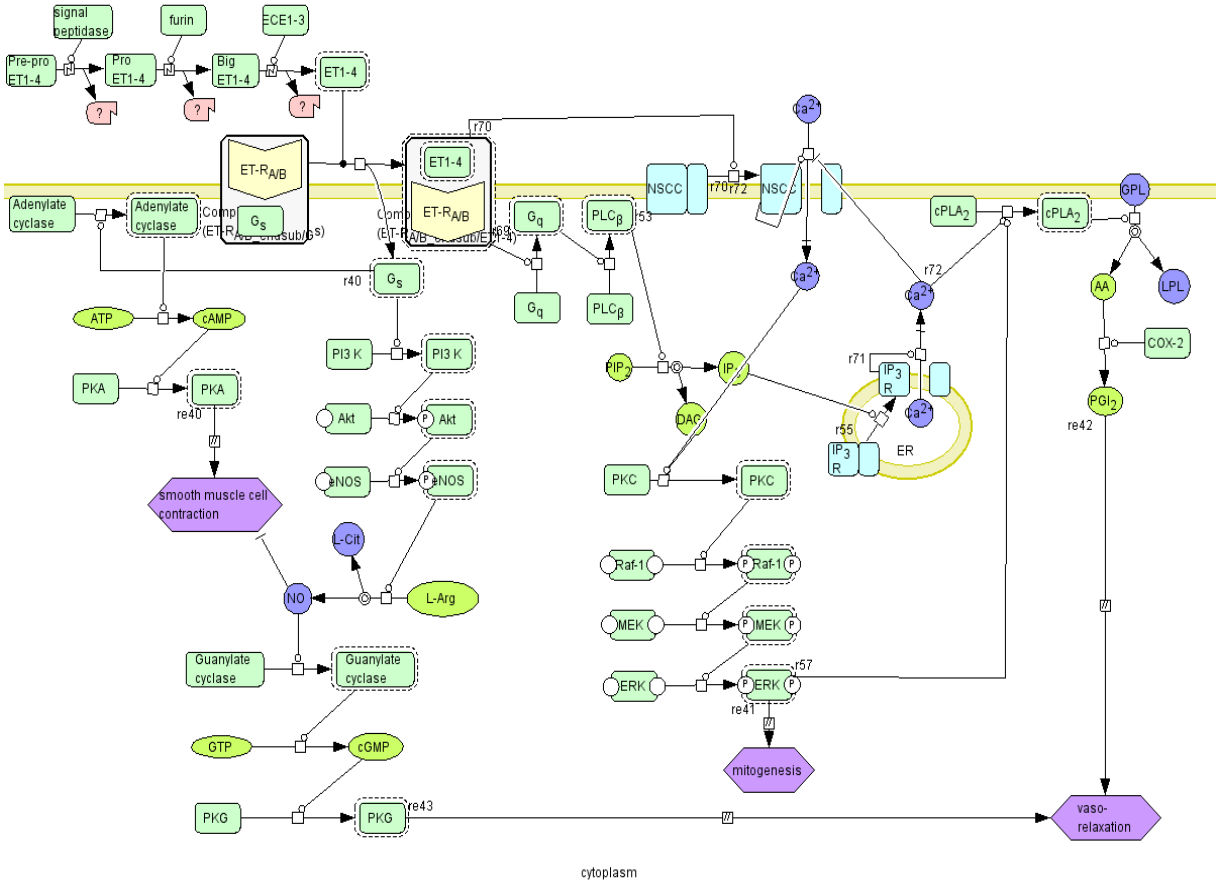

Figure 8.4.11. DAVID illustration of endothelin signalling pathway enriched in the plasma proteome analyses of NSTEMI samples. Proteins shaded in green were identified in the Orbitrap analysis.

Additionally, plasma proteomic analyses of unstable angina samples revealed similar results except pathway enrichment showed more inclination towards chemokine, cytokine and interleukin activated pathways. Except the above mentioned pathways, pathway enrichment analyses also indicated the predisposition of FGF signalling pathway, G-protein coupled receptor signalling pathway, CCKR signalling, PDGF signalling, Ras signalling etc (Figure 8.4.12). Moreover, enrichment of biological functions and molecular functions indicated that most of the proteins identified in the plasma were involved in cell adhesion, cell movement or enzymes. Some of them express at the plasma membrane of their corresponding cell types (Figure 8.4.13 and 8.4.14).

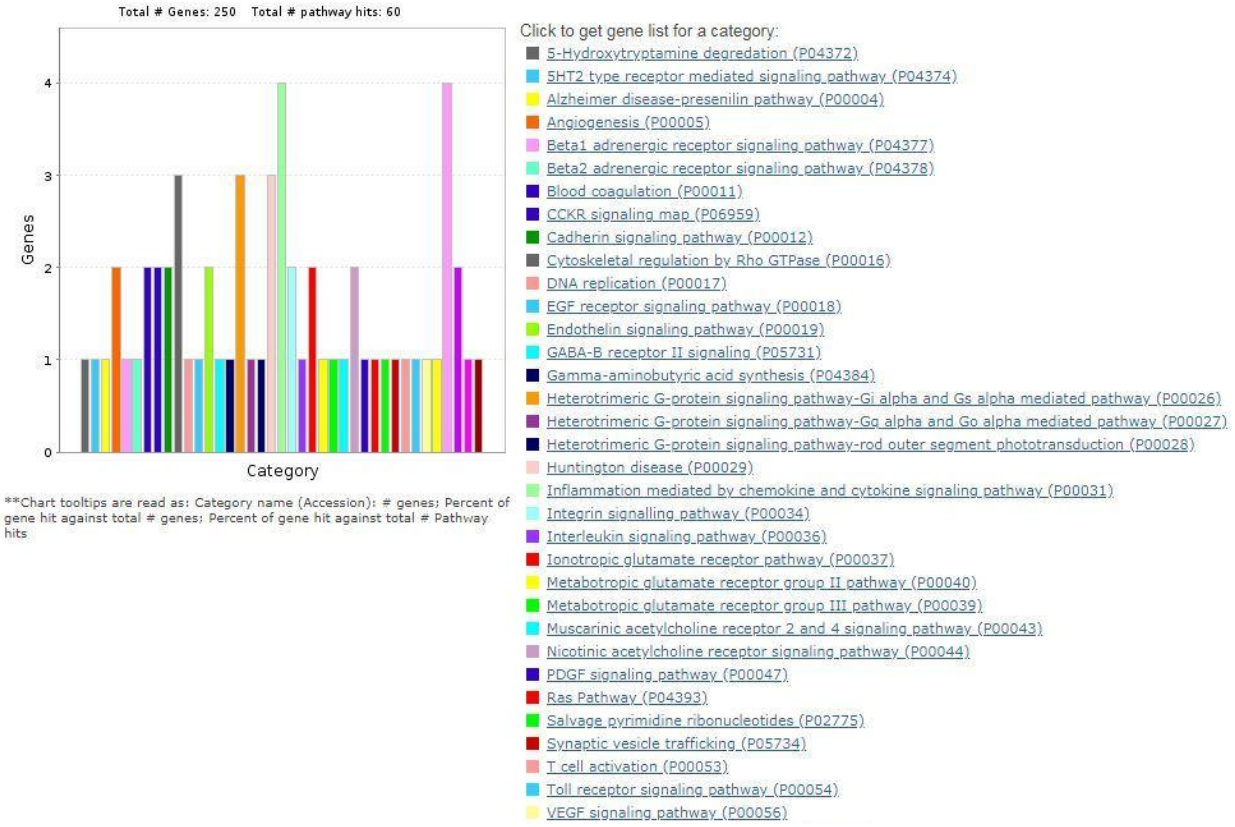

Figure 8.4.12. Bar chart showing enriched pathways in UA plasma after Panther analyses. Different pathways are marked with different colors. List of the color codes are given at the right side of the graph.

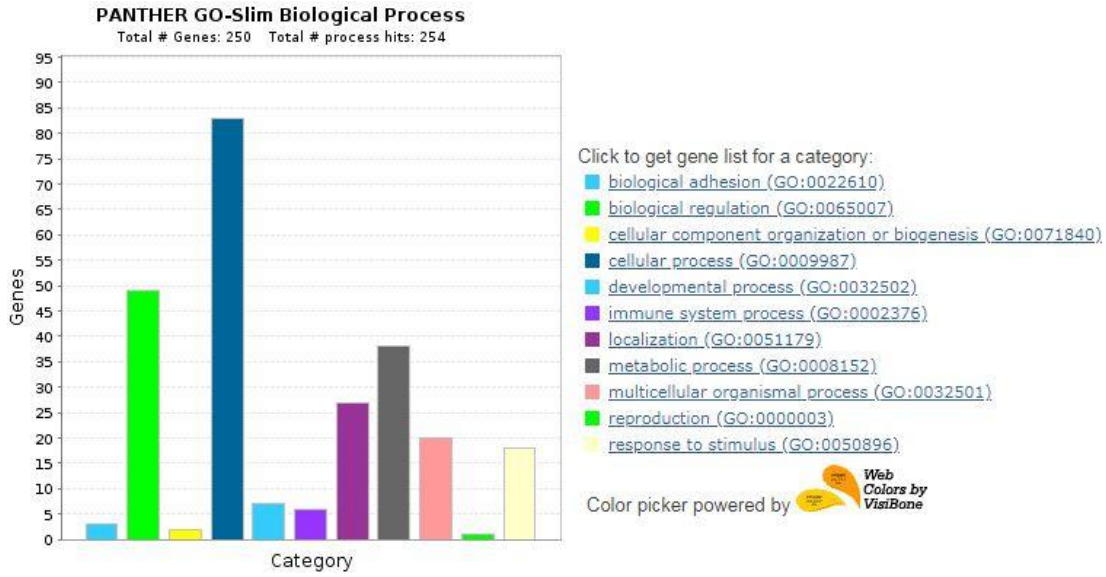

Figure 8.4.13. Bar chart showing enriched biological functions in different color codes. List of the color codes are given at the right side of the graph.

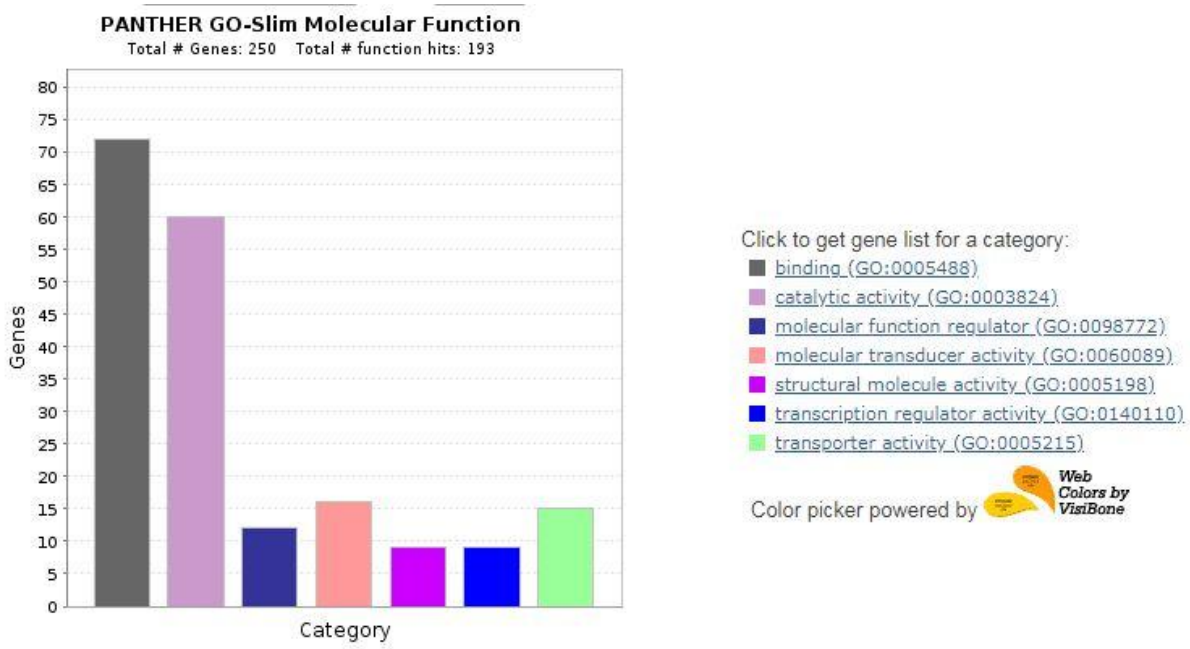

Figure 8.4.14. Bar chart showing enriched molecular functions in different color codes. List of the color codes are given at the right side of the graph.

Enriched pathways in the plasma proteome of UA samples are illustrated below (Figure 8.4.15, 8.4.16 and 8.4.17)

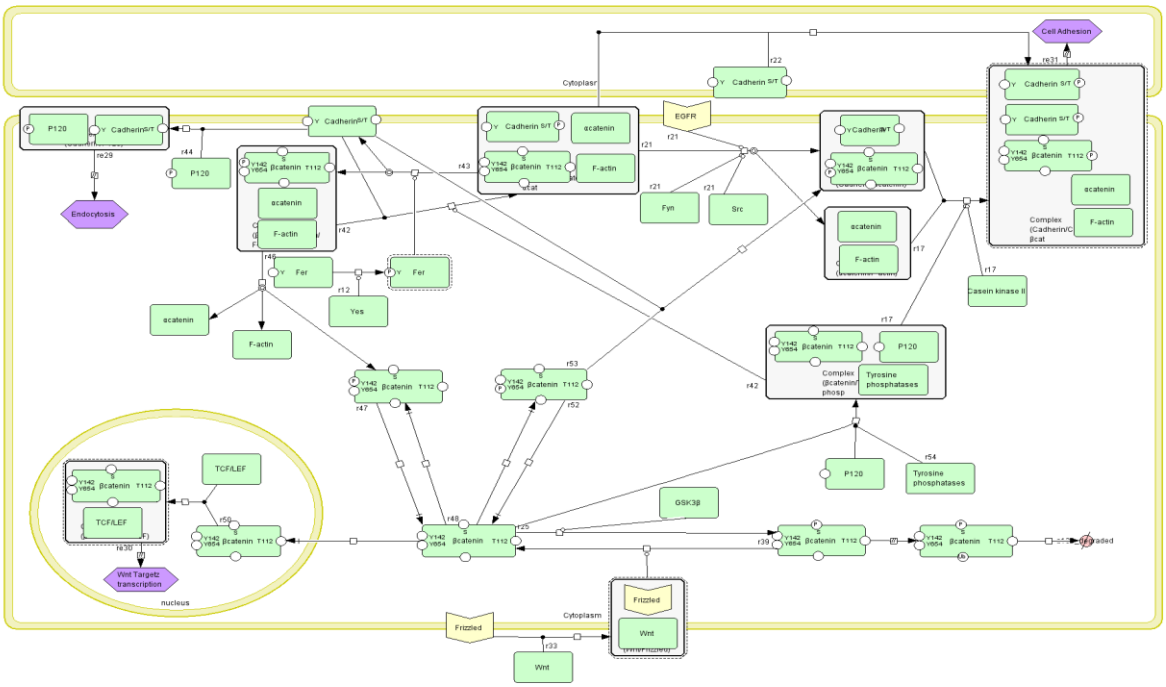

Figure 8.4.15. DAVID illustration of cadherin signalling pathway enriched in the plasma proteome analyses of UA samples. Proteins shaded in green were identified in the Orbitrap analysis of the same.

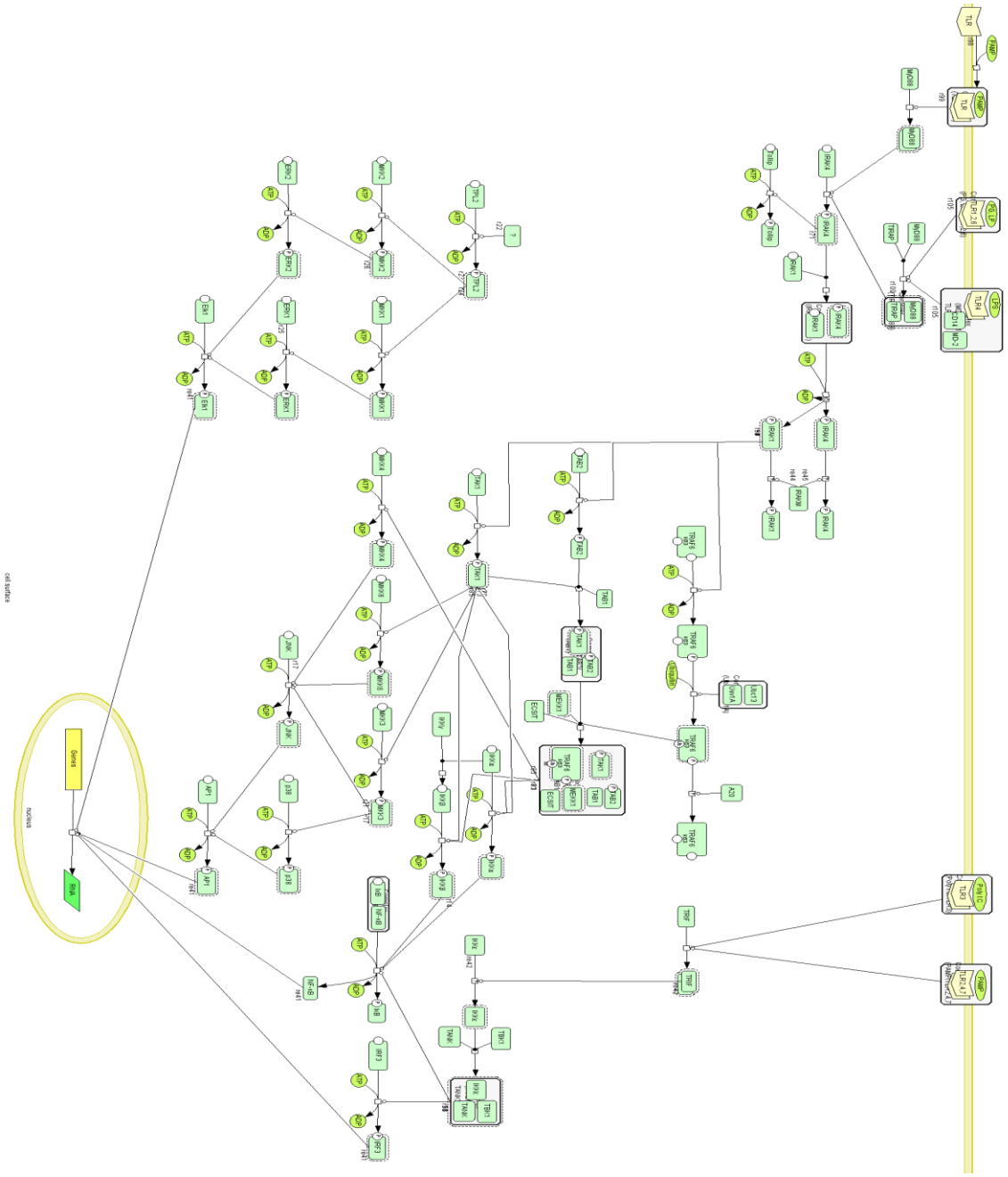

Figure 8.4.16. DAVID illustration of Toll like receptor signalling pathway enriched in the plasma proteome analyses of UA samples. Proteins shaded in green were identified in the Orbitrap analysis of the same.

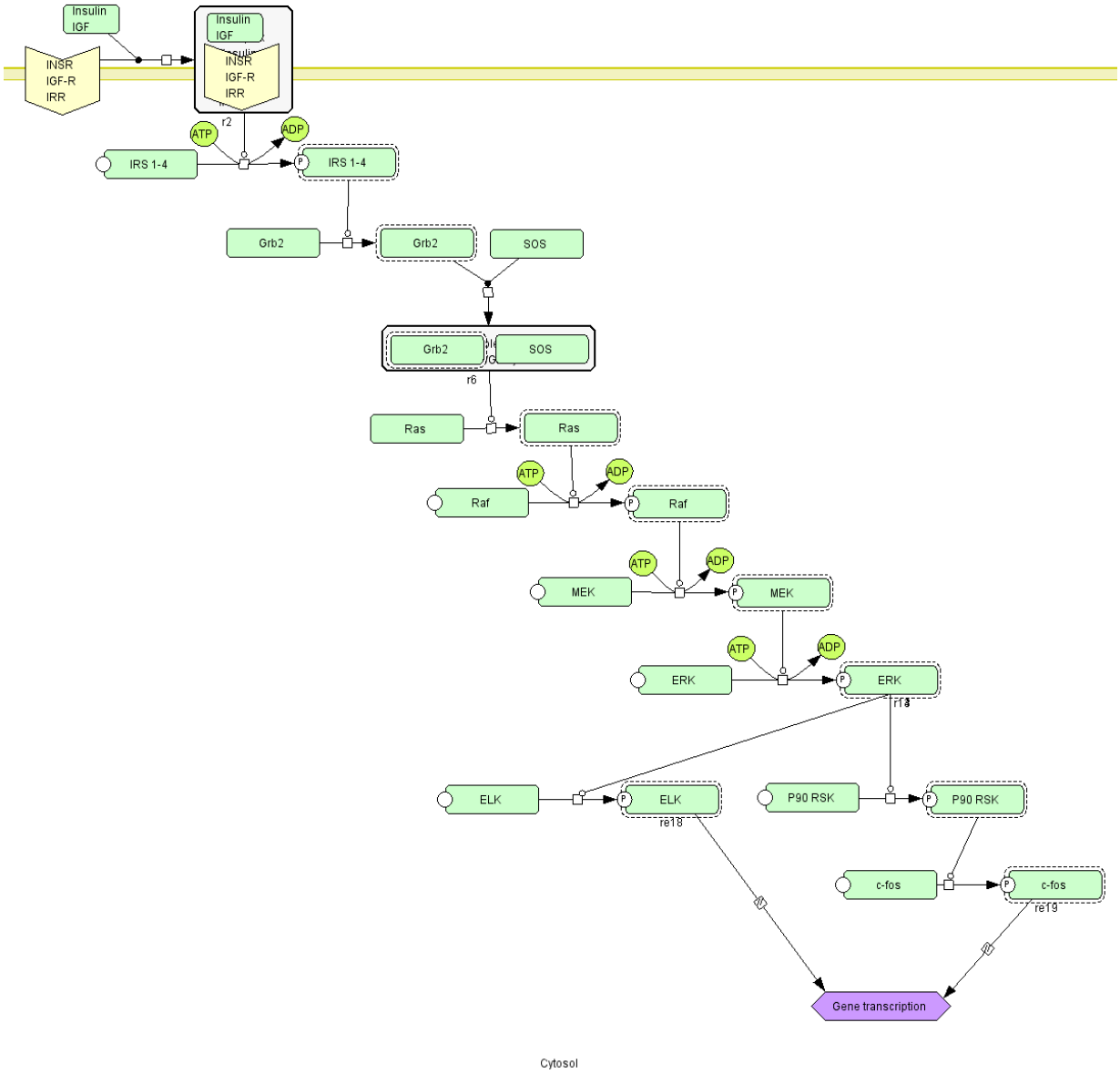

Figure 8.4.17. DAVID illustration of Insulin receptor signalling pathway enriched in the plasma proteome analyses of UA samples. Proteins shaded in green were identified in the Orbitrap analysis of the same.

8.4.1.5. Reactome analysis indicates enrichment of Dectin-1 mediated pathway in NSTEMI

Plasma proteomics of NSTEMI samples identified the presence of soluble Galectin-3 in the Orbitrap analysis. Soluble Galectin-3 is a lectin family protein which is found on the plasma and induces pro-inflammatory cytokine production, cell movement etc. As we analyzed our proteome in Reactome database to identify pathways related to atherosclerosis with the reference to the human genome; we found a significant enrichment score for Dectin-1 mediated signalling pathway which included soluble Galectin-3 as a candidate protein.

8.4.1.6. Dectin-1 interacts with soluble Galectin-3

To understand the effect of soluble Galectin-3, we studied its interacting partners initially in STRING database (Figure 8.4.18).This interaction analysis led to the identification of soluble Galectin-3 as an interacting partner which support our previous proteomic observation. The PPI score for LGALS3 and Dectin-1 is 0.825 which is far above the threshold value of 0.6. Moreover, there are experimental reports available concerning their interaction in different pathological conditions.

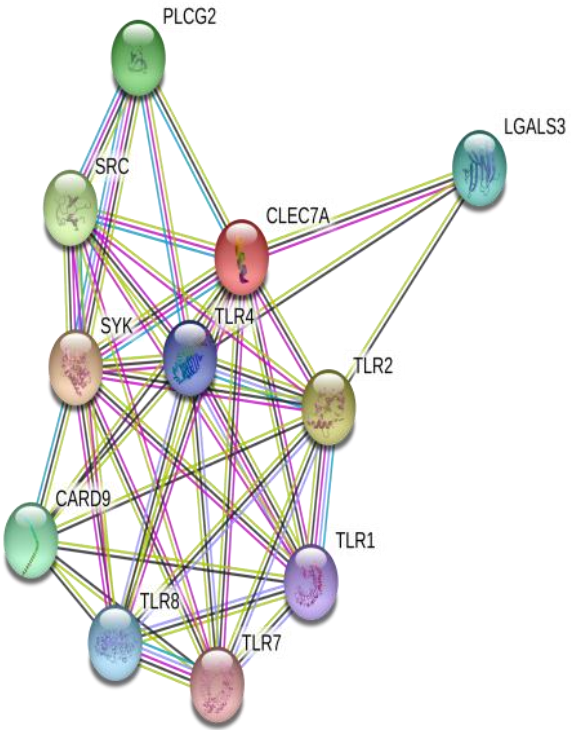

Figure 8.4.18 STRING interaction analysis of Dectin-1 (CLEC7A) shows its strong interaction with LGALS3

Moreover, in silico docking analysis between these two proteins revealed that they can interact with a significantly high docking score. We used PatchDock and ClusPro to dock the proteins and refined the models common between these two softwares using FireDock. We took the common highest scoring model from both the softwares (Figure 8.4.19).

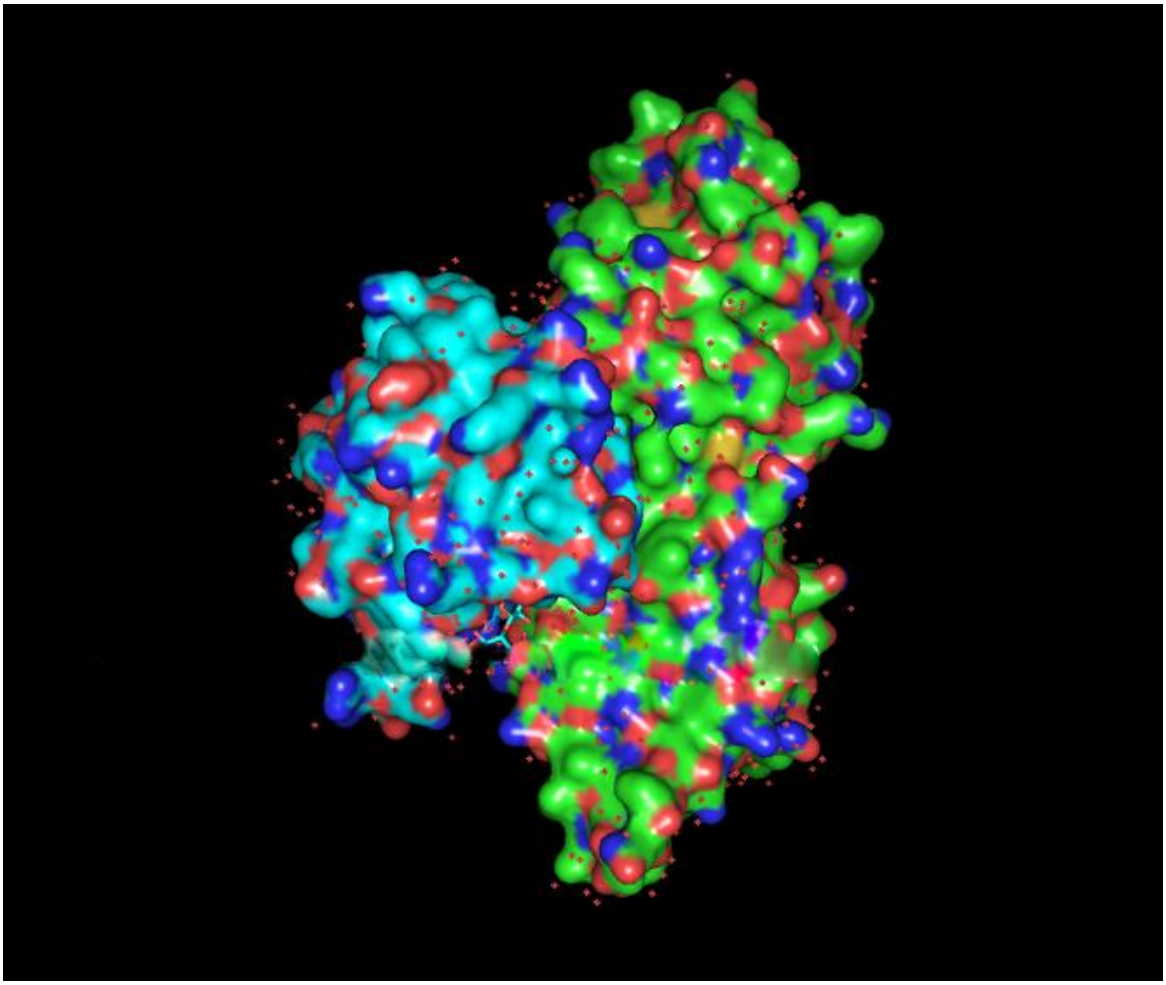

Figure 8.4.19. PyMol surface view of the highest scoring model involving soluble Gacletin-3 (Sky blue) and Dectin-1 (Green).

8.4.1.7. Interaction of soluble Galectin-3 with Dectin-1 induces TNF-α secretion from macrophages

To understand the cause-effect relationship between Galectin-3 and Dectin-1 we treated monocytes derived mcrophages overnight with recombinant Galectin-3. Furthermore, after treatment we measured the concentration of secreted TNF-α in the media. Interestingly, we found out that compared to untreated cells or controls, Galectin-3 treated cells secreted increased amount ($p<0.05$) of TNF-α in the extracellular media (Figure 8.4.20).

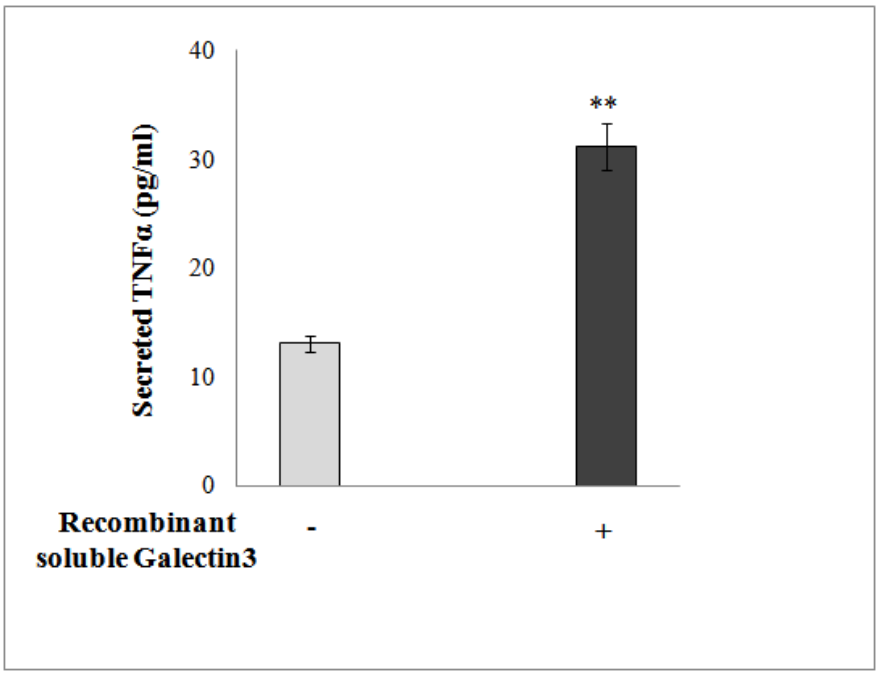

Figure 8.4.20. Level of secreted TNF-α after treatment with Galectin -3 in macrophage cells. '-'denotes absence of soluble Galectin-3 in the media and '+' denotes presence of soluble Galectin-3 in the media

8.4.2. Conclusion

We showed for the first time the involvement of different pathways in NSTEMI and UA compared to STEMI patients. This includes pathways which promote cell movement, cellular differentiation, inflammatory response pathway involving Toll like receptors etc. Identification of these pathways and new candidate proteins may help in identification of new drug targets for CAD subtypes. Moreover, for the first we showed that soluble Galectin-3 interacts with Dectin-1 to induce the secretion of TNF-α which proves the involvement of chronic inflammation in the patho-biology of NSTEMI.

DISCUSSION


CONCLUSION
DISCUSSION
RESULTS & ANALYSIS
METHODOLOGY
LITERATURE REVIEW
INTRODUCTION

Proteomics is a systemic discipline of bodily processes to deal with the large-scale characterization of protein species within a biological systems e.g. cell, a tissue, a body bio-fluid, an organism, or a cohort population. Advancing from chemical analytical platforms (e.g., mass spectrometry and other technologies), proteomics approaches have added powerful applications in cardiovascular biomedicine, most notably in: 1) the finding of circulating protein biomarkers of CAD from plasma samples; and 2) the discovery of disease mechanisms and potential therapeutic targets in cardiovascular tissues, in both preclinical models and translational studies. Present-day proteomics investigations offer powerful ways to concurrently examine tens of thousands of proteins in various samples, and understand their molecular phenotypes in health and disease.

So, the main focus of the present study was not only to present evidence that a platelet protein, sTLT1 is directly linked to atherogenesis and progression of CAD by participating in inflammatory process with the help of macrophage secreted cytokines but also to identify several possible pathophysiological protein candidates for CAD subtypes by performing proteomics studies on STEMI, NSTEMI and UA.

Increased levels of sTLT1 was reported in a small sample group of subjects (n=19) with chest pain, however, it was limited by case numbers, subject profile and insufficient statistical validation (Esponda OL et al, Clin. App. Thromb Hemost, 2015). Moreover, the association between plasma sTLT1 and clinico-pathological parameters were not studied in the report. Here, in the first two sections, we establish a robust increase in plasma sTLT1 in a relatively larger sample size, documented with clinical correlations and patho-physiological importance. Statistical association of sTLT1 with left ventricular ejection fraction (LVEF) and carotid intima-media thickness in subclinical individuals further signifies its relation to the overall atherosclerotic burden. Our results also prove that sTLT1 is distinctly correlated with GRACE score (Bradshaw PJ et al, Heart, 2006), TIMI score (Morrow DA et al, Circulation, 2000) and Framingham risk factors; thus with chances of mortality in acute CAD.

Oxidized LDL is known to be associated with atherosclerotic plaque formation and therefore, considered as a possible risk factor for subclinical CAD in apparently healthy individuals. It is imperative to each step of thrombus formation, starting from foam cell differentiation to the secretion of inflammatory cytokines into intima-medial space (Steinberg D et al,ATVB,2010). Interaction of oxLDL with CD36 promotes the activation of PI-3K pathway

to induce the secretion of pro-inflammatory cytokines (Koga MM et al, Plos One, 2012). Alternatively, CD64 activation endorses phagocytosis of oxLDL to form foam cells. As a result, significant association of sTLT1 with oxLDL in the present study is indicative of its clinical importance in subclinical cases.

Absence of any significant associations with age, sex and platelet number point toward the fact that sTLT1 is independent of its limiting factors. Multiple logistic regressions indicate sTLT1 is associated with hypertension representing a significant risk involvement with the disease. Also, comparative ROC analysis reveals that sTLT1 performs better than oxLDL and NT-proBNP as a risk factor for CAD indicating that it can be an important factor to assess the disease in subclinical and clinical cases.

It has been already reported that Fcɣ RI (CD64) is a macrophage-specific marker and plays an important role in activating the immune system and safeguarding of peripheral tolerance. Hernandez- Vargas showed that double knockout mice against ApoE and Fcɣ RI provide protection against atherosclerosis by reducing 50% of the atherosclerotic lesion area in which chemokine activation is impaired through upregulation of NF-kB (Hernandez-vergas et al, Circ.Res.2006). It has been reported that CD64 expression is notably increased in CAD in comparison with healthy control subjects via C-reactive protein (Djebara S et al, Shock, 2017). On the contrary, CD64-CRP interaction endorses uptake of oxLDL and thereby plays a significant role in the pathogenesis of CAD. All these information point out its role in foam cell formation and inflammation. The present study, for the first time, show the activation of SYK mediated pathway through interaction of Fcɣ RI with sTLT1 which is in accordance with the inflammatory role of CD64 in atherosclerosis.

Tyrosine-protein kinase, SYK, the initiator of intracellular signalling in this study, has been reported to increase the secretion of IL-1β in vascular smooth muscle cells to support atherosclerosis. SYK (L), the long isoform of SYK, increases oxLDL phagocytosis in monocytic U937 cells. Additionally, pharmacological inhibition of SYK causes the downstream suppression of MAPK, MEK and ERK; indicating its role in disease initiation and progression. Interestingly, release of thrombin-stimulated platelets was inhibited by blocking SYK suggesting its role in platelet activation. Our study for the first time establishes that SYK activation causes the secretion of pro-inflammatory cytokines through MEK/ERK pathway through the interaction of a novel thrombin induced platelet protein, sTLT1 with

CD64 (Figure 9.1). The contribution of this pathway towards inflammation and atherosclerosis may help in finding new drug targets in the near future.

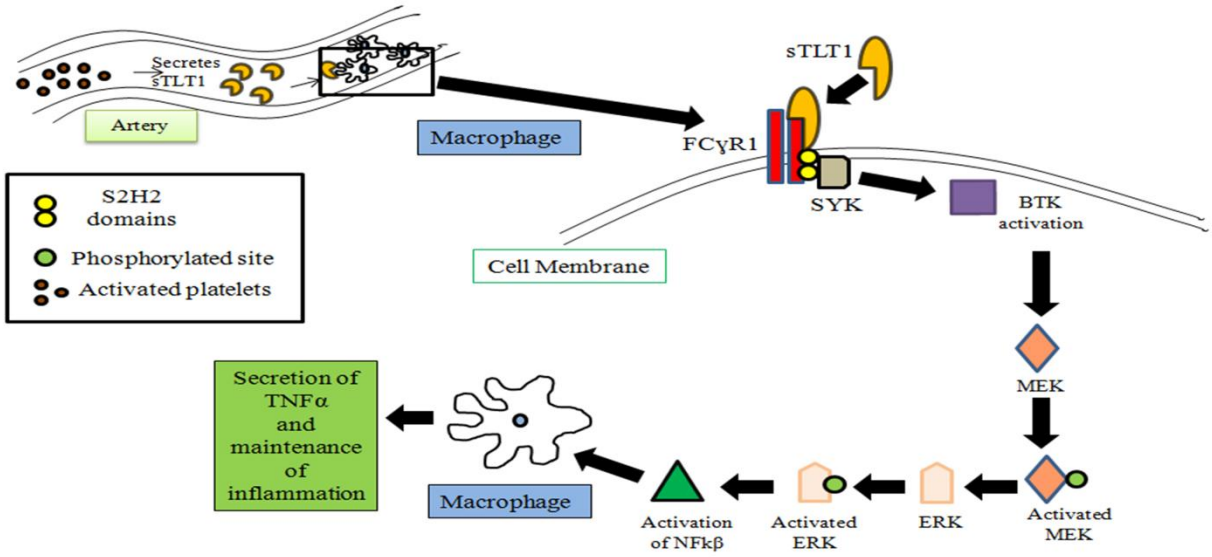

Figure 9.1. Diagrammatic representation of sTLT1 activated pathway via Fcɣ RI/SYK/ERK cascade

The role and effectiveness of oral Bruton's Tyrosine Kinase (BTK) inhibitors as a selective blocker of atherosclerotic plaque development by disrupting platelet aggregation is well known (Lindner JR,Blood,2018). Our study established that, BTK inhibitors not only help in preventing platelet aggregation but also abrogate the inflammatory effects of macrophages which might help in developing in drug development strategies in the future along with the use of SYK inhibitors.

The next section of the study reports a panel of proteins in human blood plasma relevant to the pathophysiology of coronary artery diseases utilizing extensive quantitative and qualitative proteomic experimental techniques in a case-control design followed by some biochemical validations and ex vivo experiments. Plasma collected from the subjects clinically diagnosed with STEMI, NSTEMI and UA were analyzed by high resolution MS/MS. Subsequently, validations in plasma of STEMI patient and ex vivo experiments using human cells revealed significantly deregulated reverse cholesterol transport, as well as inflammation-induction signalling which might be accountable for atherosclerosis, a critical risk factor which drives a subject towards acute coronary event. Analysis of the identified proteins indicated enriched pathways such as intrinsic and extrinsic coagulation cascades,

internalization of LDL particles, foam cell signalling, activation of inflammatory signalling etc. which are linked to arterial blockage and CAD through compromised RCT and inflammation.

Here, we used a discovery platform for proteomic identification of whole human plasma in patients suffering from coronary artery disease (CAD). Numerous reports on proteomic analysis of cardiovascular disorders are available. High resolution mass spectrometry using 4-plex iTRAQ and SRM based quantitative plasma profiling revealed an increased level of a cytoskeletal protein, vinculinin in atherosclerotic condition. Similarly, proximity extension assay on proteomics chip reported new candidates like osteoprotegrin, T-cell immunoglobulin and mucin domain (TIM)-1, growth/differentiation factor 15 (GDF-15), and growth hormone for CVD. Moreover, recent discoveries reported 85 circulating protein biomarkers among which regulators of metabolic and adipocyte homeostasis are shown to be associated with cardiovascular events in Framingham Heart Study participants (n=3523). Lygirou et al reported the identification of 3796 proteins in human plasma, out of which 100 were found to have a significant differential expression (trends verified for 39 proteins) in the case as compared to control subjects (Lygirou V et al,J Trans. Med.2018). In the present study, we further compared the plasma proteome as already catalogued in the Plasma Proteome Database (http://www.plasmaproteomedatabase.org/). In the nano-LC-MS/MS Orbitrap experiment, ABCA5, one of the key proteins identified, is yet to be indexed in the Plasma Proteome Database indicating its novel importance in CAD. We report a higher level of ABCA5 in STEMI compared to healthy control.

This study also identified another physiologically important protein, AZGP1, an adipokine, which is reported to be implicated with lipid mobilization**.** Similar to SWATH analysis it is found to be significantly decreased in STEMI compared to healthy control. It is also shown to be decreased in obese women as well as in non-alcoholic fatty liver disease (NAFLD) rat model demonstrating a significant association with the risk factor of atherosclerosis. In-silico analyses using online available softwares like ClusPro 2.0, PatchDock beta 1.3 and HADDOCK 2.2 (Kastritis PL et al,JPR, 2010) display the interaction between AZGP1 and CD36. Along with this, the thermodynamic parameters of interaction between CD36 and AZGP1 revealed the presence of a definite preferred site of attachment for the ligand confirming its role in downstream signalling. Additionally, our data on cholesterol efflux rate clearly showed the effect of AZGP1 on RCT.

It is evident from the previous reports that CD36 upon binding with oxidized LDL leads to the initiation of various pathways including NF-kB, VAV and FAK-mediated signaling which may cause chronic inflammation and macrophage trapping (Silverstein Roy L. et al,Trans. Am. Clin. Climat. Association.2010). When CD36 is reduced PPARγ is also decreased. Decrease of PPARγ regulates the expression of Scavenger Receptor-A. To examine the CD36 mediated downstream signalling, macrophages were differentiated into foam cells by OxLDL and the levels of CD36, as well as PPARγ were measured. Interestingly, the level of CD36 remained unchanged in macrophages while PPARγ is reduced in foam cells. In plasma both PPARγ and AZGP1 are reduced in STEMI subjects which is supported by an earlier report in adipocytes (Mracek T et al,JOE, 2010). It is established that the reduced level of PPARγ may cause shifting of the foam cell signalling towards RCT pathway because PPARγ regulates HDL export by controlling ABCA transporters with the help of LXRα. Hence, this lowering of PPARγ is likely to imbalance RCT. To overcome the imbalanced RCT other transporters are increased which is apparent from an increased level of ABCA5. But, parallel to this, the decrease in AZGP1 possibly could not manage the RCT balance. Also, a low level of C17ORF57 causes foam cell differentiation and a high level of PGLYRP2 induces prolonged inflammation promoting the formation of atherosclerotic lesions. The reduced level of plasma HAVCR2 also called as TIM3 (T cell immunoglobulin and mucin domain 3) is known to be inversely correlated with atherosclerosis (Foks AC et al, ATVB, 2013). Furthermore, HAVCR2 regulates the maturity of N_K T cells and $CD8^+$ T cells (Ndhlovu LC et al,Blood,2012). As a result, it is plausible that lowering of HAVCR2 could result in the deregulation of the inflammatory cytokines and foam cell differentiation.

Our data on plasma proteomics of NSTEMI and UA identified many unique proteins which are important in plaque development of both the subtypes. This is significant because of the fact that plaque composition and nature of the plaques in NSTEMI as well as UA differ drastically compared to STEMI plaques. So, it is very likely that the instability of the plaques depend upon unique protein composition and distinctive strata of pathway activation. Our enrichment analyses showed enrichment of pathways linked to atherosclerosis and inflammation. Moreover, our studies on Dectin-1 function clearly indicate a significant role of soluble Galectin-3 in chronic inflammation in NSTEMI.

So, our proteomic identification and validation reveal altered level of circulating proteins which are noteworthy for understanding the pathophysiology of coronary artery disease.

Among the significantly altered proteins, AZGP1 is a novel adipokine which might be responsible for decreased level of PPARɣ . Lowering of PPARɣ may promote imbalance in RCT in macrophage whereas the chronic inflammation is supported with an increased level of PGLYRP2. Decreased levels of HAVCR2 and C17ORF57 promote foam cell differentiation. Although, increased level of ABCA5 tends to maintain the balance of cholesterol transport yet the availability of more number of differentiated macrophages and decreased level of AZGP1 help to induce deregulation of RCT which indeed likely to play a significant role in atherosclerosis (Figure 9.2).

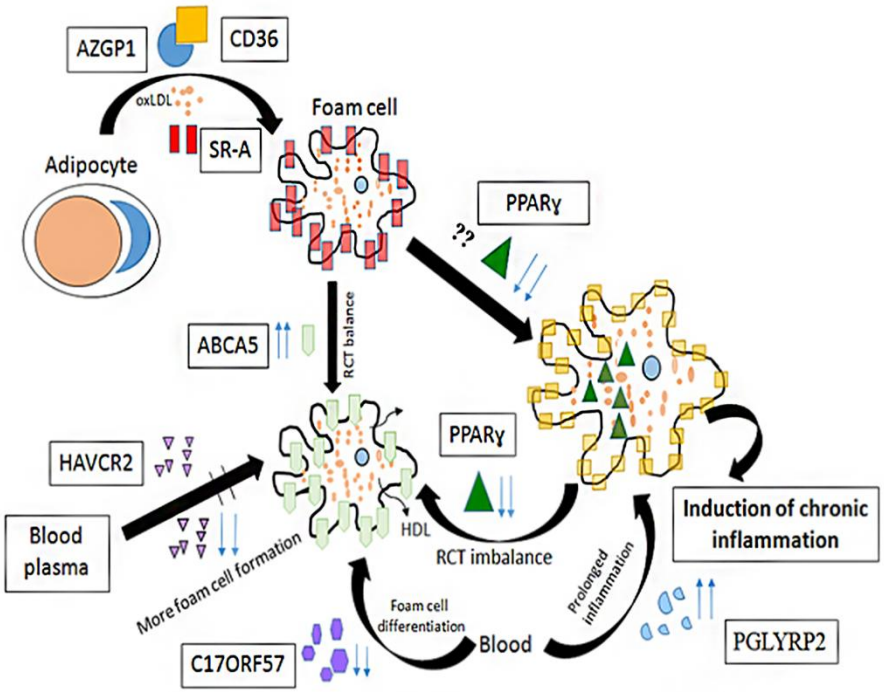

Figure 9.2. Diagrammatic representation showing the contribution of validated proteins in chronic inflammation, RCT and atherosclerosis.

Upward blue arrows indicate an increased level of the protein whereas downward blue arrows indicate a decreased level of the protein as found in the study.

REFERENCES

References

1. Benjamin EJ, Muntner P, Alonso A, Bittencourt MS, Callaway CW, Carson AP, et al. Heart Disease and Stroke Statistics-2019 Update: A Report From the American Heart Association. Circulation. 2019 Mar 5;139(10):e56-e528. PubMed PMID: 30700139.

2. Bourantas CV, Garcia-Garcia HM, Torii R, Zhang YJ, Westwood M, Crake T, et al. Vulnerable plaque detection: an unrealistic quest or a feasible objective with a clinical value? Heart. 2016 Apr;102(8):581-9. PubMed PMID: 26783236.

3. Bradshaw PJ, Ko DT, Newman AM, Donovan LR, Tu JV. Validity of the GRACE (Global Registry of Acute Coronary Events) acute coronary syndrome prediction model for six month post-discharge death in an independent data set. Heart. 2006 Jul;92(7):905-9. PubMed PMID: 16387810. Pubmed Central PMCID: 1860727.

4. Brown TM, Bittner V. Biomarkers of atherosclerosis: clinical applications. Current cardiology reports. 2008 Nov;10(6):497-504. PubMed PMID: 18950561. Pubmed Central PMCID: 2774886.

5. Carmona-Saez P, Chagoyen M, Tirado F, Carazo JM, Pascual-Montano A. GENECODIS: a web-based tool for finding significant concurrent annotations in gene lists. Genome biology. 2007;8(1):R3. PubMed PMID: 17204154. Pubmed Central PMCID: 1839127.

6. Das AA, Chakravarty D, Bhunia D, Ghosh S, Mandal PC, Siddiqui KN, et al. Elevated level of circulatory sTLT1 induces inflammation through SYK/MEK/ERK signalling in coronary artery disease. Clinical science. 2019 Nov 29;133(22):2283-99. PubMed PMID: 31713591.

7. Davi G, Patrono C. Platelet activation and atherothrombosis. The New England journal of medicine. 2007 Dec 13;357(24):2482-94. PubMed PMID: 18077812.

8. Derive M, Bouazza Y, Sennoun N, Marchionni S, Quigley L, Washington V, et al. Soluble TREM-like transcript-1 regulates leukocyte activation and controls microbial sepsis. Journal of immunology. 2012 Jun 1;188(11):5585-92. PubMed PMID: 22551551. Pubmed Central PMCID: 6382278.

9. Djebara S, Biston P, Fosse E, Daper A, Joris M, Boudjeltia KZ, et al. Time Course of CD64, a Leukocyte Activation Marker, During Cardiopulmonary Bypass Surgery. Shock. 2017 Feb;47(2):158-64. PubMed PMID: 27648690.

10. Ed Rainger G, Chimen M, Harrison MJ, Yates CM, Harrison P, Watson SP, et al. The role of platelets in the recruitment of leukocytes during vascular disease. Platelets. 2015;26(6):507-20. PubMed PMID: 26196409. Pubmed Central PMCID: 4673595.

11. El-Menyar A, Zubaid M, AlMahmeed W, Sulaiman K, AlNabti A, Singh R, et al. Killip classification in patients with acute coronary syndrome: insight from a multicenter registry. The American journal of emergency medicine. 2012 Jan;30(1):97-103. PubMed PMID: 21159479.

12. Foks AC, Ran IA, Wasserman L, Frodermann V, Ter Borg MN, de Jager SC, et al. T-cell immunoglobulin and mucin domain 3 acts as a negative regulator of atherosclerosis. Arteriosclerosis, thrombosis, and vascular biology. 2013 Nov;33(11):2558-65. PubMed PMID: 23990206.

13. Fuster V. The Vulnerable Patient: Providing a Lens Into the Interconnected Diseases of the Heart and Brain. Journal of the American College of Cardiology. 2015 Sep 1;66(9):1077-8. PubMed PMID: 26314536.

14. Gattis JL, Washington AV, Chisholm MM, Quigley L, Szyk A, McVicar DW, et al. The structure of the extracellular domain of triggering receptor expressed on myeloid cells like transcript-1 and evidence for a naturally occurring soluble fragment. The Journal of biological chemistry. 2006 May 12;281(19):13396-403. PubMed PMID: 16505478.

15. Hansson GK, Robertson AK, Soderberg-Naucler C. Inflammation and atherosclerosis. Annual review of pathology. 2006;1:297-329. PubMed PMID: 18039117.

16. Hartmann P, Schober A, Weber C. Chemokines and microRNAs in atherosclerosis. Cellular and molecular life sciences : CMLS. 2015 Sep;72(17):3253-66. PubMed PMID: 26001902. Pubmed Central PMCID: 4531138.

17. Hernandez-Vargas P, Ortiz-Munoz G, Lopez-Franco O, Suzuki Y, Gallego-Delgado J, Sanjuan G, et al. Fcgamma receptor deficiency confers protection against atherosclerosis in apolipoprotein E knockout mice. Circulation research. 2006 Nov 24;99(11):1188-96. PubMed PMID: 17053192.

18. Huang da W, Sherman BT, Lempicki RA. Systematic and integrative analysis of large gene lists using DAVID bioinformatics resources. Nature protocols. 2009;4(1):44-57. PubMed PMID: 19131956.

19. Huang da W, Sherman BT, Lempicki RA. Bioinformatics enrichment tools: paths toward the comprehensive functional analysis of large gene lists. Nucleic acids research. 2009 Jan;37(1):1-13. PubMed PMID: 19033363. Pubmed Central PMCID: 2615629.

20. Huo Y, Zhao L, Hyman MC, Shashkin P, Harry BL, Burcin T, et al. Critical role of macrophage 12/15-lipoxygenase for atherosclerosis in apolipoprotein E-deficient mice. Circulation. 2004 Oct 5;110(14):2024-31. PubMed PMID: 15451785.

21. Insull W, Jr. The pathology of atherosclerosis: plaque development and plaque responses to medical treatment. The American journal of medicine. 2009 Jan;122(1 Suppl):S3-S14. PubMed PMID: 19110086.

22. Jones DP, True HD, Patel J. Leukocyte Trafficking in Cardiovascular Disease: Insights from Experimental Models. Mediators of inflammation. 2017;2017:9746169. PubMed PMID: 28465628. Pubmed Central PMCID: 5390637.

23. Kastritis PL, Bonvin AM. Are scoring functions in protein-protein docking ready to predict interactomes? Clues from a novel binding affinity benchmark. Journal of proteome research. 2010 May 7;9(5):2216-25. PubMed PMID: 20329755.

24. Kozakov D, Hall DR, Xia B, Porter KA, Padhorny D, Yueh C, et al. The ClusPro web server for protein-protein docking. Nature protocols. 2017 Feb;12(2):255-78. PubMed PMID: 28079879. Pubmed Central PMCID: 5540229.

25. Libby P. Atherosclerosis: disease biology affecting the coronary vasculature. The American journal of cardiology. 2006 Dec 18;98(12A):3Q-9Q. PubMed PMID: 17169627.

26. Lindner JR. Btk inhibitors in atherosclerosis. Blood. 2018 Jun 14;131(24):2601-2. PubMed PMID: 29903867. Pubmed Central PMCID: 6032894 interests.

27. Lygirou V, Latosinska A, Makridakis M, Mullen W, Delles C, Schanstra JP, et al. Plasma proteomic analysis reveals altered protein abundances in cardiovascular disease. Journal of translational medicine. 2018 Apr 17;16(1):104. PubMed PMID: 29665821. Pubmed Central PMCID: 5905170.

28. Mancardi DA, Albanesi M, Jonsson F, Iannascoli B, Van Rooijen N, Kang X, et al. The high-affinity human IgG receptor FcgammaRI (CD64) promotes IgG-mediated

inflammation, anaphylaxis, and antitumor immunotherapy. Blood. 2013 Feb 28;121(9):1563-73. PubMed PMID: 23293080.

29. Marchio P, Guerra-Ojeda S, Vila JM, Aldasoro M, Victor VM, Mauricio MD. Targeting Early Atherosclerosis: A Focus on Oxidative Stress and Inflammation. Oxidative medicine and cellular longevity. 2019;2019:8563845. PubMed PMID: 31354915. Pubmed Central PMCID: 6636482.

30. Mashiach E, Nussinov R, Wolfson HJ. FiberDock: Flexible induced-fit backbone refinement in molecular docking. Proteins. 2010 May 1;78(6):1503-19. PubMed PMID: 20077569. Pubmed Central PMCID: 4290165.

31. Mi H, Muruganujan A, Casagrande JT, Thomas PD. Large-scale gene function analysis with the PANTHER classification system. Nature protocols. 2013 Aug;8(8):1551-66. PubMed PMID: 23868073. Pubmed Central PMCID: 6519453.

32. Mi H, Muruganujan A, Thomas PD. PANTHER in 2013: modeling the evolution of gene function, and other gene attributes, in the context of phylogenetic trees. Nucleic acids research. 2013 Jan;41(Database issue):D377-86. PubMed PMID: 23193289. Pubmed Central PMCID: 3531194.

33. Moore KJ, Sheedy FJ, Fisher EA. Macrophages in atherosclerosis: a dynamic balance. Nature reviews Immunology. 2013 Oct;13(10):709-21. PubMed PMID: 23995626. Pubmed Central PMCID: 4357520.

34. Morrow DA, Antman EM, Charlesworth A, Cairns R, Murphy SA, de Lemos JA, et al. TIMI risk score for ST-elevation myocardial infarction: A convenient, bedside, clinical score for risk assessment at presentation: An intravenous nPA for treatment of infarcting myocardium early II trial substudy. Circulation. 2000 Oct 24;102(17):2031-7. PubMed PMID: 11044416.

35. Mracek T, Gao D, Tzanavari T, Bao Y, Xiao X, Stocker C, et al. Downregulation of zinc-{alpha}2-glycoprotein in adipose tissue and liver of obese ob/ob mice and by tumour necrosis factor-alpha in adipocytes. The Journal of endocrinology. 2010 Feb;204(2):165-72. PubMed PMID: 19934249. Pubmed Central PMCID: 2807359.

36. Muthusamy B, Hanumanthu G, Suresh S, Rekha B, Srinivas D, Karthick L, et al. Plasma Proteome Database as a resource for proteomics research. Proteomics. 2005 Aug;5(13):3531-6. PubMed PMID: 16041672.

37. Nanjappa V, Thomas JK, Marimuthu A, Muthusamy B, Radhakrishnan A, Sharma R, et al. Plasma Proteome Database as a resource for proteomics research: 2014 update. Nucleic acids research. 2014 Jan;42(Database issue):D959-65. PubMed PMID: 24304897. Pubmed Central PMCID: 3965042.

38. Ndhlovu LC, Lopez-Verges S, Barbour JD, Jones RB, Jha AR, Long BR, et al. Tim-3 marks human natural killer cell maturation and suppresses cell-mediated cytotoxicity. Blood. 2012 Apr 19;119(16):3734-43. PubMed PMID: 22383801. Pubmed Central PMCID: 3335380.

39. Nogales-Cadenas R, Carmona-Saez P, Vazquez M, Vicente C, Yang X, Tirado F, et al. GeneCodis: interpreting gene lists through enrichment analysis and integration of diverse biological information. Nucleic acids research. 2009 Jul;37(Web Server issue):W317-22. PubMed PMID: 19465387. Pubmed Central PMCID: 2703901.

40. Nording HM, Seizer P, Langer HF. Platelets in inflammation and atherogenesis. Frontiers in immunology. 2015;6:98. PubMed PMID: 25798138. Pubmed Central PMCID: 4351644.

41. Patzelt J, Verschoor A, Langer HF. Platelets and the complement cascade in atherosclerosis. Frontiers in physiology. 2015;6:49. PubMed PMID: 25784879. Pubmed Central PMCID: 4345806.

42. Porter KA, Xia B, Beglov D, Bohnuud T, Alam N, Schueler-Furman O, et al. ClusPro PeptiDock: efficient global docking of peptide recognition motifs using FFT. Bioinformatics. 2017 Oct 15;33(20):3299-301. PubMed PMID: 28430871. Pubmed Central PMCID: 5860028.

43. Prabhakaran D, Anand S, Watkins D, Gaziano T, Wu Y, Mbanya JC, et al. Cardiovascular, respiratory, and related disorders: key messages from Disease Control Priorities, 3rd edition. Lancet. 2018 Mar 24;391(10126):1224-36. PubMed PMID: 29108723. Pubmed Central PMCID: 5996970.

44. Ramji DP, Davies TS. Cytokines in atherosclerosis: Key players in all stages of disease and promising therapeutic targets. Cytokine & growth factor reviews. 2015 Dec;26(6):673-85. PubMed PMID: 26005197. Pubmed Central PMCID: 4671520.

45. Riccioni G, Back M, Capra V. Leukotrienes and atherosclerosis. Current drug targets. 2010 Jul;11(7):882-7. PubMed PMID: 20388065.

46. Rios FJ, Koga MM, Ferracini M, Jancar S. Co-stimulation of PAFR and CD36 is required for oxLDL-induced human macrophages activation. PloS one. 2012;7(5):e36632. PubMed PMID: 22570732. Pubmed Central PMCID: 3343035.

47. Roth GA, Johnson C, Abajobir A, Abd-Allah F, Abera SF, Abyu G, et al. Global, Regional, and National Burden of Cardiovascular Diseases for 10 Causes, 1990 to 2015. Journal of the American College of Cardiology. 2017 Jul 4;70(1):1-25. PubMed PMID: 28527533. Pubmed Central PMCID: 5491406.

48. Sakakura K, Nakano M, Otsuka F, Ladich E, Kolodgie FD, Virmani R. Pathophysiology of atherosclerosis plaque progression. Heart, lung & circulation. 2013 Jun;22(6):399-411. PubMed PMID: 23541627.

49. Schneidman-Duhovny D, Inbar Y, Nussinov R, Wolfson HJ. PatchDock and SymmDock: servers for rigid and symmetric docking. Nucleic acids research. 2005 Jul 1;33(Web Server issue):W363-7. PubMed PMID: 15980490. Pubmed Central PMCID: 1160241.

50. Schneidman-Duhovny D, Inbar Y, Polak V, Shatsky M, Halperin I, Benyamini H, et al. Taking geometry to its edge: fast unbound rigid (and hinge-bent) docking. Proteins. 2003 Jul 1;52(1):107-12. PubMed PMID: 12784375.

51. Silverstein RL, Li W, Park YM, Rahaman SO. Mechanisms of cell signaling by the scavenger receptor CD36: implications in atherosclerosis and thrombosis. Transactions of the American Clinical and Climatological Association. 2010;121:206-20. PubMed PMID: 20697562. Pubmed Central PMCID: 2917163.

52. Stefanadis C, Antoniou CK, Tsiachris D, Pietri P. Coronary Atherosclerotic Vulnerable Plaque: Current Perspectives. Journal of the American Heart Association. 2017 Mar 17;6(3). PubMed PMID: 28314799. Pubmed Central PMCID: 5524044.

53. Steinberg D, Witztum JL. Oxidized low-density lipoprotein and atherosclerosis. Arteriosclerosis, thrombosis, and vascular biology. 2010 Dec;30(12):2311-6. PubMed PMID: 21084697.

54. Szklarczyk D, Gable AL, Lyon D, Junge A, Wyder S, Huerta-Cepas J, et al. STRING v11: protein-protein association networks with increased coverage, supporting functional discovery in genome-wide experimental datasets. Nucleic acids research.

2019 Jan 8;47(D1):D607-D13. PubMed PMID: 30476243. Pubmed Central PMCID: 6323986.

55. Szklarczyk D, Morris JH, Cook H, Kuhn M, Wyder S, Simonovic M, et al. The STRING database in 2017: quality-controlled protein-protein association networks, made broadly accessible. Nucleic acids research. 2017 Jan 4;45(D1):D362-D8. PubMed PMID: 27924014. Pubmed Central PMCID: 5210637.

56. Tabas-Madrid D, Nogales-Cadenas R, Pascual-Montano A. GeneCodis3: a non-redundant and modular enrichment analysis tool for functional genomics. Nucleic acids research. 2012 Jul;40(Web Server issue):W478-83. PubMed PMID: 22573175. Pubmed Central PMCID: 3394297.

57. Thomas PD, Campbell MJ, Kejariwal A, Mi H, Karlak B, Daverman R, et al. PANTHER: a library of protein families and subfamilies indexed by function. Genome research. 2003 Sep;13(9):2129-41. PubMed PMID: 12952881. Pubmed Central PMCID: 403709.

58. Thomas PD, Kejariwal A, Campbell MJ, Mi H, Diemer K, Guo N, et al. PANTHER: a browsable database of gene products organized by biological function, using curated protein family and subfamily classification. Nucleic acids research. 2003 Jan 1;31(1):334-41. PubMed PMID: 12520017. Pubmed Central PMCID: 165562.

59. Tosi F, Micaglio R, Sandri M, Castagna A, Minguzzi D, Stefanoni F, et al. Increased plasma thrombin potential is associated with stable coronary artery disease: An angiographically-controlled study. Thrombosis research. 2017 Jul;155:16-22. PubMed PMID: 28477533.

60. Tousoulis D, Charakida M, Stefanadis C. Endothelial function and inflammation in coronary artery disease. Heart. 2006 Apr;92(4):441-4. PubMed PMID: 16159981. Pubmed Central PMCID: 1860901.

61. Vacek TP, Rehman S, Neamtu D, Yu S, Givimani S, Tyagi SC. Matrix metalloproteinases in atherosclerosis: role of nitric oxide, hydrogen sulfide, homocysteine, and polymorphisms. Vascular health and risk management. 2015;11:173-83. PubMed PMID: 25767394. Pubmed Central PMCID: 4354431.

62. van der Meijden PEJ, Heemskerk JWM. Platelet biology and functions: new concepts and clinical perspectives. Nature reviews Cardiology. 2019 Mar;16(3):166-79. PubMed PMID: 30429532.

63. van Zundert GCP, Rodrigues J, Trellet M, Schmitz C, Kastritis PL, Karaca E, et al. The HADDOCK2.2 Web Server: User-Friendly Integrative Modeling of Biomolecular Complexes. Journal of molecular biology. 2016 Feb 22;428(4):720-5. PubMed PMID: 26410586.

64. Virmani R, Kolodgie FD, Burke AP, Finn AV, Gold HK, Tulenko TN, et al. Atherosclerotic plaque progression and vulnerability to rupture: angiogenesis as a source of intraplaque hemorrhage. Arteriosclerosis, thrombosis, and vascular biology. 2005 Oct;25(10):2054-61. PubMed PMID: 16037567.

65. Washington AV, Gibot S, Acevedo I, Gattis J, Quigley L, Feltz R, et al. TREM-like transcript-1 protects against inflammation-associated hemorrhage by facilitating platelet aggregation in mice and humans. The Journal of clinical investigation. 2009 Jun;119(6):1489-501. PubMed PMID: 19436112. Pubmed Central PMCID: 2689104.

PUBLICATIONS

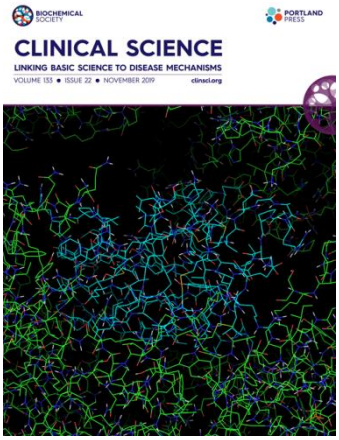

Original Articles

- **Das AA**, Chakravarty D, Bhunia D, Ghosh S, Mandal PC, Siddiqui KN, Bandyopadhyay A.(2019)Elevated level of circulatory sTLT1 induces inflammation through SYK/MEK/ ERK signalling in coronary artery disease. **Clin Sci (Lond).** Nov 29; 133(22):2283-2299. doi: 10.1042/CS20190999. PMID: 31713591.
- **Das AA**, Roy ChoudhuryK, Jagadeeshaprasad M G, Kulkarni Mahesh J., Mondal P C&Arun Bandyopadhyay.Proteomic Analysis Detects Dysregulated Reverse Cholesterol Transport in Human Subjects with ST-Segment Elevation Myocardial Infarction. (Manuscript under review)
- Yelamanchi SD, Tyagi A, Mohanty V, Dutta P, Korbonits M, Chavan S, Advani J, Madugundu AK, Dey G, Datta KK, Rajyalakshmi M, Sahasrabuddhe NA, Chaturvedi A, Kumar A, **Das AA**, Ghosh D, Jogdand GM, Nair HH, Saini K, Panchal M, Sarvaiya MA, Mohanraj SS, Sengupta N, Saxena P, Subramani PA, Kumar P, Akkali R, Reshma SV, Santhosh RS, Rastogi S, Kumar S, Ghosh SK, Irlapati VK, Srinivasan A, Radotra BD, Mathur PP, Wong GW, Satishchandra P, Chatterjee A, Gowda H, Bhansali A, Pandey A, Shankar SK, Mahadevan A, Prasad TSK. (2018)Proteomic Analysis of the Human Anterior Pituitary Gland. **OMICS**. Dec; 22(12):759-769. doi: 10.1089/omi. 2018.0160.PMID:30571610
- Cristina Vassalle, Claudio Marabotti, Siddiqui Khawer Naveed, Roy Arun, Irene Traghella, Francesca Mastorci, Alberto Marabotti, **Das Apabrita Ayan**, Banerjee Tanima, Chakravarty Devasmita, Bandyopadhyay Arun, Kyriazoula Chatzianagnostou, Mirko Passera, Simona Storti and Alessandro Pingitore. (2019) Dietary and Lifestyle Impact on Different Biochemical and Hematological Parameters in Indian Children. **EC Cardiology.** 6(10): 1002-1009.

Conference Proceedings

- Kamalika Roy Choudhury, **Apabrita Ayan Das** and Arun Bandyopadhyay. **Differential proteomic profiling of control and STEMI subjects: probable implications towards reverse cholesterol transport. J Clin. Exp. Cardiolog** .DOI: 10.4172/2155-9880-C1-086
- **Apabrita Ayan Das**, Prakash C Mandal, Khawer N Siddiqui and ArunBandyopadhyay **.**Elevated level of sTLT1 is associated with risk prediction in acute coronary syndrome. **J Clin. Exp. Cardiolog**. DOI: 10.4172/2155-9880-C1-086

Clinical Science (2019) **133** 2283–2299
https://doi.org/10.1042/CS20190999

PORTLAND PRESS

Research Article

Elevated level of circulatory sTLT1 induces inflammation through SYK/MEK/ERK signalling in coronary artery disease

Apabrita Ayan Das[1], Devasmita Chakravarty[1], Debmalya Bhunia[2], Surajit Ghosh[2], Prakash C. Mandal[3], Khawer N. Siddiqui[4] and Arun Bandyopadhyay[1]

[1]Cell Biology and Physiology Division, CSIR-Indian Institute of Chemical Biology, CN-6, Sector 5, Salt Lake, Kolkata 700091, India; [2]Organic and Medicinal Chemistry Division, CSIR-Indian Institute of Chemical Biology, Jadavpur, Kolkata 700032, India; [3]Department of Interventional Cardiology, Apollo Gleneagles Hospital, Kolkata, India; [4]Cardiac Research Division,Ruby General Hospital, Kolkata, India

Correspondence: Arun Bandyopadhyay (arunb@iicb.res.in)

The role of inflammation in all phases of atherosclerotic process is well established and soluble TREM-like transcript 1 (sTLT1) is reported to be associated with chronic inflammation. Yet, no information is available about the involvement of sTLT1 in atherosclerotic cardiovascular disease. Present study was undertaken to determine the pathophysiological significance of sTLT1 in atherosclerosis by employing an observational study on human subjects (n=117) followed by experiments in human macrophages and atherosclerotic apolipoprotein E (apoE)$^{-/-}$ mice. Plasma level of sTLT1 was found to be significantly (P<0.05) higher in clinical (2342 $\pm$ 184 pg/ml) and subclinical cases (1773 $\pm$ 118 pg/ml) than healthy controls (461 $\pm$ 57 pg/ml). Moreover, statistical analyses further indicated that sTLT1 was not only associated with common risk factors for Coronary Artery Disease (CAD) in both clinical and subclinical groups but also strongly correlated with disease severity. *Ex vivo* studies on macrophages showed that sTLT1 interacts with Fcγ receptor I (FcγRI) to activate spleen tyrosine kinase (SYK)-mediated downstream MAP kinase signalling cascade to activate nuclear factor-κ B (NF-kB). Activation of NF-kB induces secretion of tumour necrosis factor-α (TNF-α) from macrophage cells that plays pivotal role in governing the persistence of chronic inflammation. Atherosclerotic apoE$^{-/-}$ mice also showed high levels of sTLT1 and TNF-α in nearly occluded aortic stage indicating the contribution of sTLT1 in inflammation. Our results clearly demonstrate that sTLT1 is clinically related to the risk factors of CAD. We also showed that binding of sTLT1 with macrophage membrane receptor, FcγR1 initiates inflammatory signals in macrophages suggesting its critical role in thrombus development and atherosclerosis.

Introduction

Platelets are the smallest and specialised blood cells that play important roles in physiological processes including haemostasis, thrombosis, inflammation, wound healing and host defence. In atherosclerosis, platelets enrich and promote the inflammatory milieu by recruiting inflammatory cells near the lesion sites and release inflammatory mediators [1]. The interplay among platelets, endothelial cells, circulating leucocytes and progenitor cells contributes to leucocyte activation, adhesion and transmigration. Once activated, the platelet-secreted proteins set the course of next atherosclerotic events depending upon the very specific stimulus by which the platelets get activated. Thrombin, being a platelet agonist, acts as a pro-atherosclerotic mediator in cardiovascular diseases and remains consistently high in the plasma of coronary artery disease (CAD) patients [2]. So, the proteins secreted from thrombin-activated platelets may play potential roles in the manifestation of atherosclerosis as well as CAD.

Received: 25 September 2019
Revised: 08 November 2019
Accepted: 11 November 2019

Accepted Manuscript online: 12 November 2019
Version of Record published: 21 November 2019

Clinical Science (2019) **133** 2283–2299
https://doi.org/10.1042/CS20190999

TREM-like transcript 1 (TLT1), which is known to be expressed on the surface membrane of thrombin-activated platelets, is confined to megakaryocytes as well as platelets [3] and is mostly thought to be associated with thrombus formation. The truncated part of TLT1 (17 kDa), a part of the extracellular domain of the main protein, is released into the bloodstream as soluble TLT1 (sTLT1) [4]. It has already been shown, this protein promotes platelet endothelial cell interaction, actin polymerisation [5], platelet aggregation [3,6] and leucocyte activation in microbial sepsis [7], but its role in CAD as well as atherosclerosis still remains to be understood. In CAD, high levels of thrombin not only activate platelets to mediate thrombosis but also get involved in ongoing inflammatory process along with atherosclerosis through the secretion of pro-inflammatory cytokines [8]. However, sTLT1, a protein secreted from thrombin-stimulated platelets is not yet reported to be connected to inflammation. Furthermore, even though the blood thrombin levels in CAD patients and asymptomatic individuals with associated risk factors remain high [2], no information is available about the role of circulating sTLT1 in cardiovascular pathology. It is reported that triggering receptor expressed on myeloid cells like protein (TREML) group of proteins mostly bind with proteins possessing spleen tyrosine kinase (SYK) domain in their intracellular part and induce inflammation [9]. TLT1, being a member of TREML protein family, has a high possibility of involvement in inflammation. But, the specific receptors involved and the intracellular effect of this protein upon receptor binding remain largely unknown.

Fc receptors are well conserved among species and play a crucial role in maintaining cellular effector functions. Fcγ receptor I (FcγRI), being an SYK domain-associated protein, likely has its own claim as a receptor for sTLT1. It binds to immunoglobulin G (IgG) with high affinity and is constitutively expressed on monocytes, macrophages, dendritic cells and neutrophils. Interestingly, the docking mode of this protein is largely constant for most of its ligands [10]. Since, the binding affinity between FcγRI and IgG is very high, the receptors remain oversaturated with IgG even after extravasations of immune cells. But the exact role of this receptor protein in atherosclerosis remains unclear [11]. The relationship of FcγRI with cardiovascular disease was established by a study which showed FcγRI deficiency conferred protection against atherosclerosis in apolipoprotein E (apoE$^{-/-}$) mice [12]. Studies reported that saturated FcγRI binds to other ligands in an inflammatory environment to form an immune complex but the mechanism of such interactions and the role of FcγRI in intracellular signalling are still not understood.

Involvement of sTLT1 towards atherosclerosis as well as CAD pathology is still poorly understood. It is likely that sTLT1 functions via conserved Fcγ receptors and thereby contributes to CAD. In the present study, we established a strong association between plasma levels of sTLT1 with severity and progression of CAD using healthy control, asymptomatic individuals and CAD subjects. We also show that sTLT1 binds to FcγRI on macrophage surface initiating SYK-mediated signalling which might contribute to inflammation and atherosclerosis.

Experimental

Chemicals

Fmoc protected amino acids and rink amide AM resin both were purchased from Novabiochem (Merck). *N,N′*-dimethylformamide (DMF), Dichloromethane (DCM), Trifluoroacetic acid (TFA), pipyridine, *o*-(Benzotriaz ol-1-yl)-N,N,N′,N′-tetramethyluroniumhexafluorophosphate (HBTU), Diisopropylethylamine (DIEA) and diethyl ether were purchased from Spectrochem. Ethanedithiol (EDT) and phenol were bought from Merck, Darmstadt, Germany. Antibodies, ELISA kits and reagents were purchased as described in the respective methods.

Study population and study design

Fresh blood samples were collected from the subjects with CAD (n=60) on their arrival in Apollo Gleneagles Hospital, Kolkata, India. Blood from healthy (n=16), as well as asymptomatic individuals (n=41), were collected from the local population through randomized routine check-up. Post-percutaneous intervention (Post-PCI) samples were taken from the same individuals who were considered as CAD patients previously. Blood plasma was separated by centrifugation at 2500×***g*** for 10 min and stored in −80°C freezer.

The protocol was approved by the Ethics Committees of CSIR-IICB and Apollo Gleneagles Hospital, Kolkata (Reference no. IEC Ref: IEC/2013/10/32; Date of approval: 15th October, 2013). Informed consents were obtained from each individual prior to blood collection. Samples were collected according to the Declaration of Helsinki (1975). Detailed information about each individual was collected in a proforma made according to the guidelines of the Indian Council for Medical Research.

Inclusion and exclusion criteria

Subjects with CAD were enrolled for the study. Subjects other than CAD such as valvular heart disease, any chronic cardiovascular disease, diabetes, renal failure, hepatic failure, cancer, thyroid and other endocrinopathies, known genetic disorders, platelet-related disorders, collagen-related vascular disease, sepsis were excluded from the study. Healthy controls were recruited from the local population with normal systolic/diastolic blood pressure, normal blood profile, normal echocardiograph and -electrocardiograph. Carotid intima–media thickness were within normal range (<1 mm). The subjects with abnormal lipid profile and common risk factors, history of smoking or raw tobacco consumption, abnormal electrocardiogram (ECG) and echocardiography reports, carotid intima–media thickness > 1 mm were categorized as asymptomatic or subclinical subjects. Diabetic cardiomyopathy patients were excluded due to their use of anti-diabetic medications which might complicate original goal of the study.

Echocardiography

Two-dimensional trans-thoracic echocardiography with targetted M-mode and Doppler were performed using commercially available systems by trained cardiologists. Echocardiography of CAD was confirmed to the recommendation of the 2012 World Heart Federation Criteria. All measurements were made by blinded observers and the mean of the three readings was recorded. Ejection fraction was calculated by Simpson's method. Carotid intima–media thickness was determined by a trained physician using Duplex-Doppler vascular study.

Peptide synthesis

Scramble and active peptides (17 amino acids long) were synthesised. Sequences of the peptides were # **sequence 1: LQEEDAGEYGCMVDGAR (active peptide) and # sequence 2: EDGQIYVPCLQYSLPQV (scramble).** To synthesise the peptides 300 mg of rink amide AM resin was placed in a peptide vessel and swelled overnight in DMF-DCM (1:1) solvent. Five equivalent of excess Fmoc protected amino acids (depending on sequence) were coupled successively followed by Fmoc deprotection using 20% piperidine solution in CEM microwave peptide synthesiser equipped with Liberty 1. Coupling and deprotection steps were maintained for 8 min and 5 min, respectively. N,N′-DIEA and HBTU were used as an activator base and activator, respectively. DMF was used as solvent. After completion of the synthesis, the peptide attached resin was washed by DMF and DCM solvents. Peptides attached with resin were cleaved by standard resin cleavage cocktail solution containing 92.5% TFA, 2.5% milli-Q water, 2.5% EDT and 2.5% phenol. Resin attached peptide was kept for 3 h containing this peptide cleavage solution in a peptide vessel on shaker (Labnet International). After that, TFA was removed from the filtrate by nitrogen gas flow. The filtrate was added gradually to the cold diethyl ether solvent to ensure complete precipitation. The precipitation was separated by centrifugation. Finally, synthesised peptides were purified by using Shimadzu HPLC system equipped with C-18 reverse-phase HPLC column and molecular weights were confirmed by MALDI-TOF mass spectrometry (Supplementary Figure 2A–D). The purity of the peptides was checked by MALDI MS/MS (Supplementary Figure 2).

Docking analysis

Structures of SH2 domain of Fcγ RI and IgV-like domain were retrieved from PDB. The tertiary structures were optimised using Repair PDB function in FoldX to remove bad torsion angles; steric clashes and built missing atoms [13]. Visual analysis of interface residues was performed using PyMOL. Intermolecular interaction of SH2 (FcγRI) and IgV-like domain (sTLT1) were analysd via protein–protein docking and by calculating free energy of binding. PATCHDOCK, ClusPro V.2.0 and HADDOCK 2.2 (High Ambiguity Driven protein–protein Docking) servers were selected to perform receptor–ligand docking. FcγRI (SH2 domain) was defined as receptor and IgV like domain of sTLT1 was defined as ligand for all the docking servers. Structures for SH2 domain and IgV like domain were uploaded in PATCHDOCK server (clustering RMSD was set to 2.0), which utilises a fast Fourier transform (FFT) algorithm to search spatial degree of freedom between receptor as well as ligand and reports each binding mode with an energy scoring function. Same receptor–ligand pair was docked independently with ClusPro V.2.0 which uses PIPER to find pairwise interaction potentials as well as rank them on the basis of stability, semi-definite programming based under-estimation (SDU) energy and cluster size. The cluster with best statistics in both cases was chosen for further studies which were performed using HADDOCK2.2. It uses biophysical or biochemical interaction data such as chemical shift perturbation data from NMR. The information about interacting residues was introduced as ambiguous interaction restraints (AIRs) to drive the docking. Then, the structures were docked according to their intermolecular energy after calculation (that is the sum of electrostatic, van der Walls and AIR energy terms). So, lowest HADDOCK score represents the best possible interacting pair. Rigid body minimisation and then semi-rigid TAD-SA as well as final refinement in Cartesian space for the experimental pair were performed by HADDOCK2.2.

Clinical Science (2019) **133** 2283–2299
https://doi.org/10.1042/CS20190999

For this analysis, we specifically generated AIR restrained file for both the proteins and specified the probable interacting chains (as identified from other two servers) to get best cluster combination with minimum HADDOCK score.

ELISA

Distribution of cholesterol among lipoprotein subfractions in CAD subjects was determined by commercially available colorimetric assay kit using cholesterol probe (Sigma–Aldrich, U.S.A.). Distribution of the same in healthy controls and asymptomatic individuals were obtained from the diagnostic centre where they were recruited by the cardiologist involved in the present study (Khawer N. Siddiqui). Soluble TLT1 in mice and human (R&D systems, U.S.A.), oxidised low-density lipoprotein (LDL) (Uscn Life Sciences, U.S.A.) and tumour necrosis factor-α (TNF-α) in mice and human (R&D systems, U.S.A.) levels were measured by sandwich ELISA method as per the manufacturers' instructions. The detection limit of the kit was 10 pg/ml for sTLT1 and oxLDL whereas for TNF-α, it was 5.5 pg/ml. The intra-assay CV was <10% and the inter-assay CV was <12% in all the ELISA.

Western blotting

Proteins (60 μg) were resolved in 10% SDS/PAGE and Western blots from cell lysate were performed according to the previously established protocol [14]. Plasma samples were diluted (1:50) and 60 μg protein was resolved in 10% denaturing gel with pre-stained protein ladder (Fermentas #SM0671). Separated protein bands were transferred to PVDF membrane with semi-dry transfer apparatus (45 volts, 150 mA). The membranes were then incubated with 5% non-fat milk solution, followed by incubation with primary antibodies and secondary antibodies (1:4000, anti-goat; 1:5000, anti-mouse; 1:5000, anti-rabbit; AP–conjugated) with alternate wash. Blots were finally incubated with NBT/BCIP solution until the bands were visible.

The primary antibodies were diluted in 5% milk in TBST and used in indicated dilutions for signalling studies from plasma and differentiated THP1 macrophages: anti-TLT1 (1:1000, R&D Systems, U.S.A.); anti-human α-transferrin (1:2000, Sigma–Aldrich, U.S.A.); anti-IKK-β (1:500, sc-271782, Santa Cruz Biotechnology); anti-phospho-IKK-α/β (1:1000, sc-21661, Santa Cruz Biotechnology); anti-nuclear factor-κ B (NF-kB)-p65 (1:800, sc-8008, Santa Cruz Biotechnology); anti-phospho-NF-kB-p65 (1:800, sc-33020, Santa Cruz Biotechnology); anti-MEK1/2 (1:1000, #9122, Cell Signaling Technology); anti-phospho-MEK1/2 (1:500, sc-7995, Santa Cruz Biotechnology); anti-ERK1/2 (1:800, ab17942, Abcam); anti-phospho-ERK1/2 (1:1000, #4370, Cell Signaling Technology); anti-SYK (1:800, #2712, Cell Signaling Technology); anti-phospho-SYK (1:800, #2711, Cell Signaling Technology); anti-Bruton's tyrosine kinase (BTK) (1:2000, ab18934, Abcam); anti-phospho-BTK (1:800, #5082, Cell Signaling Technology) were used to immunoblot corresponding proteins. α-tubulin (1:800, Cell Signaling Technology, U.S.A.) and α-transferrin (1:2000, Sigma–Aldrich, U.S.A.) were used as the loading controls for the immunoblots from cell lysates and plasma samples, respectively.

Co-immunoprecipitation studies

Co-immunoprecipitation for sTLT1 and FcγRI was performed by Pierce Classic Magnetic IP/Co-IP Kit (Cat. no. 88804) with the same antibody used for Western blot (anti-sTLT1, R&D Systems, U.S.A.; anti-FcγRI, R&D Systems, U.S.A.). Co-IP was conducted as per the manufacturer's protocol and macrophage cell lysate loaded for each reaction was 400 μg. IgG was used as negative control for each Co-IP experiment. α-tubulin was used as loading control for Co-IP experiments (Cell Signaling Technology, U.S.A., 1:800).

Cell culture and differentiation

Human THP1 monocyte cells (ATCC) were cultured in modified RPMI 1640 medium (Gibco, U.S.A.) with 10% foetal bovine serum in 5% CO_2 incubator at 37°C. The cells (2×10^6) were seeded with 1 ml of incomplete medium in six-well plates coated with fibronectin (Corning, Biocoat, Germany) and were differentiated using 100 nM phorbol myristate acetate (PMA) (Sigma, U.S.A.) for 24 h at 37°C in 5% CO_2. Differentiated cells remained attached to the bottom of the wells. Floating cells were washed after discarding remaining media and then each well was washed with cell culture grade Dulbecco's phosphate buffer saline (DPBS) (Gibco, U.S.A.). Differentiated THP1 cells were then treated with 10 μg/ml oxidised LDL (oxLDL) (low-TIBAR, Alpha-Aesar, U.S.A.) for 48 h to differentiate into foam cells.

Treatment of differentiated cells with chemically synthesised peptides (sequence 1 or active sequence and scramble)

Differentiated macrophages were treated with Sequence 1 or active peptide and scramble peptide (2 ng/ml) for 6 h; protein was isolated by cell lysis with RIPA buffer for 30 min at 4°C at different time points. Protease inhibitor cocktail (Sigma–Aldrich, U.S.A.) and PhosStop (Roche) were used to prevent proteolysis and destabilisation of phosphoproteins, respectively.

Treatment of differentiated THP1 cells with chemically synthesised peptides and inhibitors

Differentiated THP1 cells were separately treated with active sequence or scramble sequence (2 ng/ml) and in the absence or presence of either SYK blocker, R406 (0.5 μg, 4 μg) or BTK blocker, Ibrutinib (1 μg, 2 μg) along with active sequence. After 6 h, cells were lysed with RIPA buffer for 30 min at 4°C with protease inhibitor cocktail (Sigma–Aldrich, U.S.A.) and PhosStop (Roche, Germany) to prevent proteolysis and destabilisation of phosphoproteins, respectively.

Experiments in mice

Wild-type C57BL/6 mice were received from animal house facility of CSIR-Indian Institute of Chemical Biology, Kolkata, India. ApoE$^{-/-}$ mice were obtained from CSIR-Centre for Cellular and Molecular Biology, Hyderabad, India and maintained in the animal house of CSIR-India Institute of Chemical Biology, Kolkata. The protocol was approved by the Institutional Ethics Committee (Reference no. IICB/AEC/Meeting/2018/Aug) and the animals were handled in accordance with the Committee for the Purpose of Control and Supervision of Experiments on Animals (CPCSEA), Ministry of Social Justice, and Government of India (Registration no. 147/1999/CPCSEA). In each set, ten mice were fed with normal chow diet (kcal: Protein = 25%; Carbohydrate = 58%; Fat = 17%) or high-cholesterol diet (Research Diets Inc.; Open Source DIETS; Cat no. D12336; detailed composition has been attached in Supplementary Table 1) for 2 months (45 and 60 days). Blood was collected by retro-orbital bleeding in EDTA coated vacutainer (BD, U.S.A.) for plasma collection after 45 and 60 days. Isolated plasma was stored at −80°C freezer for future experiments. Estimation of sTLT1 and TNF-α was performed by ELISA using commercially available kits (R&D Systems, U.S.A.). For histopathology, mice were deeply anaesthetised with ether and killed immediately by cervical dislocation. Animals (n=10) were killed after 45 and 60 days to dissect out their aorta and fixed with 4% formaldehyde solution. Aortic sections (8 μm) were prepared from paraffin blocks by microtome. Sections were mounted on slides and observed under a microscope after Haematoxylin–Eosin staining.

Power calculation for the study population

We performed the power calculation by considering control to cases ratio 0.5. We used the following formula for calculating sample size for quantitative variables in case–control studies.

$$\text{Sample size} = (r + 1/r) \times (SD^2(z_\beta + z_{\alpha/2}))/d^2$$

r = ratio of controls to cases
z_β = standard normal variate for power (here for 80% its 0.84)
$z_{\alpha/2}$ = standard normal variate for level of significance (1.96 for P=0.05, i.e. 5% type I error)
SD = standard deviation
d = differences of mean between control and cases.

Based on the power calculation between patient and the subclinical group, we decided to take a sample size of 63 for patients and 32 subclinical subjects whereas power calculation between subclinical and control group suggested a sample size of 24 for subclinical and 12 for the control group [15].

Statistical analysis

Data are expressed as mean ± SEM for continuous variables. Normal distributions for all continuous variables were tested using Kolmogorov–Smirnov test. One-way analysis of variance (ANOVA) was carried out to compare among three experimental groups. Otherwise non-parametric Kruskal–Wallis test was used. Differences among study groups were determined by Student's t test after testing their normality. Samples which were handled erroneously were considered as outliers. We also removed samples who had biological problems (chronic illness, ongoing medication, a high number of platelets, diabetes etc.) as biological outliers. Statistical outliers were detected by Z test and Grubb's test. The correlation between continuous variables was calculated using Pearson's Correlation Coefficient (r). The

Clinical Science (2019) **133** 2283–2299
https://doi.org/10.1042/CS20190999

Table 1 Baseline characteristics of study populations

Variables	Group 1 (*n*=16) Control	Group 2 (*n*=41) Asymptomatic	Group 3 (*n*=60) CAD	*P*-value
Age	39.6 ± 3.34	44 ±1.79	52 ±1.61	0.04
M/F	12/4	32/9	50/10	0.1006
Total cholesterol (mg/dl)	159.4 ± 7.64	174.4 ± 5.72	217.5 ± 9.44	0.0001
HDL cholesterol (mg/dl)	45 ± 3.15	41.6 ± 1.35	36.8 ± 1.5	0.07 (ns)
LDL cholesterol (mg/dl)	95 ± 6.32	107.78 ± 5.02	120.4 ± 8.20	0.01
Triglyceride (mg/dl)	117.19 ± 9.01	143.02 ± 10.88	173.1 ± 14.95	0.187 (ns)
SBP (mm/Hg)	115 ± 3	117 ± 2	120 ± 8	0.02
DBP (mm/Hg)	75 ± 2	77 ± 2	80 ± 2	0.096 (ns)
Smoking status (current/ex)	3/1	12/9	19/2	0.2365

Data are expressed as mean ± SEM and compared by one-way ANOVA. Abbreviation: HDL, high-density lipoprotein; ns, not significant.

numbers of subjects taken into account in different correlation studies are different because of the exclusion of statistical and biological outliers from the data. Multiple logistic regression analysis was performed to determine the dependence and predictive value of sTLT1 on the established risk factors and diagnosing the disease in patients. A probability value of $P \leq 0.05$ was considered as statistically significant. All these tests were performed using GraphPad Prism 8.0 and MedCalc 6.2.0 software.

Results

Baseline characteristics

The demographics of 117 individuals included in the present study are shown in Table 1. Approximately 13.7% individuals were control (n=16); 35% individuals were asymptomatic (n=41) and 51% subjects had CAD (n=60). In control group, 75% were males and 25% were females; in asymptomatic, 78% were males and 22% were females; in CAD subjects 90% were males and 10% were females. Among the control subjects four individuals were smokers but still, they were included in the group because three of them started smoking recently (1 month) and one of them was an ex-smoker (15 years ago and he smoked for 3 years only). All the patients in CAD had documented hypercholesterolaemia, hypertension and abnormal ECG and echocardiography reports. Angiography was also performed to determine the extent and degree of the blockage. The major clinical and demographic variables among the three groups were determined through one-way ANOVA (Table 1). Patients were grouped under three Killip classes, (a) Class I, 19 (31.67%); (b) Class II, 31 (51.67%); (c) Class III, 10 (16.67%). None of the subjects belonged to Class IV.

Normalisation of demographic variables

No correlation of plasma sTLT1 was found with the age of individuals within the study group (Supplementary Figure 3A). To rule out the variability bias based upon platelet number, an association of sTLT1 with platelet count was calculated which revealed no significant correlation indicating the variation of sTLT1 level was solely dependent upon the pathophysiology of the subjects (Supplementary Figure 3B). Furthermore, multiple logistic regressions indicated that plasma sTLT1 level was significantly associated with disease risk in contrast with other risk factors like hypertension (Table 2).

Soluble TLT1 level increases in CAD patients and asymptomatic individuals

In CAD subjects (n=60), sTLT1 level (2342 ± 184 pg/ml) was significantly (P<0.001) increased compared to both asymptomatic (1773 ± 118 pg/ml) and control individuals (461 ± 57 pg/ml) (Figure 1A). There was a four-fold rise in sTLT1 in asymptomatics compared to normal healthy controls (P<0.001). To validate these results, we performed Western blotting with human plasma which displayed a higher level of the protein in CAD patients (Figure 1B). It was also observed that sample collected from subjects 48 h after pro-thoracic coronary angioplasty (PTCA), the protein level (3055 ± 246 to 1757± 156) decreased significantly (P<0.001; Figure 1C). Moreover, multiple logistic regression analysis also supports these findings as sTLT1 associated with disease outcome (P=0.045, OR = 1.02, 95% CI = 1–1.04; Table 2). Majority of the patients were under anti-diuretic drugs (73.33%), anti-platelet drugs (68.3%). Very few patients (8.3%) were under anti-hypertensive drugs. However, sTLT1 level remained unaltered with the

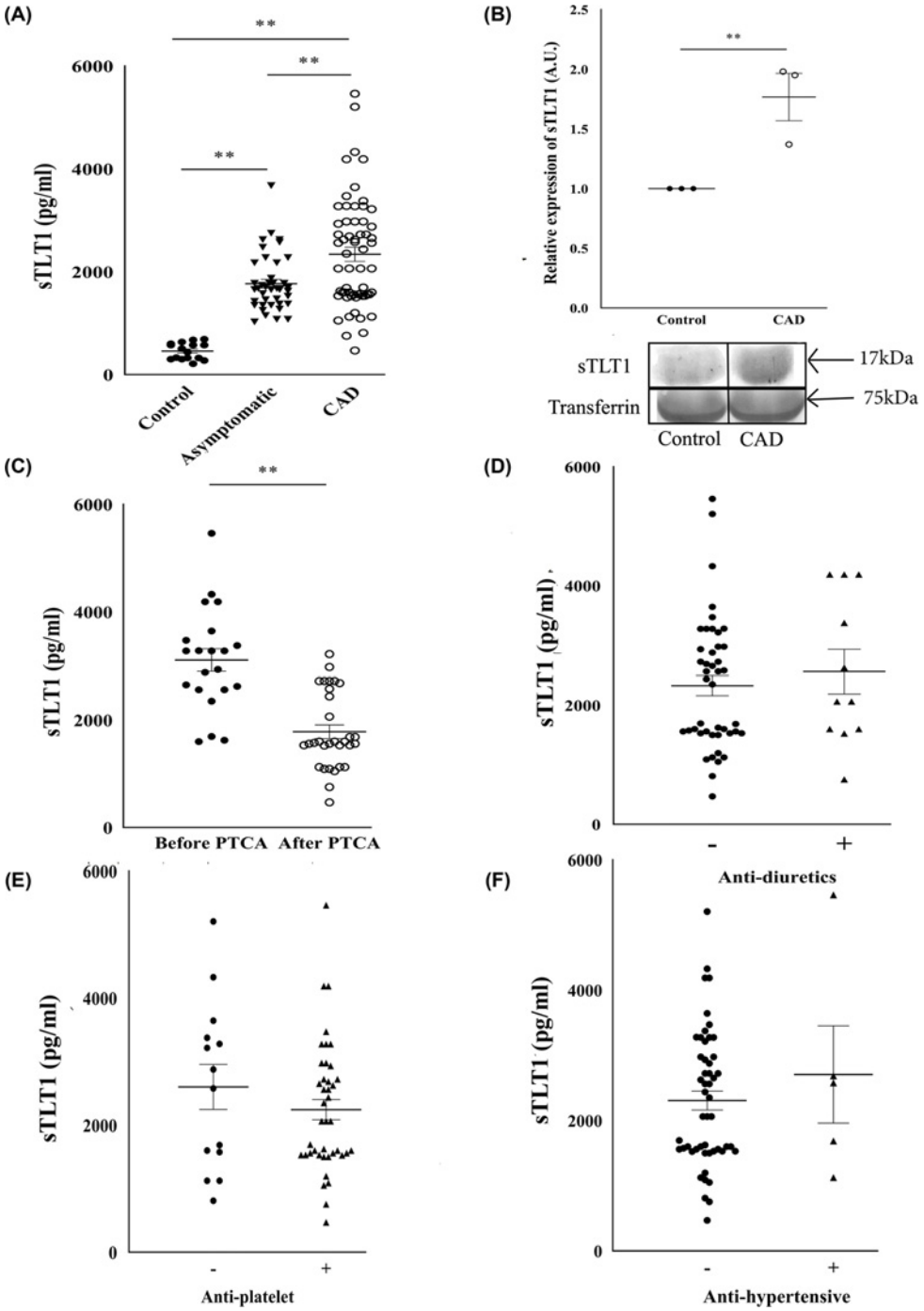

Figure 1. Estimation of soluble TLT1 levels in human plasma

Scattered plots showing plasma sTLT1 levels (mean ± SEM) in control (Black dots; n=16), asymptomatic (Inverted black triangle; n=41) and CAD (Black bordered white dots; n=60) subjects as measured by ELISA (**A**). Representative immunoblot showing sTLT1 in CAD (Black bordered white dots) and healthy control (Black dots) in human plasma as well as its densitometric analyses by ImageJ software (**B**). The delineations in the representative blot image signify that they are cropped images from the same gel. The levels of sTLT1 are also shown in patients before (Black dots; n=21) and after PTCA (Black bordered white dots; n=31) (**C**); without (−) or with (+) anti-diuretics (**D**), anti-platelet (**E**) or anti-hypertensive (**F**) medicines. CAD subjects without medication (n=44, 14, 51 representing anti-diuretics, anti-platelet and anti-hypertensive groups, respectively) are represented as black dots and CAD subjects with medications (n=11, 41, 5 representing anti-diuretics, anti-platelet and anti-hypertensive groups, respectively) were represented as black triangles. Immunoblots shown were performed in triplicates. Double asterisk (**) indicates means are significantly different at $P<0.05$.

Clinical Science (2019) **133** 2283–2299
https://doi.org/10.1042/CS20190999

Table 2 Results of multivariate logistic regression analysis for the disease risk prediction

Variable	Coefficient	Std. error	*P*
Coefficients and standard errors			
Hypertension	−0.243	2.346	0.917
sTLT1	*0.0199*	*0.001*	**0.045*
Constant	−15.93		
Variable	**Odds ratio**		**95% CI**
Odds ratios and 95% confidence intervals			
Hypertension	0.7844		0.0079–77.9517
sTLT1	*1.0201*		*1.0004–1.0402*

Significant values are indicated in italics."*" indicates significant P value
Abbreviation: sTLT1, soluble TREM-like Transcript 1.

administration of those medications (anti-diuretics, P=0.927; anti-platelet, P=0.394; anti-hypertensive, P=0.467) as shown in Figure 1D–F.

Correlation of sTLT1 level with common risk factors

We also examined the relationship of sTLT1 with common risk factors of atherosclerosis like LDL, LDL/high-density lipoprotein (HDL) ratio and oxLDL. We observed that, sTLT1 level positively correlated with LDL ($r = 0.401$, P=0.03, n=35) as well as LDL/HDL ratio ($r = 0.435$, P=0.016; n=30) in asymptomatic individuals (Supplementary Figure 1A,B, respectively). Similarly, sTLT1 level also positively correlated with LDL concentration ($r = 0.48$, P=0.003, n=35) and LDL/HDL ratio ($r = 0.445$, P=0.003, n=41) in CAD subjects (Supplementary Figure 1D,E, respectively). The level of LDL-C was borderline high in majority (69%) of the CAD subjects (n=43). Interestingly, 81% among the subjects with borderline high LDL-C had high oxLDL level (n=35). So, we examined association of oxLDL with sTLT1. Correlation studies with oxLDL revealed strong positive correlation both in plasma of asymptomatic individuals ($r = 0.491$, P=0.004, n=33) as well as CAD subjects ($r = 0.453$, P=0.002, n=43) (Supplementary Figure 1C,F, respectively).

Association of sTLT1 with the severity of CAD

Correlation analyses with left ventricular ejection fraction (LVEF) and Global Registry of Acute Coronary Events (GRACE) score were performed to establish the clinical significance of CAD. Supplementary Figure 1G, showed sTLT1 level is inversely correlated with LVEF ($r = 0.460$, P=0.004, n=40). GRACE score was calculated for 6 months (predicts the risk of MI within 6 months) based on Killip classification and it has a strong positive correlation with blood sTLT1 level ($r = 0.508$, P=0.001, n=41) (Supplementary Figure 1H). As low LVEF and higher GRACE score are directly related to disease severity; it is clear that association of sTLT1 with them would relate this protein with the severity of the disease and chances of an acute coronary event when it crosses the threshold value. Furthermore, we calculated the thrombolytic index of myocardial infarction score (TIMI score) (estimated risk of the individuals for an acute event within 14–30 days) for each patient. Patients were categorised into two distinct groups according to their TIMI score. The subjects with TIMI score < 5 was in lower risk of having another acute event whereas subjects with a TIMI score ranging from 5 to 8 are on the higher risk of another event. Interestingly, low TIMI score group (black dots; n=17) corresponded to lower level sTLT1 (1621 ± 174 pg/ml) and high TIMI score group (black squares; n=38) corresponded to higher concentration of sTLT1 (2924 ± 231 pg/ml) with a very significant P-value of <0.001 (Supplementary Figure 1I). These results strongly support the hypothesis that the plasma level of sTLT1 is associated with the severity and risk of an acute coronary event.

Receiver operating characteristics curve analysis

To determine the specific cut off concentration and predictive performance of sTLT1, receiver operating characteristics (ROC) curve analysis was performed. As shown in Supplementary Figure 1J, the ROC curve analysis with asymptomatic and control subjects revealed a cut-off value more than 875 pg/ml ($P<0.001$) with a sensitivity of 91.67% and specificity of 100% for association with CAD. The ROC curve analysis with sTLT1 concentration between asymptomatic and CAD subjects showed a cut off concentration of 2500 pg/ml with 65% sensitivity and 91% specificity ($P<0.001$) (Supplementary Figure 1K). NT-pro-BNP levels were quantified and compared

Table 3 Values of HADDOCK analysis for cluster 1

Variables	Values
HADDOCK score	-109.0 ± 4.7
Cluster size	103
RMSD from the overall lowest energy structure	1.4 ± 0.8
van der Waals energy	-33.4 ± 4.4
Electrostatic energy	-396.4 ± 88.1
Desolvation energy	1.1 ± 10.5
Restraints violation energy	25.2 ± 14.58
Buried surface area	1645.0 ± 70.0
Z-score	−2.2

with sTLT1 level in patients to compare its (sTLT1) sensitivity over NT-pro-BNP and was found to be performing better than NT-P-BNP [Area under the curve (AUC) = 89% for sTLT1over 65% for NT-pro-BNP] (Supplementary Figure 1K). Sensitivity of sTLT1 was compared with that of oxLDL among asymptomatic or subclinical subjects. Accordingly, sTLT1 is found to be performing better than oxLDL (AUC = 100% for sTLT1 over 80% for oxLDL).

sTLT1 binds with the SH2 domain of SYK

To understand the functional significance of sTLT1 *in-silico* analysis was performed. Increased level of sTLT1 in blood led us to testify the cause–effect relationship of this protein with the disease. Based on *in-silico* studies we predicted that sTLT1, being a secreted plasma protein, may interact with macrophage membrane proteins. Protein structure of sTLT1 indicated that it has a prominent IgV like domain. Based on literature mining in Uniprot, we found that 'IgV like domain' family proteins bind to SYK group of proteins. So, to identify possible interactors of sTLT1, we performed STRING interaction analysis. It identified ten probable interactors with significantly high protein–protein interaction (PPI) score ($P<0.05$) (Figure 2A). Among these interactors, FCER1G (FcεRI) not only has a SYK domain but also has a high node to node PPI score of 0.6 between sTLT1 (node 2) and FcεRI (node 1). Moreover, FcεRI is abundant on macrophage cell surface and involved in adaptive immune regulation. Based on these initial data, we examined docking of FcεRI on sTLT1.

The aim was to find out the specific region of the proteins (FcεRI and sTLT1) which frequently interacts with its ligands. Searches in PDB and Uniprot led us to identify SH2 domain (9–262 amino acids) of FcεRI and IgV like domain of sTLT1 (amino acids: 20–125) as the most frequent interacting chains. So, to determine the best possible conformation, we docked IgV like domain of sTLT1 (amino acids: 20–125) (PDB ID: 2FRG) [Figure 2B(b–d) Red portion showing the interacting surface] with SH2 domain (part of ITAM domain) of SYK in FCER1G (amino acids: 9–262) (PDB ID: 1A81) (Figure 2B(a) Red portion showing the surface of interaction) with the help of PatchDock and ClusPro 2.0. Primarily, .gz files of both the domains were uploaded for both the domains in PatchDock web server. The results presented ten probable binding conformations with minimum free energy, minimum entropy and the maximum number of weak bondings. Further to cross-validate the pairs, we repeated the docking experiments using ClusPro 2.0 and one of the predicted interaction complex was found to be common in both of the web servers. Further analysis was done on this common conformation of interacting pairs. In Figure 2C(a,b), a simple ribbon model of the common pair has been shown (IgV domain in red) from two different angles. We also determined the surface cleft of interaction of this pair through initial docking [Figure 2D (zoomed in) and 2F (zoomed out)]. Figure 2E shows possible amino acids involved in interaction in Ig V like domain in loop ribbon model. Then, we docked the proteins using HADDOCK to find out the possible angle of interaction and specific chains involved in interaction. HADDOCK results primarily indicated 8 different cluster combinations of interaction for the chosen pair. Clusters were numbered from 1 to 8 according to their HADDOCK score in increasing order. Scatter plots against HADDOCK score (y-axes) and other determining variables (x-axes) for all the clusters are presented in Figure 3A–G. These scatter plots indicate cluster 1 (marked as red triangle in the plots) to be the most appropriate cluster of interaction based since it earned minimum HADDOCK score and minimum inter-Root Mean Square Distance (i-RMSD) among the interacting chains (Table 3). Based on *in-silico* analysis, we performed co-immunoprecipitation studies of sTLT1 (chemically synthesised) and FcεRI from cellular extracts of differentiated macrophages to find out the same conclusion (Figure 3H).

Clinical Science (2019) **133** 2283–2299
https://doi.org/10.1042/CS20190999

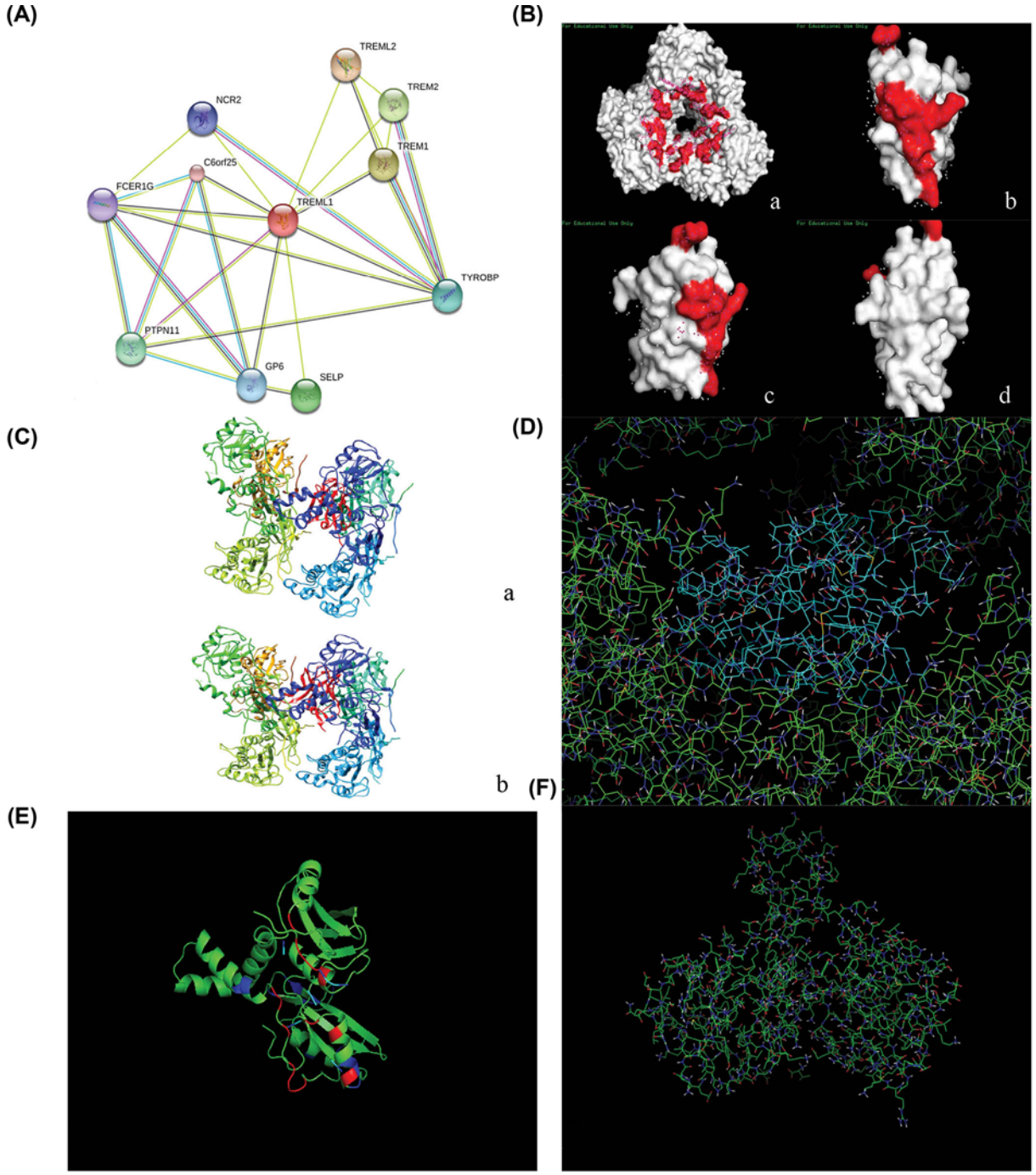

Figure 2. Molecular docking showing FcγRI interaction with sTLT1

Possible interactors for sTLT1 (TREML1) were determined by STRING analysis which indicated FcγRI (FCER1G) as a possible receptor with fairly high PPI score ($P<0.05$) (**A**). 3D model of interacting protein domains and their surface of interaction (in red) of SH2 domain (a) and IgV-like domain (b–d) were shown in PyMOL view (**B**). Common interacting complex from PatchDock and ClusPro is shown in Ribbon model (sTLT1 in red and SH2 domain of FcγRI in multicolour) from two different angles (a,b) which was used for HADDOCK2.2 analysis (**C**). Ball and stick model of the zoomed in (**D**) and zoomed out (**F**) view of sTLT1 (sky blue) - FcγRI (green) attachment cleft in HADDOCK cluster were shown in PyMOL view. Position of interacting amino acids of sTLT1 specifically highlighted in red and blue was represented as ribbon model (**E**).

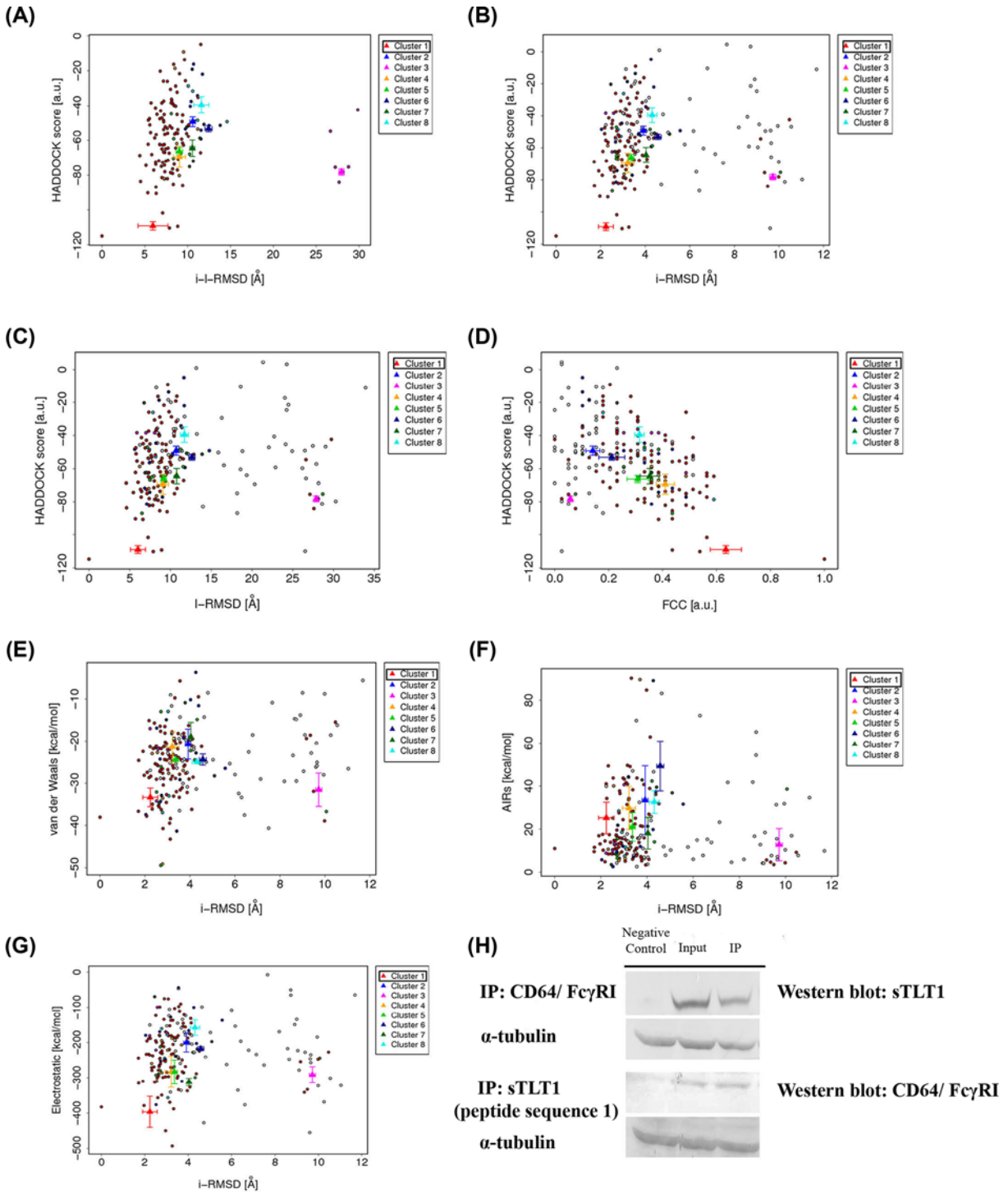

Figure 3. HADDOCK analysis and Co-IP confirms sTLT1–FcγRI interaction

The results and graphics presented in this figure (**A**–**G**) are based on water-refined models generated by HADDOCK. The clusters (indicated in colour in the graphs) are calculated based on the interface–ligand RMSDs calculated by HADDOCK, with the interface defined automatically based on all observed contacts. The various structural analyses (FCC, i-RMSD and l-RMSD) are made with the respect to the best HADDOCK model (the one marked as red triangle) with the lowest HADDOCK score. (**H**) Co-immunoprecipitation (Co-IP) experiments in macrophage cells showing FcγRI when immune-precipitated with anti-sTLT1 antibody and *vice versa* indicating the interaction of FcγRI with sTLT1. Synthetic sTLT1 protein was used as input in Co-IP of sTLT1 and cell lysate was used as input in FcγRI. α-tubulin was used in both the cases as loading control. IgG was considered as negative control for the whole experiment.

Clinical Science (2019) **133** 2283–2299
https://doi.org/10.1042/CS20190999

sTLT1 activates SYK-mediated mitogen activated protein kinase pathway

Differentiated THP1 monocyte-macrophages were treated with sTLT1 active peptide (sequence 1) and scramble (sequence 2) to find out the effect of sTLT1–FcγRI interaction. Sequence 1 treated cells showed a time-dependent phosphorylation pattern of SYK when compared to total SYK whereas scramble treated cells did not show any phosphorylation pattern. The level of activated, i.e. phosphorylated SYK is 1.4-times higher at 15 min (Figure 4A, $P<0.05$). Time-dependent study of phosphorylated BTK showed 2.9-fold increase against total BTK level at 10 min (Figure 4A, $P<0.05$). But, scramble treatment did not show phospho-BTK. Downstream analyses of BTK pathway led us to trace further into the phosphokinetics of this signalling cascade. MEK, next predominant member of this cascade, showed four-fold initial increase at 15 min to five-fold increase at 30 min compared with initial levels (Figure 4B, $P<0.05$) after active peptide treatment but not in scramble treated cells. Phosphorylated ERK showed a significant (three-fold) increase at 15 min (Figure 4B, $P<0.05$) only in cells treated with active sequence.

Activation of ERK-mediated mitogen activated protein kinase pathway induces NF-kB canonical pathway

Increased level of phosphorylated MEK (mitogen activated protein kinase (MAPK)) and ERK (MAPK kinase (MAPKK)) led us to explore further downstream of sTLT1-induced intracellular pathway. The phosphorylated IKKβ was nearly two-fold higher and the level of phosphorylated NF-kB-p65 was 1.5-fold higher after 15 min of treatment with sTLT1 active sequence compared to the effect with scramble peptide at 0 min (Figure 4C $P<0.05$). These results may indicate that activation of IKKβ directed to the phosphorylation of IkB and its gradual degradation through ubiquitination. On the other hand, this degradation of IkB results into the release of NF-kB-p65 from the inactive complex of p65-p35 that makes nuclear translocation of the molecule possible. This correlates with the high level of NF-kB-p65 in the cell lysate.

SYK antagonist R406 inhibits downstream signalling to decrease the secretion of TNF-α from THP1-derived macrophages

Differentiated macrophages were treated with SYK specific inhibitor, R406 in two different concentrations (0.5 and 2 μg) along with active peptides. Immunoblots showed that SYK was inhibited by R406 (Supplementary Figure 4A). Interestingly, BTK activation was also inhibited in response to R406 compared with active peptide alone (Supplementary Figure 4A). This indicates that BTK activation happens directly following SYK activation in response to active sTLT1 peptide. Furthermore, ERK interestingly showed the same trend as of BTK and SYK (Supplementary Figure 4A). To examine the functional significance of SYK inhibition, the level of secreted TNF-α in differentiated macrophage cell culture medium was estimated in the presence or absence of SYK antagonist. TNF-α level reduced in a dose-dependent manner ($P<0.001$) with SYK antagonist in active peptide treated group whereas it remains unchanged in response to scramble peptide (Supplementary Figure 4B). These observations indicate that sTLT1 active peptide initiates a SYK-BTK-MEK-ERK axis to promote inflammation through TNF-α secretion.

Secretion of TNF-α is derceased by BTK antagonist

To understand further the involvement of BTK-MEK-ERK axis, cells were treated in the absence or presence of BTK inhibitor, Ibrutinib, along with active peptide or scramble. Immunoblot demonstrated reduction in BTK activation by Ibrutinib. The normal pattern of activation even in the presence of BTK inhibitor in the cell culture indicates that SYK remains upstream to this axis. Ibrutinib treated cells did not show any activation of ERK suggesting that ERK remains downstream to SYK, BTK and MEK (Supplementary Figure 4C). Moreover, to check the downstream influence of this inhibition, we measured secreted TNF-α from cells treated with active peptide and scramble along with BTK antagonist. TNF-α secretion reduced in a dose-dependent manner ($P<0.001$) with Ibrutinib (Supplementary Figure 4D). These data indicated the involvement of NF-kB-p65 and IKK-β in the signalling, since the same cascade induces TNF-α secretion from macrophages. Thus the above observations suggested that sTLT1 acts through the major signalling axis consisting of SYK-BTK-MEK-ERK.

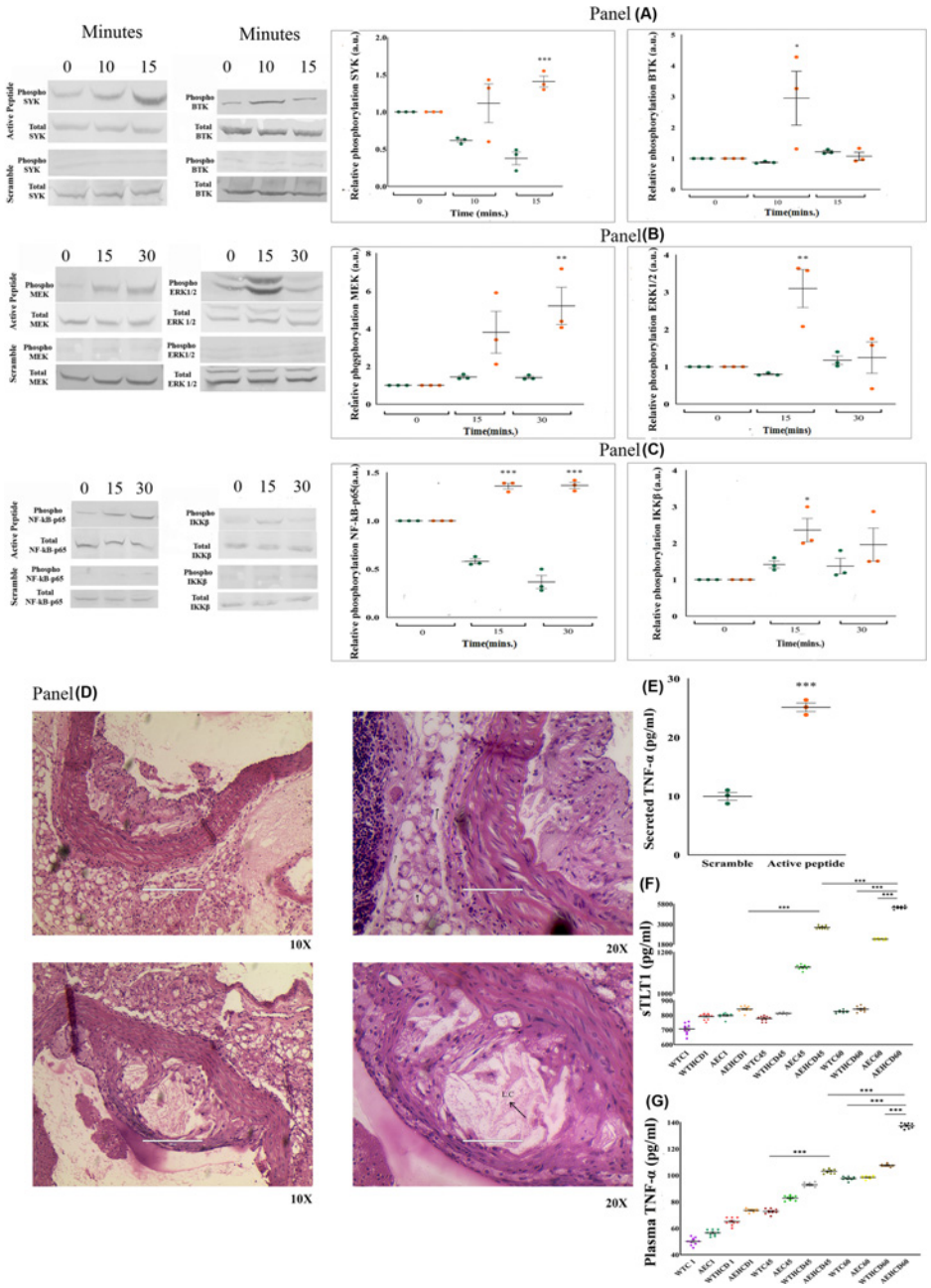

Figure 4. Induction of sTLT1 activates SYK mediated signalling to secrete TNF-α *in vivo*

Immunoblots showing phosphorylation status of SYK, BTK, MEK, ERK1/2, NF-kB-p65 and IKK-β in macrophage upon stimulations with active peptide of sTLT1 and its scramble for indicated times. Densitometric analyses of the immunoblots by ImageJ software are shown in the corresponding adjacent panels (**A–C**) to indicate the level of phosphorylation. All the blots shown are performed in triplicates. Green dots and yellow dots represent data for scramble and active peptide treatment at different time points, respectively. Histopathological images of aortic arches (cross-sections) in apoE$^{-/-}$ mice (n=10) fed with HCD for 45 days (upper panel) and 60 days (lower panel) in 10× and 20× magnifications. Arrows indicate the lipid-laden cells and L.C. designates necrotic lipid core (**D**). Scattered plots showing the level of secreted TNF-α (pg/ml) from macrophages treated with sTLT1 active peptide (yellow dots) and its scramble sequence (green dots) (**E**). Plasma concentration of sTLT1 (**F**) or TNF-α (**G**) in mice fed with chow or HCD after 45 and 60 days indicating the inflammatory state of the mice in plaque-forming stages. Asterisk (*) denotes significant difference at P<0.05. Abbreviations. WTC1, WTC45, WTC60: wild-type mice fed with chow for 1, 45 and 60 days respectively; WTHCD1, WTHCD45, WTHCD60: wild-type mice fed with high cholesterol diet for 1 day, 45 and 60 days, respectively; AEC1, AEC45, AEC60: apoE$^{-/-}$ mice fed with chow for 1, 45 and 60 days, respectively; AEHCD1, AEHCD45, AEHCD60: apoE$^{-/-}$ mice fed with high cholesterol diet for 1, 45 and 60 days, respectively. Abbreviation: HCD, high cholesterol diet.

Clinical Science (2019) **133** 2283–2299
https://doi.org/10.1042/CS20190999

sTLT1 stimulate secretion of TNF-α in THP1 derived macrophages as well as in apoE$^{-/-}$ mice

Differentiated macrophages from THP1 cells treated with synthetic peptides (sequence 1 and sequence 2) showed three-times higher level of secreted TNF-α in seq1 (active peptide) treated group compared with seq 2 or scramble treated group. Secretion of TNF-α from differentiated macrophages was induced by sTLT1 active peptide compared with that of scramble one. To connect this finding with atherosclerosis *in vivo*, plasma levels of sTLT1 and TNF-α were measured in apoE$^{-/-}$ mice fed with high cholesterol diet (HCD) and compared with those of chow-fed wild-type mice of the same strain for 45 and 60 days. Histopathological analysis (Haematoxylin–Eocene staining) of the cross-section of the aorta reveals plaque development after 45 days which progressed to advanced level of occlusion after 60 days in HCD fed mice (Figure 4D). As mentioned earlier, induction of sTLT1 active peptide increased TNF-α secretion significantly in macrophage cells (Figure 4E, P=0.0001). So, to connect further sTLT1 and TNF-α was measured in mice plasma. Plasma levels of sTLT1 increased significantly (amount ≈ 3500 pg/ml, P<0.05) in HCD fed apoE$^{-/-}$ mice after 45 days (AEHCD45) which increased further after 60 days (≈6000 pg/ml, P<0.001; AEHCD60) compared with chow fed mice (Figure 4F). Interestingly, sTLT1 level in chow fed apoE$^{-/-}$ mice (AEC60) was less (P<0.001) compared to that of HCD fed apoE$^{-/-}$ mice after 60 days (AEHCD60). On the other hand, the level of sTLT1 was similar in wild-type mice either fed with chow (WTC60) or HCD after 60 days (WTHCD60). However, sTLT1 level differs significantly (P<0.001) between HCD fed wild-type (WBHCD60) and apoE$^{-/-}$ mice after 60 days (AEHCD60).

For further understanding plasma TNF-α level was also measured in wild-type and apoE$^{-/-}$ mice either fed with chow or HCD after 45 and 60 days respectively. Interestingly, HCD fed atherosclerotic mice with distinct plaques had the highest level of TNF-α at day 60 (P<0.05; AEHCD60) compared with that of chow fed wild-type mice (WTC60) or HCD fed wild-type mice(WTHCD60) or chow fed apoE$^{-/-}$ mice (AEC60, Figure 4G). As, HCD fed apoE$^{-/-}$ mice showed an increased expression of both sTLT1 and TNF-α, it is apparent that sTLT1 induction in apoE$^{-/-}$ mice correlated with high TNF-α level and thereby indicates the maintenance of inflammation in mice as well as sTLT1-induced macrophages.

Discussion

In the present study, we present evidence that plasma sTLT1 is strongly associated with atherogenesis and progression of CAD and likely to participate in inflammatory process by stimulating macrophages for the secretion of cytokines. Elevated levels of sTLT1 was reported in a small sample size of subjects (n=19) with chest pain, however, it was limited by case numbers, subject profile and statistical validation [16]. Furthermore, the relations between sTLT1 level and clinico-pathological parameters as well as correlation with risk factors were not studied. Here we show a robust increase in plasma sTLT1 in a relatively larger sample size, documented with clinical correlations and patho-physiological significance. Association of sTLT1 with LVEF and carotid intima–media thickness (data not shown) in asymptomatic individuals further signifies its connection with the overall atherosclerotic burden. Our results show that sTLT1 is directly correlated with GRACE score [17], TIMI score and Framingham risk factors and thereby with chances of mortality in acute CAD.

OxLDL is known to associate with atherosclerotic plaque formation and therefore, considered as a potential risk factor for subclinical CAD in apparently healthy individuals [18]. It is important for each step of thrombus formation, starting from foam cell differentiation to the secretion of inflammatory cytokines into intima-medial space. Interaction of oxLDL with CD36 promotes the activation of PI-3K pathway to induce the secretion of pro-inflammatory cytokines. On the other hand, CD64 activation promotes phagocytosis of oxLDL to form foam cells. Therefore, significant association of sTLT1 with oxLDL in the present study is indicative of its clinical importance in subclinical cases.

Lack of significant association with age, sex and platelet number indicated that sTLT1 level is unbiased of its limiting factors like platelet number and age. Multiple logistic regressions reveal sTLT1 is associated with hypertension indicating a significant risk involvement with the disease. Comparative ROC curve analysis reveals that sTLT1 performs better than oxLDL and NT-proBNP as a risk factor for CAD indicating that it can be an important factor for assessing disease in subclinical and clinical cases.

It is reported that FcγRI (CD64) is a macrophage-specific marker and plays an important role in activating the immune system and maintenance of peripheral tolerance. Hernandez- Vargas showed that double knockout mice against ApoE and FcγRI confer protection against atherosclerosis by reducing 50% of the atherosclerotic lesion area in which chemokine activation is impaired through up-regulation of NF-kB [12]. It has been reported that CD64 expression is significantly increased in CAD compared with healthy control subjects via C-reactive protein (CRP)

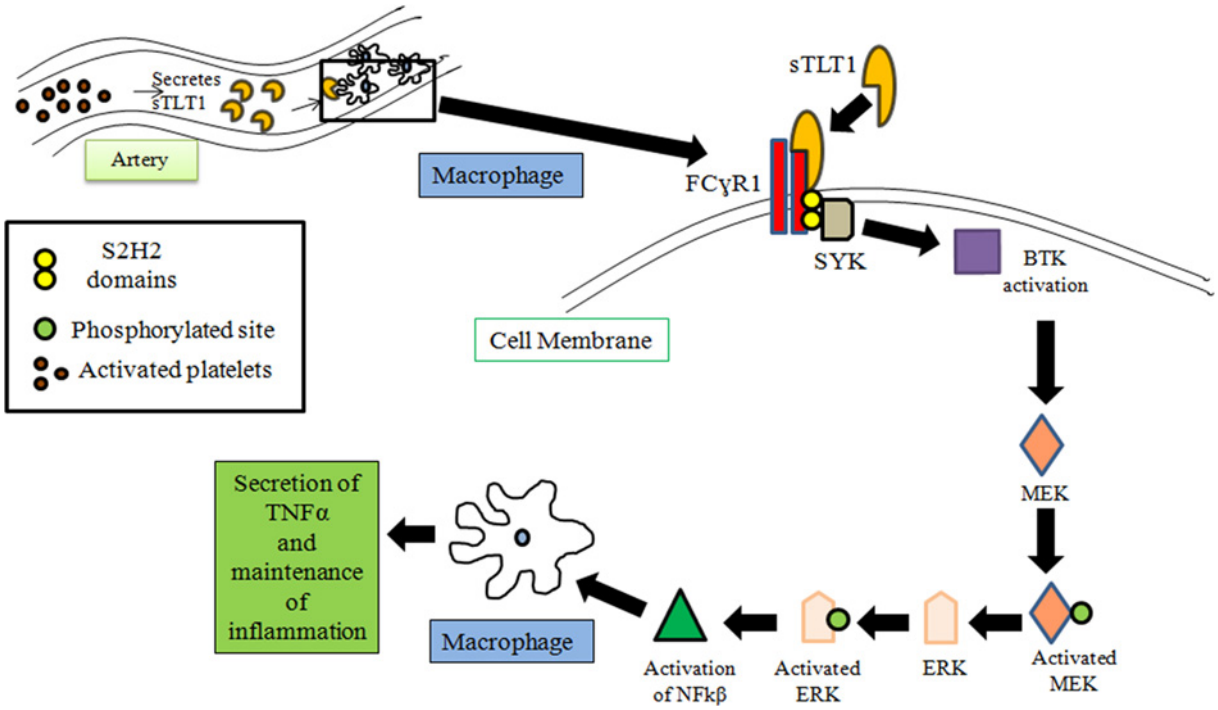

Figure 5. Diagrammatic representation of sTLT1 activated pathway via FcγRI/SYK/ERK cascade

[19]. On the other hand, CD64–CRP interaction promotes uptake of oxLDL and thereby plays a significant role in the pathogenesis of CAD [20]. All this information indicate its role in foam cell formation and inflammation. The present study, for the first time, show the activation of SYK-mediated pathway through interaction of FcγRI with sTLT1 which is in accordance with the inflammatory role of CD64 in atherosclerosis.

Tyrosine-protein kinase, SYK, the initiator of intracellular signalling in the present study, has been reported to activate the secretion of IL-1β in vascular smooth muscle cells to promote atherosclerosis [21]. SYK (L), the long isoform of SYK, promotes oxLDL phagocytosis in monocytic U937 cells. Also, SYK (L) siRNA significantly inhibits oxLDL engulfment [22]. On the other hand, pharmacological inhibition of SYK causes the downstream suppression of MAPK, MEK and ERK; indicating its role in disease initiation and progression [23]. Interestingly, release of thrombin-stimulated platelets was inhibited by blocking SYK [24]. Most of the reports indicate the role of SYK towards autophagy and foam cell formation through the MEK/ERK pathway. Our study establishes that SYK activation causes the secretion of pro-inflammatory cytokines through MEK/ERK pathway and a novel thrombin induced platelet protein, sTLT1 evoking the cascade by interacting with CD64 (Figure 5). The contribution of this pathway towards inflammation and atherosclerosis may help in finding new drug targets in the near future.

The role and efficacy of oral BTK inhibitors as a selective blocker of atherosclerotic plaque formation by disrupting platelet aggregation is well known [25]. Later studies also showed that BTK inhibitor Ibrutinib does not affect the phagocytosis in monocytes but it suppresses FcγR-mediated cytokine production [26]. Ibrutinib related studies further indicated that BTK inhibition can suppress TREM1-mediated neutrophil activation [27]. Hence, BTK activation through FcγRs may promote inflammatory cytokine production through the binding of TREM1 group of proteins. Here we show sTLT1, a TREM family member upon binding with FcγRI (a FcγR receptor) initiates BTK-mediated intracellular signalling which induces inflammatory cytokine (TNF-α) secretion through ERK/NF-kB. This information indicates that BTK inhibitors not only help in preventing platelet aggregation but also abrogate the inflammatory effects of macrophages.

Thus the present study demonstrates that high levels of sTLT1 in CAD is associated with the disease and it may be responsible for inflammatory signals in local milieu of the arterial lumen and thereby, is likely to play significant role in atherosclerotic process.

Clinical Science (2019) **133** 2283–2299
https://doi.org/10.1042/CS20190999

Clinical perspectives

- CAD is the leading cause of deaths worldwide which occurs due to atherosclerotic plaque build-up in the coronary arteries resulting into thrombotic occlusion. Current understanding about the mechanism of thrombus development indicates the importance of inflammation in local milieu of the coronary arterial lumen; however, very little is known about the signalling pathways related to inflammation. Understanding the molecular alterations and underlying signalling mechanism may help assessing the disease severity and overall disease management process.

- Our study highlights that, sTLT1, a platelet protein, is associated with CAD in clinical as well as subclinical subjects and it also facilitates inflammation by secreting TNF-α from macrophages through SYK/MEK/ERK axis.

- sTLT1 may serve as an important protein associated with the preventive efficiency of CAD. The mechanism by which sTLT1-induced inflammation, might offer novel insights into compromised resolution of inflammation in atherosclerosis and identification of new therapeutic strategies to fight CAD.

Competing Interests

The authors declare that there are no competing interests associated with the manuscript.

Funding

This work was supported by the Council of Scientific and Industrial Research, New Delhi, India [grant number MLP123 (to Arun Bandyopadhyay)]; and the Fellowship from University Grants Commission, New Delhi, India.

Author Contribution

Apabrita Ayan Das and Arun Bandyopadhyay conceived the study, designed the experiments. Apabrita Ayan Das and Devasmita Chakravarty conducted the experiments. Apabrita Ayan Das contributed to the acquisition, analysis and interpretation of the data. Debmalya Bhunia and Surajit Ghosh synthesised the peptides. Prakash C. Mandal collected the plasma samples from human subjects, provided and analysed clinical data. Khawer N. Siddiqui helped in the echocardiography of human subjects. Apabrita Ayan Das, Prakash C. Mandal, Khawer N. Siddiqui and Arun Bandyopadhyay wrote the manuscript. Surajit Ghosh critically read the manuscript. All gave final approval and have agreed to be accountable for all aspects of work ensuring integrity and accuracy. The data were not presented anywhere and all the authors have approved their acknowledgment in this manuscript.

Abbreviations

AIR, ambiguous interaction restraint; ANOVA, analysis of variance; ApoE, apolipoprotein E; AUC, area under the curve; BTK, Bruton's tyrosine kinase; CAD, coronary artery disease; DCM, dichloromethane; DIEA, diisopropylethylamine; DMF, *N,N′*-dimethylformamide; ECG, electrocardiogram; EDT, ethanedithiol; FcγRI, Fcγ receptor I; HADDOCK, High Ambiguity Driven Protein–Protein Docking; HBTU, *o*-(Benzotriazol-1-yl)-N,N,N′,N′-tetramethyluroniumhexafluorophosphate; HCD, high cholesterol diet; HDL, high-density lipoprotein; IgG, immunoglobulin G; LDL, low-density lipoprotein; LVEF, left ventricular ejection fraction; MAPK, mitogen activated protein kinase; NF-kB, nuclear factor-κ B; oxLDL, oxidised LDL; PPI, protein–protein interaction; ROC, receiver operating characteristic; sTLT1, soluble TREM like transcript 1; SYK, spleen tyrosine kinase; TFA, trifluoroacetic acid; TIMI score, thrombolytic index of myocardial infarction score; TREML, triggering receptor expressed on myeloid cells like protein; TNF-α, tumour necrosis factor-α.

References

1 Back, M., Yurdagul, Jr, A., Tabas, I., Oorni, K. and Kovanen, P.T. (2019) Inflammation and its resolution in atherosclerosis: mediators and therapeutic opportunities. *Nat. Rev. Cardiol.* **16**, 389–406, https://doi.org/10.1038/s41569-019-0169-2

2 Loeffen, R., van Oerle, R., Leers, M.P., Kragten, J.A., Crijns, H., Spronk, H.M. et al. (2016) Factor XIa and thrombin generation are elevated in patients with acute coronary syndrome and predict recurrent cardiovascular events. *PLoS ONE* **11**, e0158355, https://doi.org/10.1371/journal.pone.0158355

3 Washington, A.V., Schubert, R.L., Quigley, L., Disipio, T., Feltz, R., Cho, E.H. et al. (2004) A TREM family member, TLT-1, is found exclusively in the alpha-granules of megakaryocytes and platelets. *Blood* **104**, 1042–1047, https://doi.org/10.1182/blood-2004-01-0315

4 Gattis, J.L., Washington, A.V., Chisholm, M.M., Quigley, L., Szyk, A., McVicar, D.W. et al. (2006) The structure of the extracellular domain of triggering receptor expressed on myeloid cells like transcript-1 and evidence for a naturally occurring soluble fragment. *J. Biol. Chem.* **281**, 13396–13403, https://doi.org/10.1074/jbc.M600489200
5 Morales, J., Villa, K., Gattis, J., Castro, W., Colon, K., Lubkowski, J. et al. (2010) Soluble TLT-1 modulates platelet-endothelial cell interactions and actin polymerization. *Blood Coagul. Fibrinolysis* **21**, 229–236, https://doi.org/10.1097/MBC.0b013e3283358116
6 Washington, A.V., Gibot, S., Acevedo, I., Gattis, J., Quigley, L., Feltz, R. et al. (2009) TREM-like transcript-1 protects against inflammation-associated hemorrhage by facilitating platelet aggregation in mice and humans. *J. Clin. Investig.* **119**, 1489–1501, https://doi.org/10.1172/JCI36175
7 Derive, M., Bouazza, Y., Sennoun, N., Marchionni, S., Quigley, L., Washington, V. et al. (2012) Soluble TREM-like transcript-1 regulates leukocyte activation and controls microbial sepsis. *J. Immunol.* **188**, 5585–5592, https://doi.org/10.4049/jimmunol.1102674
8 Jaberi, N., Soleimani, A., Pashirzad, M., Abdeahad, H., Mohammadi, F., Khoshakhlagh, M. et al. (2019) Role of thrombin in the pathogenesis of atherosclerosis. *J. Cell Biochem.* **120**, 4757–4765, https://doi.org/10.1002/jcb.27771
9 Tammaro, A., Derive, M., Gibot, S., Leemans, J.C., Florquin, S. and Dessing, M.C. (2017) TREM-1 and its potential ligands in non-infectious diseases: from biology to clinical perspectives. *Pharmacol. Therapeutics* **177**, 81–95, https://doi.org/10.1016/j.pharmthera.2017.02.043
10 Lu, J. and Sun, P.D. (2015) Structural mechanism of high affinity FcgammaRI recognition of immunoglobulin G. *Immunol. Rev.* **268**, 192–200, https://doi.org/10.1111/imr.12346
11 Nimmerjahn, F. and Ravetch, J.V. (2008) Fcgamma receptors as regulators of immune responses. *Nat. Rev. Immunol.* **8**, 34–47, https://doi.org/10.1038/nri2206
12 Hernandez-Vargas, P., Ortiz-Munoz, G., Lopez-Franco, O., Suzuki, Y., Gallego-Delgado, J., Sanjuan, G. et al. (2006) Fcgamma receptor deficiency confers protection against atherosclerosis in apolipoprotein E knockout mice. *Circ. Res.* **99**, 1188–1196, https://doi.org/10.1161/01.RES.0000250556.07796.6c
13 Van Durme, J., Delgado, J., Stricher, F., Serrano, L., Schymkowitz, J. and Rousseau, F. (2011) A graphical interface for the FoldX forcefield. *Bioinformatics* **27**, 1711–1712, https://doi.org/10.1093/bioinformatics/btr254
14 Banerjee, P. and Bandyopadhyay, A. (2014) Cytosolic dynamics of annexin A6 trigger feedback regulation of hypertrophy via atrial natriuretic peptide in cardiomyocytes. *J. Biol. Chem.* **289**, 5371–5385, https://doi.org/10.1074/jbc.M113.514810
15 Charan, J. and Biswas, T. (2013) How to calculate sample size for different study designs in medical research? *Indian J. Psychol. Med.* **35**, 121–126, https://doi.org/10.4103/0253-7176.116232
16 Esponda, O.L., Hunter, R., Del Rio, J.R. and Washington, A.V. (2015) Levels of soluble TREM-like transcript 1 in patients presenting to the emergency department with chest pain. *Clin. Appl Thromb. Hemost.* **21**, 30–34, https://doi.org/10.1177/1076029614547298
17 Holvoet, P., Harris, T.B., Tracy, R.P., Verhamme, P., Newman, A.B., Rubin, S.M. et al. (2003) Association of high coronary heart disease risk status with circulating oxidized LDL in the well-functioning elderly: findings from the Health, Aging, and Body Composition Study. *Arteriosclerosis Thromb. Vasc. Biol.* **23**, 1444–1448, https://doi.org/10.1161/01.ATV.0000080379.05071.22
18 Ehara, S., Ueda, M., Naruko, T., Haze, K., Itoh, A., Otsuka, M. et al. (2001) Elevated levels of oxidized low density lipoprotein show a positive relationship with the severity of acute coronary syndromes. *Circulation* **103**, 1955–1960, https://doi.org/10.1161/01.CIR.103.15.1955
19 Devaraj, S., Chen, X., Adams-Huet, B. and Jialal, I. (2013) Increased expression of Fc-gamma receptors on monocytes in patients with nascent metabolic syndrome. *J. Clin. Endocrinol. Metab.* **98**, E1510–E1515, https://doi.org/10.1210/jc.2013-2112
20 Stancel, N., Chen, C.C., Ke, L.Y., Chu, C.S., Lu, J., Sawamura, T. et al. (2016) Interplay between CRP, atherogenic LDL, and LOX-1 and its potential role in the pathogenesis of atherosclerosis. *Clin. Chem.* **62**, 320–327, https://doi.org/10.1373/clinchem.2015.243923
21 Dautova, Y., Kapustin, A.N., Pappert, K., Epple, M., Okkenhaug, H., Cook, S.J. et al. (2018) Calcium phosphate particles stimulate interleukin-1beta release from human vascular smooth muscle cells: A role for spleen tyrosine kinase and exosome release. *J. Mol. Cell Cardiol.* **115**, 82–93, https://doi.org/10.1016/j.yjmcc.2017.12.007
22 Howard, J.C., Florentinus-Mefailoski, A., Bowden, P., Trimble, W., Grinstein, S. and Marshall, J.G. (2016) OxLDL receptor chromatography from live human U937 cells identifies SYK(L) that regulates phagocytosis of oxLDL. *Anal. Biochem.* **513**, 7–20, https://doi.org/10.1016/j.ab.2016.07.021
23 Corr, E.M., Cunningham, C.C. and Dunne, A. (2016) Cholesterol crystals activate Syk and PI3 kinase in human macrophages and dendritic cells. *Atherosclerosis* **251**, 197–205, https://doi.org/10.1016/j.atherosclerosis.2016.06.035
24 Liu, X., Yan, Y., Bao, L., Chen, B., Zhao, Y. and Qi, R. (2014) Ginkgolide B inhibits platelet release by blocking Syk and p38 MAPK phosphorylation in thrombin-stimulated platelets. *Thromb. Res.* **134**, 1066–1073, https://doi.org/10.1016/j.thromres.2014.08.025
25 Busygina, K., Jamasbi, J., Seiler, T., Deckmyn, H., Weber, C., Brandl, R. et al. (2018) Oral Bruton tyrosine kinase inhibitors selectively block atherosclerotic plaque-triggered thrombus formation in humans. *Blood* **131**, 2605–2616, https://doi.org/10.1182/blood-2017-09-808808
26 Ren, L., Campbell, A., Fang, H., Gautam, S., Elavazhagan, S., Fatehchand, K. et al. (2016) Analysis of the effects of the Bruton's tyrosine kinase (Btk) inhibitor Ibrutinib on monocyte Fcgamma receptor (FcgammaR) function. *J. Biol. Chem.* **291**, 3043–3052, https://doi.org/10.1074/jbc.M115.687251
27 Stadler, N., Hasibeder, A., Lopez, P.A., Teschner, D., Desuki, A., Kriege, O. et al. (2017) The Bruton tyrosine kinase inhibitor ibrutinib abrogates triggering receptor on myeloid cells 1-mediated neutrophil activation. *Haematologica* **102**, e191–e194, https://doi.org/10.3324/haematol.2016.152017

ECRONICON OPEN ACCESS

EC CARDIOLOGY

Research Article

Dietary and Lifestyle Impact on Different Biochemical and Hematological Parameters in Indian Children

Cristina Vassalle[1]*, Claudio Marabotti[2], Siddiqui Khawer Naveed[3], Roy Arun[3], Irene Traghella[1], Francesca Mastorci[6], Alberto Marabotti[4], Das Apabrita Ayan[5], Banerjee Tanima[5], Chakravarty Devasmita[5], Bandyopadhyay Arun[5], Kyriazoula Chatzianagnostou[1], Mirko Passera[6], Simona Storti[1] and Alessandro Pingitore[6]

[1]*Fondazione CNR-Regione Toscana G Monasterio, 56124 Pisa and 54100 Massa, Italy*

[2]*Cardiovascular Department, Ospedale della Bassa val di Cecina, Cecina, Italy*

[3]*Department of Cardiology, Ruby General Hospital, Kolkata, India*

[4]*University of Pisa, Italy*

[5]*Indian Institute of Chemical Biology, Kolkata*

[6]*Clinical Physiology Institute, National Research Council, Pisa, Italy*

***Corresponding Author:** Cristina Vassalle, Fondazione CNR-Regione Toscana G Monasterio, 56124 Pisa and 54100 Massa, Italy.

Received: July 17, 2019; **Published:** September 05, 2019

Abstract

Objective: India is characterized by the simultaneous occurrence of under- and overnutrition. In children the adoption of inappropriate feeding practices drives both to immediate and longer-term health implications, and it is one of the predisposing factor to obesity risk and noncommunicable diseases (NCDs) in adulthood.

Aim: To assess differences in disease risk biomarkers between Indian children living in a Calcutta suburb slum respect to those belonging to the high social class, according to their dietary and lifestyle habits.

Methods: Lifestyle, dietary habit (13-item food-frequency questionnaire), physiological and laboratory general and cardiometabolic risk biomarkers [blood pressure, heart rate, uric acid-UA, urea, glycated haemoglobin, electrolytes, creatinine, lipid, thyroid and inflammatory profile, hemochrome, parathormone, vitamin D, liver enzymes] were assessed in 41 Indian children (4 - 10 yrs) of the low (LSC) and high social class.

Results: LSC-children had significantly lower UA, and significantly higher HDL, and inflammatory parameters, and consumed significantly less meal number, sugar, and dairy, snacks or street food.

Conclusions: Higher inflammation in LSC children as well as higher obesity risk in Indian children adopting a Western diet must be targeted in the context of socio-economic status towards better health for all children.

Keywords: *India; Children; Urban Slums; Primordial Disease Prevention; Nutritional Transition*

Introduction

In India, the National and Family Health Survey reported that a great percentage of children is still underweight [1]. Poor living conditions in early life may cause, in adulthood, subsequent high risk for chronic clinical conditions such as depression, hypertension, diabetes mellitus, and obesity, which in turn may drive to worse non communicable disease (NCDs) [2,3]. At the same time, a parallel process of demographic and epidemiological transition are currently occurring at high rate in India, in which a change from a condition of predominance of nutritional deficiencies and infectious diseases, to those classified as degenerative chronic disease (such as cardiovascular disea-

se, cancer, and diabetes) is witnessed [4]. As developing country has become wealthier, an increasing number of Indians belonging to the upper class have abandoned their traditional eating habits and replaced them with a more Westernized diet, also associated with physical inactivity and other unhealthy lifestyle behaviors [5]. However, it must taken in account that in children, the adoption of inappropriate feeding practices, often typical of the Western diets, may drive both immediate and longer-term health implications, and it is one of the predisposing factor to subsequent obesity risk and NCDs in adulthood [6,7].

Simple anthropometric indicators giving an estimate of stunting (height-for- age z score), underweight (weight-for-age z score), wasting (weight-for-height z score), mid-upper arm circumference, and functional tests (e.g. handgrip, blood pressure), are non-invasive and cheap, and remain the first choice where access to healthcare structures is difficult. Moreover, nutritional questionnaires and dietary indexes are also important for overall dietary assessment, giving information on variability in foods, quality of diets, and diet–disease relationships. However, blood tests are routinely done in worldwide healthcare settings, to help the determination of a risk/diseased or a healthy status. A panel of general blood tests commonly include metabolic parameters (e.g. glucose, lipid profile), nitrogen metabolites (e.g. urea, creatinine, uric acid), electrolytes and important enzymes (e.g. liver aminotransferases).

Aim of the Study

Aim of the present study was to assess differences between Indian children living in a slum in Calcutta suburb respect to those belonging to the high social class, regarding lifestyle and dietary habits, blood pressure and heart rate, and biochemical general, inflammatory and cardiometabolic risk biomarkers.

Material and Methods

Participants

The study was conducted in a tertiary care hospital in India in apparently healthy children aged 4 - 10 yr belonging to the low (n = 29, 12 females) and high (n = 12, 9 females) social class. None of the female reported menarche.

Low social class children living in a slums located in the suburbs of Kolkata City were enrolled in January 2016 at Department of Cardiology, Ruby General Hospital (West Bengal, India), where the non-governmental organization (Usthi Foundation), which give children access to healthcare and take care of their school attendance, cooperated with local physicians.

Children from high-social class were recruited from staff and doctor's children. Social status was estimated on the basis of their family income.

The study was approved by the local Ethics Committee: the investigation conformed to the principles outlined in the Declaration of Helsinki. All parents gave their informed consent before the study.

Dietary and lifestyle assessment

At enrolment participants' nutritional and lifestyle habits were assessed by using a semi-structured interview. In particular, for lifestyle habits, school frequency, hours of sleep per night, usual bedtime, smoke/alcohol assumption, menarche age, and job activity were evaluated.

For dietary intake food frequency per week (e.g. street food, cereals, legumes, eggs, meat) were estimated. Also, hygienic conditions at home (presence of bath, kitchen, and potable water availability) were considered.

Autonomic and biochemical measurements

Blood pressure and heart rate measurements were carried out by means of an automatic recorder (OMRON digital arm BP monitoring) allowing 3-minute intervals between single readings. Accordingly, blood pressure values, reported in the present study, represent the average of at least three recordings obtained from each child. Fasting blood samples were centrifuged at 2500g, for 10 minutes, and stored at -80°C until assayed. Biochemical analysis included the evaluation of the following biomarkers: uric acid (UA), urea, glycated hemoglobin (HbA1c), electrolytes, creatinine, lipid profile, and inflammatory parameters (C-reactive protein CRP, erythrocyte sedimentation rate

ESR), hematological parameters, thyroid-stimulating hormone (TSH), vitamin D (vitD), parathyroid hormone (PTH), serum glutamate pyruvate transaminase (SGPT, also known as alanine aminotransferase), serum glutamate oxaloacetate transaminase (SGOT, also known as aspartate aminotransferase), gamma-glutamyl transpeptidase (GGT). Standard automated laboratory methods were used to estimate biomarker concentration (INTEGRA 400, Roche, Cobas-E411, USA, Mindray BC5380, Germany)

Anthropometric measures

Anthropometric measurements (weight, height) were taken three times and averaged, and body mass index (BMI) calculated. Mid-Upper Arm Circumference (MUAC) was measured at the mid-point between the tip of the shoulder and the tip of the elbow.

Z scores (weight for age, WAZ; height for age, HAZ; BMI for age, BAZ) were calculated using the WHO Anthro software (WHO Anthro version 3.2.2, January 2011; http://www.who.int/childgrowth/software/en/).

Statistical analysis

Student's t test and χ^2 test for continuous and categorical variables, respectively, were used. Owing to skewness, log transformation of C reactive protein (CRP), gamma-glutamyl transferase (GGT), parathyroid hormone (PTH) was used. The relationship between two continuous parameters was performed by using simple regression analysis. Continuous variables with univariate association of $p \leq 0.05$ were evaluated by a multivariate regression analysis to estimate independent factors in determining WAZ, HAZ, BAZ and MUAC values. Data are expressed as mean ± SD. Analyses were performed using StatView software (specify version). A p value ≤ 0.05 was considered statistically significant.

Results

Anthropometric characteristics and dietary and lifestyle habits according to social status

Demographic and physiologic characteristics of children enrolled in the study are reported in table 1. Children belonging to the low social class had lower Z-scores and MUAC with respect to high social class children (Table 2). In particular, girls in the high social class and boys in the low social class had respectively the highest and lower WAZ, HAZ and BAZ (Table 2).

	Low class	High class	p
Number	29	12	-
Males	13 (45)	4 (33)	ns
Age (years)	7.8 ± 1.5	8.3 ± 1.3	ns
Diastolic blood pressure (mmHg)	78 ± 8	76 ± 9	ns
Sistolic blood pressure (mmHg)	113 ± 11	110 ± 10	ns
Heart rate (bpm)	91 ± 14	101 ± 16	< 0.05

Table 1: *Demographic and physiological characteristics of children enrolled in the study. Data are expressed as mean ± SD or number (%).*

	Low class		High class		
	Girls	Boys	Girls	Boys	p
WAZ	-0.9 ± 1.3	-1.8 ± 1.1	1.6 ± 1.1	0.4 ± 2.1	< 0.001
HAZ	-0.4 ± 1.0	-1.3 ± 0.9	0.9 ± 1.1	0.4 ± 1.8	< 0.001
BHZ	-1.0 ± 1.4	-1.5 ± 1.0	1.5 ± 1.0	0.2 ± 2.0	< 0.001
MUAC	16.7 ± 2.2	16.5 ± 1.9	21.0 ± 3.1	18.2 ± 5.9	< 0.01

Table 2: *Z-scores and mid-upper arm circumference according to social class and gender. WAZ: Weight for Age; HAZ: Height for Age; BAZ: BMI for Age; MUAC: Mid-Upper Arm Circumference.*

No differences between children were found in lifestyle habits (Table 3). For dietary intake assessment, when stunting was defined as a low height-for-age for children (as a measure of past -chronic - child undernutrition) [8], 4 (13%) stunted children (with z-scores < -2.00) were found between children living into the slum. When underweight was defined as low weight-for-age (as an index of both past (chronic) and present (acute) undernutrition, 7), 9 (31%) children (with z-scores < -2.00) living into the slum were found to be underweight. Instead, in the HSC group, 6 children resulted overweight (50%), and 1 obese (8%). Moreover, children living in slums consumed a low number of meals ($p < 0.05$), reported no habitual sugar ($p = 0.06$), and dairy ($p < 0.01$) consumption, and no consumption of snacks and street food ($p < 0.001$). No difference for consumption of cereals, roots/tubers, legumes, meat, fish/seafood, oil/fats, fruits/vegetables, spices, and eggs was observed between the two groups of children (Table 3).

Lifestyle	Low class	High class	p
School frequency	29 (100)	12 (100)	ns
Sleep hours/night	9.4 ± 0.3	8.9 ± 0.4	ns
Usual bedtime	21 ± 1	22 ± 1	ns
Smoking habit/alcohol assumption	-	-	-
Job activity	-	-	-
Meal number/day	3	4	< 0.05
Diet consumption/week			
Street food	0 (0)	8 (67)	< 0.001
Cereals	29 (100)	12 (100)	ns
Legumes	28 (97)	12 (100)	ns
Dairy	14 (48)	12 (100)	ns
Eggs	28 (97)	12 (100)	ns
Meat	27 (93)	12 (100)	ns
Fish and seafood	25 (86)	9 (75)	ns
Oil/fat	12 (41)	7 (58)	ns
Sugar/Honey	22 (76)	12 (100)	0.06
Fruits and vegetables	29 (100)	12 (100)	ns
Tea	20 (69)	11 (92)	ns
Spices	29 (100)	12 (100)	ns
Hygienic conditions			
Bath	26 (90)	11 (92)	ns
Kitchen	29 (100)	12 (100)	ns
Potable water	13 (45)	6 (50)	ns

Table 3: *Lifestyle habits and dietary intake of children enrolled in the study. Data are expressed and mean±SD or number (%).*

Biochemical markers according to social status

As concerns biochemical markers, low social class children presented lower UA ($p < 0.001$), and higher HDL ($p < 0.05$) levels (Table 4). They also showed higher creatinine ($p \leq 0.001$) and potassium ($p < 0.001$), and lower sodium ($p < 0.05$) and chloride ($p < 0.001$) (Table 4). Moreover, inflammatory parameters were higher in low social class children (ESR, neutrophil to lymphocyte ratio) (Table 4). No differences in the other analytes or parameters were observed (Table 4).

	Low social class (Mean ± Std dev)	High social class (Mean ± SD)	p-value
ESR (mm/h)	24.9 ± 8.7	20 ± 4.5	0.08
Hemoglobin (g/dL)	12.7 ± 0.9	12.9 ± 1.1	ns
WBC (x10^9/L)	10 ± 2.5	9 ± 3	ns
N/L	2.6 ± 1.4	1.7 ± 0.6	0.03
Platelets (x10^9/L)	2.7 ± 0.7	3 ± 0.9	ns
Uric acid (mg/dL)	3.5 ± 0.6	4.3 ± 0.6	< 0.001
Urea (mg/dL)	19.4 ± 3.6	18.7 ± 7.8	ns
HbA1c (%)	5.4 ± 0.3	5.3 ± 0.3	ns
Sodium (meq/L)	137.5 ± 1.5	138.8 ± 1.9	< 0.05
Potassium (meq/L)	4.7 ± 0.4	4.2 ± 0.2	< 0.0001
Chloride (meq/L)	98.8 ± 2.3	104.3 ± 1.1	< 0.0001
Creatinine (mg/dL)	0.6 ± 0.1	0.5 ± 0.2	< 0.01
SGPT (IU/L)	22.6 ± 5.6	28.5 ± 16.7	ns
SGOT (IU/L)	31.1 ± 5.4	28.2 ± 5.5	ns
γ-GT (IU/L)	11.2 ± 2.5	10.9 ± 4.4	ns
CRP (mg/dL)	1.3 ± 0.5	1.5 ± 1.4	ns
Total cholesterol (mg/dL)	158.6 ± 26	159.1 ± 25	ns
HDL (mg/dL)	58.8 ± 9	50.6 ± 15	< 0.05
LDL (mg/dL)	73.8 ± 24	79 ± 24	ns
VLDL (mg/dL)	26 ± 3.4	18 ± 4.2	ns
Triglycerides (mg/dL)	131.1 ± 16.6	126 ± 20	ns
TSH (mU/L)	3.8 ± 2	3.7 ± 2	ns
Vitamin D3 (ng/mL)	16 ± 4.8	13.6 ± 12	ns
PTH (pg/mL)	43.4 ± 13	43 ± 19	ns

Table 4: *Biochemical parameters in LSC and HSC Indian Children.*

ESR: Erythrocyte Sedimentation Rate; WBC: White Blood Cells; N/L: Neutrophils to Lymphocytes Ratio; HbA1c: Glycated Hemoglobin; SGPT: Serum Glutamic Pyruvic Transaminase; SGOT: Serum Glutamic Oxaloacetic Transaminase; γ-GT: Gamma Glutamyl Transferase; CRP: C-Reactive Protein; HDL: High-Density Lipoprotein; LDL: Low Density Lipoprotein; VLDL: Very Low Density Lipoprotein; TSH: Thyroid-Stimulating Hormone; PTH: Parathyroid Hormone.

Interestingly, all LSC children had CRP levels above 0.6 mg/dl (age-reference limit adopted). Moreover, for it concerns 25(OH)D levels, only one male children in the HSC showed sufficient levels (above 30 ng/mL).

Correlation of WAZ, HAZ, BAZ and MUAC in the overall population

WAZ: Inversely correlated with creatinine ($r = -0.36$, $p < 0.05$), vitamin D ($r = -0.33$, $p \leq 0.05$), M/L ($r = -0.3$, $p \leq 0.05$), and directly with UA ($r = 0.51$, $p < 0.001$), chloride ($r = 0.43$, $p < 0.01$), SGPT ($r = 0.5$, $p < 0.001$), hematocrit ($r = 0.32$, $p < 0.05$). WAZ was significantly higher in children consuming street food ($p < 0.01$), and dairy ($p < 0.05$), and negatively correlated with sleep hours ($p < 0.001$).

Multiple regression analysis identified creatinine (T value -2.1, $p < 0.05$), and sleep hours (T value -3, $p < 0.01$) as independent variables for WAZ.

HAZ: Inversely correlated with creatinine ($r = -0.31$, $p \leq 0.05$), N/L ($r = -0.35$, $p < 0.05$), M/L ($r = -0.36$, $p < 0.05$), SGOT ($r = -0.37$, $p < 0.01$), and directly with UA ($r = 0.37$, $p < 0.05$), chloride ($r = 0.43$, $p < 0.01$), PTH ($r = 0.42$, $p < 0.01$). HAZ was significantly higher in children consuming street food ($p < 0.05$), and dairy ($p < 0.05$), and negatively correlated with sleep hours ($p < 0.05$).

Creatinine (T value -2.3, $p < 0.05$) and PTH (T value 2.7, $p \leq 0.01$) remained as independent correlates of HAZ after multivariate adjustment.

BAZ: Inversely correlated with creatinine ($r = 0.35$, $p < 0.05$), vitD ($r = -0.36$, $p < 0.05$), HDL ($r = -0.4$, $p < 0.05$), and directly with UA ($r = 0.52$, $p < 0.001$), chloride ($r = 0.4$, $p \leq 0.01$), SGPT ($r = 0.55$, $p < 0.001$). BAZ was significantly higher in children consuming street food ($p < 0.01$), dairy ($p < 0.05$), and negatively correlated with sleep hours ($p < 0.001$).

At the multivariate regression analysis, HDL (T value -2, $p \leq 0.05$), creatinine (T value -2.1, $p < 0.05$), SGPT (T value 2.4, $p < 0.05$), sleep hours (T value -3.5, $p \leq 0.001$) remained the only independent determinant for BAZ.

MUAC: Directly correlated with UA ($r = 0.47$, $p < 0.01$), chloride ($r = 0.35$, $p < 0.05$), SGPT ($r = 0.57$, $p < 0.001$), Hbg ($r = 0.37$, $p < 0.05$), GGT ($r = 0.41$, $p < 0.01$), GFR ($r = 0.32$, $p < 0.05$), and inversely with HDL ($r = -0.34$, $p < 0.05$), and vitamin D ($r = -0.48$, $p < 0.01$). MUAC was significantly higher in children consuming street food ($p < 0.01$), dairy ($p < 0.05$), and negatively correlated with sleep hours ($p < 0.001$).

At the multivariate analysis sleep hours remained as the only significant determinant for MUAC (T value -3.1, $p < 0.01$).

Discussion

In the present study, we evidenced that a significant percentage of Indian children living in a slums is stunted/underweight, and has higher levels of inflammatory markers respect to those belonging to the high social class. On the contrary, high social class children, which adopted a Western dietary pattern, had higher percentage of overweight and higher levels of biochemical parameters, representing conventional risk factors for NCDs, which correlates to nutritional indices. Moreover, sleep quality intended as hours of sleep per night per hours, emerges as an important determinant for nutritional indices, suggesting that also inadequate sleep may contribute to cardio-metabolic risk in children independently from their socio-economic status.

Malnutrition is a big public health problem in India, where nearly 60 million children are estimated to be underweight [9]. In particular, this problem is diffuse especially among the poor and vulnerable social classes, and it sets in mostly during the first years of life. Parameters related to nutrition and growth are determinants of their successive survival, cognitive development, and lifelong health. Restricted growth in young children is a risk factor for mortality from infectious diseases and for poor physical and cognitive development throughout life [10,11].

Recent research suggests that social and economic status (SES) exposures during childhood are powerful predictors of health in adulthood, suggesting how physiological, behavioral, or psychological pathways can link the childhood SES experience to adult health [12].

In this context, social background and nutritional differences significantly affect inflammatory parameters in adolescent worldwide [13,14]. However, there is a lot of heterogeneity according to social class. In particular, at the same time India is a country in rapid nutritional and demographic transition, in which life expectancy is increasing and we witness change from undernutrition to overweight and obesity. A study conducted in 45 villages in East and West Godavari in Andhra Pradesh on sample size of 180.162 subjects, showed that the peak prevalence of many non-communicable diseases occurs at a younger age than in developed countries, recommending the challenge to implement appropriate prevention strategies [15]. Thus, subjects belonging to high social class are experiencing an epidemic of obesity-hyperglycemia, largely due to demographic and lifestyle changes, which is reflected in a growing burden of NCDs [16]. A review on school Indian children, including 11 studies, estimated a prevalence of overweight and obesity among 8.5 - 29.0% and 1.5 - 7.4% respectively [17]. We found more than half children belonging to HSC group with overweight/obesity and adverse Western feeding habits. Interestingly, we previously observed that UA (a main blood antioxidant, but also a cardiovascular risk factor if present at high levels) progressively growth from underweight to normal weight and overweight/obese Indian children ($p < 0.01$) [18]. Moreover, as food inta-

ke and fructose content may significantly affect the development of hyperuricemia, the adoption of Western diet (high fats and fructose content), street-food consuming (high content in saturated fats and poor in fibers, vitamins and antioxidants) and sedentary habit may favor UA elevation [19]. Accordingly, Indian children in the high social class, which habitually consume street food, presented higher UA levels respect to those who do not consume this kind of food [18]. Thus, early identification of overweight during childhood, which is of considerable clinical and public health relevance, may be particularly important among Indian children. By contrast, higher inflammatory parameters in low social class children, possibly associated to multiple factors linked to socio-economic disadvantage, such as the result of high levels of infection exposure, inappropriate infant, child feeding, lacking care practices, can also represent an important link in the pathophysiology of NCDs later in adulthood. Interestingly, sleep duration, which is a known risk factor for obesity and metabolic risk both in adults and children of other ethnic groups, emerges as a determinant of nutritional indices, independent on Indian children social status [19-21]. The high prevalence of hypovitaminosis D, likely also related to skin colour, suggest the need of supplementation and physiological level restoring in all children, beyond their belonging to different social classes.

One limitation for the present study is the limited number of children enrolled, although the great number of biomarkers considered, and significance of the differences observed reinforce our results. Accordingly, the multifactorial nature of child stunting and underweight offers many entry points for clinical and educational solutions and suggests that the impact of any intervention remains influenced by the combined effects of all variables within the determinants of health.

In conclusion, the co-existence of undernutrition and overnutrition in the Indian children population level poses a unique public health challenge. Interventional strategies for primary prevention of NCD risk in adulthood, possibly starting at a very young age, and focused on increased physical activity and healthy lifestyle behaviors (e.g. sleep hours) and food options, must be optimized in the socio-economic context of children. In this setting, the identification and use of simple and valid biochemical markers may be helpful to track these changes so as to understand and prevent late-life health outcomes, pursuing better health for all children.

Acknowledgment

Authors thank the *Bhalobasa* ONLUS (Perignano, Pisa, Italy) for the valuable contribution to the research mission.

Bibliography

1. NFHS-4, National and Family Health Survey (2015-2016).
2. Mendenhall E., *et al*. "Non-communicable disease syndemics: poverty, depression, and diabetes among low-income populations". *Lancet* 389.10072 (2017): 951-963.
3. Vassalle C., *et al*. "Antioxidants in the diet and cognitive function: which role for the Mediterranean life-style?" *Journal of Prevention of Alzheimer's Disease* 4.1 (2017): 58-64.
4. Yadav S and Arokiasamy P. "Understanding epidemiological transition in India". *Global Health Action* 7 (2014): 23248.
5. Shrivastava U., *et al*. "Obesity, Diabetes and Cardiovascular Diseases in India: Public Health Challenges". *Current Diabetes Reviews* 13.1 (2016): 65-80.
6. Bhargava M., *et al*. "Overweight and Obesity in School Children of a Hill State in North India: Is the Dichotomy Urban-Rural or Socio-Economic? Results from a Cross-Sectional Survey". *PLoS One* 11.5 (2016): e0156283.
7. Misra A., *et al*. "Nutrition transition in India: secular trends in dietary intake and their relationship to diet-related non-communicable diseases". *Journal of Diabetes* 3.4 (2011): 278-292.
8. Srivastava A., *et al*. "Nutritional status of school-age children - A scenario of urban slums in India". *Archives of Public Health* 70.1 (2012): 8.

9. Bryce J., *et al*. "Maternal and child undernutrition, effective action at national level". *Lancet* 371.9611 (2008): 510-526.

10. Black RE., *et al*. "Maternal and child undernutrition: global and regional exposures and health consequences". *Lancet* 371.9608 (2008): 243-260.

11. Grantham-McGregor S., *et al*. "Developmental potential in the first 5 years for children in developing countries". *Lancet* 369.9555 (2007): 60-70.

12. Galobardes B., *et al*. "Is the association between childhood socioeconomic circumstances and cause-specific mortality established? Update of a systematic review". *Journal of Epidemiology and Community Health* 62.5 (2008): 387-390.

13. Chen E., *et al*. "Role models and the psychological characteristics that buffer low-socioeconomic-status youth from cardiovascular risk". *Child Development* 84.4 (2013): 1241-1252.

14. Kruger HS., *et al*. "Stunting, adiposity, and low-grade inflammation in African adolescents from a township high school". *Nutrition* 26.1 (2010): 90-99.

15. Joshi R., *et al*. "Chronic diseases now a leading cause of death in rural India--mortality data from the Andhra Pradesh Rural Health Initiative". *International Journal of Epidemiology* 35.6 (2006): 1522-1529.

16. Ganie MA., *et al*. "Prevalence, risk factors and consequences of overweight and obesity among schoolchildren: a cross-sectional study in Kashmir, India". *Journal of Pediatric Endocrinology and Metabolism* 30.2 (2017): 203-209.

17. Srihari G., *et al*. "Nutritional status of affluent Indian school children: what and how much do we know?" *Indian Pediatrics* 44.3 (2007): 204-213.

18. Mastorci F., *et al*. "Undernutrition and Overnutrition Burden for Diseases in Developing Countries: The Role of Oxidative Stress Biomarkers to Assess Disease Risk and Interventional Strategies". *Antioxidants (Basel)* 6.2 (2017): E41.

19. Vassalle C., *et al*. "Uric Acid for Cardiovascular Risk: Dr. Jekyll or Mr. Hide?" *Diseases* 4 (2016): E12.

20. Sayin FK and Buyukinan M. "Sleep Duration and Media Time Have a Major Impact on Insulin Resistance and Metabolic Risk Factors in Obese Children and Adolescents". *Childhood Obesity* 12.4 (2016): 272-278.

21. Aziz M., *et al*. "The Association of Sleep Duration and Morbid Obesity in a Working Population: The Baptist Health South Florida Employee Study". *Metabolic Syndrome and Related Disorders* 15.2 (2016): 59-62.

Volume 6 Issue 10 October 2019

OMICS A Journal of Integrative Biology
Volume 22, Number 12, 2018

DOI: 10.1089/omi.2018.0160

Research Articles

Proteomic Analysis of the Human Anterior Pituitary Gland

Soujanya D. Yelamanchi,[1] Ankur Tyagi,[2] Varshasnata Mohanty,[2] Pinaki Dutta,[3] Márta Korbonits,[4] Sandip Chavan,[1] Jayshree Advani,[1,5] Anil K. Madugundu,[1,5–7] Gourav Dey,[1,5] Keshava K. Datta,[1] M. Rajyalakshmi,[8] Nandini A. Sahasrabuddhe,[1] Abhishek Chaturvedi,[9] Amit Kumar,[10] Apabrita Ayan Das,[11] Dhiman Ghosh,[12] Gajendra M. Jogdand,[10] Haritha H. Nair,[13] Keshav Saini,[14] Manoj Panchal,[15] Mansi Ashwinsinh Sarvaiya,[16] Soundappan S. Mohanraj,[17] Nabonita Sengupta,[18] Priti Saxena,[14] Pradeep Annamalai Subramani,[19] Pradeep Kumar,[20] Rakhil Akkali,[21] Saraswatipura Vishwabrahmachar Reshma,[22] Ramachandran Sarojini Santhosh,[23] Sangita Rastogi,[24] Sudarshan Kumar,[25] Susanta Kumar Ghosh,[19] Vamshi Krishna Irlapati,[26] Anand Srinivasan,[27] Bishan Das Radotra,[28] Premendu P. Mathur,[29] G. William Wong,[30] Parthasarathy Satishchandra,[31] Aditi Chatterjee,[1] Harsha Gowda,[1] Anil Bhansali,[3] Akhilesh Pandey,[1,5–7,32–35] Susarla K. Shankar,[36,37] Anita Mahadevan,[36,37] and T.S. Keshava Prasad[1,2]

Abstract

The pituitary function is regulated by a complex system involving the hypothalamus and biological networks within the pituitary. Although the hormones secreted from the pituitary have been well studied, comprehensive analyses of the pituitary proteome are limited. Pituitary proteomics is a field of postgenomic research that is crucial to understand human health and pituitary diseases. In this context, we report here a systematic proteomic

[1]Institute of Bioinformatics, International Technology Park, Bangalore, India.
[2]Center for Systems Biology and Molecular Medicine, Yenepoya Research Centre, Yenepoya (Deemed to be University), Mangalore, India.
[3]Department of Endocrinology, Postgraduate Institute of Medical Education and Research, Chandigarh, India.
[4]Department of Endocrinology, Barts and the London School of Medicine, Queen Mary University of London, London, United Kingdom.
[5]Manipal Academy of Higher Education, Manipal, India.
[6]Center for Molecular Medicine, National Institute of Mental Health & Neurosciences, Bangalore, India.
[7]Department of Laboratory Medicine and Pathology and Center for Individualized Medicine, Mayo Clinic, Rochester, Minnesota.
[8]Department of Biotechnology, BMS College of Engineering, Bangalore, India.
[9]Department of Biochemistry, Melaka Manipal Medical College, Manipal Academy of Higher Education, Manipal, India.
[10]Institute of Life Sciences, Nalco Square, Bhubaneswar, India.
[11]Cell Biology and Physiology Division, Indian Institute of Chemical Biology, Kolkata, India.
[12]Protein Engineering and Neurobiology Laboratory, Department of Biosciences and Bioengineering, Indian Institute of Technology, Bombay, India.
[13]Division of Cancer Research, Rajiv Gandhi Centre for Biotechnology, Thiruvananthapuram, India.
[14]Faculty of Life Sciences and Biotechnology, South Asian University, New Delhi, India.
[15]Department of Life Science, Central University of South Bihar, Gaya, India.
[16]Padmashree Dr. D.Y. Patil Medical College, Hospital and Research Centre, Pune, India.
[17]Department of Plant Sciences, School of Life Sciences, University of Hyderabad, Hyderabad, India.
[18]Neuroinflammation Laboratory, National Brain Research Centre, Manesar, India.
[19]Department of Molecular Parasitology, National Institute of Malaria Research, Bangalore, India.
[20]Department of Biotechnology, VBS Purvanchal University, Jaunpur, India.
[21]Department of Biotechnology, Indian Institute of Technology, Madras, India.
[22]Department of Biotechnology, PES University, Bangalore, India.
[23]School of Chemical and Biotechnology, SASTRA University, Thanjavur, India.
[24]Microbiology Laboratory, National Institute of Pathology, New Delhi, India.
[25]Proteomics and Structural Biology Laboratory, Animal Biotechnology Center, National Dairy Research Institute, Karnal, India.
[26]Dr Reddy's Institute of Life Sciences, University of Hyderabad, Hyderabad, India.
[27]Department of Pharmacology, Postgraduate Institute of Medical Education and Research, Chandigarh, India.
[28]Department of Histopathology, Postgraduate Institute of Medical Education and Research, Chandigarh, India.
[29]Department of Biochemistry and Molecular Biology, School of Life Sciences, Pondicherry University, Pondicherry, India.
[30]Department of Physiology, Johns Hopkins University School of Medicine, Baltimore, Maryland.
[31]Department of Neurology, National Institute of Mental Health and Neuro Sciences, Bangalore, India.
[32]McKusick-Nathans Institute of Genetic Medicine, Johns Hopkins University School of Medicine, Baltimore, Maryland.
Departments of [33]Biological Chemistry, [34]Pathology and [35]Oncology, Johns Hopkins University School of Medicine, Baltimore, Maryland.
[36]Department of Neuropathology, National Institute of Mental Health and Neuro Sciences, Bangalore, India.
[37]Human Brain Tissue Repository, National Institute of Mental Health and Neuro Sciences, Neurobiology Research Centre, Bangalore, India.

profiling of human anterior pituitary gland (adenohypophysis) using high-resolution Fourier transform mass spectrometry. A total of 2164 proteins were identified in this study, of which 105 proteins were identified for the first time compared with high-throughput proteomic-based studies from human pituitary glands. In addition, we identified 480 proteins with secretory potential and 187 N-terminally acetylated proteins. These are the first region-specific data that could serve as a vital resource for further investigations on the physiological role of the human anterior pituitary glands and the proteins secreted by them. We anticipate that the identification of previously unknown proteins in the present study will accelerate biomedical research to decipher their role in functioning of the human anterior pituitary gland and associated human diseases.

Keywords: proteomics, anterior pituitary, diagnostics, biomarkers, ophthalmology, endocrinology

Introduction

The pituitary gland, often referred as the master endocrine gland, regulates various biological processes, including growth, water balance, reproductive functions, secretion and release of milk, response to stress, pigmentation, basal metabolism, and various other physiological activities in the body to maintain homeostasis. These functions are mediated through hormones secreted from adenohypophysis and neurohypophysis, which are two separate anatomical regions of the pituitary gland with distinct developmental origin, morphology, histology, ultrastructure, and physiological roles (Fig. 1A).

Anterior pituitary gland is the glandular portion of the pituitary secreting key hormones, such as growth hormone (GH), prolactin (PRL), luteinizing hormone, follicle-stimulating hormone, thyroid-stimulating hormone, and adrenocorticotropic hormone (ACTH). Posterior pituitary gland comprised specialized glial cells called pituicytes and axons of neurons arising from the hypothalamus releasing oxytocin and vasopressin.

The functions of the pituitary gland are classically regulated by the hypothalamus through stimulatory (e.g., gonadotropin-releasing hormone, thyrotropin-releasing hormone, and corticotropin-releasing hormone) and inhibitory factors (somatostatin and dopamine). In addition, neurotransmitters (serotonin, gamma-amino butyric acid, and vasoactive intestinal peptide) as well as cytokines (interleukin [IL]-1, IL-2, and IL-6) and neuropeptides have been found to regulate the synthesis and release of hormones from pituitary glands (Jorgensen et al., 2003; Karanth and McCann, 1991; Yasin et al., 1994).

Similarly, molecules expressed in the nonendocrine folliculostellate cells are also involved in the regulation of hormonal secretion from the anterior pituitary gland. For instance, S100, basic fibroblast growth factor, and IL-6 proteins secreted from folliculostellate cells stimulate the secretion of anterior pituitary gland hormones in a paracrine manner (Allaerts and Vankelecom, 2005).

Mass spectrometry (MS)-based studies using different fractionation techniques have been carried out to identify proteins from human pituitary glands. In one such study, 7596 proteins were shown to be expressed from human pituitary gland through MS-based analysis (Liu et al., 2017). In another study, 1660 proteins were reported using multidimensional separation by liquid chromatography (Liu et al., 2011). Furthermore, 1449 proteins were reported using multiple gel-based technologies (Zhao et al., 2005). Similarly, using a protein array containing 1005 antibodies, 316 proteins were identified from pituitary glands (Ribeiro-Oliveira et al., 2008).

Although the hormones secreted from the pituitary have been well studied, comprehensive analyses of the pituitary proteome are limited. Pituitary proteomics is a field of postgenomic research that is crucial to understand human health and pituitary diseases. In this context, we report here a systematic proteomic profiling of human anterior pituitary gland (adenohypophysis) using high-resolution Fourier transform MS.

Materials and Methods

Sample collection

The study was approved by the Scientific Ethics Committee of National Institute of Mental Health and Neuro Sciences (NIMHANS, Bangalore, India). Subsequently, pituitary glands were obtained from the Human Brain Tissue Repository (National Research Facility), NIMHANS, Bangalore, India. An informed written consent had been obtained from close relatives after having ascertained that no objection has been expressed by the deceased to any of his/her organs being used after his/her death for research/educational purposes. The Human Brain Tissue Repository has been authorized to collect the tissues during autopsy and to store them.

Anterior pituitary gland tissues were collected from three male victims of road traffic accidents. After death, the bodies were immediately transported and maintained at 4°C in the mortuary. The tissues were harvested between 9 and 17 h after death (Supplementary Table S1). Anterior pituitary gland ($n = 3$) tissues were dissected from human pituitary glands at the time of autopsy. Histological examination of a segment of pituitary glands was carried out to distinguish anterior pituitary gland to confirm the absence of adenomas and inflammation (Supplementary Fig. S1).

Protein extraction and normalization

Anterior pituitary gland tissues were homogenized individually in liquid nitrogen using mortar and pestle. Protein from these tissues was extracted in urea lysis buffer (9 M urea, 20 mM HEPES, 1 mM sodium orthovanadate, 1 mM β-glycerophosphate, and 2.5 mM sodium pyrophosphate). The lysates were subjected to centrifugation at 13,000 rpm for 15 min at 4°C. Supernatant from each tissue lysate was collected and protein estimation was carried out by bicinchoninic acid assays (Pierce, USA). Protein samples were normalized based on protein amounts, as verified on 10% sodium dodecyl sulfate/polyacrylamide gel electrophoresis (SDS-PAGE).

Five hundred micrograms of protein from each of the three tissue samples was pooled to get a 1.5 mg protein pool from

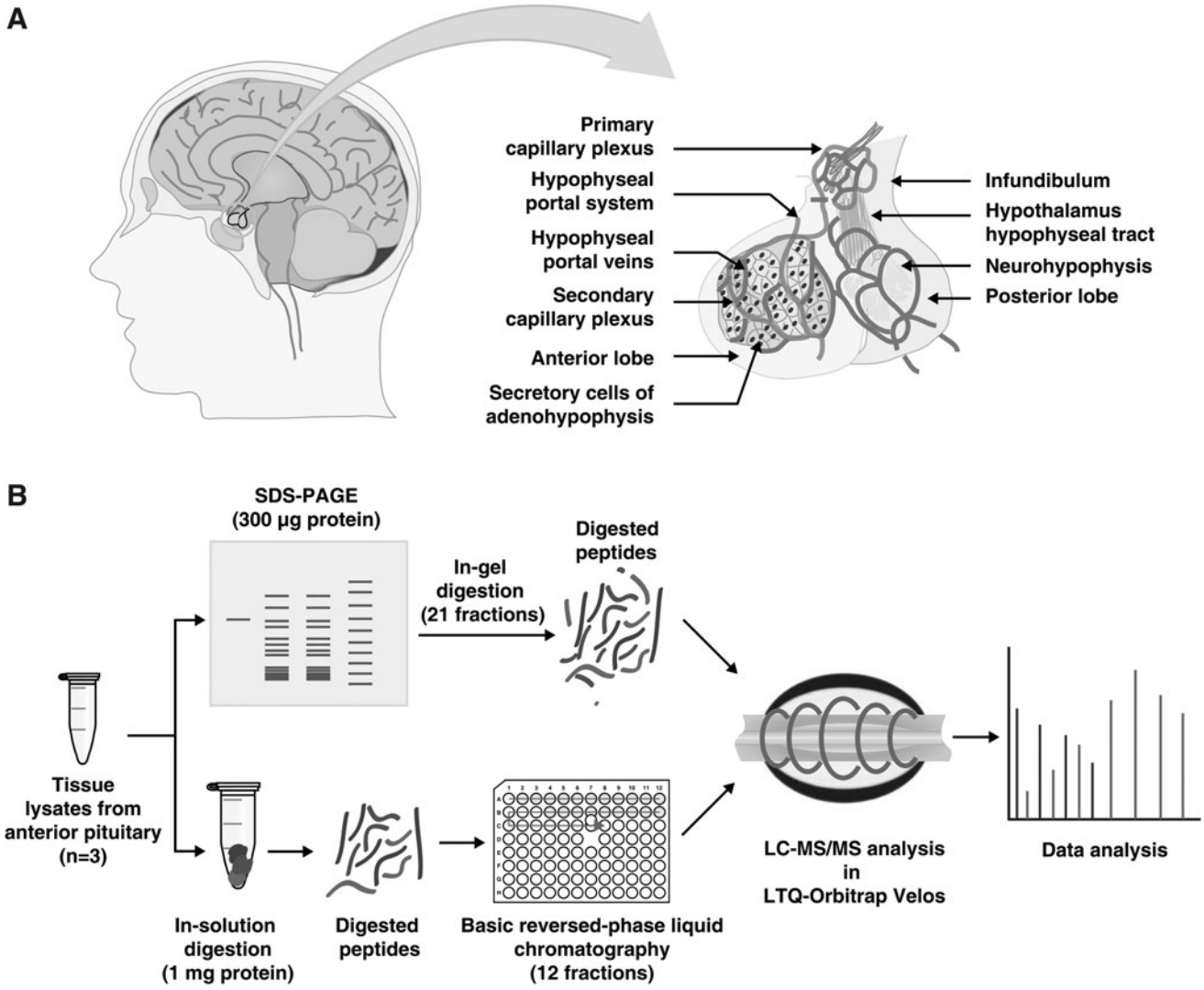

FIG. 1. Schematic representation of anatomical structure and proteomic analysis of human pituitary gland. **(A)** The detailed structure of human pituitary glands. **(B)** The methodology used using different fractionation techniques and LC-MS/MS analysis for the identification of proteins from human adenohypophysis. LC-MS/MS, liquid chromatography–mass spectrometry/mass spectrometry.

adenohypophysis. Three hundred micrograms of protein from the pooled sample underwent in-gel digestion, while a 1 mg aliquot was subjected to in-solution digestion.

In-gel digestion

Protein-level fractionation was performed as described previously (Yelamanchi et al., 2016a). Briefly, 300 μg of protein from adenohypophysis was resolved on the 10% SDS-PAGE gel. The gel was stained with colloidal Coomassie blue stain and each lane was cut into 21 bands. Gel bands were completely destained with 40 mM ammonium bicarbonate in 40% acetonitrile. Reduction was carried out using 5 mM dithiothreitol and alkylation by 20 mM iodoacetamide. In-gel digestion was performed using trypsin (Promega, Madison, WI, USA), with the enzyme and substrate ratio of 1:20 (w/w), for 12 h at 37°C. In-gel digested peptides were subjected to peptide extraction followed by cleaning up using C_{18} stage tips (3M Empore high-performance extraction disks).

In-solution digestion and basic pH reversed-phase liquid chromatography (bRPLC)

In-solution digestion was carried out with 1 mg of protein from the pooled lysate essentially as described previously (Balakrishnan et al., 2014; Harish et al., 2015). Reduction and alkylation of cysteine residues were carried out using 5 mM dithiothreitol (60°C for 45 min) and 20 mM iodoacetamide, respectively. Reduced and alkylated samples were subjected to trypsin digestion with the enzyme and substrate ratio of 1:20 (w/w) at 37°C for 16 h. This was followed by cleaning up of the digested samples on Sep-Pak C_{18} columns (WAT051910; Waters Corporation, Milford, MA, USA). Samples were lyophilized (Operon, Gyeonggi-do, Korea) and stored at −80°C.

The in-solution digested peptides were subjected to basic pH reversed-phase liquid chromatography fractionation on XBridge (C_{18}, 5 μm 250×4.6 mm column) (Waters Corporation) coupled to an Agilent 1200 series HPLC system containing a binary pump, autosampler, UV detector, and a

fraction collector. Solvents such as 7 mM triethylammonium bicarbonate (TEABC) in water at pH 8.4 and 7 mM TEABC in 90% acetonitrile, pH 8.4, were used as mobile phase A and B, respectively. Fractionation was carried out on 1 mg equivalent peptides from adenohypophysis at a flow rate of 1 mL/min using the following gradient: 1% B for 0–5 min, 10% B for 5–10 min, 10–35% B for 10–40 min, and 100% B for 40–45 min. A total of 96 fractions collected were further pooled to obtain a total of 12 fractions. The fractions were vacuum dried and stored at −80°C.

Liquid chromatography–mass spectrometry/mass spectrometry analysis

Anterior pituitary gland protein fractions were subjected to liquid chromatography–mass spectrometry/mass spectrometry (LC-MS/MS) analysis on LTQ-Orbitrap Velos mass spectrometer (Thermo Scientific, Bremen, Germany) connected to an Easy nano-LC II system (Thermo Scientific) for peptide separation through reversed-phase chromatography method. The peptides were loaded onto a trap column (2 cm × 75 μm, 5 μm) and fractionated on an analytical column (10 cm × 75 μm, 3 μm). The columns were packed in-house using C_{18} material (Magic C_{18} AQ, 100 Å). The sample was loaded on a trap column at a flow rate of 3 μL/min using 0.1% formic acid (solvent A). The peptides were separated on an analytical column at LC gradient of 5% to 30% solvent B (100% acetonitrile, 0.1% formic acid) over a period of 65 min at a flow rate of 350 nL/min.

Each peptide fraction was run over a total time period of 70 min. The spray voltage was set to 2.0 kV, and the data were acquired in a data-dependent manner. Twenty most intense precursor ions were chosen for fragmentation in higher energy collisional dissociation (HCD) mode. The scans were acquired using Orbitrap mass analyzer at a resolution of 60,000 and 15,000 for MS and MS/MS, respectively, at 400 m/z. Thirty-nine percent of normalized collision energy was used to fragment the peptides. The automatic gain control for full MS was set to 1×10^6 ions and for MS/MS was set to 5×10^4 ions with a maximum time of accumulation of 100 and 300 ms, respectively. The lock mass option was enabled for accurate mass measurements. Polydimethylcyclosiloxane (m/z, 445.1200025) ions were used for internal calibration.

Data analysis

LC-MS/MS data analysis was carried out by using Proteome Discoverer platform, version 2.1 (Thermo Scientific). The data were searched against NCBI Human RefSeq 81 database, which contained 110,386 unique protein sequences with known contaminants using SequestHT and Mascot (Version 2.4) search algorithms. The search parameters used were set as indicated—precursor mass tolerance was set to 20 ppm and fragment mass tolerance to 0.05 Da. Oxidation of methionine and acetylation at protein N-terminus was set as variable modification, while carbamidomethylation of cysteine was set as fixed modification.

Other search parameters included two missed cleavages by trypsin and 1% false discovery rate (FDR). Gene Ontology (GO) terms on biological processes, cellular components, and signal peptides were acquired from Human Protein Reference Database (HPRD) (Goel et al., 2012; Keshava Prasad et al., 2009). Signal peptide domains were also fetched from SignalP version 4.1 (http://cbs.dtu.dk/services/SignalP), for the proteins that lack domain information from HPRD. The data were compared with two published studies on human proteome, comprising one such study from our group (Kim et al., 2014; Wilhelm et al., 2014). Furthermore, human anterior pituitary gland data were also compared with Human Protein Atlas (HPA; http://proteinatlas.org) (Uhlen et al., 2015) containing antibody-based proteomic evidence.

Data availability

The MS data from anterior pituitary gland were submitted to the ProteomeXchange Consortium (http://proteomexchange.org) via the PRIDE partner repository (Vizcaino et al., 2013) with the data set identifier PXD005819.

Results and Discussion

LC-MS/MS-based proteomic analysis of anterior pituitary gland was performed using two different fractionation techniques, as illustrated in Figure 1B. A total of 33 separate LC-MS/MS runs were analyzed using high-resolution Fourier transform mass spectrometer. The analysis resulted in the identification of 2164 proteins that were supported by 12,076 peptides and 120,971 peptide spectrum matches. A complete list of peptides and proteins identified from anterior pituitary gland is given in Supplementary Table S2.

A total of 1395 proteins were identified with multiple peptide evidence. We identified 200 N-terminally acetylated peptides, which enabled us to confirm translational start sites of 187 proteins. A representative MS/MS spectrum for peptides of some of these proteins is depicted in Figure 2. Functional categorization of human anterior pituitary gland proteome was performed based on biological processes and cellular components using the data acquired from HPRD (Goel et al., 2012; Keshava Prasad et al., 2009). GO classification of human anterior pituitary gland proteins is shown in Figure 3A and B.

Anterior pituitary gland proteome was compared with our recent study describing a draft map of human proteome, which comprised proteomes from 30 different human tissues or primary cells (Kim et al., 2014). We also compared human anterior pituitary gland data with another MS-based study that comprises human proteins from 60 tissues, 13 body fluids, 147 cell lines, and public repositories (Wilhelm et al., 2014). Besides these, the data were also mapped to HPA that includes proteins identified from 45 healthy tissues (Uhlen et al., 2015).

Protein expression data from human pituitary glands have not been appended in all these three databases till date. We identified two proteins that are not found in these databases, including putative V-set and immunoglobulin domain-containing-like protein IGHV4OR15-8-like (LOC102723407) and ES1 protein homolog, mitochondrial (LOC102724023). The data from the current study will serve as a baseline for future studies that can help in understanding the organ physiology under normal and disease conditions.

Proteins that are previously not reported

Proteomics of human pituitary gland has been carried out previously by some of the research groups using the high-resolution MS-based approach (Table 1). In this study, we identified an additional 105 proteins from the human anterior pituitary gland that were not reported in any of the earlier studies (Supplementary Table S3).

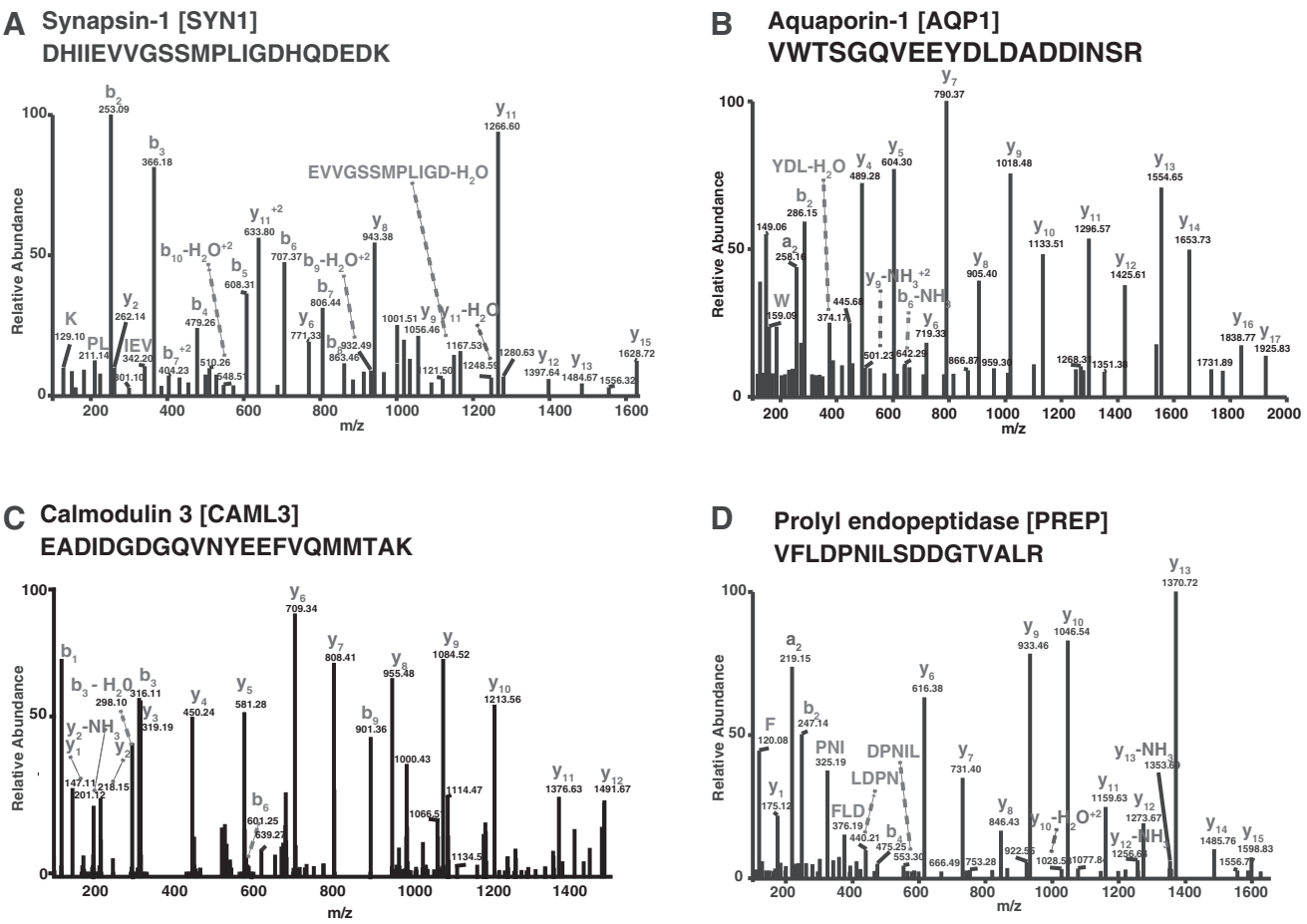

FIG. 2. Representative MS/MS spectra. MS/MS spectra for peptides corresponding to proteins identified from human pituitary gland—**(A)** synapsin-1 [SYN1]; **(B)** aquaporin-1 [AQP1]; **(C)** calmodulin [CALM3]; and **(D)** prolyl endopeptidase [PREP]. The fragmented ions are indicated as b, y, and a ions. Internal fragmented ions are also clearly represented.

Anterior pituitary gland proteins associated with aryl-hydrocarbon receptor signaling

We identified a large number of aryl-hydrocarbon receptor (AHR) signaling network proteins from this study. AHR upon stimulation with ligand activates a series of signaling cascades that are known to be associated with distinct physiological processes in the body, including detoxification process, immunoregulation, gene regulation, and homeostasis (Yelamanchi et al., 2016). Activated AHR has been reported to regulate the mRNA expression of PRL, lutropin subunit beta (LHB), and chromogranin A (CHGA) in pituitary gland (Cao et al., 2011; Moran et al., 2012). Aryl-hydrocarbon interacting protein (AIP) interacts with ligand-bound AHR in the cytosol and translocates into the nucleus leading to transcriptional repression of AHR (Ramadoss et al., 2004).

Previous reports have shown that decreased AHR expression and mutation in AIP gene are associated with GH-secreting pituitary adenomas (Iacovazzo et al., 2016; Jaffrain-Rea et al., 2009). We identified 24 proteins to be enriched in the AHR signaling pathway. The pathway map highlighting the proteins identified in this study is shown in Figure 4.

Significance of anterior pituitary gland proteins with secretory potential

The anterior pituitary gland is well known for secreting distinct hormones. Proteins destined to be secreted from cell usually harbor an N-terminal 15–30 amino acid sequence called a signal peptide, which regulates the translocation/secretion of secretory proteins through the secretory pathway. As the pituitary gland is a secretory endocrine gland, it is reasonable to investigate other lesser known proteins with secretory potential. Therefore, we analyzed signal peptide containing proteins expressed in the pituitary gland. Signal peptide information was available for 336 pituitary gland proteins in HPRD and we combined these data with infor mation from SignalP. In total, 480 proteins were found to contain signal peptides in our study (Supplementary Table S4).

All the known peptide hormones of anterior pituitary gland were identified in this study. A literature search was carried out to analyze the functional significance of anterior pituitary gland proteins with secretory potential. Secretogranin-3 (SCG3), a secretory protein, has been found to be localized in secretory granules of endocrine cells in adenohypophysis (Sakai et al., 2003).

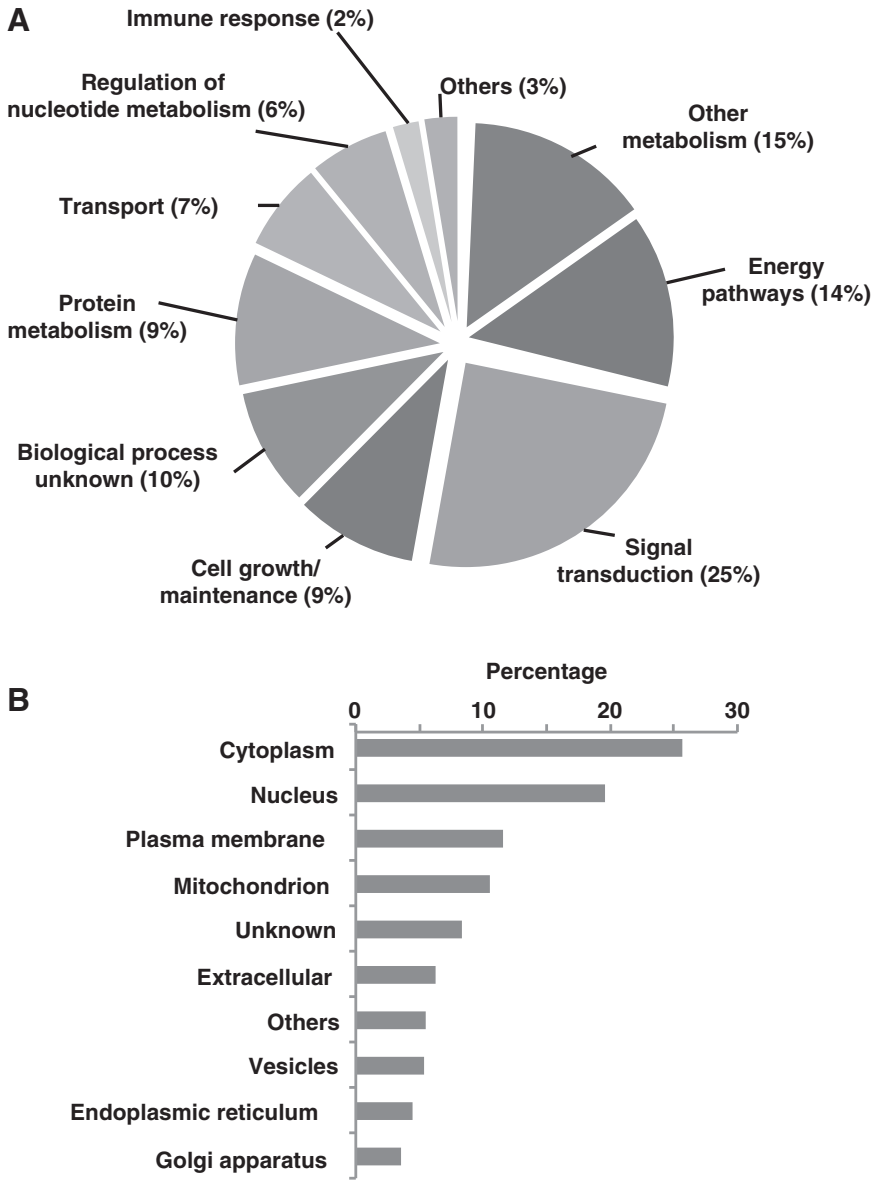

FIG. 3. GO analysis. **(A)** Biological processes such as signal transduction, protein metabolism, and transport were the GO terms derived from human adenohypophysis proteins; **(B)** cellular components, including cytoplasm, nucleus, extracellular and plasma membrane, are illustrated. GO, Gene Ontology.

Previously, it has been reported that CHGA, another secretory protein identified in this study, colocalized with SCG3 to endocrine cells of pituitary gland and pancreas. Similar to most hormones, CHGA and chromogranin B are synthesized as preprohormone and proteolytically processed into multiple smaller peptide hormones with distinct biological functions. CHGA can give rise to peptide hormones that regulate hormone secretion from the parathyroid chief cells (Russell et al., 1994), insulin secretion from the pancreatic islets (Tatemoto et al., 1986), and catecholamine release from the adrenal medulla (Mahata et al., 1997).

VGF nerve growth factor inducible (*VGF*) is a secreted neuroendocrine hormone with an important central metabolic and reproductive role (Jethwa and Ebling, 2008). Mice lacking VGF are infertile and have dramatically reduced fat mass and body weight despite consuming more calories per gram body weight (Hahm et al., 1999). As a preprohormone, VGF is proteolytically processed by neuroendocrine convertases (PCSK1 and PCSK2) into multiple smaller isoforms, each possessing distinct biological functions in the central nervous system with regard to modulating food intake (Jethwa et al., 2007) and reproduction (Succu et al., 2004). A partial list of hitherto signal peptide containing proteins from human anterior pituitary gland is provided in Table 2.

Folliculostellate proteins identified from human anterior pituitary gland

Anterior pituitary gland comprises different groups of endocrine cells that regulate various functional activities in the body through the secretion of hormones. It also harbors

TABLE 1. SUMMARY OF PREVIOUS STUDIES ON HUMAN PITUITARY PROTEOMICS

	Sample preparation	*# Proteins*	*#Peptides*	*MS/MS spectra*	*Instrument and resolution used*	*Search algorithm*	*Reference*
1	Immunoaffinity depletion and high-pH HPLC separation	7596	121,315	436,104	TripleTOF 5600 (MS1 and MS2 40000 and 20000)	Mascot	Liu et al. (2017)
2	In-gel digestion and 2D-HPLC (SCX and RPLC)	1660	42,055	89,314	LTQ-Orbitrap XL	SEQUEST	Liu et al. (2011)
3	In-gel digestion (isoelectric focusing and SDS-PAGE)	1449	6295	—	LCQ Deca XP Plus ion trap	SEQUEST	Zhao et al. (2005)
4	In-solution digestion	1007	14,301	—	Q-TOF	ProteinLynx Global Server	Krishnamurthy et al. (2011)
5	2D gel electrophoresis	316	—	—	BD powerblot western array	—	Ribeiro-Oliveira et al. (2008)
6	In-gel digestion isoelectric focusing	127	—	—	LCQ Deca	SEQUEST	Giorgianni et al. (2003)
7	2D gel electrophoresis	28	—	—	Voyager DE-RP and LCQ Deca	—	Zhan and Desiderio (2003)

HPLC, high-performance liquid chromatography; 2D, two dimensional; SDS-PAGE, sodium dodecyl sulfate/polyacrylamide gel electrophoresis; MS, mass spectrometry; SCX, strong cation exchange; RPLC, reverse phase liquid chromatography.

another group of nonendocrine star-shaped cells with long cytoplasmic processes known as the folliculostellate cells. These cells are restricted to anterior pituitary gland portion of the pituitary gland and are known to form gap junctions and network-like structures surrounding the endocrine cells (Inoue et al., 1999).

In this study, we identified a number of proteins that have been described to be expressed in folliculostellate cells. Annexin A1 (ANXA1), expressed in these nonendocrine cells, is known to inhibit the release of ACTH from adenohypophysis (Tierney et al., 2003). Macrophage migration inhibitory factor, a proinflammatory cytokine, functions as an autocrine or paracrine factor in folliculostellate cells and provides protection against infection or inflammation (Tierney et al., 2005). Glutamine synthetase (GLUL), which has been identified in folliculostellate cells, utilizes ammonia for the synthesis of glutamine. Hence, folliculostellate cells can also function as scavengers of ammonia (Shirasawa and Yamanouchi, 1999).

Matrix metalloproteinase-9 (MMP9) is reported to regulate the proliferation of folliculostellate cells (Ilmiawati et al., 2012). Metalloproteinase inhibitor 2 (TIMP2) is secreted from the folliculostellate cells and promotes the survival of endocrine cells of the pituitary gland (Matsumoto et al., 1993). Ciliary neurotrophic factor (CNTF) receptor subunit alpha identified in this study induces the proliferation of folliculostellate cells on stimulation with CNTF (Perez Castro et al., 2000). Previous reports have shown that CNTF forms gap junctions between these cells (Sakuma et al., 2002). Protein S100-B (S100B) has been reported to regulate the secretion of PRL from lactotrophs (Ishikawa et al., 1983).

Anterior pituitary gland proteins associated with diseases

Anterior pituitary gland proteins have been reported to be involved in various human diseases. Beta-2-syntrophin (SNTB2), follicle stimulating hormone subunit beta (FSHB), and neuronal pentraxin-2 (NPTX2) have been reported to be differentially expressed in prolactinomas (Evans et al., 2008). A calcium binding protein secretagogin (SCGN), which is highly expressed in pituitary glands, has been reported to be associated with nonfunctional pituitary adenomas (Gartner et al., 2001). The cochaperone, AIP, has been shown to interact with many biologically significant proteins, including guanine nucleotide-binding protein subunit alpha-13 (GNA13), which destabilizes AIP-AhR complex, thus regulating AhR translocation to the nucleus.

In addition, AIP interaction with cGMP-dependent 3′, 5′-cyclic phosphodiesterase (PDE2A) has been shown to decrease mitogenic effects by reducing cAMP levels. This indicates that AIP has tumor suppressor activity in pituitary tumor cells (Trivellin and Korbonits, 2011).

Mutational studies have shown that AIP is associated with familial isolated pituitary adenoma (Vierimaa et al., 2006), pituitary adenoma with neuronal choristoma, and sporadic pituitary adenoma. Similarly, mutation in G-protein subunit alpha S (GNAS) gene is reported to be associated with the McCune-Albright syndrome (Weinstein et al., 1991). cAMP-dependent protein kinase type I-alpha regulatory subunit (PRKAR1A) is associated with Carney complex-related pituitary adenomas. Tissue alpha-L-fucosidase (FUCA1)

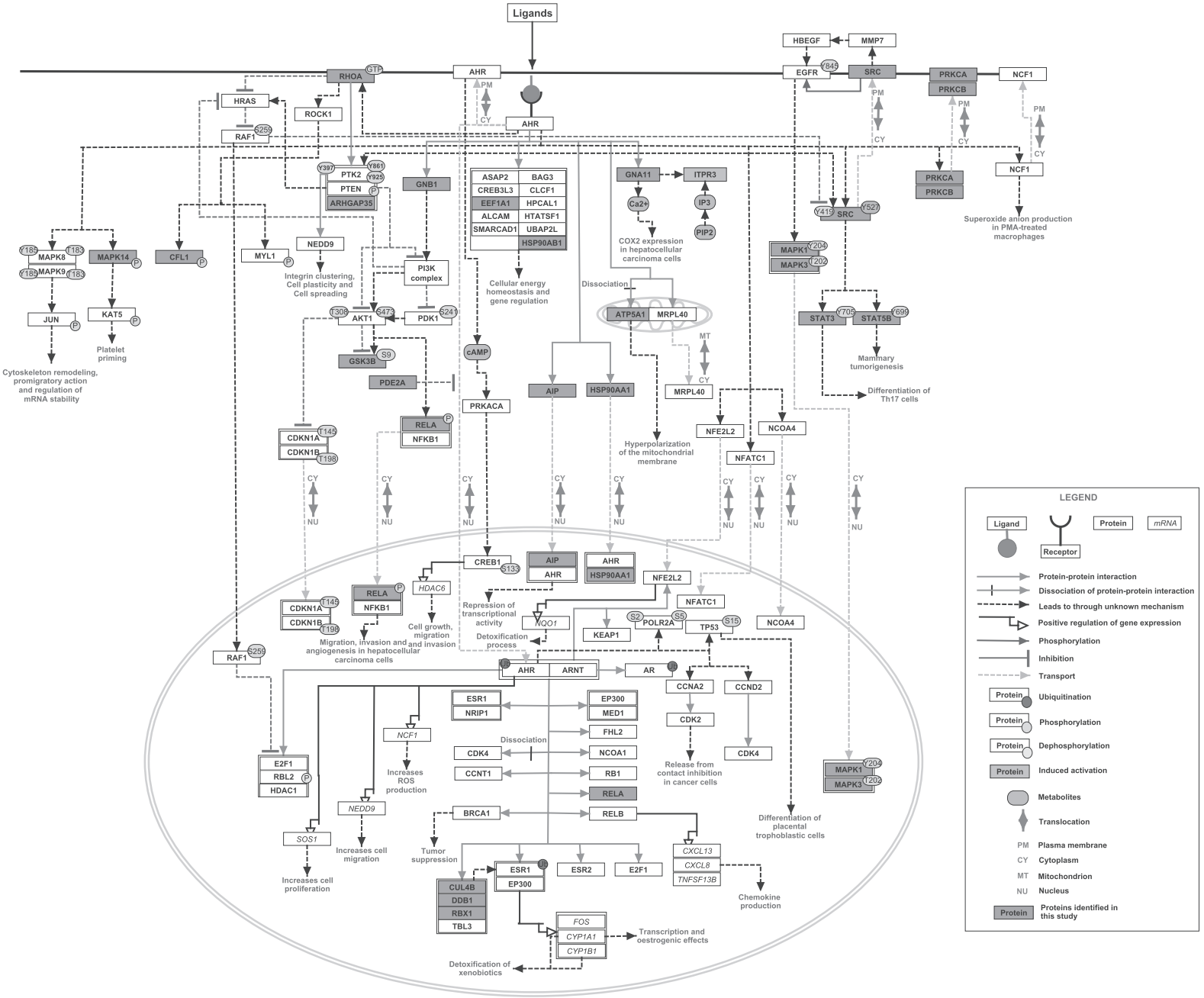

FIG. 4. Aryl-hydrocarbon signaling pathway. The signaling pathway map exhibiting distinct reactions under receptor activation. Twenty-four proteins were identified to be associated with this pathway, as highlighted.

Table 2. A Partial List of Signal Peptide Containing Proteins Identified from Human Anterior Pituitary Gland

	Gene symbol	*Protein*	*RefSeq accession*	*Molecular function*
1	*SYNPR*	Synaptoporin	NP_001123475.1	Auxiliary transport protein activity
2	*SORT1*	Sortilin 1	NP_002950.3	Receptor activity
3	*CDH2*	Cadherin-2	NP_001783.2	Cell adhesion molecule activity
4	*HPX*	Hemopexin precursor	NP_000604.1	Protein binding
5	*GM2A*	Ganglioside GM2 activator	NP_000396.2	Transporter activity
6	*VASN*	Vasorin	NP_612449.2	Growth factor binding
7	*FUCA1*	Tissue alpha-L-fucosidase	NP_000138.2	Hydrolase activity
8	*MRC2*	C-type mannose receptor 2	NP_006030.2	Receptor activity
9	*IPO9*	Importin-9	NP_060555.2	Transporter activity
10	*NIPSNAP3B*	Protein NipSnap homolog 3B	NP_060846.2	Transporter activity
11	*CMPK1*	UMP-CMP kinase isoform a	NP_057392.1	Catalytic activity
12	*EPHX1*	Epoxide hydrolase 1	NP_001129490.1	Hydrolase activity
13	*SERINC1*	Serine incorporator 1	NP_065806.1	Protein binding
14	*KNG1*	Kininogen-1	NP_000884.1	Protease inhibitor activity
15	*SLC22A13*	Solute carrier family 22 member 13	NP_004247.2	Auxiliary transport protein activity

has previously been reported to be associated with colorectal cancer (Otero-Estevez et al., 2013). SNTB2, PDE2A, and FUCA1 have not previously been reported from human pituitary gland.

We compared the proteomic data from anterior pituitary gland with the genes associated with sporadic pituitary adenoma from the genome-wide association study database that comprises information related to mutations in genes and the disease association. We identified protocadherin-related 15 (PCDH15) from this study. Previous reports have shown that mutation in *PCDH15* gene is associated with Usher syndrome and hearing loss. Furthermore, *PCDH15* gene expression was known to be linked with pituitary development in mice (Ye et al., 2015).

We also identified aminophospholipid transporter, class I, type 8A (ATP8A2) and Wiskott–Aldrich syndrome protein family member 3 (WASF3) in this study when compared with expression Quantitative Trait Loci (eQTL) analysis. Previous reports have shown that mutation in ATP8A2 was found to be linked to several human neurological disorders such as cognitive disorders, optic dystrophy, hypotonia, and cerebellar ataxia mental retardation and dysequilibrium (CAMRQ) syndrome (McMillan et al., 2018). Furthermore, overexpression of *WASF3* gene is known to play an active role in the development of cancer (Teng et al., 2013).

Conclusions

Pituitary gland is known as the master gland and regulates most of the endocrine functions in the human body. It should be noted that the proteins analyzed in this study were from the male anterior pituitary gland and it is indeed possible that the female anterior pituitary gland could be different in terms of its proteome.

The present data set will serve as a vital resource for further investigations on the physiological role of human pituitary glands and the proteins secreted by them. Notably, experimental standards for high-throughput proteomics have been evolving for over a decade (Hogan et al. 2006), and advances in omics analyses for health and disease have now become crucial for a system-scale understanding of the pituitary gland pathophysiology (Zhan and Desiderio, 2016). Moreover, we anticipate that the identification of novel proteins in this study will accelerate biomedical research to decipher their role in the functioning of human pituitary gland and associated human diseases.

Acknowledgments

We acknowledge the contribution of Late Dr. Kanchan Mukherjee for the design of the study and critical review of this article. We also acknowledge Late Dr. Gururao S. Desai for his contribution in experiments and article writing. We thank Thermo Scientific and Sciex for access to instrumentation. The study was supported by a research grant ''DBT Programme Support on Neuroproteomics of Neurological Disorders'' to IOB and NIMHANS by DBT, Government of India (BT/01/COE/08/05). Human brain tissues for the study were obtained from the Human Brain Tissue Repository, a National Research Facility, Department of Neuropathology, NIMHANS, Bangalore, India.

This publication was partly supported by a subaward from The Johns Hopkins University, with funds provided from the National Institute of Neurological Disorders and Stroke (NINDS) (Grant Number: 1RO1NS055628-01A2). The contents of the study are solely the responsibility of the authors and do not represent the official views of NINDS or JHU. J.A. is a recipient of Senior Research Fellowships from the Council for Scientific and Industrial Research (CSIR), Government of India. A.T. is a recipient of Senior Research Fellowship from Yenepoya (deemed to be University). V.M. is a recipient of Junior Research Fellowship from Yenepoya (deemed to be University).

Author Disclosure Statement

The authors declare that no conflicting financial interests exist.

References

Allaerts W, and Vankelecom H. (2005). History and perspectives of pituitary folliculo-stellate cell research. Eur J Endocrinol 153, 1–12.

Balakrishnan L, Nirujogi RS, Ahmad S, et al. (2014). Proteomic analysis of human osteoarthritis synovial fluid. Clin Proteomics 11, 6.

Cao J, Patisaul HB, and Petersen SL. (2011). Aryl hydrocarbon receptor activation in lactotropes and gonadotropes interferes with estradiol-dependent and -independent preprolactin, glycoprotein alpha and luteinizing hormone beta gene expression. Mol Cell Endocrinol 333, 151–159.

Evans CO, Moreno CS, Zhan X, et al. (2008). Molecular pathogenesis of human prolactinomas identified by gene expression profiling, RT-qPCR, and proteomic analyses. Pituitary 11, 231–245.

Gartner W, Lang W, Leutmetzer F, Domanovits H, Waldhausl W, and Wagner L. (2001). Cerebral expression and serum detectability of secretagogin, a recently cloned EF-hand Ca(2+)-binding protein. Cereb Cortex 11, 1161–1169.

Giorgianni F, Desiderio DM, and Beranova-Giorgianni S. (2003). Proteome analysis using isoelectric focusing in immobilized pH gradient gels followed by mass spectrometry. Electrophoresis 24, 253–259.

Goel R, Harsha HC, Pandey A, and Prasad TS. (2012). Human protein reference database and human proteinpedia as resources for phosphoproteome analysis. Mol Biosyst 8, 453–463.

Hahm S, Mizuno TM, Wu TJ, et al. (1999). Targeted deletion of the Vgf gene indicates that the encoded secretory peptide precursor plays a novel role in the regulation of energy balance. Neuron 23, 537–548.

Harish G, Mahadevan A, Pruthi N, et al. (2015). Characterization of traumatic brain injury in human brains reveals distinct cellular and molecular changes in contusion and pericontusion. J Neurochem 134, 156–172.

Hogan JM, Higdon R, and Kolker E. (2006). Experimental standards for high-throughput proteomics. OMICS 10, 152–157.

Iacovazzo D, Caswell R, Bunce B, et al. (2016). Germline or somatic GPR101 duplication leads to X-linked acrogigantism: A clinico-pathological and genetic study. Acta Neuropathol Commun 4, 56.

Ilmiawati C, Horiguchi K, Fujiwara K, and Yashiro T. (2012). Matrix metalloproteinase-9 expression in folliculostellate cells of rat anterior pituitary gland. J Endocrinol 212, 363–370.

Inoue K, Couch EF, Takano K, and Ogawa S. (1999). The structure and function of folliculo-stellate cells in the anterior pituitary gland. Arch Histol Cytol 62, 205–218.

Ishikawa H, Nogami H, and Shirasawa N. (1983). Novel clonal strains from adult rat anterior pituitary producing S-100 protein. Nature 303, 711–713.

Jaffrain-Rea ML, Angelini M, Gargano D, et al. (2009). Expression of aryl hydrocarbon receptor (AHR) and AHR-interacting protein in pituitary adenomas: Pathological and clinical implications. Endocr Relat Cancer 16, 1029–1043.

Jethwa PH, and Ebling FJ. (2008). Role of VGF-derived peptides in the control of food intake, body weight and reproduction. Neuroendocrinology 88, 80–87.

Jethwa PH, Warner A, Nilaweera KN, et al. (2007). VGF-derived peptide, TLQP-21, regulates food intake and body weight in Siberian hamsters. Endocrinology 148, 4044–4055.

Jorgensen H, Kjaer A, Knigge U, Moller M, and Warberg J. (2003). Serotonin stimulates hypothalamic mRNA expression and local release of neurohypophysial peptides. J Neuroendocrinol 15, 564–571.

Karanth S, and McCann SM. (1991). Anterior pituitary hormone control by interleukin 2. Proc Natl Acad Sci U S A 88, 2961–2965.

Keshava Prasad TS, Goel R, Kandasamy K, et al. (2009). Human protein reference database—2009 update. Nucleic Acids Res 37, D767–D772.

Kim MS, Pinto SM, Getnet D, et al. (2014). A draft map of the human proteome. Nature 509, 575–581.

Krishnamurthy D, Levin Y, Harris LW, Umrania Y, Bahn S, and Guest PC. (2011). Analysis of the human pituitary proteome by data independent label-free liquid chromatography tandem mass spectrometry. Proteomics 11, 495–500.

Liu X, Guo Z, Sun H, Li W, and Sun W. (2017). Comprehensive map and functional annotation of human pituitary and thyroid proteome. J Proteome Res 16, 2680–2691.

Liu Y, Zhuang D, Hou R, et al. (2011). Shotgun proteomic analysis of microdissected postmortem human pituitary using complementary two-dimensional liquid chromatography coupled with tandem mass spectrometer. Anal Chim Acta 688, 183–190.

Mahata SK, O'Connor DT, Mahata M, et al. (1997). Novel autocrine feedback control of catecholamine release. A discrete chromogranin a fragment is a noncompetitive nicotinic cholinergic antagonist. J Clin Invest 100, 1623–1633.

Matsumoto H, Ishibashi Y, Ohtaki T, Hasegawa Y, Koyama C, and Inoue K. (1993). Newly established murine pituitary folliculo-stellate-like cell line (TtT/GF) secretes potent pituitary glandular cell survival factors, one of which corresponds to metalloproteinase inhibitor. Biochem Biophys Res Commun 194, 909–915.

McMillan HJ, Telegrafi A, Singleton A, et al. (2018). Recessive mutations in ATP8A2 cause severe hypotonia, cognitive impairment, hyperkinetic movement disorders and progressive optic atrophy. Orphanet J Rare Dis 13, 86.

Moran TB, Brannick KE, and Raetzman LT. (2012). Aryl-hydrocarbon receptor activity modulates prolactin expression in the pituitary. Toxicol Appl Pharmacol 265, 139–145.

Otero-Estevez O, Martinez-Fernandez M, Vazquez-Iglesias L, Paez de la Cadena M, Rodriguez-Berrocal FJ, and Martinez-Zorzano VS. (2013). Decreased expression of alpha-L-fucosidase gene FUCA1 in human colorectal tumors. Int J Mol Sci 14, 16986–16998.

Perez Castro C, Nagashima AC, Pereda MP, et al. (2000). The gp130 cytokines interleukin-11 and ciliary neurotropic factor regulate through specific receptors the function and growth of lactosomatotropic and folliculostellate pituitary cell lines. Endocrinology 141, 1746–1753.

Ramadoss P, Petrulis JR, Hollingshead BD, Kusnadi A, and Perdew GH. (2004). Divergent roles of hepatitis B virus X-associated protein 2 (XAP2) in human versus mouse Ah receptor complexes. Biochemistry 43, 700–709.

Ribeiro-Oliveira A, Jr., Franchi G, Kola B, et al. (2008). Protein western array analysis in human pituitary tumours: Insights and limitations. Endocr Relat Cancer 15, 1099–1114.

Russell J, Gee P, Liu SM, and Angeletti RH. (1994). Inhibition of parathyroid hormone secretion by amino-terminal chromogranin peptides. Endocrinology 135, 337–342.

Sakai Y, Hosaka M, Hira Y, et al. (2003). Immunocytochemical localization of secretogranin III in the anterior lobe of male rat pituitary glands. J Histochem Cytochem 51, 227–238.

Sakuma E, Herbert DC, and Soji T. (2002). Leptin and ciliary neurotrophic factor enhance the formation of gap junctions

between folliculo-stellate cells in castrated male rats. Arch Histol Cytol 65, 269–278.
Shirasawa N, and Yamanouchi H. (1999). Glucocorticoids induce glutamine synthetase in folliculostellate cells of rat pituitary glands in vivo and in vitro. J Anat 194 (Pt 4), 567–577.
Succu S, Cocco C, Mascia MS, et al. (2004). Pro-VGF-derived peptides induce penile erection in male rats: Possible involvement of oxytocin. Eur J Neurosci 20, 3035–3040.
Tatemoto K, Efendic S, Mutt V, Makk G, Feistner GJ, and Barchas JD. (1986). Pancreastatin, a novel pancreatic peptide that inhibits insulin secretion. Nature 324, 476–478.
Teng Y, Ghoshal P, Ngoka L, Mei Y, and Cowell JK. (2013). Critical role of the WASF3 gene in JAK2/STAT3 regulation of cancer cell motility. Carcinogenesis 34, 1994–1999.
Tierney T, Christian HC, Morris JF, Solito E, and Buckingham JC. (2003). Evidence from studies on co-cultures of TtT/GF and AtT20 cells that annexin 1 acts as a paracrine or juxtacrine mediator of the early inhibitory effects of glucocorticoids on ACTH release. J Neuroendocrinol 15, 1134–1143.
Tierney T, Patel R, Stead CA, Leng L, Bucala R, and Buckingham JC. (2005). Macrophage migration inhibitory factor is released from pituitary folliculo-stellate-like cells by endotoxin and dexamethasone and attenuates the steroid-induced inhibition of interleukin 6 release. Endocrinology 146, 35–43.
Trivellin G, and Korbonits M. (2011). AIP and its interacting partners. J Endocrinol 210, 137–155.
Uhlen M, Fagerberg L, Hallstrom BM, et al. (2015). Proteomics. Tissue-based map of the human proteome. Science 347, 1260419.
Vierimaa O, Georgitsi M, Lehtonen R, et al. (2006). Pituitary adenoma predisposition caused by germline mutations in the AIP gene. Science 312, 1228–1230.
Vizcaino JA, Cote RG, Csordas A, et al. (2013). The PRoteomics IDEntifications (PRIDE) database and associated tools: Status in 2013. Nucleic Acids Res 41, D1063–D1069.
Weinstein LS, Shenker A, Gejman PV, Merino MJ, Friedman E, and Spiegel AM. (1991). Activating mutations of the stimulatory G protein in the McCune-Albright syndrome. N Engl J Med 325, 1688–1695.
Wilhelm M, Schlegl J, Hahne H, et al. (2014). Mass-spectrometry-based draft of the human proteome. Nature 509, 582–587.
Yasin SA, Costa A, Forsling ML, and Grossman A. (1994). Interleukin-1 beta and interleukin-6 stimulate neurohypophysial hormone release in vitro. J Neuroendocrinol 6, 179–184.
Ye Z, Li Z, Wang Y, et al. (2015). Common variants at 10p12.31, 10q21.1 and 13q12.13 are associated with sporadic pituitary adenoma. Nat Genet 47, 793–797.
Yelamanchi SD, Kumar M, Madugundu AK, et al. (2016). Characterization of human pineal gland proteome. Mol Biosyst 12, 3622–3632.
Yelamanchi SD, Solanki HS, Radhakrishnan A, et al. (2016). Signaling network map of the aryl hydrocarbon receptor. J Cell Commun Signal 10, 341–346.
Zhan X, and Desiderio DM. (2003). Heterogeneity analysis of the human pituitary proteome. Clin Chem 49, 1740–1751.
Zhan X, and Desiderio DM. (2016). Editorial: Systems biological aspects of pituitary tumors. Front Endocrinol (Lausanne) 7, 86.
Zhao Y, Giorgianni F, Desiderio DM, Fang B, and Beranova-Giorgianni S. (2005). Toward a global analysis of the human pituitary proteome by multiple gel-based technology. Anal Chem 77, 5324–5331.

Address correspondence to:
T.S. Keshava Prasad, PhD
Center for Systems Biology and Molecular Medicine,
Yenepoya Research Centre, Yenepoya
(Deemed to be University)
Mangalore 575 018
India

E-mail: keshav@yenepoya.edu.in

Anita Mahadevan, MD
Human Brain Tissue Repository
Neurobiology Research Centre
National Institute of Mental Health and Neuro Sciences
Bangalore 560 029
India

E-mail: anita_mahadevan@yahoo.com

Susarla K. Shankar, MD
Human Brain Tissue Repository
Neurobiology Research Centre
National Institute of Mental Health and Neuro Sciences
Bangalore 560 029
India

E-mail: shankarsk2004@gmail.com

Abbreviations Used

2D = two dimensional
ACTH = adrenocorticotropic hormone
AHR = aryl-hydrocarbon receptor
AIP = aryl-hydrocarbon interacting protein
ANXA1 = annexin A1
CHGA = chromogranin A
CNTF = ciliary neurotrophic factor
CRH = corticotropin-releasing hormone
GH = growth hormone
GLUL = glutamine synthetase
GNA13 = guanine nucleotide-binding protein subunit alpha-13
GO = Gene Ontology
HPA = Human Protein Atlas
HPLC = high-performance liquid chromatography
HPRD = Human Protein Reference Database
IL = interleukin
LC-MS/MS = liquid chromatography–mass spectrometry/mass spectrometry
MMP9 = matrix metalloproteinase-9
NIMHANS = National Institute of Mental Health and Neuro Sciences
NPTX2 = neuronal pentraxin-2
PCDH15 = protocadherin-related 15
SCG3 = secretogranin-3
SCGN = secretagogin
SDS-PAGE = sodium dodecyl sulfate/polyacrylamide gel electrophoresis
SNTB2 = beta-2-syntrophin
TEABC = triethylammonium bicarbonate

Kamalika Roy Choudhury et al., J Clin Exp Cardiolog 2017, 8:12(Suppl)
DOI: 10.4172/2155-9880-C1-086

Differential proteomic profiling of control and STEMI subjects; probable implications towards reverse cholesterol transport

Kamalika Roy Choudhury, Apabrita Ayan Das and Arun Bandyopadhyay
CSIR-Indian Institute of Chemical Biology, India

Statement of the Problem: Atherosclerotic lesions in humans typically develop over years to decades; one of the longest incubation periods of disease onset in humans. Acute coronary syndrome (ACS) includes unstable angina and acute myocardial infarction. Atherosclerosis is the major source of mortality in the developed countries, claiming more lives than all types of cancer combined. WHO predicts atherosclerosis to become an epidemic in developing countries like India in coming years as it acquires western lifestyles. Only few reports are available on the plasma proteome profile of ACS. In this study, we used STEMI patients and age and sex matched control subjects.

Methodology & Theoretical Orientation: We used nano LC-MS orbitrap mass spectrometer and SWATH-MS to annotate proteins and identify differential expressions between control and ACS samples respectively. We used GeneCodis 3.0 and PANTHER for pathway enrichment analysis.

Findings: Using nano LC-MS orbitrap mass spectrometer we identified ~3000 proteins from control and STEMI patients respectively. We also performed SWATH-MS to identify differential expressions of proteins, if any. 65 proteins (27 downregulated, 38 upregulated) show differential expressions between control and STEMI patients. Some protein expression patterns were validated using western blotting and ELISA to look into the molecular detail. Here we intend to focus on the reverse cholesterol transport (RCT) pathway.

Conclusion & Significance: We found downregulation of ZAG, a novel adipokine in ACS patients from SWATH and validated using western and ELISA. Upregulation of a novel ATP binding cassette transporter, ABCA5, was observed in STEMI using orbitrap-MS. We show here that these might be responsible for the alteration in reverse cholesterol transport pathway during ACS which has a great impact on atherosclerotic pathway.

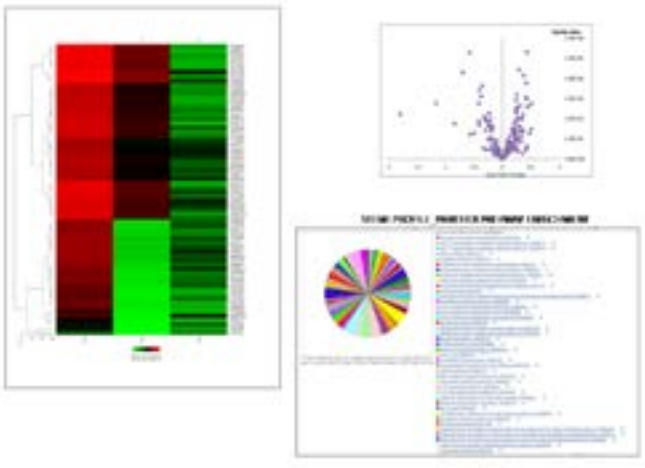

Biography

Kamalika Roy Choudhury did her PhD from SINP, India on Cell Biology and Proteomics of Huntington's disease. She is currently working on cardiovascular translational research; looking for proteomic alterations and post translational modifications during acute coronary syndrome.

withkamalika@gmail.com

Apabrita Ayan Das et al., J Clin Exp Cardiolog 2017, 8:12(Suppl)
DOI: 10.4172/2155-9880-C1-086

Elevated level of sTLT1 is associated with risk prediction in acute coronary syndrome

Apabrita Ayan Das[1], **Prakash C Mandal**[2], **Khawer N Siddiqui**[3] and **Arun Bandyopadhyay**[1]
[1]CSIR-Indian Institute of Chemical Biology, India
[2]Apollo Gleneagles Hospital, India
[3]Ruby General Hospital, India

Statement of the Problem: Soluble TREM like transcript 1(sTLT1) is reported to be associated with major processes related to atherosclerosis and Acute Coronary Syndrome. Hence, our study aimed to determine the association of sTLT1 with Coronary Heart Disease and its ability to predict the risk in the aforementioned disease.

Methodology: 117 subjects with or without Acute Coronary Syndrome were enrolled and plasma levels of soluble TREM like Transcript 1, NT-proBNP, oxidized LDL and other cholesterols were estimated. Subclinical cases were identified by lipid profiling, electrocardiogram and echocardiography. Regression analysis and ROC analysis were performed to determine the predictive value of this protein.

Findings: sTLT1 level was significantly ($p<0.05$) higher in ACS subjects and asymptomatic than that of control subjects. The level of sTLT1 was not only associated with common risk factors of ACS in both patient and asymptomatic groups but also correlated with disease severity and it was also significantly associated (1338±375 pg/ml) with intima-media thickness in asymptomatic individuals (>1mm). Cut-off values of sTLT1 were found to be 875 pg/ml and 2500 pg/ml in asymptomatic and ACS subjects respectively, as revealed by Receiver operating characteristic (ROC) curve analysis. Multiple linear and logistic regression analysis revealed that sTLT1 level would independently predict ACS as it is significantly associated (Linear Regression: $P<0.0001$, $r=0.674$) (Logistic Regression: $P=0.045$, OR=1.02, 95% CI=1 to 1.04) with disease risk.

Conclusion & Significance: Circulating sTLT1 represents a promising candidate for risk prediction in asymptomatic as well as ACS subjects which may reduce mortality rate by leading better prognosis.

Biography

Apabrita Ayan Das is working on Cardiovascular Biology. He had pursued his MSc from Banaras Hindu University. Currently, he is pursuing his PhD under Dr. Arun Bandyopadhyay in CSIR-Indian Institute of Chemical Biology, India. His research is mainly focused on identifying novel prognostic and diagnostic marker for acute coronary syndrome and elucidates their role in coronary heart disease.

apabritaayan@gmail.com

इंटरनेशनल सोसायटी ऑफ हार्ट रिसर्च (भारतीय अनुभाग) का 14वीं वार्षिक बैठक

14th Annual Meeting of International Society for Heart Research Indian Section

27th to 29th January 2017 at CSIR Institute of Genomics and Integrative Biology, Delhi

Prof. N.K. Ganguly Award

This is to certify that Dr./Mr./Ms. Apabsita Ayan Das has won the Prof. N.K Ganguly award in the 14th Annual Meeting of International Society for Heart Research Indian Section organised at the CSIR Institute of Genomics and Integrative Biology, Delhi from 27th to 29th January 2017

Shantanu Sengupta
Organizing Secretary

Subir Kumar Maulik
Secretary,
ISHR Indian Section

K.K Talwar
President,
ISHR Indian Section

Institute of Bioinformatics

WORKSHOP ON CLINICAL PROTEOMICS

Held on July 29 - August 01, 2013

INSTITUTE OF BIOINFORMATICS, BANGALORE

CERTIFICATE

This is to certify that **Mr. Apabrita Ayan Das** *from* **Indian Institute of Chemical Biology, Kolkata** *participated in this workshop.*

T. S. Keshava Prasad, Ph. D.

Institute of Bioinformatics I.T.P.L.

Ravi Sirdeshmukh, Ph. D.

Certificate of Recognition

conferenceseries.com

One Commerce Center-1201, Orange St. #600, Wilmington, Zip 19899, Delaware, USA
Ph: +1-888-843-8169, Fax: +1-650-618-1417, Toll free: +1-800-216-6499

Conference Series and the Editors of Journal of Clinical & Experimental Cardiology, Journal of Cardiovascular Diseases & Diagnosis, International Publisher of Science, Technology and Medicine and Journal of Cardiovascular Diseases & Diagnosis wish to thank

Prof/Dr. **Apabrita Ayan Das**

CSIR-Indian Institute of Chemical Biology, India

for his phenomenal and worthy oral presentation on

"Elevated level of sTLT1 is associated with risk prediction in acute coronary syndrome"

at the "22nd World Cardiology Conference"

held during December 11-12, 2017 in Rome, Italy

Sergey Suchkov
Sechenov University, Moscow Engineering Physical University (MEPhI) and National Alliance for Translational Medicine, Russian Federation

World Cardiology 2017 Organizing Committee Members

Rainer Moosdorf	Guy Hugues Fontaine	Fekry El Deeb	Marco Picichè
University Hospital of Giessen and Marburg, Germany	Pitié-Salpêtrière Hospital France	Zulekha Hospitals UAE	San Bortolo Hospital Italy

INTERNATIONAL CONFERENCE ON MOLECULAR SIGNALLING: RECENT TRENDS IN BIOSCIENCES

NOVEMBER 20-22, 2015

Organized by

DEPARTMENT OF ZOOLOGY

NORTH-EASTERN HILL UNIVERSITY, SHILLONG - 793022

Certificate of Participation

This is to certify that Prof. /Dr. / Mr. / Ms. Abhrita Ayan Das

CSIR-IICB, Kolkata *participated / ~~delivered an invited lecture~~ / presented a paper / ~~chaired a Session~~ in the International Conference on Molecular Signalling: Recent Trends in Biosciences organized by the Department of Zoology, North-Eastern Hill University, Shillong - 793 022.*

PROF. B. B. P. GUPTA
Secretary, ICMS 2015
Secretary
ICMS- 2015
Department of Zoology
NEHU, Shillong

PROF. N. SAHA
Convener, ICMS 2015
Convener
ICMS- 2015
Department of Zoology
NEHU, Shillong

VIT®
UNIVERSITY
(Estd. u/s 3 of UGC Act 1956)
Vellore-632 014, Tamil Nadu, India.
www.vit.ac.in

C.B.S.T

Centre for Bio-Separation Technology

7th Annual Meeting of Proteomics Society, India - 2015

3rd – 6th December 2015

CERTIFICATE

This is to certify that **Dr/Mr/Ms/Mrs.** Apabrita Ayan Das ..... has participated in **workshop/ conference** of **7th** annual meeting conducted by Centre for Bio-Separation Technology (CBST), VIT University, Vellore under the aegis of **Proteomics Society, India.**

Prof. Surekha Zingde
President
Proteomic Society, India

Dr. G. Viswanathan
Chancellor
VIT University

Prof. M. A.Vijayalakshmi
Convener, PSI-2015
Director, CBST

इंटरनेशनल सोसायटी ऑफ हार्ट रिसर्च (भारतीय अनुभाग) का 14वीं वार्षिक बैठक

14th Annual Meeting of International Society for Heart Research Indian Section

27th to 29th January 2017 at CSIR Institute of Genomics and Integrative Biology, Delhi

This is to certify that ~~Dr./Mr.~~/Ms. Aparbita Ayan Das has participated as a delegate in the 14th Annual Meeting of International Society for Heart Research (Indian Section) organized at the CSIR Institute of Genomics and Integrative Biology (CSIR-IGIB) at Delhi, India from 27th to 29th January, 2017

Shantanu Sengupta
Organizing Secretary

Subir Kumar Maulik
Secretary,
ISHR Indian Section

K.K Talwar
President,
ISHR Indian Section

ISHR International Society for Heart Research

IGIB INSTITUTE OF GENOMICS & INTEGRATIVE BIOLOGY Genomics Knowledge Partner

GENOMEET2017
CSIR Institute of Genomics and Integrative Biology

8th ANNUAL MEETING OF PROTEOMICS SOCIETY, INDIA
3rd MEETING OF ASIA OCEANIA AGRICULTURAL PROTEOMICS ORGANIZATION

International Conference on Functional & Interaction Proteomics: Application in Food & Health

Certificate of Participation

Presented to

Apabrita Ayan Das

for participation in

8th Annual Meeting of Proteomics Society, India

3rd Meeting of Asia Oceania Agricultural Proteomics Organization

organised by NIPGR, New Delhi, India

14th - 17th December 2016

President PSI

President AOAPO

Convener

Proteomics Society, India
(Regd. No 286/2009, Registrar of Societies, RR(Dist) Dist, A.P, India)

Certificate of Participation

IIT BOMBAY

Presented to

Mrs. Apabrita Ayan Das

For participating at the 6th Annual Meeting of the Proteomics Society, India PS(I) held at IIT Bombay during 7-9 December, 2014

S. Zingde

Dr. Surekha Zingde
President, PS(I)

Sanjeeva Srivastava

Dr. Sanjeeva Srivastava
Convener

Proteomics Society, India
(Regd.No 286/2009, Registrar of Societies, RRS and Dist, A.P, India)

IIT BOMBAY

Certificate of Participation

Presented to

Mr. Apabrita Ayan Das

For successfully attending the workshop on Targeted Proteomics conducted at the 6th Annual Meeting of the Proteomics Society, India PS(I) held at IIT Bombay during 10-11 Dec, 2014

S. Zingde

Dr. Surekha Zingde
President, PS(I)

Sanjeeva Srivastava

Dr. Sanjeeva Srivastava
Convener